

**THE DESIGN AND OPTIMIZATION OF
MULTISCALE HYBRID NANOCOMPOSITE
STRUCTURES FOR VIBRATION AND BUCKLING
BEHAVIOR**

**A Thesis Submitted to
the Graduate School İzmir Institute of Technology
in Partial Fulfillment of the Requirements for the Degree of**

DOCTOR OF PHILOSOPHY

in Mechanical Engineering

**By
Ozan AYAKDAŞ**

**July 2024
İZMİR**

We approve the thesis of **Ozan AYAKDAŞ**

Examining Committee Members:

Prof. Dr. H. Seçil ARTEM
Mechanical Engineering, İzmir Institute of Technology

Prof. Dr. Alper TAŞDEMİRCİ
Mechanical Engineering, İzmir Institute of Technology

Prof. Dr. Kutlay SEVER
Mechanical Engineering, İzmir Katip Çelebi University

Prof. Dr. Evren MELTEM TOYGAR
Mechanical Engineering, Dokuz Eylül University

Prof. Dr. Engin AKTAŞ
Civil Engineering, İzmir Institute of Technology

16 July 2024

Prof. Dr. H. Seçil ARTEM
Supervisor,
Mechanical Engineering,
İzmir Institute of Technology

Assoc. Prof. Dr. Levent AYDIN
Co-Supervisor,
Mechanical Engineering,
İzmir Katip Çelebi University

Prof. Dr. M. İ. Can DEDE
Head of Department of
Mechanical Engineering

Prof. Dr. Mehtap EANES
Dean of the Graduate School

ACKNOWLEDGMENTS

Firstly, I would like to express my sincere gratitude to my supervisor, Prof. Dr. Hatice Seil ARTEM, for her invaluable mentorship, patience, and insightful guidance throughout my Ph.D. studies. I am deeply grateful to my co-supervisor, Assoc. Prof. Dr. Levent AYDIN, for his contributions, encouragement and motivation throughout my academic journey. I would also like to appreciate my Ph.D. committee members, Prof. Dr. Alper TAŐDEMIRCI and Prof. Dr. Kutlay SEVER, for their support and valuable feedback. I am also grateful to my Ph.D. thesis examining committee members, Prof. Dr. Evren Meltem TOYGAR and Prof. Dr. Engin AKTAŐ, for their constructive suggestions and contributions.

My warm thanks go to my research group colleagues and friends, Dr Melih SAVRAN and A. Harun SAYI, for their assistance and support throughout my Ph.D. studies.

Above all, I owe my deepest gratitude to my dear wife, Seda AYAKDAŐ, for her unwavering support, care and love throughout my academic journey. I am also deeply grateful to my parents, AyŐe AYAKDAŐ and Ahmet AYAKDAŐ, who have always supported and encouraged me - thank you for being my pillars of strength. I would also like to thank my brother, Melih AYAKDAŐ, for his constant support and his presence.

Finally, I would like to acknowledge the funding provided by the YÖK Council of Higher Education 100/2000 Doctoral Scholarship, which supported my dissertation work within the framework of this scholarship.

ABSTRACT

THE DESIGN AND OPTIMIZATION OF MULTISCALE HYBRID NANOCOMPOSITE STRUCTURES FOR VIBRATION AND BUCKLING BEHAVIOR

This thesis presents multiscale hybrid natural fiber-reinforced nanocomposite structures as viable alternatives to the traditional synthetic carbon and glass fiber composites commonly used in industries like automotive, aviation, and aerospace. These alternatives were created using stochastic optimization methods—Differential Evolution, Simulated Annealing, and Nelder-Mead algorithms—to optimize critical buckling load, fundamental frequency, and factor of safety, while reducing weight and cost. A broad range of design variables were employed, including fiber volume fraction, stacking sequences, and the volume content of Carbon Nanotubes (CNTs) or Graphene Platelets (GPLs) in each layer. The effective material properties of matrices reinforced with CNTs or GPLs were determined using the Modified Halpin-Tsai equations and the rule of mixtures, accounting for the agglomeration effects of the nanofillers. Vibration, buckling, and failure analyses of multiphase hybrid fiber-reinforced nanocomposite structures were performed using both analytical methods (Navier's solution with First-order Shear Deformation Theory (FSDT) and Classical Laminated Theory (CLT)) and the Finite Element Method (FEM). A multi-objective optimization problem was strategically executed using the Penalty Function approach to propose optimal eco-friendly, lightweight, and cost-effective alternatives to conventional composite materials, aiming for maximum mechanical response with minimal weight and cost. Additionally, optimal nanocomposite driveshaft designs were proposed for future automotive applications, featuring hybrid Carbon/Flax/CNT structures with non-uniform fiber and CNT distribution, accounting for agglomeration effects. The results indicated that optimizing natural fibers with GPLs or CNTs in engineering structures offers substantial benefits, enhancing both environmental sustainability and composite material performance in terms of weight, cost, frequency, and buckling properties.

ÖZET

ÇOK ÖLÇEKLİ HİBRİT NANOKOMPOZİT YAPILARIN TİTREŞİM VE BURKULMA DAVRANIŞLARI İÇİN TASARIMI VE OPTİMİZASYONU

Bu tezde, otomotiv, havacılık ve uzay sanayi gibi endüstrilerde yaygın olan geleneksel sentetik karbon ve cam elyaf takviyeli kompozit yapılara alternatif olarak çok fazlı hibrit doğal fiber takviyeli nanokompozit yapılar sunulmaktadır. Alternatif tasarımların kritik burkulma yükünü, doğal frekansını ve yapısal güvenlik faktörünü maksimize etmek için Differential Evolution, Simulated Annealing, ve Nelder-Mead stokastik optimizasyon yöntemleri kullanılmıştır. Fiber hacim oranı, fiber oryantasyon açısı ve her tabakadaki Karbon Nanotüplerin (CNT) veya Grafen Plaketlerin (GPL) hacim içeriği eş zamanlı olarak tasarım değişkenleri olarak kullanılmıştır. CNT veya GPL ile güçlendirilmiş matrislerin etkili malzeme özellikleri, nanodolgu maddelerinin kümelenme etkileri göz önünde bulundurularak Modifiye Halpin-Tsai denklemleri ve karışım kuralı kullanılarak hesaplanmıştır. Çok fazlı ara hibrit fiber tabakalı nanokompozit yapıların vibrasyon, burkulma ve hasar analizleri, hem analitik yöntemler (Navier çözümü ile Birinci Derece Kayma Deformasyon Teorisi (FSDT) ve Klasik Laminasyon Teorisi (CLT)) hem de Sonlu Elemanlar Metodu (FEM) kullanılarak yapılmıştır. Maksimum mekanik özellik ve minimum ağırlık ve maliyet için çok amaçlı optimizasyon problemleri, geleneksel kompozit yapılara çevre dostu, hafif ve düşük maliyetli alternatifler önerebilmek amacıyla Ceza Fonksiyonu yaklaşımı kullanılarak stratejik bir şekilde gerçekleştirilmiştir. Ayrıca, otomotiv endüstrisinde potansiyel gelecekteki uygulamalar için optimum nanokompozit tahrik mili tasarımları, kalınlık boyunca kümelenme etkileri dahil olmak üzere eşit olmayan şekilde dağılmış fiber ve CNT dağılımına sahip hibrit Karbon/Keten/CNT takviyeli yapılarla önerilmiştir. Genel sonuçlar, doğal fiberlerin GPL veya CNT ile optimize edilmesinin, mühendislik yapılarında sadece çevresel sürdürülebilirlik açısından değil, aynı zamanda ağırlık, maliyet, frekans ve burkulma özelliklerine dayalı kompozit malzeme tasarımının performansı açısından da avantajlar sağladığını göstermiştir.

TABLE OF CONTENTS

LIST OF FIGURES	ix
LIST OF TABLES	xiii
CHAPTER 1. INTRODUCTION	1
1.1. Literature Survey.....	1
1.2. Research Significance	9
1.3. Motivation, Objectives and Originality	11
CHAPTER 2. COMPOSITE MATERIALS.....	15
2.1. Classification of Composites	15
2.2. Nanocomposites	19
2.3. Natural Fibers and Natural Fiber Nanocomposites.....	24
2.4. Application of the Hybrid Composites, Natural Fiber Composites and Nanocomposites.....	28
CHAPTER 3. MECHANICAL ANALYSIS.....	33
3.1. Laminate Constitutive Equations for CLPT and FSDT	35
3.2. Classical Laminated Plate Theory.....	37
3.2.1. Vibration of the Simply Supported Composite Plate	37
3.2.2. Buckling of Simply Supported Composite Plates Under Compressive Loads.....	39
3.2.3. Stress-Strain Analysis	41
3.2.4. Failure Analysis	43
3.2.5. Driveshaft Problem	45
3.3. First- Order Shear Deformation Theory.....	46
3.3.1. Vibration of the Laminated Composite Plate by Simply Supported Boundary Conditions	48
3.3.2. Buckling of the Laminated Composite Plate by Simply Supported Boundary Conditions	49

CHAPTER 4. MATERIAL PROPERTIES	51
4.1. Halpin-Tsai Model	53
4.1.1. Carbon Nanotube Reinforced Matrix	53
4.1.2. Three-Phase Fiber/CNT Reinforced Matrix Composite	54
4.1.3. Graphene Reinforced Matrix	55
4.1.4. Graphene and Fiber Reinforced Matrix	56
4.2. Modified Halpin-Tsai Model	57
4.2.1. CNT-Reinforced Matrix Composite Model	57
4.2.2. Fiber Reinforced Nanocomposite Lamina Constants	60
4.3. Functionally Graded Graphene Reinforced Matrix	61
4.4. Eshelby-Mori Tanaka Model for Nanocomposite Structures	62
CHAPTER 5. OPTIMIZATION.....	66
5.1. Single-Objective Optimization	66
5.2. Multi-objective Optimization.....	67
5.3. Stochastic Optimization Algorithms.....	67
5.3.1. Differential Evolution Algorithm.....	68
5.3.2. Nelder-Mead Algorithm.....	69
5.3.3. Simulated Annealing Algorithm	71
CHAPTER 6. VIBRATION PROBLEMS	73
6.1. Benchmark Problems	73
6.1.1. Problem B1.....	74
6.1.2. Problem B2.....	76
6.1.3. Problem B3.....	77
6.1.4. Problem B4.....	79
6.1.4.1. Problem B4.1	80
6.1.4.2. Problem B4.2.....	82
6.1.5. Problem B5.....	83
6.1.6. Problem B6.....	87
6.1.6.1. Problem B6.1	87
6.1.6.2. Problem B6.2.....	89
6.2. Single-Objective Problems	90

6.2.1. Problem 1	93
6.2.2. Problem 2	94
6.2.3. Problem 3	96
6.2.4. Problem 4	97
6.2.5. Problem 5	100
6.2.6. Problem 6	104
6.3. Multi-Objective Optimization Problems.....	106
6.3.1. Problem 1.	109
6.3.2. Problem 2.	117
6.3.3. Problem 3.	124
6.3.3.1. Finite Element Analysis of the Optimum Cases	133
 CHAPTER 7. BUCKLING PROBLEMS	 138
7.1. Benchmark Problem.....	138
7.1.1. Problem B1.....	139
7.1.2. Problem B2.....	141
7.1.3. Material Model Verification	143
7.2 Single-Objective Optimization Problem.....	147
7.2.1. Problem 1	147
7.3. Multi-objective Optimization Problem	151
7.3.1. Problem 1.	153
 CHAPTER 8. NANOCOMPOSITE DRIVESHAFT PROBLEM	 159
8.1. Benchmark Problem.....	160
8.1.1. Finite Element Analysis of Composite Driveshafts	162
8.2. Nanocomposite Driveshaft Optimization Problem.....	167
 CHAPTER 9. CONCLUSION	 177
 REFERENCES	 180

LIST OF FIGURES

<u>Figure</u>	<u>Page</u>
Figure 2.1. Classification of composite materials.....	15
Figure 2.2. Composite types according to reinforcement shape.....	17
Figure 2.3. Different types of carbon-based nanofillers	20
Figure 2.4. Classification of natural fibres according to origin, with examples.....	25
Figure 2.5. Images of the most widely used natural fibers	26
Figure 2.6. Manufacturing process of the Ramie/Carbon hybrid composites in four distinct layer sequences.....	27
Figure 2.7. The material composition details of the commercial aircraft models the Boeing 787 and the Airbus A380	29
Figure 2.8. A) Porsche Motorsport 718 Cayman GT4 CS MR with full natural fiber body kit, b) Tesla race car S P100D showing a body made from natural fibers, c) McLaren F1 seat reinforced with Bcomp	30
Figure 2.9. Nanocomposite applications a) carbon fibre/graphene nanocomposites application on Orbex Prime rocket b) Lockheed Martin F-35 Lightning II c) Nasa Space Launch System and forward skirt structure	31
Figure 3.1. Geometry of the laminated plate	34
Figure 3.2. Schematic illustration of a unidirectional fiber-reinforced composite lamina, with the inclusion of GPLs in the polymer matrix.....	34
Figure 3.3. Thin laminated composite plate subjected to biaxial in-plane loading	39
Figure 3.4. Resultant forces and moments on a laminate	41
Figure 3.5. Composite cylindrical hollow shaft.....	45
Figure 4.1. Hierarchy of the three-phase GPLs/fiber/polymer multiscale composites	51
Figure 4.2. Concept of multiscale graphene nano platelets (a) and carbon nanotube (b) reinforced polymer composites.....	52
Figure 4.3. Unidirectional fiber-reinforced composite lamina with MWCNT inclusion	58
Figure 4.4 Illustration of the CNTs half-wavelength.....	59
Figure 4.5. Geometry and coordinate system of the FG-GPLs composite plates.....	61
Figure 4.6. Partial agglomeration of CNTs.....	63

<u>Figure</u>	<u>Page</u>
Figure 5.1. Flowchart of the DE algorithm.....	69
Figure 5.2. Flowchart of the NM algorithm.....	70
Figure 5.3. Flowchart of the SA algorithm.....	72
Figure 6.1. Dimensions and boundary conditions of plate	82
Figure 6.2. Glass fiber/CNT reinforced nanocomposite plate	84
Figure 6.3. Different GPL distribution patterns.....	88
Figure 6.4. Young’s modulus of the CNT reinforced composites for different agglomeration factor and comparison with experimental and analytical results	90
Figure 6.5. Schematic illustration of a unidirectional fiber-reinforced composite laminate	91
Figure 6.6. Illustration of the symbols for inter ply hybrid fiber/GPLs reinforced nanocomposites layer by layer.....	92
Figure 6.7. Comparison of natural frequencies. Costs. And weights for optimum designs formulated in Problems 1–4.....	99
Figure 6.8. Contour plots of the frequency for hybrid [C/C/F/F]s composite plates with varying graphene weight and fibre orientation angles of each layer.....	103
Figure 6.9. Variation of the natural frequencies with increasing in flax ply for constant total ply thickness of the hybrid composite plate.....	105
Figure 6.10. Illustration of the symbols for inter ply hybrid and non-hybrid fiber/CNTs reinforced nanocomposites for two-phase and three -phase composites	108
Figure 6.11. Comparison of the optimum design results for maximum fundamental frequency and minimum weight	116
Figure 6.12. Comparison of the optimum design results for maximum fundamental frequency and minimum cost.....	123
Figure 6.13. Comparison of the optimum design results for maximum fundamental frequency, minimum cost and minimum weight	132
Figure 6.14. Representation of the designs.....	134
Figure 6.15. Mode shapes of vibration of [C/C/K/K]s-CNT multiscale nanocomposite plate with SSSS boundary condition	136

<u>Figure</u>	<u>Page</u>
Figure 7.1. Laminated composite plate with 64 layers Structure	140
Figure 7.2. Young's modulus of CNT-reinforced matrix as a function of Vcnt (vol%) for various fa agglomeration factors	144
Figure 7.3. Young's modulus of CNT-reinforced matrix as a function of Vcnt (vol%) for various fw waviness factors.	145
Figure 7.4. a) Agglomeration effects on Critical Buckling Load for [90/90/90/90]s plates with 0.60 volume fraction of fiber and a/b=0.5. b) comparison of how variations in fiber orientation angle and volume fraction affect Ncr	146
Figure 7.5. Layered symmetric-balanced laminated composite	147
Figure 7.6. Comparison of the optimum design results for maximum critical buckling load and minimum weight	158
Figure 8.1. General visual representation of the placement and role of the drive shaft in the vehicle's transmission system.....	159
Figure 8.2. General dimension of the composite driveshaft	161
Figure 8.3. Mesh used in FEA model	163
Figure 8.4. Boundary conditions and loadings of static and buckling analysis in Autodesk Inventor NASTRAN Software	163
Figure 8.5. Boundary conditions and loadings of normal modes analysis in Autodesk Inventor NASTRAN Software	164
Figure 8.6. Finite Element Analysis Results for (a) Stress Components and (b) Puck Failure Indexes	166
Figure 8.7. Comparison of the optimum design results minimum weight design results for multiphase hybrid and non-hybrid fiber/CNT reinforced nanocomposite driveshafts.....	170
Figure 8.8. Finite Element Analysis Results for a) Stress Components and b) Puck Failure Indexes for multiphase hybrid Flax/Carbon/CNT reinforced nanocomposite driveshafts	173
Figure 8.9. Finite Element Analysis Results for 4th carbon/cnts ply of hybrid nanocomposite driveshaft a) Shear Stress Component (s12) and b) Puck Failure Index	174

<u>Figure</u>	<u>Page</u>
Figure 8.10. First buckling mode shape of a hybrid nanocomposite driveshaft.....	175
Figure 8.11. The first eight mode shapes of natural frequency of a simply supported composite drive shaft.....	176

LIST OF TABLES

<u>Table</u>	<u>Page</u>
Table 2.1. Differences between thermosets and thermoplastics	16
Table 2.2. Mechanical Properties of some plant fibers compared to glass and carbon fibers.....	18
Table 2.3. The overview of the cnts reinforced matrix materials improvements	22
Table 2.4. The overview of the Graphene reinforced matrix materials improvements ..	23
Table 2.5. The advantages and disadvantages of natural fiber composites over traditional petroleum-based composites	24
Table 5.1. Three optimization methods options	71
Table 6.1. Material Properties of the gpls, matrix, flax carbon and glass fibers	73
Table 6.2. Comparison of optimum results for non-dimensionalized frequencies Ω of graphene/fiber reinforced nanocomposite plates	75
Table 6.3. Comparison of design efficiency factors (Ω_{\max} / Ω_0) of the optimum design for graphene/fiber reinforced nanocomposite plates	75
Table 6.4. Comparison of optimum results for non-dimensionalized frequencies Ω and design efficiency factors (Ω_{\max} / Ω_0) of graphene/fiber reinforced nanocomposite plates.....	77
Table 6.5. Comparison of optimum weight fraction sequence results for non- dimensionalized frequencies Ω of graphene/fiber reinforced nanocomposite plates	78
Table 6.6. Comparison of design efficiency factors (Ω_{\max} / Ω_0) of the optimum design for graphene/fiber reinforced nanocomposite plates	79
Table 6.7. General description of benchmark problems B4	80
Table 6.8. Material Properties of the CNT, matrix, glass fibers	80
Table 6.9. Comparison of non-dimensional frequencies Ω obtained by analytical and numerical solution (Autodesk NASTRAN) with different methods from the literature for glass fiber reinforced with SSSS square plate.....	81
Table 6.10. Comparison of non-dimensional frequencies Ω obtained by analytical and numerical solution (NASTRAN) with different methods from the literature for CNT-Glass fiber reinforced with SSSS square plate	83
Table 6.11. Description of the Optimization Problems	84

<u>Table</u>	<u>Page</u>
Table 6.12. Comparison of the optimum stacking sequences result of the weight minimization problem for DE, SA and NM algorithms with SQP38 method for different frequency constraints Ω_0	85
Table. 6.13. Comparison of the optimum volume fraction design results for each layer in the weight minimization problem using DE, SA, and NM algorithms versus the SQP method for different frequency constraints Ω_0	85
Table 6.14. Comparison of the DE, SA, and NM algorithms' optimum weight content designs per layer in the weight minimization problem with the SQP approach for various frequency constraints Ω_0	86
Table 6.15. Comparison of the DE, SA, and NM algorithms' minimum weight results for structures in the weight minimization problem with the SQP approach for various frequency constraints.....	86
Table 6.16. Comparison of the effect of GPLs distribution patterns on dimensionless natural frequencies according to different mode shapes.....	89
Table 6.17. Hill's moduli of SWCNT.....	89
Table 6.18. Material Properties of the GPLs, matrix, flax carbon and glass fibers.....	92
Table 6.19. Description of the Optimization Problems	93
Table 6.20. Optimum stacking sequences results of the carbon, flax and glass fiber reinforced composite plates.....	94
Table 6.21. Optimum Stacking Sequences Results of the Carbon-Flax and Carbon-Glass fiber reinforced composite plates.....	95
Table 6.22. Optimum stacking sequences and weight content of gpls results of the carbon, flax and glass fiber reinforced composite plates.....	97
Table 6.23. Optimum Stacking Sequences and weight content of gpls results of the Carbon-Flax and Carbon-Glass, Glass-Flax fiber reinforced composite plates.....	99
Table 6.24. Comparison of optimum design for non-dimensionalized frequencies Ω of carbon, flax and glass fiber reinforced nanocomposite plates for different aspect ratios(a/b),	101
Table 6.25. Comparison of optimum design for non-dimensionalized frequencies Ω of carbon, flax and glass fiber reinforced nanocomposite plates for different aspect ratios(a/b),	102

<u>Table</u>	<u>Page</u>
Table 6.26. Optimum Stacking Sequences and weight content of GPLs results of the Carbon-Flax fiber reinforced composite plates according to variation of flax ply number	106
Table 6.27. Mathematical definitions of optimization problems for two-phase (fiber/matrix) composites and three phase (fiber/GPLs/matrix) nanocomposite plates	107
Table 6.28. Material Properties of Fiber and Matrix for Problem 1, 2 and 3.	108
Table 6.29. Comparison of optimum Stacking sequence, volume fraction of fiber and weight fraction of CNT distribution results for maximum fundamental frequency and minimum weight of composite plates	111
Table 6.30. Comparison of optimum fundamental frequency and minimum weight with the related cost and comparing the results to the reference design	114
Table 6.31. Comparison of optimum Stacking sequence, volume fraction of fiber and weight fraction of CNT distribution results for maximum fundamental frequency and minimum cost of composite plates,.....	118
Table 6.32. Comparison of optimum fundamental frequency and minimum cost with the related weight and comparing the results to the reference design	121
Table 6.33. Comparison of optimum Stacking sequence, volume fraction of fiber and weight fraction of CNT distribution results for maximum fundamental frequency and minimum weight of composite plates	126
Table 6.34. Comparison of optimum fundamental frequency, minimum cost and minimum weight and comparing the results to the reference design	129
Table 6.35. Optimum design results of the Problem 3	134
Table 6.36. Optimum material properties for layer by layer	134
Table 6.37. Comparison of the FEM results with analytical method for optimum cases	135
Table 7.1. Different load cases, lengths, and widths considered for 64-layer laminated composite plate.....	139

<u>Table</u>	<u>Page</u>
Table 7.2. Optimum stacking sequences and buckling load factors obtained for 64-layer laminated composite plate with graphite/epoxy layers under different load cases.....	140
Table 7.3. Comparison of nondimensional buckling loads, $N = N_{cr}\alpha^2/E_2h^3$, for simply supported cross-ply laminated rectangular plates under uniaxial compressions.....	142
Table 7.4. Comparison of nondimensional buckling loads, $N = N_{cr}\alpha^2/E_2h^3$, for simply supported cross-ply laminated rectangular plates under biaxial compressions.....	142
Table 7.5. Comparison of the modified Halpin-Tsai Model results for variable V_{cnt} . Mechanical properties of MWCNT-reinforced nanocomposite matrix.....	143
Table 7.6. Material Properties of the CNT, matrix, flax carbon and glass fibers.....	148
Table 7.7. Comparison of critical buckling load capacity, stacking sequences and weight for 16 layered symmetric-balanced CNT added laminated composites.....	149
Table 7.8. Mathematical definitions of optimization problems for two-phase (fiber/matrix) composites and three phase (fiber/GPLs/matrix) nanocomposite plates.....	152
Table 7.9. Material properties of fiber and matrix for buckling Problem 1.....	153
Table 7.10. Comparison of optimum Stacking sequence, volume fraction of fiber and weight fraction of CNT distribution results for maximum critical buckling load and minimum weight of composite plates,.....	155
Table 7.11. Comparison of optimum critical buckling loads and minimum weights and comparing the results to the reference design.....	156
Table 8.1. Design specification of the driveshaft.....	161
Table 8.2. Mechanical Properties of the Carbon/Epoxy, Carbon/CNT/Epoxy and Basalt /bio-epoxy composite materials.....	162
Table 8.3. Mesh Set up in Autodesk NASTRAN.....	165
Table 8.4. A summary of comparison for composite drive shaft design parameters calculations; Critical Torsional Buckling Load, Fundamental Frequency and Factor of Safety.....	165
Table 8.5. Material Properties for driveshaft optimization problems.....	167

<u>Table</u>	<u>Page</u>
Table 8.6. Optimum Stacking Sequences, Volume Fraction of Fiber and Carbon Nanotubes sequences for composite Driveshaft	168
Table 8.7. Minimum weight, natural frequencies, critical torsional buckling loads and safety factor results of optimum Multiphase Fiber reinforced nanocomposite Driveshafts	169
Table 8.8. Material Properties of each ply for optimum inter-ply hybrid Flax/Carbon/CNTs nanocomposite driveshafts with Modified Halpin-Tsai Model	171
Table 8.9. A comparison of the natural frequencies, critical torsional buckling load, and factor of safety results obtained from Finite Element Analysis (FEA) and Analytical Methods for the optimum hybrid nanocomposite driveshaft	172

CHAPTER 1

INTRODUCTION

1.1. Literature Survey

Nanocomposites are composite materials containing at least one or more reinforcing components in the nanoscale range, including graphene nanoparticles (GNPs) and carbon nanotubes (CNTs). These inclusions result in composites that are lighter and stiffer, as mentioned by numerous studies¹. The optimization of nanocomposite properties in terms of nanoscale reinforcements and stacking sequences has the potential to enable further design improvements and the production of lighter composites. Both graphene platelets and carbon nanotubes are characterised by a number of similar properties, including a high specific strength-to-weight ratio, high electrical resistivity and thermal conductivity. Graphene consists of graphite atoms bonded in hexagonal lattice structures, forming a two-dimensional (2D) material, while carbon nanotubes are three-dimensional (3D) structures created by rolling up sheets of graphene^{2,3}. The values of Young's modulus, inherent strength, and thermal conductivity for a defect-free graphene nanoplate are approximately 1.0 TPa, 42 N/m, and 5300 W/(m·K), respectively⁴. It was found that the addition of 0.3 wt% CNTs reinforcement in resin to a composite plate resulted in an improvement in flexural modulus and flexural strength by 11.6% and 18.0%, respectively⁵. Despite the excellent properties of carbon nanotubes (CNTs), two-dimensional graphene has garnered considerable attention. This is primarily due to the higher manufacturing costs of CNTs, their highly anisotropic mechanical properties, and challenges in achieving sufficiently uniform dispersion within matrix materials. Furthermore, some studies suggest that graphene nanofillers and their derivatives offer greater advantages for designers seeking to achieve superior structural properties^{6,7}. In a study conducted by Rafiee et al.⁸, the elastic modulus of an epoxy matrix reinforced with graphene, single-walled carbon nanotubes (SWCNTs), and multi-walled carbon nanotubes (MWCNTs) at a weight fraction of 0.1% was investigated. The results showed that the Young's modulus of the graphene-reinforced composite increased by 30%, whereas the carbon nanotube-reinforced composite observed only a 3% increase in

Young's modulus.⁸ The reinforcement of epoxy composites with graphene nanoplatelets and carbon nanotubes (CNTs) has been the subject of numerous studies, which have revealed that graphene-reinforced epoxy composites possess exceptional potential. This is as a result of their superior shear strength, enhanced Young's modulus and reduced manufacturing costs in comparison to CNTs-reinforced composites.^{9,10}

The increasing demand for low-cost, lightweight, and environmentally friendly materials has led to a significant growth in the use of natural fibre-reinforced composites over the past few decades. This trend is observable across a range of industrial sectors, including automotive, aerospace, naval and civil construction. The utilization of high-performance natural fibers, including hemp, flax, jute, kenaf, and sisal, has been on the rise, replacing synthetic fibers and consequently reducing the carbon footprint and other environmentally deleterious effects associated with synthetic fibers. This aligns with the Kyoto Protocol regulations and the biodegradability requirements in Europe. Natural fiber composites provide several advantages, including lightweight and low cost. The lightweight nature of these composites enhances fuel efficiency in automotive applications, particularly in electric and hybrid vehicles¹¹. Recently, some components of automobiles, including door panels, seatback structures and instrument panels, are being manufactured using FFRCs (flax fibre-reinforced composites). It is estimated that the application of plant fibres in the automotive industry may increase by 54%, as documented in the referenced literature¹². The surface areas for load transmission within a polymer matrix are typically smaller for major plant fibres, including hemp, jute, coir, ramie, and various other natural fibres. Among these, flax fibres are particularly noteworthy as an excellent choice due to the high surface area for load transmission offered by retted flax bundles, which makes them highly effective in reinforcing polymer composites^{13,14}. Currently, flax is regarded as the most viable alternative to synthetic fibres in the automotive industry, given its superior tensile strength and modulus¹⁵. In experimental studies investigating the acoustic and vibrational damping properties of flax fiber-reinforced composites, it was observed that their acoustic absorption and vibration damping capabilities are superior to those of glass fiber-reinforced composites, which were found to be 21.42 % and 51.03 %, respectively¹⁶. Therefore, the use of flax fibres can be considered an appropriate substitute for glass fibres in applications that necessitate a high level of sound and vibration damping. It is a proof of the replacement of natural fibres with synthetic fibres for the vibration-related problems. However, it is important that natural fibres possess a number of disadvantages, including low water resistance and

rapid moisture absorption, as well as low stiffness and strength properties¹⁷. The shortcomings resulted from the nature of the flax fibers which can easily interact with water molecules. As a result of the above-mentioned characteristics, a relatively weak bond between the fibres and the matrix is observed in the case of flax-reinforced composites¹⁸⁻²⁰. The key to removing this disadvantage is material hybridization, which is achieved by combining synthetic and natural fibres in a polymer matrix²¹.

In engineering systems subjected to vibrations, determining the natural frequency is crucial to prevent resonance from external excitations. Consequently, numerous studies have focused on the design and optimization of composites that experience vibrations. Adali and Duffy²² utilized the laminate thickness and the total number of layers as design variables with the objective of minimizing the cost of symmetric, angle-ply graphite/glass hybrid laminates subject to a frequency constraint. The results showed that the material cost of the hybrid design was significantly lower than that of a graphite laminate. In a further study focusing on hybrid composite plates and shells, Ma et al. have proposed a simultaneous multi-scale optimization framework. This framework enables the parallel optimization of fibre volume fractions, fibre orientations and the stacking sequence, utilising the Discrete Material Optimization (DMO) method.²³ The study of hybrid composite structures has been a major area of research due to their potential to reduce costs, weight and failure index while improving safety. In hybrid composites, the design approach typically includes the use of high-stiffness and high-cost materials in the outer layers, with low-stiffness and low-cost materials employed in the inner layers. The objective of the study by Abachizadeh and Tahani²⁴ is to optimise the natural frequency and minimize the cost of hybrid graphite/glass epoxy laminates. The study employed the Genetic Algorithm and Simulated Annealing for optimization purposes, demonstrating the beneficial effects of the hybridisation process in reducing weight while maintaining an acceptable natural frequency. Haichao An et al.²⁵ successfully resolved the optimal design problem involving hybrid graphite/glass epoxy composite laminates, with the objective of minimising costs while maximising both frequency and frequency gaps. In this study, a genetic algorithm was employed to optimise the stacking sequence of the laminate, with high-stiffness material positioned in the skin layers and low-stiffness material situated in the core layers. The incorporation of flax fiber in hybrid composites has been the focus of numerous optimization studies²⁶⁻²⁹. Flax fibers are a more cost-effective, accessible, and environmentally friendly alternative to glass fibers. In the study conducted in Savran and Aydın, the frequency of hybrid graphite-flax/epoxy and

graphite-glass/epoxy composite plates was maximized³⁰.

This study employed Differential Evolution (DE), Nelder-Mead (NM), and Simulated Annealing (SA) to solve the optimal design problem. The findings indicated that using graphite-flax/epoxy is a superior option compared to graphite-glass/epoxy in terms of maximizing natural frequency and minimizing cost. Hosseinzadeh et al.³¹ investigated the use of flax fibres as an efficient alternative to glass fibres in composites for the multi-objective optimization of hybrid composite plates, with the objective of minimizing costs and maximizing frequency gaps. The results demonstrated that the incorporation of flax fibres into composite materials can provide a cost-effective solution, enhance the natural frequency, and reduce the gaps between the natural frequencies. The optimal design of hybrid composite beams subjected to distinct boundary conditions was investigated by Megahed et al.³². The design variables included the fibre type, volume fraction, layer thickness, and fibre orientation. The solutions were obtained using a particle swarm optimization (PSO) algorithm. The results indicated that laminates based on hybrid designs comprising carbon and flax fibres demonstrated the optimal combination of lightweight and low-cost characteristics, with maximum natural frequencies.

Designs of three-phase nanocomposites, which include a nanoscale component, fiber, and matrix, offer additional opportunities for optimizing composite laminates. Nanoscale reinforcement, such as graphene nanoplatelets, can transfer a significant amount of stress from the polymer matrix to the reinforcing material, as observed in various studies³³. However, the use of a nanoscale reinforcement in a polymer matrix may lead to a number of issues. The issues include the high cost of nano reinforcements, non-uniform dispersion in the matrix and coalescing leading to weak zones in the matrix. Presence of weak zones in the matrix can inadvertently affect the stiffness and strength of the laminate. In consideration of these challenges, the optimization of the design process assumes a crucial role in the development of two-phase and three-phase nano-reinforced composite structures. Study by Kamarian et al.³⁴ utilized a stacking sequence optimization approach to enhance the natural frequencies of multiphase composite plates (CNT/fiber/polymer) by utilizing the Mori-Tanaka model to ascertain the material properties and the Firefly Algorithm to derive the optimization results. Optimal design and parametric studies demonstrate that the natural frequency of nanocomposite plates can be significantly increased by optimizing the stacking sequences and the distribution of reinforcing materials across the thickness. In their study, Xiang et al.³⁵ investigated the

optimization of the lay-up of functionally graded CNT-reinforced conical shells using the genetic algorithm and the first-order shear deformation theory (FSDT). Their results indicated that the content and distribution of CNTs, as well as the stacking sequence, have a significant impact on the maximisation of the vibration frequency. The study by Yousefi et al.³⁶, based on FSDT and particle swarm optimization, aimed to optimize CNTs/polymer/fiber conical panels. The findings demonstrated that optimizing the stacking sequence and the distribution of CNTs and fibers can enhance the natural frequency of the panels and reduce the material cost. Regarding multiphase nanocomposites, the work by Jeawon et al.³⁷ focused on the optimal design of a three-phase graphene/fiber-reinforced laminated nanocomposite. The design variables included graphene and fiber contents, layer thicknesses, and fiber orientations, all aimed at achieving the highest natural frequency. It was found that the most beneficial outcomes from Sequential Quadratic Programming (SQP) suggested that non-uniform distributions of graphene and fibres, as well as fibre orientations, are highly beneficial for enhancing the efficiency of the design process. Further studies on the optimization of multiphase composite laminates with frequency, cost and weight design objectives are presented in³⁸⁻⁴¹. Experimental studies on the vibration characteristics of laminates reinforced with flax fibres and carbon nanotubes have been conducted and reported upon. It has been demonstrated that the incorporation of CNTs in flax fibre-reinforced laminates resulted in an increase in the vibration frequency, whereas the inclusion of graphite led to an improvement in the damping characteristics of the laminates^{42,43}. In an experimental study, Shanmugam and Meenakshisundaram⁴⁴ introduced an innovative concept for hybrid (flax/E-glass/epoxy) fiber reinforced polymer (HFRP) composites by adding graphene as a nanofiller. The results demonstrated that the addition of 0.6 weight percentage of graphene to HFRP composite laminates significantly enhanced the strength of the composites, indicating their suitability for utilization in structural and automotive applications.

In addition to the requirement for environmentally-friendly materials due to the End-of-Life Vehicles Directives and Euro 5 and Euro 6 regulations on emissions, designers must also consider the costs and the weight of the materials. Studies on reinforcing composites with graphene or carbon nanotube indicated that even small amounts of these materials can greatly improve the mechanical properties of composites. There is a prevailing trend in industries to employ carbon and glass fiber-reinforced composites with the underlying assumption that their lower cost and weight outweigh

other factors. Present study seeks to establish that a minimal inclusion of GPL reinforcement in combination with natural flax fibers in singly or hybrid form with synthetic fibers, can yield designs that are not only eco-friendly but also having a higher natural frequency, lower cost and weight as compared to using glass and carbon fibers as reinforcements.

Many studies on the stability of laminated composite plates have focused on rectangular plates and examined the effect of design parameters such as boundary conditions, fiber orientation, and geometric aspect ratio on stability. Thin composite structures are prone to instability, resulting in buckling when subjected to mechanical or thermal loading. The buckling behavior of composite plates includes complex analysis, and more details can be found in references ⁴⁵⁻⁴⁸ Carbon nanotubes (CNTs) are a significant additive material for high-performance structural composites and hold great potential for various applications, making them an object of interest for scientists and researchers who are highly invested in nanostructures⁴⁹. As the dimensions of these structures reduce to micro and nano scales, both experimental and atomistic simulations have demonstrated that the size effect on mechanical properties becomes increasingly significant ⁵⁰. A single-walled carbon nanotube (SWCNT) is a cylinder with a diameter of 1 nm, while a multi-walled carbon nanotube (MWCNT) consists of a concentric form and a separated array of cylinders, ranging from 2 to 100 nm in diameter and tens of microns in length ⁵¹. The another studies reported the experimental elastic properties of both SWCNT and MWCNT, revealing that the elastic modulus of CNTs can vary widely, ranging from 200 GPa to 5.6 TPa. CNT-based fiber-reinforced polymer (FRP) composite materials have high strength-to-weight and stiffness-to-weight ratios ^{52,53}. Studies have shown their potential in various applications, and there is growing interest in analyzing their performance in bending, buckling, and vibration ⁵⁴⁻⁵⁹. Research conducted by Madenci et al. ⁶⁰ explored the impact of carbon nanotubes (CNTs) on the buckling behavior of FRP composites. Their findings showed a significant increase in load-carrying capacity for the clamped-clamped boundary condition in both CNT and NEAT samples. In fact, these samples exhibited an average load-carrying capacity that was 268% and 282% higher, respectively, compared to the simple-simple condition in carbon fiber reinforced polymer composite. Madenci ⁶¹ also conducted free vibration analysis of FG-CNT composite beams and estimated the effective material properties of nanobeams using the mixing rule. In another study, Qian et al. ⁶² demonstrated that adding just 1% by weight of CNT to the matrix material can increase the composite's hardness by 36-

42% and its tensile strength by 25%. Zhu et al.⁶³ analyzed the stress-strain curve of 1 and 4 wt% CNT-reinforced epoxy resin and discovered a 30-70% increase in the elastic modulus for these weight fractions. Tarfaoui et al.⁶⁴ studied the effect of CNT in CNTs-reinforced composites with different volume fractions and found that an increase in the CNT volume fraction decreased the material properties by 0.5-2% after reaching a specific value.

Drive shafts are a crucial part of the transmission of motion from the differential to the wheels or rotors in many industries such as automotive, marine, energy, etc. In these applications, driveshafts are typically subjected to torsional, bending and normal forces in order to transfer power and torque from the engine to the gears⁶⁵. Driveshafts must be designed based on three design criteria for these applications; torque transmission capability, buckling torque capability and bending natural frequency⁶⁶. Although steel driveshafts are commonly used in the automotive industry, recent developments in manufacturing processes have led to the use of composite driveshafts as a viable alternative due to their light weight and high stiffness properties to meet rising demands in high torque transfer from powerful engines⁶⁷⁻⁶⁹.

Over the past few years, many studies have been conducted on composite driveshaft design and application to propose effective designs using different design variables and materials. One of the recent papers on composite driveshafts, the design and analysis performance compared to see different fibre materials such as carbon, Kevlar, glass and boron with the same matrix material⁷⁰. The research findings indicate that critical buckling torque and dynamic properties are influenced by two crucial design parameters: fiber orientation angles and stacking sequences. In a further study, the drive shaft made of glass epoxy resin was examined for its torsional strength, its natural frequency, and its performance parameters at critical speeds for light vehicles⁷¹. The proposed composite design is indicated as the strongest option, with a 73% weight reduction compared to conventional steel driveshafts. The other study by Savran et al. [7] on optimal composite driveshaft design problems selected fiber orientations, layer numbers, and thicknesses as design variables, with manufacturing scenarios, torsional buckling, and bending frequency serving as constraints. For different glass-epoxy materials, designs that weighs between 0.7289 kg and 2.3800 kg showed a significant weight reduction of up to 69%. The marine application of a composite drive shaft has been investigated by Bilalis et al.⁷² to see the possibility of replacing the conventional steel shaft. The optimum lay-up design of the carbon fibre-reinforced plastic shaft has

been proposed through the use of a finite element model, analytical methods and optimization algorithms. According to the results of the study, the composite shafts were 61.2% lighter than the steel shafts that were currently in use, including the flanges. Other recent research have also been conducted to compute the torsional stiffness of carbon fiber reinforced composites using a balanced laminate design, based on finite element analysis and classical laminate plate theory, as mentioned in ⁷³⁻⁷⁵. Shinde et al. ⁷¹ optimized the glass epoxy composite drive shaft for outer diameter 55 mm, inner diameter 32 mm, percentage fiber volume fraction 0.7 and stacking sequence [55/-55/55-55]s. They investigated the optimized composite drive shaft experimentally by measuring natural frequency and achieving torsion test. Their results showed that the torsional strength and natural frequency of the glass epoxy composite drive shaft are enough large for the replacement of steel drive shaft with obtaining weight reduction about 52%.

Fibre-reinforced composites have progressively replaced conventional metallic materials in applications where weight is an important consideration. In a further stage of these application in materials science, nanocomposites are also predicted to revolutionize the future of the composites industry in terms of their mechanical, thermal, electrical, optical and other properties^{76,77}. The main advantage of polymeric nanocomposites is that they incorporate at least one dimension of nanoscale reinforcement, providing a very high surface to volume ratio and excellent interfacial contact with the matrix [23]. The addition of CNTs in filament winding E-glass/Bisphenol-A epoxy cylinders was studied by Tasyürek and Tarakçioğlu et al to examine the behaviour of fatigue crack growth rate and surface crack. The findings demonstrated that the inclusion of CNTs improved fatigue life by enhancing inter-laminar adhesion ⁷⁸. In a different recent study⁷⁹, filament wound nanocomposite cylinders composed of epoxy resin and carbon nanotube (CNT) nanofillers showed improvements of up to 22% and 216%, respectively, in their interlaminar shear strength and fracture toughness characteristics. In the other recently published study, the material properties of an automotive drive shaft made of hybrid fiber-reinforced composite were found to be greatly enhanced by the addition of MWCNTs. Regards to CNTs' improved characteristics, natural frequency and critical buckling torque increased by up to 60% and 145%, respectively ⁸⁰. Furthermore, research suggested that optimizing CNT dispersion and distribution into polymer matrices may help future efforts to increase the stiffness, strength, and low weight of aerospace and automotive structures. Searle et al. conducted a study of the mechanical properties and environmental performance of carbon/epoxy, basalt/epoxy, and carbon nanotube (CNT) reinforced

carbon/epoxy composite driveshafts in order prove the viability of substituting existing steel driveshafts with composite alternatives⁸¹. The mechanical outperformance of driveshafts was investigated using a finite element method (FEA) tool and classical laminated plate theory (CLPT). The results showed that a composite drive shaft can outperform a steel shaft mechanically with careful design—up to 90% mass savings and a 50% greater Factor of Safety. Applications that involve racing automobiles, where weight reduction is essential, may utilize the C/E or C/CNT/E.

1.2. Research Significance

Lightweight composite structures, characterized by high stiffness, exceptional strength-to-weight ratios, and cost efficiency, are vital in engineering fields such as aerospace, marine, and automotive engineering. However, under dynamic loads, these structures are susceptible to buckling and resonance because of their slenderness. This can be achieved by enforcing eigenvalue buckling and frequency constraints on the component throughout its design phase. This ensures that its properties remain away from fundamental frequencies of resonance and critical buckling load values. To create successful designs that meet these requirements in engineering applications, composite materials have been increasingly utilized due to their lightweight and high strength advantages in recent decades. On the other hand, advances in nanocomposites, such as the addition of nanoscale reinforcements like carbon nanotubes and graphene nanoplatelets to the matrix materials, have led to improvements in the weight advantage of composite materials.⁸²⁻⁸⁴ On the contrary, the widespread use of synthetic fiber-reinforced composites, like carbon fiber and petroleum-based glass fiber, which surged by the late 20th century, has significantly increased greenhouse gas emissions from both production and waste. To address these environmental concerns and the rising oil prices, there has been a growing trend towards natural fiber-reinforced composites, aiming to reduce resource consumption.⁸⁵ The use of natural fiber also brings disadvantages such as weak matrix fiber interaction.⁸⁶ To overcome these disadvantages and promote more sustainable structures, recent applications have emerged in the use of hybrid synthetic-natural fibers or nano-reinforcement in matrix materials⁸⁷.

In order to comprehensively achieve these goals, the structural optimization of nanocomposites incorporating a hybrid fiber/nanofiller/matrix combination is more

mathematically complex than traditional two-phase fiber-reinforced composites, due to the including of macro, micro, and nanoscale elements. It is not feasible to take into account all of the effective parameters in the such complex optimization problems for nanocomposites in order to achieve accurate optimal results in an acceptable length of time. Therefore, meta-heuristic algorithms (Differential Evolution, Simulated Annealing, Particle Swarm Optimization, and Genetic Algorithms) in particular have been presented as stochastic optimization strategies for achieving global optimal results⁸⁸. These algorithms have much lower computing costs and time while providing accurate results. In the literature, numerous studies aim to maximize buckling load and fundamental frequency while minimizing cost and weight for two-phase composite engineering structures without nano reinforcements. These studies often employ stochastic optimization algorithms such as DE, SA, PSO and GA by using design variables such as fiber orientation angles, fiber volume fraction, number of layers, stacking sequences⁸⁹. For multiphase inter-ply hybrid fiber/nanofiller-reinforced nanocomposite structures, the multi-objective optimization approach involves maximizing natural frequency or critical buckling load while minimizing weight and cost. Finding the global optimum solution requires solving nonlinear objective functions that involve the summation of complex equations, such as fundamental frequency, critical buckling load, cost, and weight. This complexity increases due to the numerous continuous and discrete design variables, along with constraints that include nonlinear equations. These parameters include the weight content of nanofillers (CNTs or GNPs), fiber orientation angles, and fiber volume content for each layer. Elastic material constants of each ply are calculated parametrically using semi-empirical and micro-mechanical nonlinear material modeling equations at the nano, micro, and macro levels. The semi-empirical model is also crucial for predicting the agglomeration effects of nanofillers. By adjusting these variables, it is possible to achieve optimal, non-uniform material properties tailored to meet specific mechanical requirements such as maximum natural frequency, critical buckling load, and minimum failure index. Another challenge related to the development of parametric optimization equations is the writing of formulations related to the vibration, buckling and stress-strain behaviour of structures using Classical Laminate Plate Theory (CLPT) or First Order Shear Deformation Theory (FSDT) and nano-, micro- and macro-scale material model equations for hybrid nanocomposite structures. It is possible to propose lightweight structural designs composed of natural and synthetic fibres reinforced with nanofillers such as CNTs or GNPs after overcoming the challenges associated with the mechanical

design of hybrid or non-hybrid fibre reinforced nanocomposite structures. These designs make it possible to maximize the natural frequency and critical buckling loads, while minimizing the failure index, the weight and the cost of the design. This possible designs is particularly beneficial for applications such as automotive and aerospace, where stiffness and strength-to-weight and cost ratios are important, as well as being biodegradable and environmentally friendly.

1.3. Motivation, Objectives and Originality

After a detailed literature review, it is evident that the design limits for vibration, buckling and failure properties of traditional synthetic carbon and glass fibre reinforced composites have been extensively investigated by using stochastic optimization methods, particularly in sectors such as aerospace and automotive where weight reduction and cost are critical. Meanwhile, advances in nanocomposites have significantly improved the mechanical properties of traditional composites in terms of weight efficiency, particularly with the incorporation of large surface area nanofillers such as carbon nanotubes and graphene nanoplatelets.

There is a widespread utilization in industries due to the fact that traditional carbon or glass fiber reinforced composites are reliable with their mechanical properties. The other consideration, related to carbon nanotubes or graphene nanoplatelets that these are expensive and negative side like agglomeration properties to utilize in matrix materials of fiber reinforced composite structures. There is a growing interest in the use of natural fibre reinforced composites due to the increasing demand for environmentally friendly and sustainable materials. Stochastic optimization methods have shown that by designing the nanofiller material, the fibre volume fraction and the fibre orientation angles in each layer, natural fibre reinforced materials can achieve properties that are equivalent to those of synthetic fibre reinforced materials. By solving these complex optimization problems, it may be possible to develop natural fibre reinforced composite structures using CNTs and GPLs at or below the hybridization or agglomeration level with synthetic fibers. This may be the beginning of a new trend in the composites industry.

The use of nanofillers requires semi-empirical micromechanical models to accurately describe the properties of each layer, taking into account the agglomeration and waviness effects of the nano-reinforcement. Therefore, mathematically complex

issues such as non-linear objective functions, non-linear constraints and continuous-discrete design variables need to be solved in order to propose optimal hybrid fibre-reinforced nanocomposite structures in terms of natural frequency, buckling load and failure index against different loads. It is therefore possible to propose more environmentally friendly and biodegradable composite designs with minimum cost and weight compared to traditional fibre reinforced composite structures by overcoming these complex issues in mechanical analysis and formulating mathematical optimization problems.

The objectives of the PhD thesis can be listed as follows

1. To propose optimum design of hybrid and non-hybrid natural/synthetic fiber/CNTs or GPLs reinforced nanocomposite structures for vibration and buckling problems of engineering structures by using multiscale design variables; fiber orientation angles, fiber volume fraction, and the weight fraction of graphene nanoplatelets or carbon nanotubes
2. To incorporate Classical Lamination Plate Theory (CLPT) and First-order Shear Deformation Theory (FSDT) with the Navier solution and multiscale nanocomposite material models; the Modified Halpin-Tsai Model and the Rule of Mixtures.
3. To implement all models used in thesis within Wolfram Mathematica software for comprehensive problems of vibration, buckling and failure analysis of nanocomposite plates and driveshafts. To solve these models with optimization algorithms DE, SA and NM in this software.
4. To give comparison of Stochastic Optimization Search algorithms: Differential Evolution, Simulated Annealing and Nelder Mead results for minimum weight design of glass/CNTs reinforced composite plate vibration problems.
5. To examine the suitability of these methods for complicated multiscale nanocomposite design problem by analyzing the optimization performance, convergence rates, and correctness of each algorithm's solutions.
6. To compare the optimal design of inter-ply hybrid synthetic/natural fiber-reinforced composite plates, both with and without the inclusion of nanofillers such as carbon nanotubes (CNTs) and graphene nanoplatelets (GPLs).

7. To propose ecofriendly, cost-effective, lightweight natural fiber/nanofiller reinforced composite designs for vibration and buckling issues in engineering structures.
8. To explore the potential of natural fibers as a cost-effective and lightweight alternative to traditional carbon fibers, which have been extensively utilized in existing application.
9. To investigate the impact of volume fraction, stacking sequences, and non-uniform CNT fillers—taking into account the agglomeration and waviness effects of nanofillers—on multi-objective optimization problems for maximum critical buckling loads and fundamental frequencies with minimum weight and costs.
10. To propose a design methodology for a multiscale hybrid natural fiber/CNTs reinforced driveshaft using fundamental frequency, failure criteria, and critical buckling torque as design parameters.
11. To determine failure loads of optimized inter-ply hybrid fiber/CNTs reinforced nanocomposite driveshafts using Tsai-Wu (for analytical solution) and Puck (for finite element analysis) failure theories.
12. To analyze and compare the optimal solutions for multiscale nanocomposite plates and driveshaft problems using the Autodesk NASTRAN commercial FEA solver in conjunction with analytical solutions.

Originality of the thesis can be summarized as follows:

1. In the literature, related to optimization studies of multiscale hybrid fiber/CNTs or GPLs nanofiller reinforced composites for vibration and buckling problems haven't investigated yet. Although there are a few studies on analysis and single-objective optimization of carbon fiber/GPLs or glass fiber/CNTs reinforced composites for maximum fundamental frequency or minimum weight design, by using single and multi-objective optimization approaches on hybrid and non-hybrid Natural (Flax-Kenaf-Jute-Ramie) and synthetic (Carbon-Glass) fiber/CNTs or GPLs nanocomposites problems are not available in terms of weight and cost. Therefore, present study fills the gap in the available literature related to nanocomposite design and multi-objective optimization.

2. In the present thesis, a single-objective optimization approach has been considered to verify the optimization studies mathematically using DE, SA, and NM methods. Additionally, a multi-objective approach, incorporating a penalty function, is utilized for the first time to optimize combinations of natural frequency, critical buckling load, cost, and weight of multiscale hybrid nanocomposite laminates.
3. For the first time, the agglomeration and waviness effects of CNTs are included in vibration, buckling, and driveshaft problems using the Modified Halpin-Tsai Models.
4. The optimum design of multiscale hybrid Flax/Carbon fiber/CNTs reinforced nanocomposite driveshafts are firstly carried out in the literature for minimum weight design. The effects of varying weight fractions of CNTs and volume fractions of fibers for each ply are demonstrated by optimizing multiscale driveshaft problems.
5. Finite Element Analysis (FEA) of optimally designed hybrid natural/synthetic fiber-reinforced nanocomposite structures was conducted using Autodesk NASTRAN commercial software. The material properties were optimized through stochastic methods applied within modified Halpin-Tsai models. This study analysis and fills existing gaps in the literature regarding FEA and optimization tools.
6. By using stochastic optimization methods, the material properties of each ply with non-uniform nanofiller and fiber content are designed. This approach enables the proposal of alternative, more eco-friendly, and sustainable structures with natural fiber-reinforced nanocomposites, instead of traditional synthetic (carbon or glass) fibers, for addressing vibration, buckling, and driveshaft problems.

CHAPTER 2

COMPOSITE MATERIALS

Composite materials are typically defined as a composition of two or more constituent materials with notably different physical or chemical properties. The combination of these unique materials produces a material with characteristics that are distinct from those of its individual elements⁹⁰. The combination of attractive properties, including stiffness, resilience and durability, corrosion resistance and low weight, has contributed to the accelerated adoption of composite materials in engineering and material science applications in recent decades^{91,92}.

2.1. Classification of Composites

Composite materials can be categorised into four main types based on the shape of the reinforcement, the scale, the type of matrix and the bio-composite Figure⁹³.

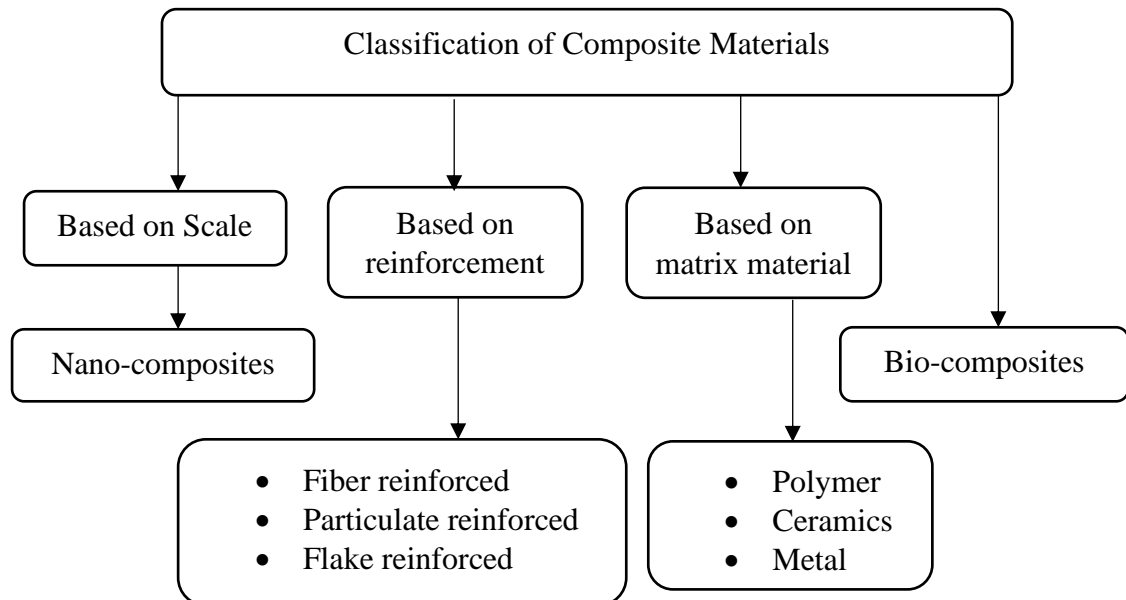


Figure 2.1. Classification of composite materials.(Source: Rajak 2019⁹³)

There are three main types of matrix materials for composites: Polymer Matrix Composites (PMCs), Ceramic Matrix Composites (CMCs), and Metal Matrix Composites (MMCs).

Polymer matrix materials (PMC) consist of a matrix of either thermoset or thermoplastic materials, reinforced with dispersed reinforcing fibres. These fibres can be made of carbon, glass, Kevlar or metals and give the composite improved mechanical properties⁹⁴⁻⁹⁶. Due to their greater strength and resistance to high temperatures, thermosets are more widely used in applications than thermoplastics and it can be easily prepared mixing resin with hardener⁹⁷. The diversities between thermosets and thermoplastics are denoted in Table 2.1⁹⁸.

Table 2.1. Differences between thermosets and thermoplastics (Source: Kaw 2005⁹⁸)

Thermoplastics	Thermosets
Soften on heating and pressure, and thus easy to repair	Decompose on heating
High strains to failure	Low strains to failure
Indefinite shelf life	Definite shelf life
Can be reprocessed	Cannot be reprocessed
Not tacky and easy to handle	Tacky
Short cure cycles	Long cure cycles
Higher fabrication temperature and viscosities have made it difficult to process	Lower fabrication temperature
Excellent solvent resistance	Fair solvent resistance

The most common composite structures used in aerospace, defence and automotive industries are made by stacking and bonding thin layers of fibre and polymer owing to PMC's cost-effective properties with enabling desired shape using easy handling techniques and simple fabrication methods⁹⁹.

Ceramic matrix composites (CMCs) are composed of ceramic matrix such as carbon, silicon carbide (SiC), aluminium oxide (Al₂O₃) and silicon nitride (SiN) where is embeded fibers in these matrix materials in order to overcome the brittleness of

monolithic ceramics¹⁰⁰. CMCs are primarily known for their unique property where the matrix fails before the fibers under load, which distinguishes them from polymer or metal matrix composites. This failure mode helps to protect the brittle fibres. CMCs are manufactured using gas or liquid phase methods, where the matrix is formed around the fibres from gaseous or liquid precursors¹⁰¹.

Metal Matrix Composites (MMCs) consist of a metal matrix, typically made of aluminum, magnesium, copper, or titanium, combined with ceramic or metal reinforcements. This combination provides superior properties, such as high strength, increased stiffness, controlled thermal expansion, and enhanced wear resistance, making MMCs extensively utilized in the automotive and aerospace industries¹⁰². However, their high stiffness and abrasive nature lead to significant tool wear during machining, necessitating the use of unconventional machining techniques¹⁰³.

Regarding reinforcement, composites can be divided into three main parts: particles, flakes and fibres. (Figure 2.2).

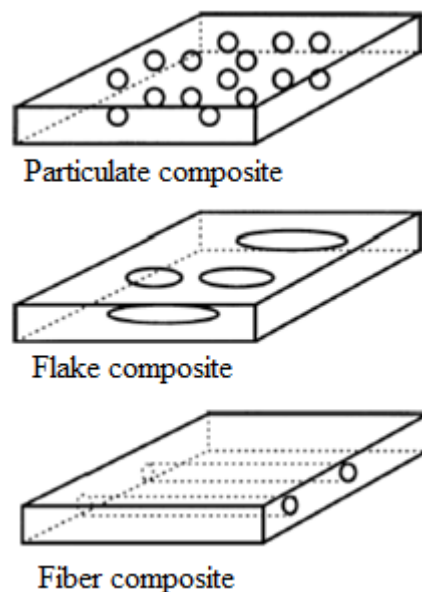


Figure 2.2. Composite types according to reinforcement shape (Source: Kaw 2005⁹⁸)

Particulate composites, which involve randomly dispersed alloy and ceramic particles within matrix materials, are considered to be isotropic. These composites offer several benefits such as increased strength, higher operating temperatures and improved oxidation resistance. Examples of particle reinforced composites include rubber with aluminium particles, silicon with carbide motes and concrete with gravel and sand⁹⁸.

Flake composites incorporate flat, thin reinforcements such as aluminum, glass, mica and silver into the matrix. Flake composites' main advantages are low cost, high strength and high flexural modulus. However, the difficulty of changing the orientation of the flakes is a notable challenge⁹⁸.

Fibre reinforced composites are generally composed of continuous long or discontinuous short fibres reinforced with matrices. These reinforced synthetic fibers like glass, carbon, basalt and kevlar improve material properties like high strength, rigidity and resistance to chemicals, temperature and wear¹⁰⁴⁻¹⁰⁷.

Table 2.2. Mechanical properties of some plant fibers compared to glass and carbon fibers
(Source: Osorio 2011¹⁰⁸)

Fiber	Density (gr/cm ³)	Diameter (µm)	Elongation at failure (%)	Tensile strength (MPa)	E-Modulus (GPa)
Bagasse	-	490	-	70	-
Coir	1.2	-	30	175	4-6
Cotton	1.5-1.6	20	7.0-8.0	287-597	5-13
Curaua	1.38	66	3.9	913	30
Flax	1.5	50-100	2.7-3.2	345-1035	50-70
Hemp	1.10	120	1.6	389-900	35
Henequen	-	180	3.7-5.9	430-570	10-16
Jute	1.3	260	1.5-1.8	393-773	26
Kenaf	1.31	106	1.8	427-519	23-27
Pineapple	1.32	-	2.4	608-700	25-29
Ramie	1.50	34	3.6-3.8	400-398	24-32
Sisal	1.5	50-80	2.0-2.5	337-413	8-10
Bamboo	0.88-1.1	100-200	-	391-713	18-55
E-glass	2.5	9-15	2.5	1200-1500	70
Carbon (PAN)	1.4	5-9	1.4-1.8	4000	230-240

The use of natural fiber reinforcement has recently gained growing popularity among researchers by improving impact toughness and fatigue strength properties with chemical treatment. Additionally, they are abundantly available at low cost, biodegradable and eco-friendly, and have a lower density compared to synthetic fibers¹⁰⁹. A general comparison of the mechanical properties and densities of the most widespread

natural fibers, as well as synthetic fibers like e-glass and carbon fiber, is provided in the Table 2.2 below. In terms of their specific properties, it is claimed that they can be compared to glass fibres, taking into consideration advantages that they are sustainable and environmentally friendly.

Bio-composites have been developed in response to the demand for biodegradable and environmentally friendly materials. They can be classified into two categories: fully green composites and partially green composites. Fully green composites utilise biopolymeric matrices, whereas partially green composites employ petrochemical resins. In both categories, natural fibres are utilised for reinforcement purposes. In general, all biopolymers are compostable; however, there are non-bio-based materials employed in the manufacture of biodegradable and compostable plastics¹¹⁰.

Nanocomposites are materials with at least one dimension at nanometre, typically 100nm or smaller. Nanocomposites are high performance materials¹¹¹. They offer unique properties and design possibilities not found in conventional composites. These superior properties can be achieved using relatively small amounts of reinforcing nanomaterials. The two primary reasons for these enhanced properties are: (a) the superior characteristics of nano-reinforcements compared to traditional reinforcing fibers, and (b) their exceptionally high surface area to volume ratio, which allows for greater interfacial interaction with the matrix.

2.2. Nanocomposites

Nanocomposites are made up of two or more different materials with different physical and chemical properties, which often exist in different phases that are separated by an interface. Recently, significant attention has been given to adding nano-sized fillers to composites, creating nanocomposites. The nanofillers can be considered to be of three types: (a) zero-dimensional (nanoparticles, such as metal oxide and ceramic oxide nanoparticles); (b) one-dimensional (nanotubes and nanowires, such as carbon nanotubes and titanium oxide nanotubes); and (c) two-dimensional (nanoplatelets, such as layered silicates, nanoclays and graphene) (d) three-dimensional (graphite). From a design perspective, nanocomposites can be classified into two main groups: (a) two-phase nanocomposites composed of a polymer matrix and nanofillers, and (b) three-phase composites comprising a polymer matrix, fibrous reinforcements, and nanofillers¹¹².The

modification of the composite in this way is generally responsible for a change to the nature of the interphase between the reinforcement and the matrix, which contributes to the generation of new properties. Then, these properties control the impressive characteristics observed in nanocomposites. The different types of carbon-based nanofillers are given as Figure 2.3¹¹³.

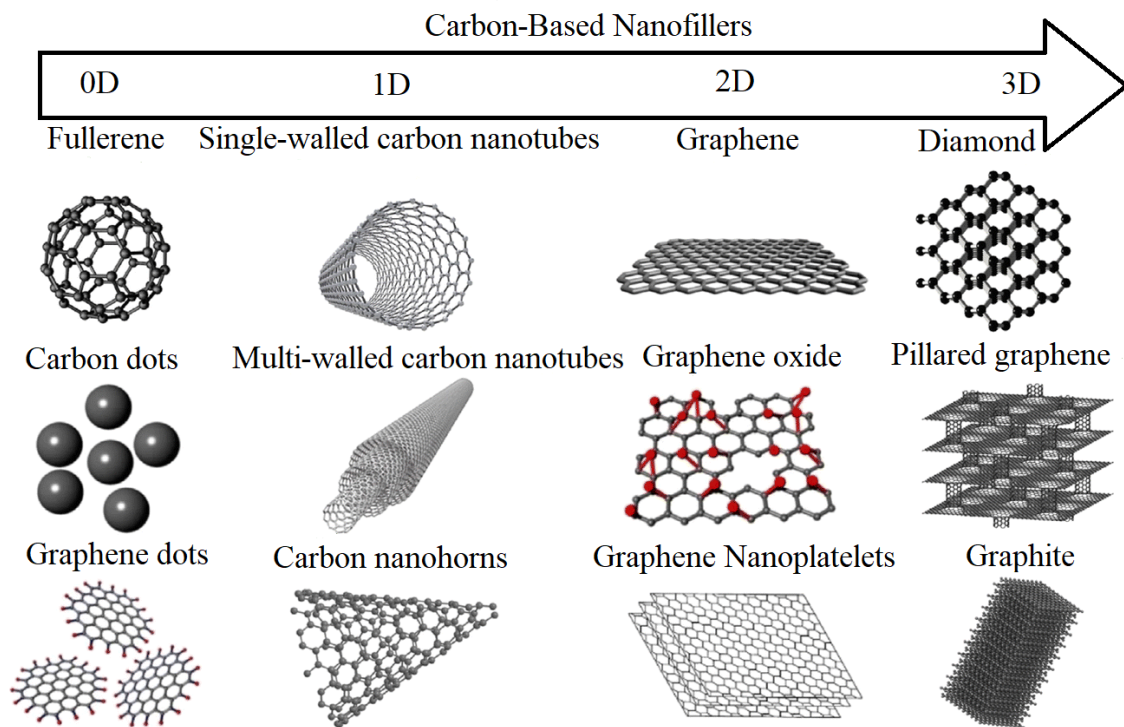


Figure 2.3. Different types of carbon-based nanofillers. (Source: Darwish 2024¹¹³)

Zero-dimensional nanofillers, generally referred to as nanoparticles (e.g., nanosilica, alumina nanoparticles), are typically incorporated into nanocomposite systems to enhance various desired properties. These improvements may include increased mechanical properties of the matrix, such as elastic modulus, tensile strength, and fatigue resistance. These materials, known for their superior properties, are manufactured by distributing nanoparticles in the matrix or coating nanofillers onto fibers. Nanoparticles enhance fiber-matrix bonding due to their large surface area, leading to effective stress transfer and improved rigidity. This results in fewer unoccupied spaces and better interaction between fiber and matrix, enhancing the mechanical characteristics of the material¹¹¹. Typically, nanoparticles are used to change the mechanical properties of composite materials. They can also be used, as well, to stimulate particular

nonstructural reactions. For instance, Kagawa reported noticeable effects of nanoparticles on epoxy resin reinforced with nanosilica, showing a connection between the nanoparticles and their optical characteristics¹¹⁴.

The most common one-dimensional nanofillers are nanotubes, composed of a sequence of atoms arranged in a long, thin cylindrical structure. They can be synthesized using materials such as carbon, TiO₂, silica, and silicon carbide¹¹². A carbon nanotube (CNT) can be defined as a series of carbon atoms arranged in a tubular shape, formed by at least one layer of graphite. The classification of carbon nanotubes (CNT) can be based on the number of layers comprising the tube: single-walled (SWCNT) and multi-walled (MWCNT). Both SWCNTs and MWCNTs have been widely employed to improve the characteristics of an array of composites and nanocomposites across a diverse range of applications⁸².

Recently, carbon nanotubes have been utilized to enhance the interfacial bonding of epoxy-based composites by being homogeneously dispersed within the matrix. These carbon nanofillers facilitate load transfer between the fibers and the epoxy by reinforcing previously weak interfacial regions. The utilisation of carbon-based nanofillers in epoxy composites is a prevailing strategy to satisfy the elevated mechanical property requirements inherent to aerospace, automotive, and marine applications¹¹⁵. Carbon nanotubes (CNTs) have recently emerged as a promising reinforcement option for composite materials, exhibiting important potential to enhance mechanical properties. Experimental studies have demonstrated the capacity of CNTs to effectively bear load in the context of nanocomposites. It is also noteworthy that the exceptional thermal conductivity of CNTs has been identified as a key property, leading to the development of a silicon wafer coated with a graphene layer, which results in a highly efficient heating film^{116,117}. To have a precise view of all effects of carbon nanotubes (CNTs) reinforced epoxy composites on the performance of epoxy composites is summarized Table 2.3.

Nanoplatelet based nanocomposites have very thin (several nm) layers deposited in the polymer matrix. The other 2D nanoplatelets consist of graphene (graphene nanoplatelets), used as nanofillers in traditional materials¹¹⁸. Graphene, an allotrope of carbon, consists of a single layer of carbon atoms arranged in a densely packed honeycomb crystal lattice. It has a variety of potential with beneficial implements. It has also been thoroughly researched and used in the creation of composites and nanocomposites¹¹².

Table 2.3. The overview of the CNTs reinforced matrix materials improvements

Nanofiller	Reinforcement Fraction (wt.%)	Name of the Property	Improvement Reported (%)	Reference
DWCNTs	0.5	Tensile strength	8	71 ¹¹⁹
		Tensile Modulus	15	
MWCNTs	1	Tensile strength	100	75 ¹²⁰
		Tensile Modulus	100	
	4	Tensile strength	150	
		Tensile Modulus	294	
SWCNTs	1	Tensile strength	25	76 ¹²¹
		Tensile Modulus	30	
		% Elongation	30	
	4	Tensile strength	23	
		Tensile Modulus	68	
DWCNTs	0.1	Tensile modulus	6	77 ¹²²
SWCNTs	1	Tensile strength	30	81 ⁸
		Tensile Modulus	14	
SWCNTs	0.5	Tensile Modulus	25	82 ¹²³
SWCNTs	1	Tensile strength	16	83 ¹²⁴
		% Elongation	25	
SWCNTs		Tensile strength	17	
		% Elongation	27	
SWCNTs	0.1	Tensile strength	11	84 ¹²⁵
MWCNTs		Tensile strength	14	
MWCNTs-L	1	%Elongation	57	85 ¹²⁶
		Impact strength	63	
MWCNTs-H	1	%Elongation	33	
		Impact strength	84	
MWCNTs	0.3	Flexural strength	29	86 ¹²⁷
		Modulus	8	
		% Elongation	89	
MWCNTs	0.5	Tensile strength	8	87 ¹²⁸
	1	Tensile Modulus	17	
MWCNTs	0.5	Tensile Modulus	12	88 ¹²⁹
MWCNTs	1	% Elongation	23	89 ¹³⁰
		Tensile Modulus	3	

The effects of graphene platelets (GPLs) on the mechanical properties of epoxy composites have been reported, revealing that a tensile strength improvement of approximately 40% is possible due to the large surface area and unique surface

characteristics of the graphene platelets⁸. The general comparison with regard to the effect of Graphene on the mechanical properties of reinforced composites is given in Table 2.4.

Table 2.4. The overview of the graphene reinforced matrix materials improvements

Nanofiller	Reinforcement Fraction (wt.%)	Name of the Property	Improvement Reported (%)	Reference
Graphene	0.5	Tensile strength	18	23 ¹³¹
Graphene oxide	0.25	Tensile strength	36	66 ¹³²
Graphene oxide	0.1	Tensile strength	25	67 ¹¹⁶
	0.1	% Elongation	38	
	0.25	Tensile strength	46	
	0.25	% Elongation	70	
	0.5	Tensile strength	62	
	0.5	% Elongation	59	
Graphene	0.1	Tensile strength	40	84 ¹²⁵
Graphene	0.1	Flexural strength	10	90 ¹³³
		Flexural modulus	7	
Graphene oxide	0.25	Tensile strength	32	91 ¹³⁴
		Flexural strength	85	
		Flexural modulus	65	
		Impact strength	103	
Graphene-MH	0.1	Tensile strength	31	92 ¹³⁵
Graphene-ME	0.1	Tensile strength	20	
Graphene-MA	0.1	Tensile strength	16	
Graphene-MH	0.3	Impact strength	89	
Graphene-ME	0.3	Impact strength	27	
Graphene-MA	0.3	Impact strength	22	
Graphene-MH	0.1	Flexural strength	15	
Graphene-ME	0.1	Flexural strength	16	
Graphene-MA	0.1	Flexural strength	30	
AE-Graphene	2	Flexural modulus	15	93 ¹³⁶
Graphene oxide	1	Tensile strength	16	94 ¹³⁷
	1	Flexural strength	38	
	1.5	Tensile strength	46	
	1.5	Flexural modulus	48	
f-Graphene	0.5	Tensile strength	38	95 ¹³⁸
	1	Tensile modulus	14	
Graphene oxide	0.5	Tensile strength	6	97 ¹³⁹

2.3. Natural Fibers and Natural Fiber Nanocomposites

Natural fibres have attracted interest from industry and scientists due to their specific properties compared to traditional synthetic fibres¹⁴⁰. High strength, high sustainability, biodegradability, low specific density and low cost are some of the unique characteristics of these fibres. Besides these advantages, natural fibers are suitable materials as reinforcements for polymer composites as they reduce tool wear. The general advantages of bio composites reinforced with natural fibres as compared to composites reinforced with synthetic fibres are shown in Table 2.5.

Table 2.5. The advantages and disadvantages of natural fiber composites over traditional petroleum-based composites. (Source: Gholampour 2020¹⁴¹)

Advantages	Disadvantages
Biodegradability	poor resistance to flame
Lightweight	Low moisture resistance
Cost-effective	Low impact resistance
Sustainability	Not suitable with a higher processing temperature
Eco-friendly	Variation in quality
Better thermal performance and insulation	Complex supply chain of natural fibers geographic locations and availability
Low energy consumption	/
Best alternatives for replacing synthetic fibers	/

Natural fibres are divided into three categories: animal fibres, vegetable fibres and mineral fibres. There are four main classes of plant based natural fibres: seed (Cotton, Coir and Kapok), leaf (Sisal, Agave, Pineapple and Abaca), bast (Kenaf, Ramie, Hemp, Jute and Flax) and stem (Wood, Straw and Bamboo) Figure 2.4.

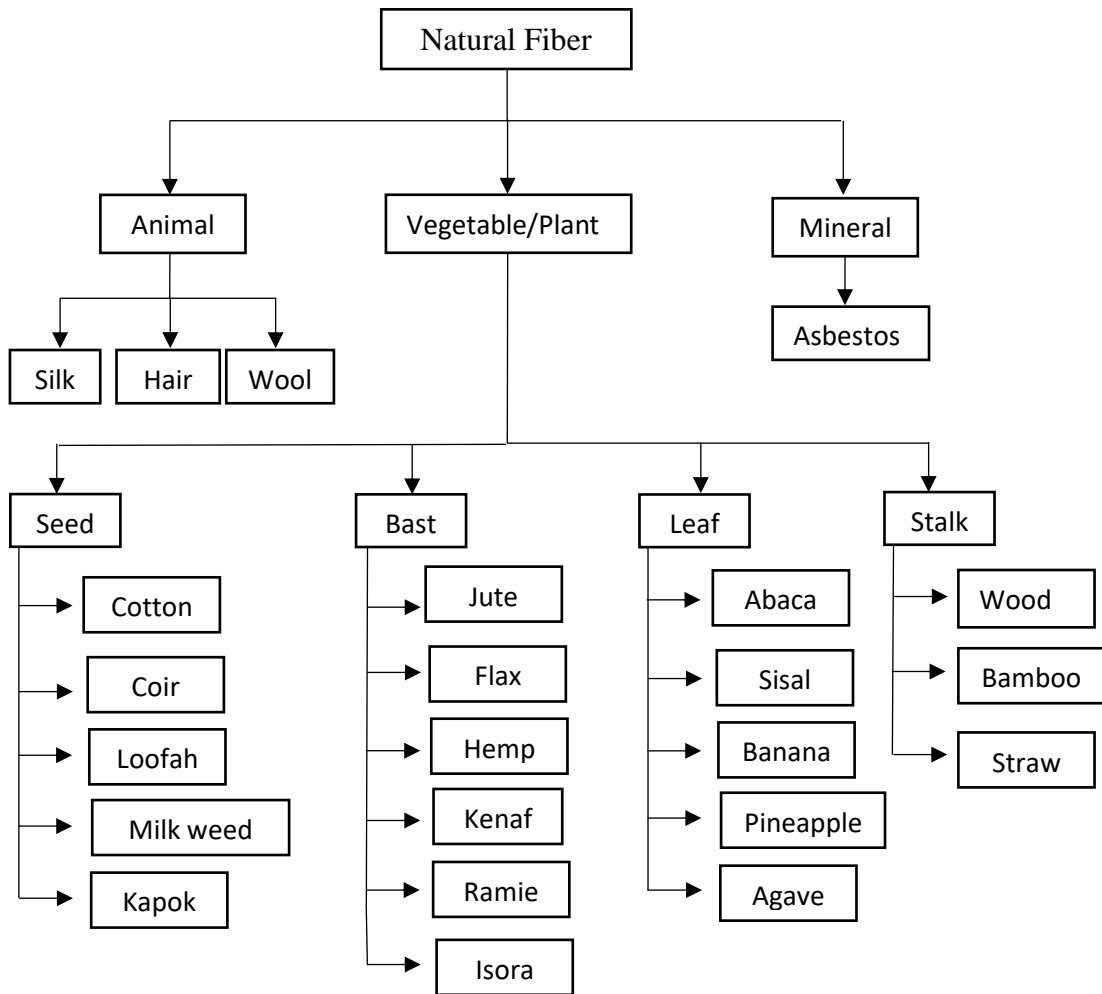


Figure 2.4. Classification of natural fibres according to origin, with examples.

(Source: Rahman 2019¹⁴²)

Flax fibre, which is one of the strongest candidates to replace synthetic fibres such as glass fibre, is obtained from the plant stem, which is stronger than that of cotton¹⁴³. They have better mechanical properties than synthetic fibres. For example, they have a lower specific density and higher strength¹⁴⁴. Thermoplastic, thermoset, and biodegradable flax fiber composites offer great mechanical characteristics¹⁴⁵. Flax fibres are also suitable for using to produce natural fibre reinforced nanocomposites with graphene nanofillers due to the low cost of producing and versatile processing routes. It was also reported that flax/epoxy/graphene reinforced nanocomposites showed a 61% increase in tensile strength compared to unfilled nanocomposites with increased flame resistance¹⁴⁶. Ramie is a green functional bast fibre that has fewer wrinkles, looks smooth and offers increased absorbency and breathability. Before any useful industrial processing

can occur, the ramie fibres' gummy components must be removed by degumming. It is one of the most biodegradable natural fibres with high strength, antibacterial and fire resistant properties¹⁴⁷. Ramie fibres are also suitable for use in nanocomposites with CNTs to improve mechanical properties such as flexural strength. This can be increased by up to 20.5% by adding 1.0 wt% CNTs to the matrix¹⁴⁸. Apart from flax and ramie, the most commonly used natural fibres are cotton, kenaf, hemp, jute, sisal and bamboo. The Figure 2.5 shows images of these natural fibres.



Figure 2.5. Images of the most widely used natural fibre. (Source: Hasan 2020¹⁴⁹)

The hybridization of the fibres in reinforced polymer composites is another method of mixing the positive properties of the two or more fibres by adjusting them layer by layer for each fibre. It can offer great advantages by combining the most appropriate properties of these different fibres to meet the requirements of the wide range of applications in engineering structures. It can also reduce the cost and weight of composites¹⁵⁰. In this context, hybridisation of natural and synthetic fibres is the most popular approach to reduce cost and weight and to increase biodegradability and sustainability. Hybrid ramie and carbon fibre composites are also investigated. The lay-up configuration is compared in terms of flexural strength and modulus. It is found that the use of carbon fibres in the outer layers results in higher flexural strength and modulus of elasticity than that in the inner layer¹⁵¹. The manufacturing method and lay-up

configurations of the Ramie/carbon hybrid composites in four different lay-up sequences are also shown in Figure 2.6.

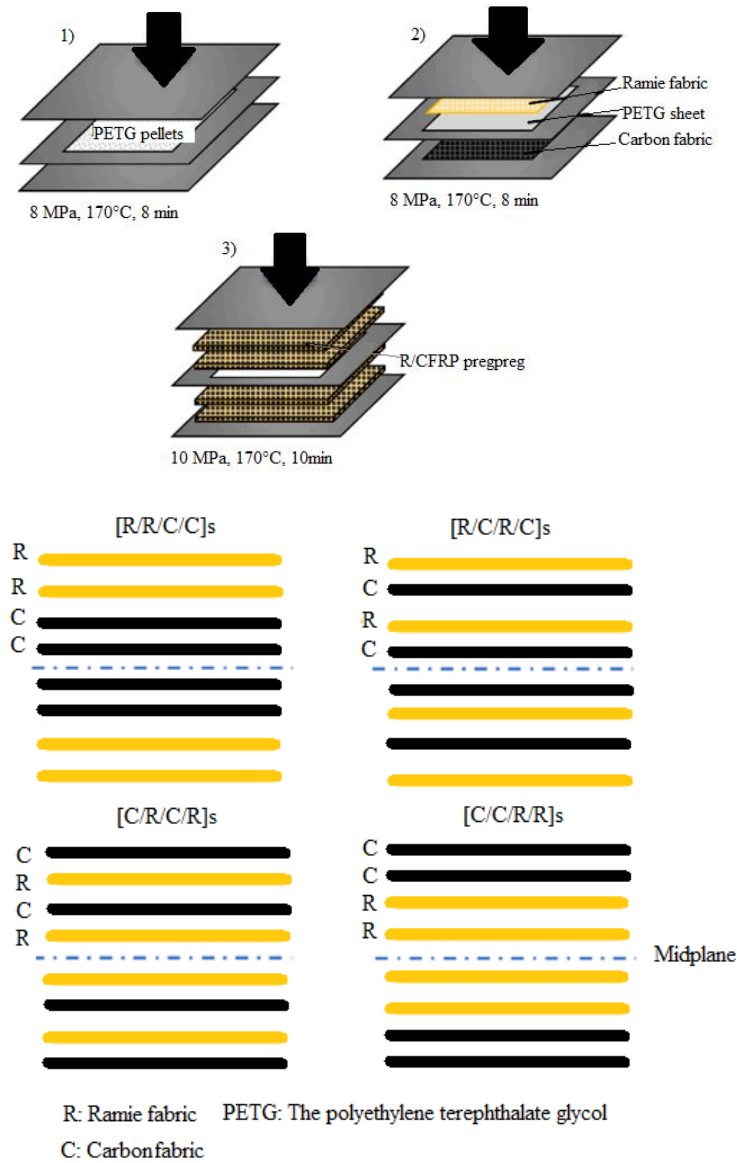


Figure 2.6. Manufacturing process of the ramie / carbon hybrid composites in four distinct layer sequences. (Source: Zhao¹⁵¹)

Hybrid natural/synthetic fiber-reinforced composites are increasingly attractive for applications in the automobile, aerospace, transportation, and military sectors. The flexural and impact strengths of hybrid carbon/flax, carbon/kenaf, glass/flax, and glass/kenaf composite structures have been studied for these purposes. Among these

combinations, the carbon/flax/epoxy composite demonstrates the highest flexural modulus¹⁵².

2.4. Application of the Hybrid Composites, Natural Fiber Composites and Nanocomposites

Nowadays, in aircraft, spacecraft, cars, helicopters, boats, sports equipment, medical and construction structures, composite materials have a wide range of industrial applications. The one of the most widespread applications are for composites are aircraft materials because of its advantages to create structures with aerodynamic efficiency together with the lower weight compared to conventional aircraft materials such as aluminium, steel etc. The major parts of the world's most famous aircraft, the 787 and A380, are made of composite materials. The details of the use of materials are shown in the Figure 2.7 for the 787 and A380 models¹⁵³.

The use of natural fibre composites is increasing due to their relatively low cost and environmentally friendly properties, despite their relatively poor mechanical properties compared to synthetic carbon fibres, which are widely used in industrial applications. In the automotive industry, for example, natural fibres such as flax, kenaf and ramie are already being used in parts such as side panels, door panels, seat backs, boot elements, bonnets, roof upholstery, centre consoles and interior parts that are of secondary importance in terms of load-bearing capacity¹⁵⁴⁻¹⁵⁷. The natural fibres are also employed in the aerospace and space industries for applications including secondary parts, trunk load floors, interior fitting elements and satellite structures¹⁵⁸⁻¹⁶². Additionally, several prominent automotive manufacturers, including Bcomp, Porsche Motorsport, Tesla, and McLaren, have successfully employed natural fibre-reinforced composites in critical vehicle components¹⁶³. In the Porsche 718 Cayman GT4 CS MR, the natural fibres present in the vehicle's main body parts have been replaced with carbon fibres. This substitution has been achieved through the utilisation of an autoclave process Figure 2.8 (a). The cost savings and carbon footprint reductions are provided at 30% and 75%, respectively. In the Tesla S P100D race car model, a weight saving of 500 kg on body panels has been achieved through the utilisation of natural fibres Figure 2.8 (b). In the McLaren F1 Racing car seats, natural flax fibre composites were replaced with carbon

fibres, which have the advantage of providing five times better vibration absorption and a reduction in cost by 30 per cent Figure 2.8c.

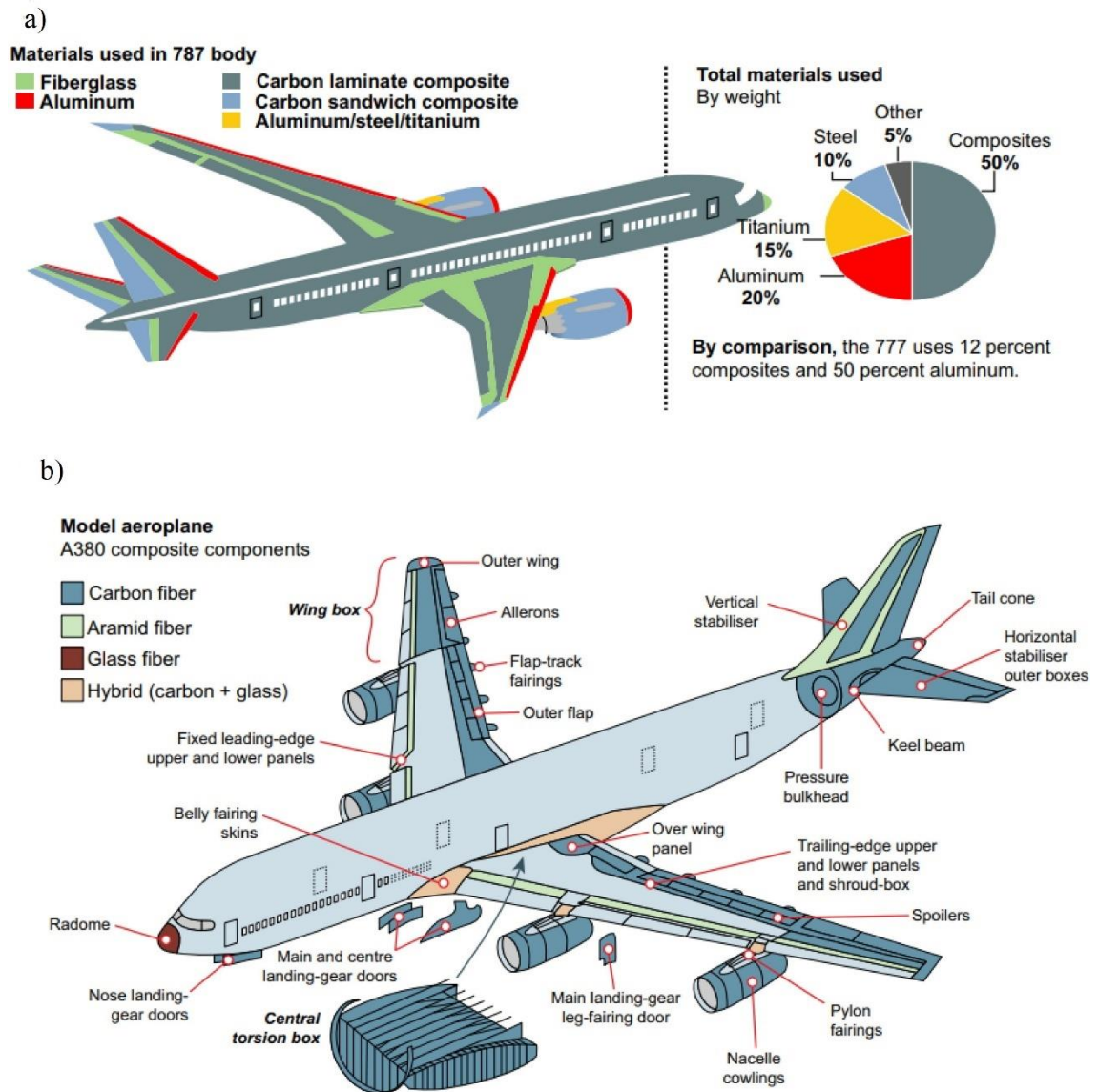


Figure 2.7. The material composition details of the commercial aircraft models the Boeing 787 and the Airbus A380 (Source: Etri 2024¹⁵³)

Nanocomposites with carbon nanotubes and graphene nanofillers are developed for extensive application fields such as aerospace, aviation, automotive application to improve the material's durability, fatigue resistance, strength and toughness properties^{164,165}. Synthetic and natural fibre/graphene nanocomposites are used for

military applications such as interior parts of military vehicles, air and space platforms, EMI shielding effects and personal protective equipment structural applications^{166,167}.

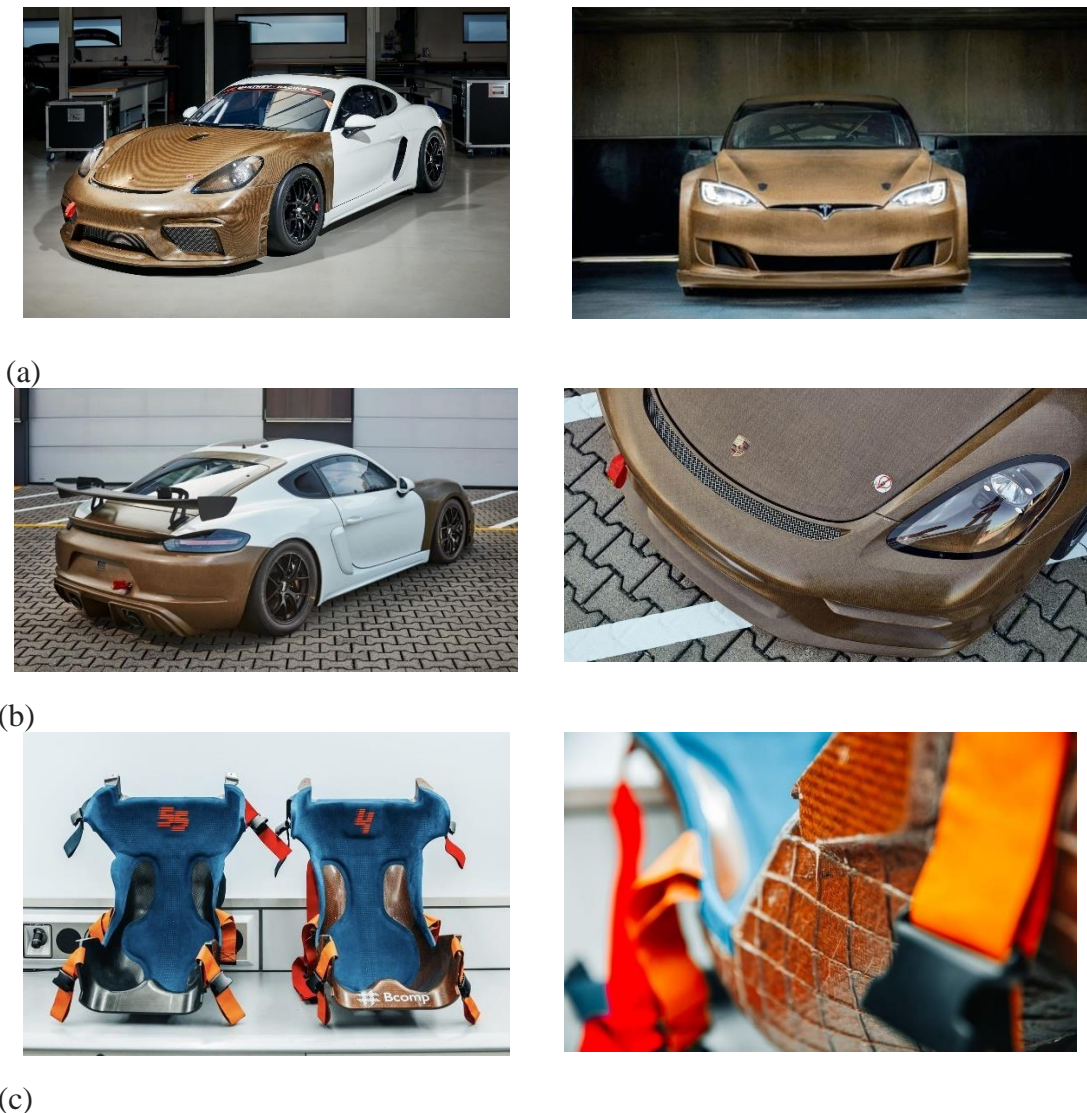


Figure 2.8. (a) Porsche Motorsport 718 Cayman GT4 CS MR with full natural fiber body kit, (b) Tesla race car S P100D showing a body made from natural fibers, (c) McLaren F1 seat reinforced with BCOMP (Source: Elseify 2021¹⁶³)

Carbon fibre/graphene reinforced nanocomposite panels are also used in NASA's Space Launch System forward skirt structure¹⁶⁸ which is shown in Figure 2.9 (c). In a further application related to graphene-based nanocomposites, the recent application of carbon fibre/graphene nanocomposites to the main structures, parts and fuel tanks of the Orbex Prime rocket, developed by the UK-based private company Orbes, represents a significant advancement in the field of rocket technology (see in Figure 2.9 (a)¹⁶⁹). The

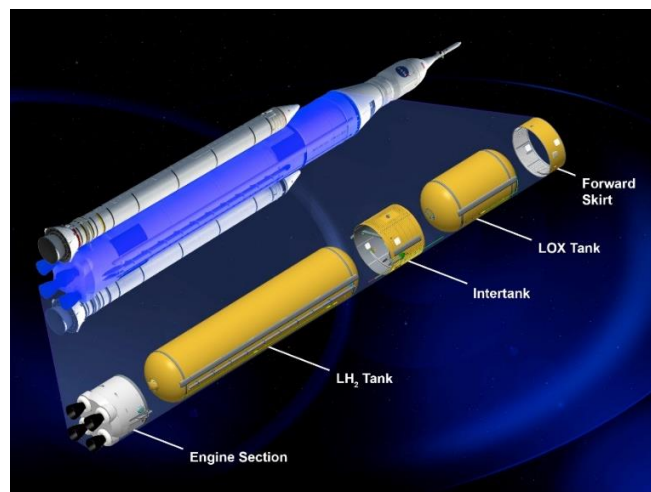
other current application of carbon nanotube (CNT) - reinforced nanocomposites is mentioned by Lockheed Martin in relation to the F-35 Lightning II model (Figure 2.9 (b)). It is proposed that CNT-reinforced thermoset epoxy composites will replace carbon fibre composite structures for the F-35 wingtip fairings material⁸⁰.



(a)



(b)



(c)

Figure 2.9. Nanocomposite applications (a) carbon fibre/graphene nanocomposites application on Orbex Prime rocket (Source: Scalia 2023¹⁶⁹) (b) Lockheed Martin F-35 Lightning II (Source: Defence 2024¹⁷⁰) (c) Nasa Space Launch System and forward skirt structure (Source: NASA 2020¹⁷¹)

In relation to the utilisation of nanomaterials in the context of aerospace structures, the National Aeronautics and Space Administration (NASA) has published a series of roadmaps outlining the potential applications of carbon-based nanofillers. It is stated that CNTs are an attractive material for the reduction of vehicle mass, the improvement of damage tolerance and thermal protection¹⁷². In the case of solving potential issues associated with the dispersion of the matrix material, the utilisation of CNT will be a highly promising avenue for improvement of the aerospace structures.

CHAPTER 3

MECHANICAL ANALYSIS

Composite laminates are composed of stacked layers of different composite materials and fiber orientations. Composite laminates are designed with planar dimensions that exceed their thickness. Composite laminates are often used in applications where membrane strength and flexural strength are required. For this reason, composite laminates are considered to be plate elements¹⁷³.

Analysis of composite plates can be classified as follows;

1. Equivalent single-layer theories (ESL) (2-D)
 - Classical laminated plate theory
 - Shear deformation laminated plate theories
2. Three-dimensional elasticity theory (3-D)
 - Traditional elasticity approach
 - Layer-wise theories
3. Multiple model methods (2-D and 3-D)

By making assumptions about the deformation kinematics or stress distribution through the laminate thickness, the Equivalent Single Layer (ESL) panel theories are derived from the 3-D elasticity theory. These assumptions are used to simplify the 3-D problem to a 2-D analysis. In this thesis, ESL theories, specifically the Classical Laminate Plate Theory (CLPT) and the First Order Shear Deformation Theory (FSDT), are used to solve the problems in laminated composite plates¹⁷³.

The simplest ESL laminated plate theory is the classical laminated plate theory (CLPT) which is an extension of the Kirchhoff (classical) plate theory to laminated composite plate. The displacement field implies that straight lines normal to the xy-plane before deformation remain straight and normal to the midsurface after deformation. The Kirchhoff assumption amounts to neglecting both transverse shear and transverse normal effects deformation is due entirely bending and in-plane stretching¹⁷³.

FSDT extends the kinematics of CLPT by incorporating transverse shear deformation into its assumptions, where the transverse shear strain is considered constant through the thickness. This inclusion relaxes the constraint of normality imposed by the classical laminate plate theory. On the other hand, FSDT requires shear correction factors

that are complex to determine for arbitrarily laminated composite panel structures. ESL models, in addition to being relatively simple and cost-effective, often deliver sufficiently accurate predictions of global responses in thin to moderately thick laminates, including total deflections, critical buckling loads, and fundamental frequencies with their corresponding mode shapes¹⁷³.

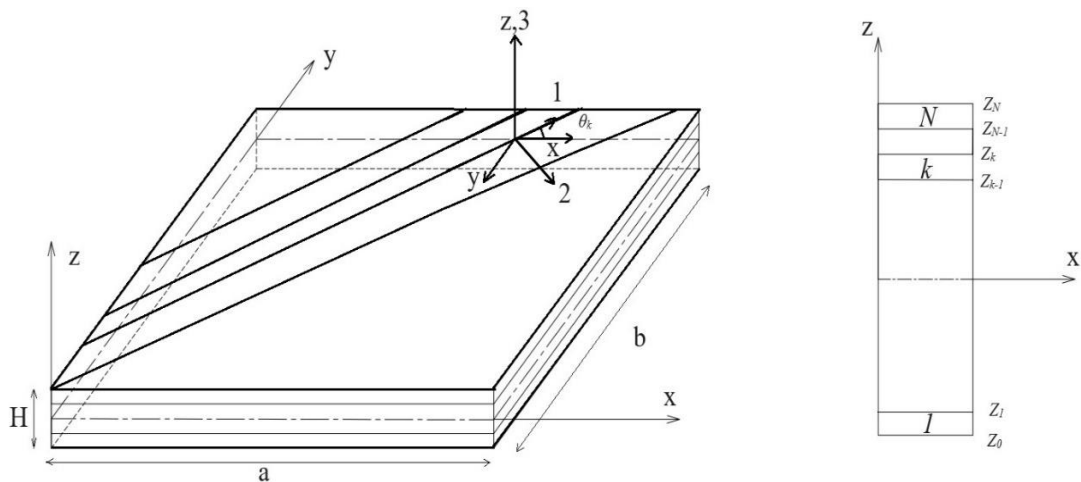


Figure 3.1. Geometry of the laminated plate (Source: Jeawon 2021³⁷)

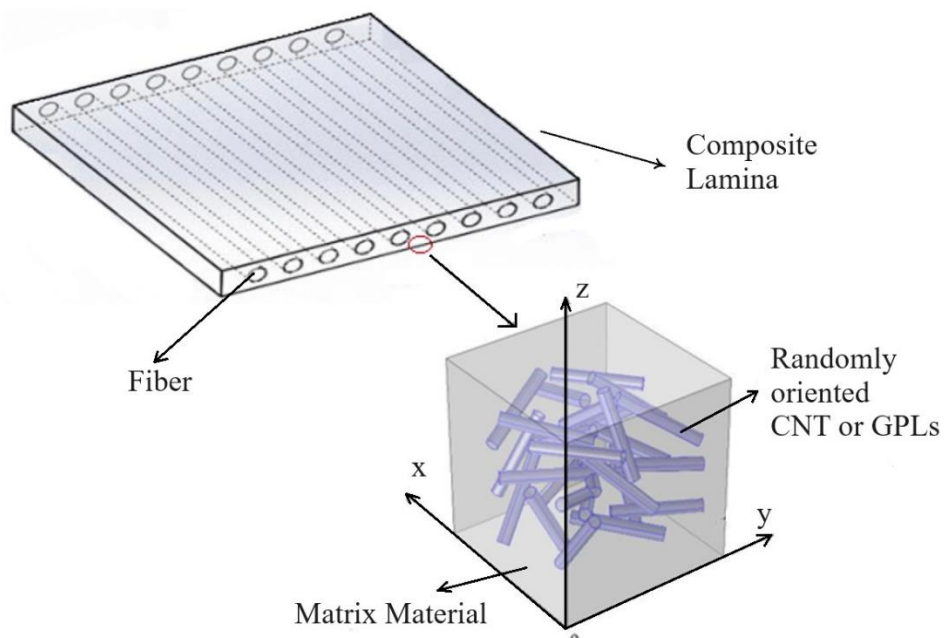


Figure 3.2. Illustration of a unidirectional fiber-reinforced composite lamina, with the inclusion of GPLs in the polymer matrix (Source: Georgantinos 2021⁸⁰)

In this study, the vibration, buckling and stress-strain analysis are considered for a laminated composite plate as shown in Figure 3.1 which is having length a , width b and a total thickness of H in the x , y and z -direction, respectively. The composite plate is composed of N lamina and each k^{th} lamina is oriented at an angle θ_k according to the laminate coordinate x . At the mid-plane of the plate, z - axis which is normal to the mid-plane coincides with the xy - plane. $z = z_k$ and $z = z_{k-1}$ shows the vertical coordinates of the top and bottom of the k^{th} layer.

Carbon nanotubes or graphene nanoplatelets and fibres as reinforcements with different or the same volume fractions in each lamina are incorporated in the polymer matrix of the laminated composite plate (see in Figure 3.2). Optimum design can also be achieved by varying the fibre orientation angles, layer thicknesses and weight fractions of nanofillers and fibres.

3.1. Laminate Constitutive Equations for CLPT and FSDT

The constitutive equations of CLPT and FSDT are given by combining here. Consider a rectangular plate composed of N layers and each layer possesses a plane of elastic symmetry to the x - y plane, constitutive equations of each k^{th} lamina can be written as¹⁷³;

$$\begin{Bmatrix} \sigma_x \\ \sigma_y \\ \sigma_{xy} \\ \sigma_{yz} \\ \sigma_{xz} \end{Bmatrix} = \begin{bmatrix} Q_{11}^k & Q_{12}^k & 0 & 0 & 0 \\ Q_{12}^k & Q_{22}^k & 0 & 0 & 0 \\ 0 & 0 & Q_{66}^k & 0 & 0 \\ 0 & 0 & 0 & Q_{44}^k & 0 \\ 0 & 0 & 0 & 0 & Q_{55}^k \end{bmatrix} \begin{Bmatrix} \varepsilon_x \\ \varepsilon_y \\ \gamma_{xy} \\ \gamma_{yz} \\ \gamma_{xz} \end{Bmatrix} \quad (3.1)$$

where Q_{ij}^k are the material constants in the material axes of the layer given as

$$Q_{11}^{(k)} = \frac{E_1^{(k)}}{(1 - \nu_{12}^{(k)} \nu_{21}^{(k)})} \quad (3.2)$$

$$Q_{12}^{(k)} = Q_{12}^{(k)} = \frac{\nu_{21}^{(k)} E_2^{(k)}}{(1 - \nu_{12}^{(k)} \nu_{21}^{(k)})} \quad (3.3)$$

$$Q_{22}^{(k)} = \frac{E_2^{(k)}}{(1 - \nu_{12}^{(k)} \nu_{21}^{(k)})} \quad (3.4)$$

$$Q_{66}^{(k)} = G_{12}^{(k)} \quad (3.5)$$

$$Q_{44}^{(k)} = G_{23}^{(k)} \quad (3.6)$$

$$Q_{55}^{(k)} = G_{13}^{(k)} \quad (3.7)$$

where $E_1^{(k)}$, $E_2^{(k)}$ are the longitudinal and transverse moduli, $\nu_{12}^{(k)}$, $\nu_{21}^{(k)}$ are the Poisson's ratios, $G_{12}^{(k)}$, $G_{23}^{(k)}$ and $G_{13}^{(k)}$ are the shear moduli of the k^{th} layer and ks is a shear correction factor taken as 5/6 (for FSDT). The reduced stiffness $Q_{ij}^{(k)}$ of the k^{th} lamina can be transformed to $\bar{Q}_{ij}^{(k)}$ as

$$\begin{Bmatrix} \sigma_x \\ \sigma_y \\ \sigma_{xy} \\ \sigma_{yz} \\ \sigma_{xz} \end{Bmatrix}^{(k)} = \begin{bmatrix} \bar{Q}_{11}^k & \bar{Q}_{12}^k & \bar{Q}_{16}^k & 0 & 0 \\ \bar{Q}_{12}^k & \bar{Q}_{22}^k & \bar{Q}_{26}^k & 0 & 0 \\ \bar{Q}_{16}^k & \bar{Q}_{26}^k & \bar{Q}_{66}^k & 0 & 0 \\ 0 & 0 & 0 & \bar{Q}_{44}^k & \bar{Q}_{45}^k \\ 0 & 0 & 0 & \bar{Q}_{45}^k & \bar{Q}_{55}^k \end{bmatrix} \begin{Bmatrix} \varepsilon_x \\ \varepsilon_y \\ \gamma_{xy} \\ \gamma_{yz} \\ \gamma_{xz} \end{Bmatrix} \quad (3.8)$$

Where $Q_{ij}^{(k)}$ are the transformed material constants given as

$$\bar{Q}_{11}^{(k)} = Q_{11}^{(k)} \cos^4 \theta + 2 (Q_{12}^{(k)} + 2Q_{66}^{(k)}) \sin^2 \theta \cos^2 \theta + Q_{22}^{(k)} \sin^4 \theta \quad (3.9)$$

$$\bar{Q}_{12}^{(k)} = 2 (Q_{11}^{(k)} + Q_{22}^{(k)} - 4Q_{66}^{(k)}) \sin^2 \theta \cos^2 \theta + Q_{12}^{(k)} (\sin^4 \theta + \cos^4 \theta) \quad (3.10)$$

$$\bar{Q}_{22}^{(k)} = Q_{11}^{(k)} \sin^4 \theta + 2 (Q_{12}^{(k)} + 2Q_{66}^{(k)}) \sin^2 \theta \cos^2 \theta + Q_{22}^{(k)} \cos^4 \theta \quad (3.11)$$

$$\begin{aligned} \bar{Q}_{16}^{(k)} &= (Q_{11}^{(k)} - Q_{12}^{(k)} - 2Q_{66}^{(k)}) \sin \theta \cos^3 \theta \\ &+ (Q_{12}^{(k)} - Q_{22}^{(k)} + 2Q_{66}^{(k)}) \sin^3 \theta \cos \theta \end{aligned} \quad (3.12)$$

$$\begin{aligned} \bar{Q}_{26}^{(k)} &= (Q_{11}^{(k)} - Q_{12}^{(k)} - 2Q_{66}^{(k)}) \sin^3 \theta \cos \theta \\ &+ (Q_{12}^{(k)} - Q_{22}^{(k)} + 2Q_{66}^{(k)}) \sin \theta \cos^3 \theta \end{aligned} \quad (3.13)$$

$$\begin{aligned} \bar{Q}_{66}^{(k)} &= (Q_{11}^{(k)} + Q_{22}^{(k)} - 2Q_{12}^{(k)} - 2Q_{66}^{(k)}) \sin^2 \theta \cos^2 \theta \\ &+ Q_{66}^{(k)} (\sin^4 \theta + \cos^4 \theta) \end{aligned} \quad (3.14)$$

$$\bar{Q}_{44}^{(k)} = Q_{44}^{(k)} \cos^2 \theta + Q_{55}^{(k)} \sin^2 \theta \quad (3.15)$$

$$\bar{Q}_{45}^{(k)} = (Q_{55}^{(k)} - Q_{44}^{(k)}) \cos\theta \sin\theta \quad (3.16)$$

$$\bar{Q}_{55}^{(k)} = Q_{55}^{(k)} \cos^2\theta + Q_{44}^{(k)} \sin^2\theta \quad (3.17)$$

In the Classical Laminated Plate Theory (CLPT), the terms $\bar{Q}_{45}^{(k)}$, $\bar{Q}_{44}^{(k)}$, $\bar{Q}_{55}^{(k)}$, σ_{yz} and σ_{xz} , are neglected because the shear strain terms γ_{yz} and γ_{xz} are not considered. However, in the First Order Shear Deformation Theory (FSDT), these terms are included in the stiffness matrices.

3.2. Classical Laminated Plate Theory

3.2.1. Vibration of the Simply Supported Composite Plate

For CLPT, the displacement field can be defined in the following form¹⁷³:

$$u(x, y, z, t) = u_0(x, y, t) - z \frac{\partial w_0}{\partial x} \quad (3.18)$$

$$v(x, y, z, t) = v_0(x, y, t) - z \frac{\partial w_0}{\partial y} \quad (3.19)$$

$$w(x, y, z, t) = w_0(x, y, t) \quad (3.20)$$

The displacement components u_0 , v_0 and w_0 represent the midplane (where $z=0$) displacements for the plate. The governing equation for the free vibration of a symmetric laminate can be expressed as follows¹⁷³:

$$D_{11} \frac{\partial^4 w_0}{\partial x^4} + 2(D_{12} + 2D_{66}) \frac{\partial^4 w_0}{\partial x^2 \partial y^2} + D_{22} \frac{\partial^4 w_0}{\partial y^4} + I_0 \ddot{w}_0 - I_2 \left(\frac{\partial^2 \ddot{w}_0}{\partial x^2} + \frac{\partial^2 \ddot{w}_0}{\partial y^2} \right) = 0 \quad (3.21)$$

where

$$\ddot{w}_0 = \frac{\partial^2 w_0}{\partial t^2} \quad (3.22)$$

h is the total thickness of the laminate, t is time and ρ_0 is the mass density. I_0 and I_2 are the moments of inertia written as

$$I_0 = \sum_{k=1}^N \rho_0^{(k)} (z_{k+1} - z_k) \quad (3.23)$$

$$I_2 = \frac{1}{3} \sum_{k=1}^N \rho_0^{(k)} (z_{k+1}^3 - z_k^3) \quad (3.24)$$

A solution is assumed for the system,

$$W_{mn}(t) = W_{mn}^0 e^{i\omega t} \quad (3.25)$$

ω represents the natural frequency. The boundary conditions for the simply supported plate are given as

$$\begin{aligned} w &= 0 \text{ at } x = 0, w = 0 \text{ at } y = 0 \\ M_x &= 0 \text{ at } x = 0, M_y = 0 \text{ at } y = 0 \end{aligned} \quad (3.26)$$

Substituting Equation (3.25) into the Equation (3.21), it is found as

$$\begin{aligned} \{D_{11}\alpha^4 + 2(D_{12} + 2D_{66})\alpha^2\beta^2 + D_{22}\beta^4 - \omega^2[I_0 + (\alpha^2 + \beta^2)I_2]\} \\ \times W_{mn} \sin(\alpha x) \sin(\beta y) = 0 \end{aligned} \quad (3.27)$$

Since the Equation 3.27 must hold for every value of x and y (where $0 < x < a$ and $0 < y < b$), it follows that the expression within the brackets must be equal to zero for each corresponding value of m and n .

$$\omega_{mn}^2 = \frac{\pi^4}{\bar{I}_0 b^4} \left[D_{11} m^4 \left(\frac{b}{a}\right)^4 + 2(D_{12} + 2D_{66}) m^2 n^2 \left(\frac{b}{a}\right)^2 + D_{22} n^4 \right] \quad (3.28)$$

$$\tilde{I} = I_0 + I_2 \left[\left(\frac{m\pi}{a}\right)^2 + \left(\frac{n\pi}{b}\right)^2 \right] \quad (3.29)$$

When the rotary inertia I_2 is not considered, the resonant frequency of a rectangular, specially orthotropic laminate can be written by the following expression¹⁷³:

$$\omega_{mn}^2 = \frac{\pi^4}{I_0 b^4} \left[D_{11} m^4 \left(\frac{b}{a} \right)^4 + 2(D_{12} + 2D_{66}) m^2 n^2 \left(\frac{b}{a} \right)^2 + D_{22} n^4 \right] \quad (3.30)$$

the fundamental frequency is obtained when $m = 1$ and $n = 1$:

$$\omega_{11}^2 = \frac{\pi^4}{I_0 b^4} \left[D_{11} \left(\frac{b}{a} \right)^4 + 2(D_{12} + 2D_{66}) \left(\frac{b}{a} \right)^2 + D_{22} \right] \quad (3.31)$$

3.2.2. Buckling of Simply Supported Composite Plates Under Compressive Loads

As previously illustrated, the laminated composite plate is being supported along all four edges and is now exhibiting orthotropic characteristics. The geometric dimensions and fibre configuration of the plate are defined by four parameters: length (a), width (b), total thickness (h) and fibre orientation angle (θ) in the x , y , z and 1 directions, respectively (Fig. 1). The composite plate is subjected to biaxial in-plane loads per unit length, designated as N_x and N_y . For the purpose of this analysis, it is assumed that the composite laminated plate is homogeneous in composition and that the layers have an identical thickness.

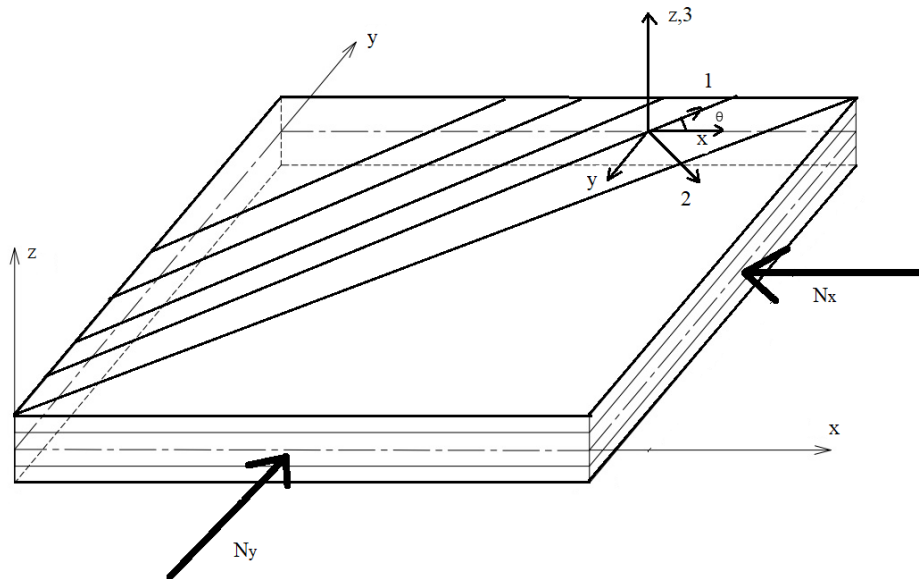


Figure 3.3. Thin laminated composite plate subjected to biaxial in-plane loading

The governing equation for the buckling problem of the symmetric laminate can be defined as follows¹⁷³:

$$\begin{aligned} D_{11} \frac{\partial^4 w}{\partial x^4} + 2(D_{12} + 2D_{66}) \frac{\partial^4 w}{\partial x^2 \partial y^2} + D_{22} \frac{\partial^4 w}{\partial y^4} \\ = \lambda \left(N_x \frac{\partial^2 w}{\partial x^2} + N_y \frac{\partial^2 w}{\partial y^2} + N_{xy} \frac{\partial^2 w}{\partial x \partial y} \right) \end{aligned} \quad (3.32)$$

The deflection in the z-direction (denoted by w) is determined by the bending stiffness D_{ij} , as previously defined:

$$w(x, y) = \sum_{m=1}^{\infty} \sum_{n=1}^{\infty} A_{mn} \sin \frac{m\pi x}{a} \sin \frac{n\pi y}{b} \quad (3.33)$$

The boundary conditions for the simply supported plate are given as

$$\begin{aligned} w = 0 \text{ at } x = 0, w = 0 \text{ at } y = 0 \\ M_x = 0 \text{ at } x = 0, M_y = 0 \text{ at } y = 0 \end{aligned} \quad (3.34)$$

In a specially orthotropic laminate, the fiber configurations consist solely of 0° and 90° orientations. In this scenario, the stiffness matrix elements $A_{16} = A_{26} = B_{16} = B_{26} = D_{16} = D_{26} = 0$. It is provided for a detailed explanation of the application of the specially orthotropic case in composite laminates, particularly for buckling problems⁴⁷. However, in cases where the laminated composite is not specially orthotropic, the bending–twisting terms D_{16} and D_{26} will only be neglected only if non-dimensional parameters satisfy specific conditions:

$$\gamma \leq 0.2, \delta \leq 0.2 \quad (3.35)$$

where

$$\gamma = D_{16} (D_{11}^3 D_{22})^{-1/4}, \delta = D_{26} (D_{11} D_{22}^3)^{-1/4} \quad (3.36)$$

The buckling load factor equation can be obtained as follows by substituting Equation 3.33 into Equation 3.32 under the boundary conditions given in Equation 3.34 as¹⁷³

$$\lambda_b = \frac{\pi^2 \left[D_{11} \left(\frac{m}{a} \right)^4 + 2(D_{12} + 2D_{66}) \left(\frac{m}{a} \right)^2 \left(\frac{n}{a} \right)^2 + D_{22} \left(\frac{n}{a} \right)^4 \right]}{N_x \left(\frac{m}{a} \right)^2 + N_y \left(\frac{n}{a} \right)^2 + N_{xy} \left(\frac{m}{a} \right) \left(\frac{n}{b} \right)} \quad (3.37)$$

Here the applied loads are represented by N_x and N_y , the buckling load factor is represented by λ_b and the integer values m and n correspond to various mode shapes. Then, the buckling loads are defined as $N_{xb} = N_x \lambda_b$ and $N_{yb} = N_y \lambda_b$. Using a suitable combination of m and n , the lowest buckling load factor (λ_{cb}) can be computed as the critical load factor. For the problems solved in this thesis, m and n are considered to be 1 or 2, and the smallest value among $\lambda_b(1,1), \lambda_b(1,2), \lambda_b(2,1), \lambda_b(2,2)$ produces λ_b . Furthermore, when unit loads are applied, the critical load equals to λ_{cb} .

3.2.3. Stress-Strain Analysis

The strain components at any point within the laminate that are in equilibrium with the reference plane can be expressed as⁹⁸

$$\begin{bmatrix} \varepsilon_x \\ \varepsilon_y \\ \gamma_{xy} \end{bmatrix} = \begin{bmatrix} \varepsilon_x^0 \\ \varepsilon_y^0 \\ \gamma_{xy}^0 \end{bmatrix} + z \begin{bmatrix} \kappa_x \\ \kappa_y \\ \kappa_{xy} \end{bmatrix} \quad (3.38)$$

The stress-strain relationship for the k^{th} layer of a laminated composite plate, based on the considering the Classical Laminated Plate Theory can be written in the following form:

$$\begin{bmatrix} \sigma_x \\ \sigma_y \\ \sigma_{xy} \end{bmatrix}_k = \begin{bmatrix} \bar{Q}_{11} & \bar{Q}_{12} & \bar{Q}_{16} \\ \bar{Q}_{12} & \bar{Q}_{22} & \bar{Q}_{26} \\ \bar{Q}_{16} & \bar{Q}_{26} & \bar{Q}_{66} \end{bmatrix}_k \left(\begin{bmatrix} \varepsilon_x^0 \\ \varepsilon_y^0 \\ \gamma_{xy}^0 \end{bmatrix} + z \begin{bmatrix} \kappa_x \\ \kappa_y \\ \kappa_{xy} \end{bmatrix} \right) \quad (3.39)$$

Here, $[\bar{Q}_{ij}]_k$, $[\varepsilon^0]$ and $[\kappa]$ represents the in plane elements of the transformed reduced stiffness matrix under plane stress condition, the strains of midplane and curvatures, respectively. The elements of transformed reduced stiffness matrix $[\bar{Q}_{ij}]$ can be calculated using the procedure previously described in this section.

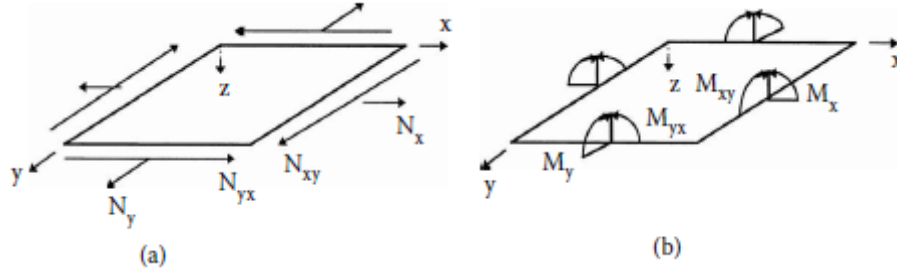


Figure 3.4. Resultant forces and moments on a laminate.(Source: Kaw 2005⁹⁸)

The moment resultants M_x , M_y and M_{xy} and the applied normal-shear force resultants N_x , N_y and N_{xy} (per unit width) have the following relations on laminate (Figure 3.4).

$$\begin{bmatrix} N_x \\ N_y \\ N_{xy} \end{bmatrix} = \begin{bmatrix} A_{11} & A_{12} & A_{16} \\ A_{12} & A_{22} & A_{26} \\ A_{16} & A_{26} & A_{66} \end{bmatrix} \begin{bmatrix} \varepsilon_x^0 \\ \varepsilon_y^0 \\ \gamma_{xy}^0 \end{bmatrix} + \begin{bmatrix} B_{11} & B_{12} & B_{16} \\ B_{12} & B_{22} & B_{26} \\ B_{16} & B_{26} & B_{66} \end{bmatrix} \begin{bmatrix} \kappa_x \\ \kappa_y \\ \kappa_{xy} \end{bmatrix}$$

$$\begin{bmatrix} N_x \\ N_y \\ N_{xy} \end{bmatrix} = \begin{bmatrix} B_{11} & B_{12} & B_{16} \\ B_{12} & B_{22} & B_{26} \\ B_{16} & B_{26} & B_{66} \end{bmatrix} \begin{bmatrix} \varepsilon_x^0 \\ \varepsilon_y^0 \\ \gamma_{xy}^0 \end{bmatrix} + \begin{bmatrix} D_{11} & D_{12} & D_{16} \\ D_{12} & D_{22} & D_{26} \\ D_{16} & D_{26} & D_{66} \end{bmatrix} \begin{bmatrix} \kappa_x \\ \kappa_y \\ \kappa_{xy} \end{bmatrix} \quad (3.40)$$

It is possible to define the matrices [A], [B], and [D] given in Equations 3.41 and 3.42 as

$$A_{ij} = \sum_{k=1}^n [(\bar{Q}_{ij})]_k (h_k - h_{k-1}), i = j = 1,2,6 \quad (3.41)$$

$$B_{ij} = \frac{1}{2} \sum_{k=1}^n [(\bar{Q}_{ij})]_k (h_k^2 - h_{k-1}^2), i = j = 1,2,6 \quad (3.42)$$

$$D_{ij} = \frac{1}{3} \sum_{k=1}^n [(\bar{Q}_{ij})]_k (h_k^3 - h_{k-1}^3), i, j = 1, 2, 6 \quad (3.43)$$

The [A]matrix represents the extensional stiffness, relating in-plane forces to in-plane strains. The [B]matrix denotes the coupling stiffness, linking forces to mid-plane strains and moments to mid-plane curvatures. Finally, the [D] matrix represents the bending stiffness, relating moments to curvatures⁹⁸.

The expressions for stress and strain, based on the Classical Laminated Plate Theory, can be formulated in the local coordinate system (1, 2). The relationship between local and global stresses in an angled lamina can be expressed as follows⁹⁸:

$$\begin{bmatrix} \sigma_1 \\ \sigma_2 \\ \sigma_{12} \end{bmatrix} = [T] \begin{bmatrix} \sigma_x \\ \sigma_y \\ \sigma_{xy} \end{bmatrix} \quad (3.44)$$

Similarly, the local and global strains are related by the following equation:

$$\begin{bmatrix} \varepsilon_1 \\ \varepsilon_2 \\ \varepsilon_{12} \end{bmatrix} = [R][T][R]^{-1} \begin{bmatrix} \varepsilon_x \\ \varepsilon_y \\ \varepsilon_{xy} \end{bmatrix} \quad (3.45)$$

where

$$[R] = \begin{bmatrix} 1 & 0 & 0 \\ 0 & 1 & 0 \\ 0 & 0 & 2 \end{bmatrix} \quad (3.46)$$

and [T] transform matrix,

$$[T] = \begin{bmatrix} c^2 & s^2 & 2sc \\ s^2 & c^2 & -2sc \\ -sc & sc & c^2 - s^2 \end{bmatrix} \quad (3.47)$$

where $c = \cos \theta$, $s = \sin \theta$.

3.2.4. Tsai-Wu Failure Criterion

In accordance with the theoretical assumption, a failure scenario for Tsai-Wu failure criterion is initiated when the following expression is validated⁸¹.

$$F_{ij}\sigma_i\sigma_j + F_i\sigma_i = IF \quad (3.48)$$

where IF is the indicator of failure.

$$(F_1\sigma_1 + F_2\sigma_2)(FoS) + (F_{11}\sigma_1^2 + F_{22}\sigma_2^2 + F_{66}\tau_{12}^2 - 2F_{12}\sigma_1\sigma_2)(FoS)^2 = 1 \quad (3.49)$$

for solution of quadratic equation gives Factor of Safety(FoS):

$$FoS = \frac{1}{2A} \left(\sqrt{B^2 + 4A} - B \right)$$

$$A = F_{11}\sigma_1^2 + F_{22}\sigma_2^2 + F_{66}\tau_{12}^2 - 2F_{12}\sigma_1\sigma_2$$

$$B = F_1\sigma_1 + F_2\sigma_2 \quad (3.50)$$

The value of F12 can be determined through the implementation of a biaxial tension test. In order to calculate this value, an empirical expression is put forth as follows¹⁷⁴:

$$F_1 = \frac{1}{(\sigma_1^T)_{ult}} + \frac{1}{(\sigma_1^C)_{ult}}$$

$$F_{11} = -\frac{1}{(\sigma_1^T)_{ult}(\sigma_1^C)_{ult}}$$

$$F_2 = \frac{1}{(\sigma_2^T)_{ult}} + \frac{1}{(\sigma_2^C)_{ult}}$$

$$F_{22} = -\frac{1}{(\sigma_2^T)_{ult}(\sigma_2^C)_{ult}}$$

$$F_{12} = -\frac{1}{2}\sqrt{F_{11}F_{22}}$$

$$F_{66} = \frac{1}{(\tau_{12}^F)_{ult}^2} \quad (3.51)$$

3.2.5. Driveshaft Problem

To analyse the behavior of the composite laminated driveshaft, the Classical Laminate Theory (CLT) was selected as the appropriate methodology. A schematic view of the shaft is presented below.

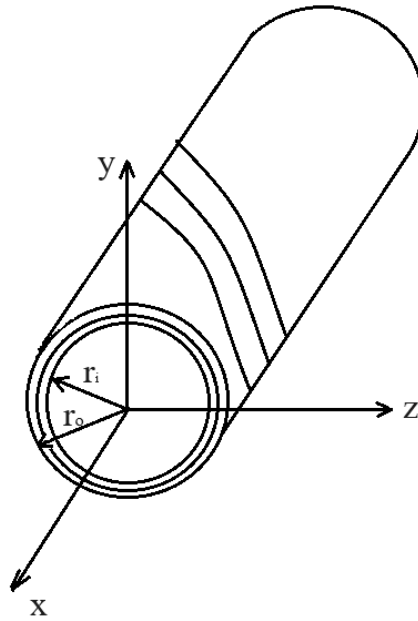


Figure 3.5. Composite cylindrical hollow shaft

The axial and hoop directions can be defined by the combined elements of the matrix $[A_{ij}]$ and the total thickness, which are given respectively as follows ¹⁷⁵:

$$E_x = \frac{1}{t} \left[A_{11} - \frac{A_{12}^2}{A_{22}} \right] \quad (3.52)$$

$$E_h = \frac{1}{t} \left[A_{22} - \frac{A_{12}^2}{A_{11}} \right] \quad (3.53)$$

where A_{11} , A_{12} and A_{22} are the corresponding elements of matrix A_{ij} , t represents the total thickness of the layers.

Once the applied torque exceeds the critical torsional buckling load T_{cr} , an orthotropic thin-walled hollow cylindrical shaft will begin to exhibit torsional buckling behaviour⁹⁸.

$$T_{cr} = (2\pi r_m^2 t)(0.272)(E_x E_h^3)^{1/4} \left(\frac{t}{r_m}\right)^{3/2} \quad (3.54)$$

where r_m , is the mean radius of the cylinder.

It is seen that torsional buckling is proportional to E_x 1/4 and E_h 3/4. It is apparent that in order to increase the torsional buckling of the composite driveshaft, 90 degree layers needs to be added.

The most important factor effecting the driveshafts in the dynamical engineering system is natural frequency. Thus, the natural frequency needs to be greater than the frequency of the vibration sources on the vehicle in order to prevent any negative effects on NVH (Noise, Vibration, Harshness). Designers must design driveshafts with a higher natural frequency (f_n) than the engine's vibration range because the combustion engine is the main source of vibration in the vehicle. It can be expressed in terms of the following equation⁹⁸:

$$f_n = \frac{\pi}{2} \sqrt{\frac{g E_x I}{W_u L^4}} \quad (3.55)$$

where g = gravity acceleration, W_u = weight per unit length, I = moment of inertia, L = length of the shaft. For the thin-walled tube, the moment of inertia can be given by

$$I = \frac{\pi}{4} (r_o^4 - r_i^4) \quad (3.56)$$

where r_o and r_i is the outer and inner radius of the driveshaft, respectively.

3.3. First-Order Shear Deformation Theory

The FSDT, based on the displacement relationship described in, is the other most widely used theory:

$$u(x, y, z, t) = u_0(x, y, t) + z\phi_x(x, y, t) \quad (3.57)$$

$$v(x, y, z, t) = v_0(x, y, t) + z\phi_y(x, y, t)$$

$$w(x, y, z, t) = w_0(x, y, t)$$

where u , v and w are the displacements along to the (x, y, z) coordinates, u_0 , v_0 and w_0 are the displacements for at a point on the mid-plane of the panel. ϕ_x and ϕ_y indicate rotations around the x and y axes, respectively. Using the relations between deformation and displacement, bending and shearing deformations can be defined as

$$\begin{Bmatrix} \varepsilon_{xx} \\ \varepsilon_{yy} \\ \gamma_{yz} \\ \gamma_{xz} \\ \gamma_{xy} \end{Bmatrix} = \begin{Bmatrix} \varepsilon_{xx}^{(0)} \\ \varepsilon_{yy}^{(0)} \\ \gamma_{yz}^{(0)} \\ \gamma_{xz}^{(0)} \\ \gamma_{xy}^{(0)} \end{Bmatrix} + z \begin{Bmatrix} \varepsilon_{xx}^{(1)} \\ \varepsilon_{yy}^{(1)} \\ \gamma_{yz}^{(1)} \\ \gamma_{xz}^{(1)} \\ \gamma_{xy}^{(1)} \end{Bmatrix} = \begin{Bmatrix} \frac{\partial u_0}{\partial x} + \frac{1}{2} \left(\frac{\partial w_0}{\partial x} \right)^2 \\ \frac{\partial v_0}{\partial y} + \frac{1}{2} \left(\frac{\partial w_0}{\partial y} \right)^2 \\ \frac{\partial w_0}{\partial y} + \phi_y \\ \frac{\partial w_0}{\partial x} + \phi_x \\ \frac{\partial u_0}{\partial y} + \frac{\partial v_0}{\partial x} + \frac{\partial w_0}{\partial x} \frac{\partial w_0}{\partial y} \end{Bmatrix} + z \begin{Bmatrix} \frac{\partial \phi_x}{\partial x} \\ \frac{\partial \phi_y}{\partial y} \\ 0 \\ 0 \\ \frac{\partial \phi_x}{\partial y} + \frac{\partial \phi_y}{\partial x} \end{Bmatrix} \quad (3.58)$$

The stress resultants (N_s , M_s and Q_s) are related to the displacement gradients and they can be expressed in terms of the displacements (u_0 , v_0 , w_0) by the relations:

$$\begin{Bmatrix} N_{xx} \\ N_{yy} \\ N_{xy} \end{Bmatrix} = \begin{bmatrix} A_{11} & A_{12} & A_{16} \\ A_{12} & A_{22} & A_{26} \\ A_{16} & A_{26} & A_{66} \end{bmatrix} \begin{Bmatrix} \frac{\partial u_0}{\partial x} + \frac{1}{2} \left(\frac{\partial w_0}{\partial x} \right)^2 \\ \frac{\partial v_0}{\partial y} + \frac{1}{2} \left(\frac{\partial w_0}{\partial y} \right)^2 \\ \frac{\partial u_0}{\partial y} + \frac{\partial v_0}{\partial x} + \frac{\partial w_0}{\partial x} \frac{\partial w_0}{\partial y} \end{Bmatrix} + \begin{bmatrix} B_{11} & B_{12} & B_{16} \\ B_{12} & B_{22} & B_{26} \\ B_{16} & B_{26} & B_{66} \end{bmatrix} \begin{Bmatrix} \frac{\partial \phi_x}{\partial x} \\ \frac{\partial \phi_y}{\partial y} \\ \frac{\partial \phi_x}{\partial y} + \frac{\partial \phi_y}{\partial x} \end{Bmatrix} \quad (3.59)$$

$$\begin{aligned}
\begin{Bmatrix} M_{xx} \\ M_{yy} \\ M_{xy} \end{Bmatrix} &= \begin{bmatrix} B_{11} & B_{12} & B_{16} \\ B_{12} & B_{22} & B_{26} \\ B_{16} & B_{26} & B_{66} \end{bmatrix} \begin{Bmatrix} \frac{\partial u_0}{\partial x} + \frac{1}{2} \left(\frac{\partial w_0}{\partial x} \right)^2 \\ \frac{\partial v_0}{\partial y} + \frac{1}{2} \left(\frac{\partial w_0}{\partial y} \right)^2 \\ \frac{\partial u_0}{\partial y} + \frac{\partial v_0}{\partial x} + \frac{\partial w_0}{\partial x} \frac{\partial w_0}{\partial y} \end{Bmatrix} \\
&+ \begin{bmatrix} D_{11} & D_{12} & D_{16} \\ D_{12} & D_{22} & D_{26} \\ D_{16} & D_{26} & D_{66} \end{bmatrix} \begin{Bmatrix} \frac{\partial \phi_x}{\partial x} \\ \frac{\partial \phi_y}{\partial y} \\ \frac{\partial \phi_x}{\partial y} + \frac{\partial \phi_y}{\partial x} \end{Bmatrix}
\end{aligned} \tag{3.60}$$

$$\begin{Bmatrix} Q_y \\ Q_x \end{Bmatrix} = K \begin{bmatrix} A_{44} & A_{45} \\ A_{45} & A_{55} \end{bmatrix} \begin{Bmatrix} \frac{\partial w_0}{\partial y} + \phi_y \\ \frac{\partial w_0}{\partial x} + \phi_x \end{Bmatrix} \tag{3.61}$$

where A_{ij} are called extensional stiffnesses, D_{ij} the bending stiffnesses and B_{ij} the bending-extensional coupling stiffnesses. A , B and D are defined in terms of the lamina stiffnesses $\bar{Q}_{ij}^{(k)}$ as

$$\begin{aligned}
(A_{ij}, B_{ij}, D_{ij}) &= \sum_{k=1}^N \int_{z_k}^{z_{k+1}} \bar{Q}_{ij}^{(k)} (1, z, z^2) dz, (i, j \rightarrow 1, 2, 6) \\
(A_{44}, A_{45}, A_{55}) &= \sum_{k=1}^N \int_{z_k}^{z_{k+1}} (\bar{Q}_{44}^{(k)}, \bar{Q}_{45}^{(k)}, \bar{Q}_{55}^{(k)}) dz, (i, j \rightarrow 1, 2, 6)
\end{aligned} \tag{3.62}$$

3.3.1. Vibration of the Laminated Composite Plate by Simply Supported Boundary Conditions

The governing equation of laminated plate under mechanical loadings is derived by using Hamilton's principle as given:

$$0 = \int_0^T (\delta U + \delta V - \delta K) dt \tag{3.63}$$

where U, V and K are the virtual strain energy, virtual work done and the virtual kinetic energy by the mechanical forces of the laminated composite plate, respectively. After the substituting mechanical loads equations and displacements into Hamilton's principle and applying Navier approach to the equations of motion, the analytical solutions can be obtained as¹⁷⁶

$$\begin{pmatrix} k_{11} & k_{12} & 0 & k_{14} & k_{15} \\ k_{12} & k_{22} & 0 & k_{24} & k_{25} \\ 0 & 0 & k_{33} & k_{34} & k_{35} \\ k_{14} & k_{24} & k_{34} & k_{44} & k_{45} \\ k_{15} & k_{25} & k_{35} & k_{45} & k_{55} \end{pmatrix} - \omega^2 \begin{pmatrix} I_0 & 0 & 0 & 0 & 0 \\ 0 & I_0 & 0 & 0 & 0 \\ 0 & 0 & I_0 & 0 & 0 \\ 0 & 0 & 0 & I_2 & 0 \\ 0 & 0 & 0 & 0 & I_2 \end{pmatrix} \begin{pmatrix} U_{mn} \\ V_{mn} \\ W_{mn} \\ X_{mn} \\ Y_{mn} \end{pmatrix} = \begin{pmatrix} 0 \\ 0 \\ 0 \\ 0 \\ 0 \end{pmatrix} \quad (3.64)$$

$$\begin{aligned} k_{11} &= A_{11}\alpha^2 + A_{66}\beta^2 \\ k_{24} &= k_{15} \\ k_{22} &= A_{66}\alpha^2 + A_{22}\beta^2 \\ \left. \begin{aligned} k_{14} &= B_{11}\alpha^2 + B_{66}\beta^2, k_{15} = (B_{12} + B_{66})\alpha\beta \\ k_{25} &= B_{66}\alpha^2 + B_{22}\beta^2 \end{aligned} \right\} \begin{array}{l} \text{for} \\ \text{antisymmetric} \\ \text{cross-ply} \end{array} \\ \left. \begin{aligned} k_{14} &= 2B_{16}\alpha\beta, k_{15} = B_{16}\alpha^2 + B_{26}\beta^2 \\ k_{25} &= 2B_{26}\alpha\beta \end{aligned} \right\} \begin{array}{l} \text{for} \\ \text{antisymmetric} \\ \text{angle-ply} \end{array} \\ k_{33} &= \kappa(A_{55}\alpha^2 + A_{44}\beta^2), k_{34} = \kappa A_{55} \alpha, k_{35} = \kappa A_{44} \beta \\ k_{44} &= D_{11}\alpha^2 + D_{66}\beta^2 + \kappa A_{55}, \\ k_{55} &= D_{66}\alpha^2 + D_{22}\beta^2 + \kappa A_{44}, k_{45} = (D_{12} + D_{66})\alpha\beta \end{aligned} \quad (3.65)$$

where κ is the shear correction factor.

3.3.2 Buckling of the Laminated Composite Plate by Simply Supported Boundary Conditions

For the buckling analysis of FSDT, it is assumed that the only applied loads are the in-plane forced loads:

$$N_x = -N_{cr}, \quad N_y = -kN_{cr}, \quad k = \frac{N_y}{N_x} \quad (3.66)$$

and all other mechanical and thermal loads are zero. It can be written from reference¹⁷⁶ as

$$\begin{bmatrix} k_{11} & k_{12} & 0 & k_{14} & k_{15} \\ k_{12} & k_{22} & 0 & k_{24} & k_{25} \\ 0 & 0 & S & k_{34} & k_{35} \\ k_{14} & k_{24} & k_{34} & k_{44} & k_{45} \\ k_{15} & k_{25} & k_{35} & k_{45} & k_{55} \end{bmatrix} \begin{Bmatrix} U_{mn} \\ V_{mn} \\ W_{mn} \\ X_{mn} \\ Y_{mn} \end{Bmatrix} = \begin{Bmatrix} 0 \\ 0 \\ Q_{mn} \\ 0 \\ 0 \end{Bmatrix}$$

(3.67)

where $S = k_{33} - N_{cr}(\alpha^2 + k\beta^2)$. N_{cr} is the critical buckling loads.

CHAPTER 4

MATERIAL PROPERTIES

In this study, three-phase multi-scale carbon nanotubes (CNTs) or graphene nanoplatelets (GPLs) and fiber-reinforced polymer nanocomposites are considered as the laminated composite materials. The approach focuses on improving the material's mechanical properties by adding a small amount of nano-reinforcement. The multiphase nanocomposite structures consist of isotropic matrix, nanoreinforcement (GPLs or CNTs) and fibers. Two different approaches are used to model matrix materials containing randomly distributed nanofillers (GPLs or CNTs), taking into account the presence or absence of agglomeration, waviness and orientation effects. These approaches use the Halpin-Tsai model and the modified Halpin-Tsai model. The Halpin-Tsai model, the modified Halpin-Tsai model and the rule of mixtures are applied to derive the effective material properties for the nano-reinforced matrix. The hierarchical process is shown in Figure 4.1.

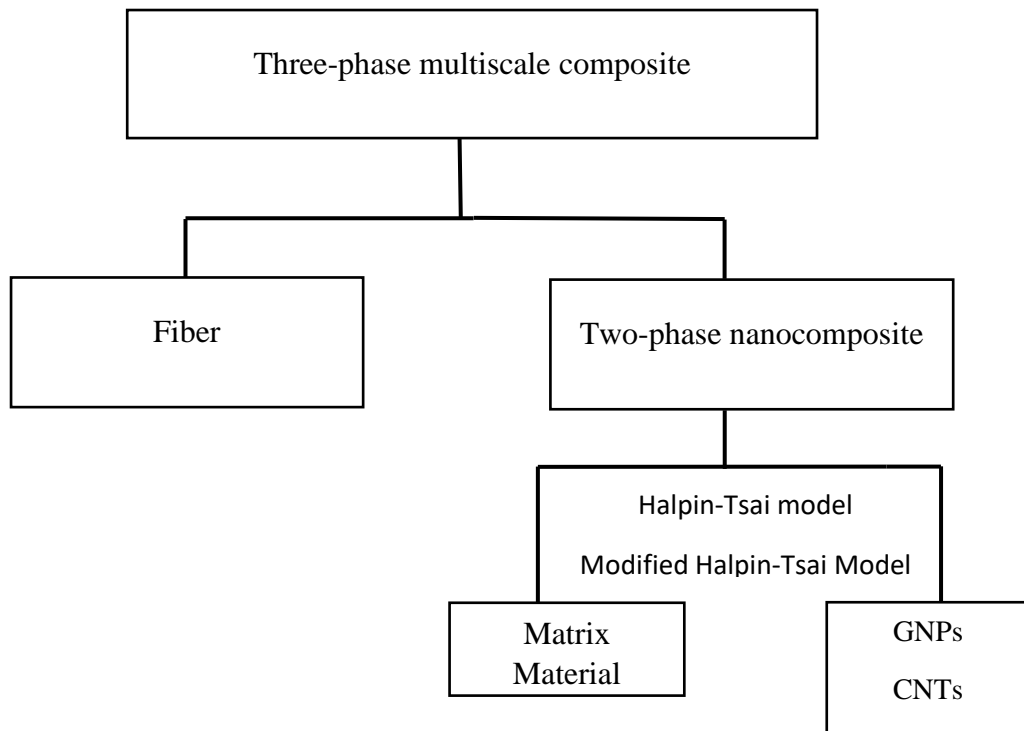
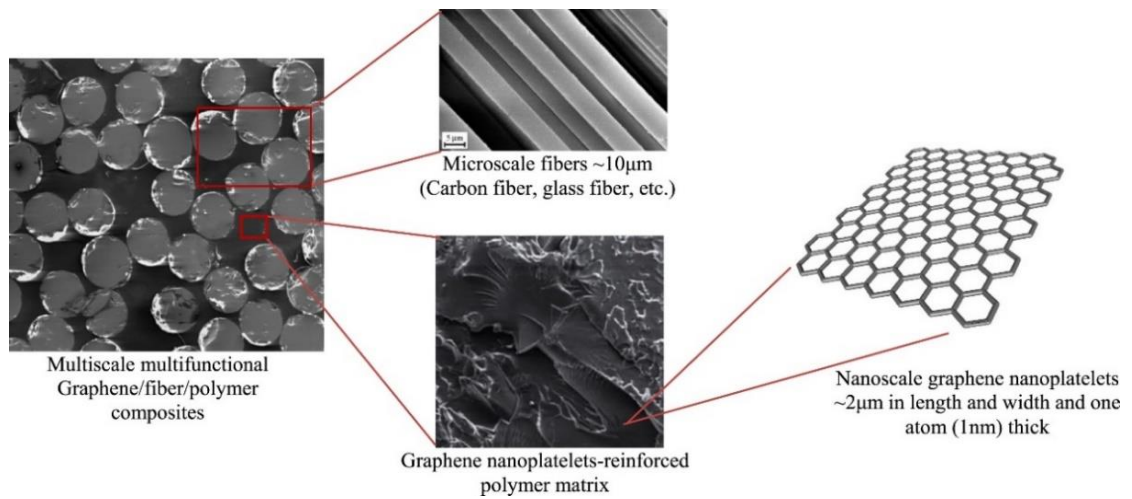
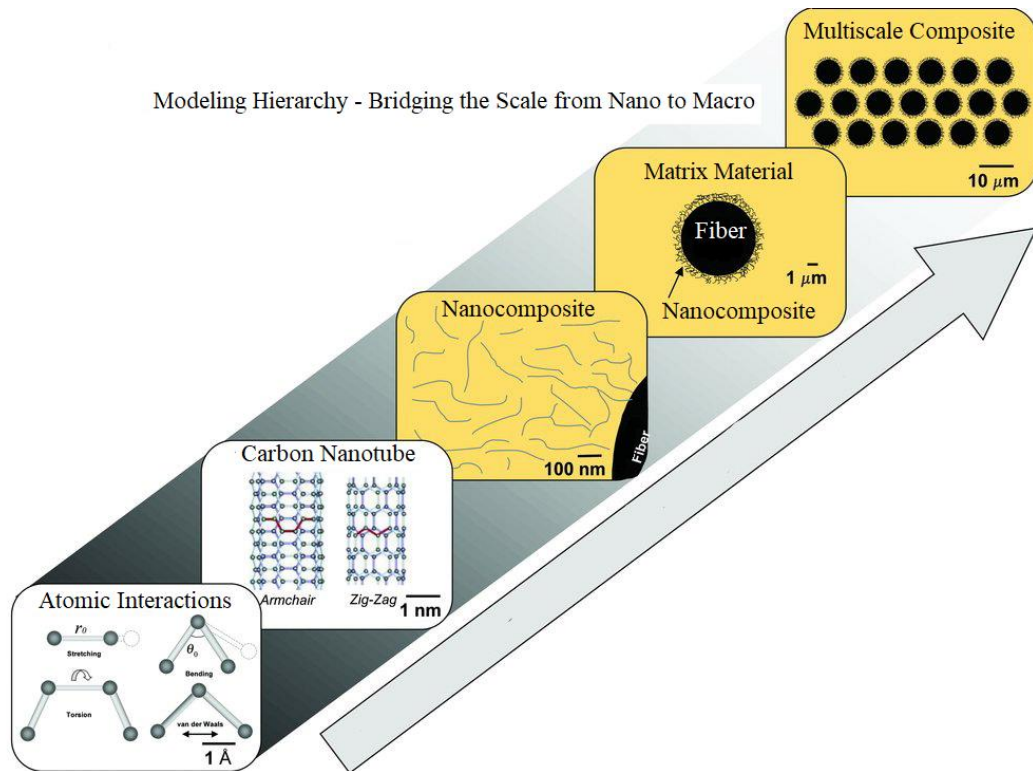


Figure 4.1. Hierarchy of the three-phase GNPs or CNTs/fiber/polymer multiscale composites. (Source: Gholami 2018¹⁷⁷)



(a)



(b)

Figure 4.2. (a) Concept of multiscale graphene nano platelets and carbon nanotube
 (b) reinforced polymer composites (Source: Rafiee 2018, Godara 2020^{178,179})

Numerous investigations have been conducted to determine the effective material properties of GPLs or CNTs reinforced laminates using micromechanical

homogenization approaches³¹⁻³⁴. Initially, these approaches were applied to define the effective material properties of two-phase fiber-reinforced composites¹⁸⁰. Subsequently, the same methodology has been extended to obtain the effective material properties of three-phase CNTs or graphene/fiber-reinforced laminates in various publications^{177,178}.

The elastic constants of three-phase graphene/fibre reinforced composites are determined using micromechanical equations. The multi-scale behaviour of both multi-scale graphene nanoplatelets and multi-scale carbon nanotube reinforced polymer composites is described in Figure 4.2 (a) and 4.2 (b).

4.1. Halpin-Tsai Model

4.1.1. Carbon Nanotube Reinforced Matrix

Using the Halpin-Tsai model, two-phase random CNTs-dispersed matrix elastic properties can be defined using micromechanical equations. For two-phase CNTs reinforced matrix properties, the CNTM index is used, where CNT stands for carbon nanotube properties and M for matrix properties. The elastic modulus of the CNT reinforced matrix can be written by³⁸

$$E_{CNTM} = \frac{E_M}{8} \left[5 \left(\frac{1 + 2\beta_{dd}V_{CNT}}{1 - \beta_{dd}V_{CNT}} \right) + 3 \left(\frac{1 + 2(l_{CNT}/d_{CNT})\beta_{dl}V_{CNT}}{1 - \beta_{dl}V_{CNT}} \right) \right] \quad (4.1)$$

where β_{dd} and β_{dl} coefficients can be calculated by

$$\beta_{dd} = \frac{(E_{CNT}/E_M) - (d_{CNT}/4t_{CNT})}{(E_{CNT}/E_M) + (d_{CNT}/2t_{CNT})} \quad (4.2)$$

$$\beta_{dl} = \frac{(E_{CNT}/E_M) - (l_{CNT}/4t_{CNT})}{(E_{CNT}/E_M) + (l_{CNT}/2t_{CNT})} \quad (4.3)$$

where l_{CNT} , d_{CNT} and t_{CNT} are the parameters related to length, diameter and the thickness of the carbon nanotubes, respectively.

The Poisson's ratio and the shear modulus of the CNT reinforced matrix are given by

$$v_{CNTM} = v_{CNT} V_{CNT} + v_M(1 - V_{CNT}) \quad (4.4)$$

$$G_{CNTM} = \frac{E_{CNTM}}{2(1 + v_{CNTM})} \quad (4.5)$$

The volume content of carbon nanotubes V_{CNT} can be expressed in terms of the weight fraction, denoted by W_{CNT} , as follows:

$$V_{CNT} = \frac{W_{CNT}}{W_{CNT} + (\rho_{CNT}/\rho_M)(1 - W_{CNT})} \quad (4.6)$$

$$\rho_{CNTM} = \rho_{CNT} V_{CNT} + \rho_M(1 - V_{CNT}) \quad (4.7)$$

4.1.2. Three-Phase Fiber/CNTs Reinforced Matrix Composite

The elastic moduli and density of each ply for the three-phase laminate (Carbon fiber/CNTs/matrix) are computed from the equations as given¹⁷⁷;

$$E_{11} = E_{F11} V_F + E_{CNTM}(1 - V_F) \quad (4.8)$$

$$E_{22} = \left(\frac{V_F}{E_{F11}} + \frac{1 - V_F}{E_{CNTM}} - V_F (1 - V_F) \frac{v_F^2(E_{CNTM}/E_{F22}) + v_{CNTM}^2(E_{F22}/E_{CNTM}) - 2v_F v_{CNTM}}{V_F E_{F22} + (1 - V_F) E_{CNTM}} \right)^{-1} \quad (4.9)$$

$$G_{12} = \left(\frac{V_F}{G_F} + \frac{1 - V_F}{G_{CNTM}} \right)^{-1} \quad (4.10)$$

$$v_{12} = v_F V_F + v_{CNTM}(1 - V_F) \quad (4.11)$$

$$\rho = \rho_F V_F + \rho_{CNTM}(1 - V_F) \quad (4.12)$$

4.1.3. Graphene Reinforced Matrix

Mechanical properties of graphene nanoplatelets reinforced matrix; Young's and shear modulus, Poisson's ratio and density are computed by using micromechanical equations shown in the equations³⁷. Young's modulus of the GPLs reinforced matrix can be expressed in

$$E_{GM} = \left(\frac{3}{8} \frac{1 + \xi_L \eta_L V_{GPL}}{1 - \eta_L V_{GPL}} + \frac{5}{8} \frac{1 + \xi_w \eta_w V_{GPL}}{1 - \eta_w V_{GPL}} \right) \times E_M \quad (4.13)$$

Here subscripts GPL, M and GM represent graphene nanoplatelets (GPL), the matrix (M) and the GPLs reinforced matrix (GM). V_{GPL} is the volume content of GPLs. Parameters ξ_L and ξ_w are corresponding properties of the length (l_{GPL}), the width (w_{GPL}) and the thickness (h_{GPL}) of GPLs given by

$$\xi_L = 2 \frac{l_{GPL}}{h_{GPL}}, \xi_w = 2 \frac{w_{GPL}}{h_{GPL}} \quad (4.14)$$

and η_L , η_w can be calculated in terms of Young's modulus E_{GPL} of the graphene nanoplatelets and E_M of the matrix as³⁷

$$\eta_L = \frac{(E_{GPL}/E_M) - 1}{(E_{GPL}/E_M) + \xi_L} \quad (4.15)$$

$$\eta_w = \frac{(E_{GPL}/E_M) - 1}{(E_{GPL}/E_M) + \xi_w} \quad (4.16)$$

The volume content of graphene nanoplatelets can be calculated in terms of its weight fraction W_{GPL} as

$$V_{GPL} = \frac{W_{GPL}}{W_{GPL} + (\rho_{GPL}/\rho_M)(1 - W_{GPL})} \quad (4.17)$$

where ρ_{GPL} and ρ_M shows the mass densities of graphene nanoplatelets and the polymer matrix, respectively.

Poisson's ratio, shear modulus and the density of the graphene reinforced matrix can be expressed as

$$v_{GM} = v_{GPL}V_{GPL} + v_M(1 - V_{GPL}) \quad (4.18)$$

$$G_{GPL} = \frac{E_{GM}}{2(1 + v_{GM})} \quad (4.19)$$

$$\rho_{GM} = \rho_{GPL}V_{GPL} + \rho_M(1 - V_{GPL}) \quad (4.20)$$

4.1.4. Graphene and Fiber Reinforced Matrix

In order to advance the mechanical properties of the composite, fiber reinforcement is implemented to graphene reinforced matrix as unidirectional and continuous. Young's moduli, shear modulus, Poisson's ratio and density of the graphene/fiber reinforced nanocomposite are defined in the following form³⁷;

$$E_{11} = E_{F11}V_F + E_{GM}(1 - V_F) \quad (4.21)$$

$$E_{22} = E_{GM} \left(\frac{E_{F22} + E_{GM} + (E_{F22} - E_{GM})V_F}{E_{F22} + E_{GM} - (E_{F22} - E_{GM})V_F} \right) \quad (4.22)$$

$$G_{12} = G_{13} = G_{GM} \left(\frac{G_{F22} + G_{GM} + (G_{F22} - G_{GM})V_F}{G_{F22} + G_{GM} - (G_{F22} - G_{GM})V_F} \right) \quad (4.23)$$

$$G_{23} = \frac{E_{22}}{2(1 + v_{23})} \quad (4.24)$$

$$v_{12} = v_{F12}V_F + v_{GM}(1 - V_F) \quad (4.25)$$

$$v_{23} = v_{F12}V_F + v_{GM}(1 - V_F) \left(\frac{1 + v_{GM} + \frac{v_{12}E_{GM}}{E_{11}}}{1 - v_{GM}^2 + \frac{v_{12}v_{GM}E_{GM}}{E_{11}}} \right) \quad (4.26)$$

$$\rho = \rho_F V_F + \rho_{GM}(1 - V_F) \quad (4.27)$$

Indications G_M and F refer to graphene-reinforced matrix and fibers, respectively. V_F and ρ_F symbolise the fiber volume content and the density of fibers.

4.2. Modified Halpin-Tsai Model

4.2.1. CNTs-Reinforced Matrix Composite Model

Under the assumption of uniform dispersion of CNTs in the polymer matrix, the H-T model in equation estimates the Young's modulus of straight aligned CNT-reinforced nanocomposites. Using the well-established H-T micromechanical model, the Young's modulus of an aligned straight CNT-reinforced polymer nanocomposite can be predicted as follows¹⁸¹:

$$E_{m-cnt} = E_m \left(\frac{1 + 2R\delta V_{cnt}}{1 - \delta V_{cnt}} \right) \quad (4.28)$$

where R and δ can be written as follows;

$$R = \left(\frac{L_{cnt}}{d_{cnt}} \right), \delta = \frac{(E_{cnt}/E_m) - 1}{(E_{cnt}/E_m) + 2R} \quad (4.29)$$

where E_m , E_{cnt} , V_{cnt} , d_{cnt} and L_{cnt} shows the elastic modulus of the matrix, elastic modulus of CNTs, volume fraction of CNTs, outer diameter of the CNTs and length of the CNTs, respectively.

On the contrary, assumptions related to uniform dispersion of CNTs into matrix material are not easy for real applications due to the tendency of orientation, waviness, and agglomeration for CNTs. Schematic drawings of the layer of the multi-scale CNTs fibre reinforced nanocomposite can be seen in Figure 4.3.

In the modified H-T model, these effects are considered by using three critical factors: waviness, orientation, and agglomeration to estimate mechanical properties more realistically. Initially, the orientation factor is included in Equation 4.30 to describe the

random orientation level of CNTs in nanocomposites ply¹⁸². Equation can be rewritten as;

$$\delta = \frac{(f_R E_{cnt}/E_m) - 1}{(f_R E_{cnt}/E_m) + 2R} \quad (4.30)$$

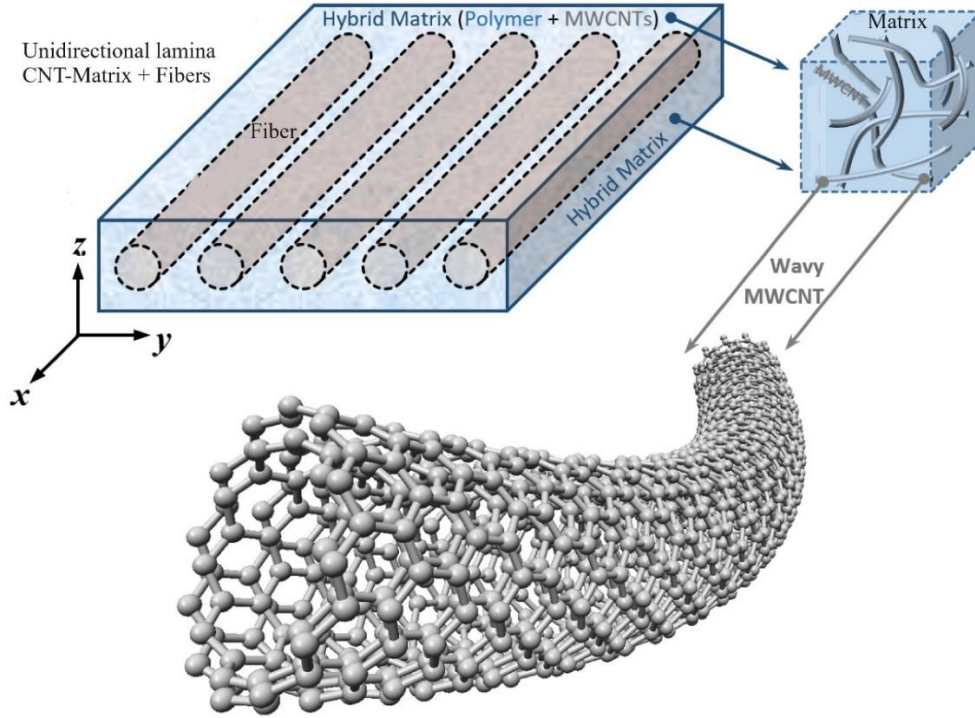


Figure 4.3. Unidirectional fiber-reinforced composite lamina with MWCNT inclusion
(Source: Georgantzinos 2021¹⁸²)

A CNT is assumed to be randomly oriented in two dimensions when its length is larger than the sample thickness, which is given as $f_R = 1/3$, and randomly oriented in three dimensions when its length is much smaller than the sample thickness, which is given as $f_R = 1/6$. The orientation factor is assumed to be $f_R = 1/6$ in this thesis problems. Additionally, Equation (4.30) can be rewritten by including a waviness factor for CNTs or MWCNTs into the matrix of nanocomposites.

$$\delta = \frac{(f_R f_W E_{cnt}/E_m) - 1}{(f_R f_W E_{cnt}/E_m) + 2R} \quad (4.31)$$

where the waviness factor f_w can be written as Equation 4.32. It is assumed to be equal to $f_w = 0.6$. Here A and W can be obtained from the half-wavelength which given in Figure 4.4.

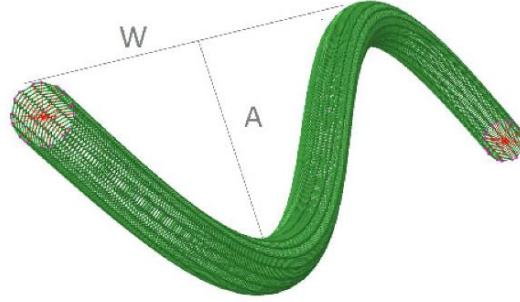


Figure 4.4. Illustration of the CNTs half-wavelength (Source: Georgantzinos 2021¹⁸²)

$$f_w = 1 - \left(\frac{A}{W}\right) \quad (4.32)$$

The agglomeration effects can be added into equation by using an agglomeration efficiency factor, f_A . And by combining the parameters α and β related to degree of CNT agglomeration, f_A can be written in equation. For the problems in these thesis, the α and β are assumed to be equal to 10 and 0.9, respectively.

$$\delta = \frac{(f_R f_w f_A E_{cnt}/E_m) - 1}{(f_R f_w f_A E_{cnt}/E_m) + 2R} \quad (4.33)$$

$$f_A = \exp(-\alpha V_{cnt}^\beta) \quad (4.34)$$

The efficiency factors for multiphase fibre/CNT reinforced nanocomposite structures can be modified to describe the material properties of the structures in accordance with characterisation methods based on the factors of the nanocomposite manufacturing process.

The shear modulus, Poisson's ratio, density of the CNT-matrix can be written as the following equations⁸⁰.

$$G_{m-cnt} = \frac{E_{m-cnt}}{2(\nu_{m-cnt} + 1)} \quad (4.35)$$

$$v_{m-cnt} = v_m \quad (4.36)$$

$$\rho_{m-cnt} = \rho_{cnt}V_{cnt} + \rho_mV_m \quad (4.37)$$

where ρ_{cnt} , ρ_m , V_{cnt} and V_m are the densities of the nanotube and matrix, volume fraction of the nanotube and matrix, respectively.

4.2.2. Fiber Reinforced Nanocomposite Lamina Constants

By using rule of mixture, unidirectional Young's modulus (E_f), density (ρ_c) and poisson's ratio (v_{12}) of the fiber/CNTs reinforced lamina properties can be written as follows⁸⁰;

$$E_1 = E_fV_f + E_{m-cnt}V_{m-cnt} \quad (4.38)$$

$$\rho_c = \rho_fV_f + \rho_{m-cnt}V_{m-cnt} \quad (4.39)$$

$$v_{12} = v_fV_f + v_{m-cnt}V_{m-cnt} \quad (4.40)$$

where ρ_f , V_f and V_{m-cnt} the density of the fibers, volume fraction of the fibers and CNT reinforced matrix, respectively.

For the Young's modulus E_2 , Poisson's ratio v_{23} and shear modulus G_{12} and G_{23} , semi-empirical models have been developed to obtain results that are closer to the experimental results and more accurate than the rule of mixtures models. The equations of the H-T semiempirical models can be written as follows;

$$\frac{P}{P_{m-cnt}} = \left(\frac{1 + \xi\eta V_f}{1 - \eta V_f} \right) \quad (4.41)$$

$$\eta = \frac{(P_f/P_{m-cnt}) - 1}{(P_f/P_{m-cnt}) - \xi} \quad (4.42)$$

where P means the E_2 , v_{23} , G_{12} and G_{23} of the fiber/CNTs reinforced matrix properties. P_{m-cnt} and η are also show the properties of CNT-matrix and experimental factor, respectively. The reinforcing factor ξ is defined according to geometry of fiber and

packing and loading conditions. $\zeta = 2$ for E_2 and $\zeta = 1$ for ν_{23} , G_{12} and G_{23} for circular fibres in a square pattern¹⁸³.

4.3. Functionally Graded Graphene Reinforced Matrix

The other technique for creating composite plates reinforced with graphene is to functionally grade the thickness of the plate using four different distributions, namely UD, FG-V, FG-O, and FG-X. Figure 4.5 shows these distributions.

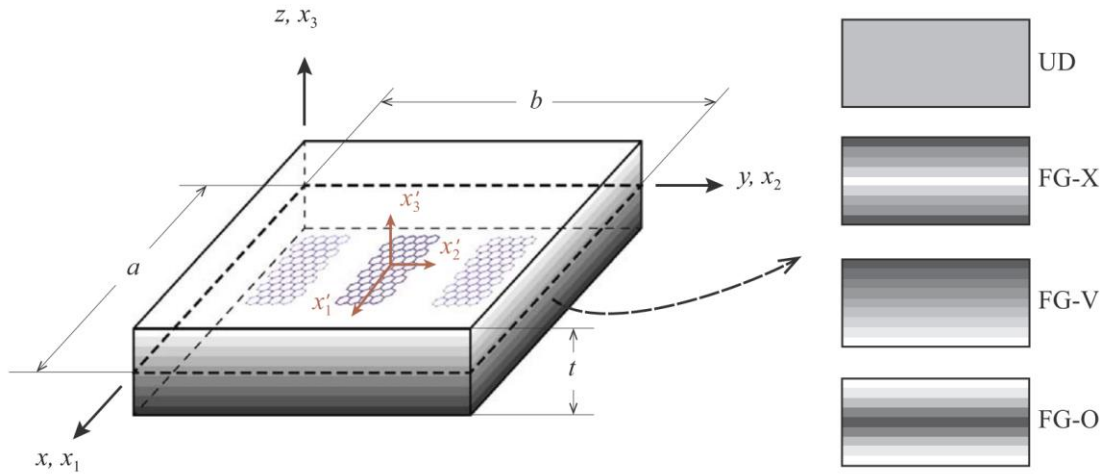


Figure 4.5. Geometry and coordinate system of the FG-GNPs composite plates.

(Source: Garcia Macias 2018¹⁸⁴)

According to their distributions, the GNPs volume fraction V_{GNPs} for an individual layer can be expressed by following equations which is the function of the thickness coordinate z ¹⁸⁴:

$$V_{GPL^*}(z) = V_{GPL} \quad (UD) \quad (4.43)$$

$$V_{GPL^*}(z) = \left(\frac{2|Z|}{t}\right)^k (k+1)V_{GPL} \quad (FG-X) \quad (4.44)$$

$$V_{GPL^*}(z) = \left(\frac{t+2Z}{2t}\right)^k (k+1)V_{GPL} \quad (FG-V) \quad (4.45)$$

$$V_{GPL^*}(z) = \left(\frac{t-2Z}{t}\right)^k (k+1)V_{GPL} \quad (FG-O) \quad (4.46)$$

where V_{GPL} , k and t refer to volume content of the GPLs, power law index and thickness of the plate, respectively.

4.4. Eshelby-Mori Tanaka Model for Nanocomposite Structures

The effective mechanical properties can be estimated for a CNT reinforced polymer by considering the aggregation of CNTs, which is done based on the Eshelby-Mori Tanaka scheme¹⁸⁵. The volume fraction of CNTs can be calculated in term of mass fraction of CNTs (w_r) as follows:

$$F_r = \frac{1}{1 + \frac{\rho_r}{\rho_m} \left(\frac{1}{w_r} - 1 \right)} \quad (4.47)$$

And the volume fraction of polymer matrix can be obtained using the following relation:

$$F_m = 1 - F_r \quad (4.48)$$

The CNTs have a tendency to cluster together because of their low bending stiffness (i.e., high length-to-diameter ratio and small elastic modulus in the radial direction) and the interfacial bonding between CNTs and the polymeric matrix. As shown in Fig. 3.4, some CNTs scatter in the matrix in random directions, while the others appear in the cluster form.

The effect of the CNTs agglomeration on the elastic properties of the randomly oriented CNT-reinforced composites has been studied utilizing a two-parameter micromechanics model as follows¹⁸⁶:

$$\mu = \frac{V_{in}}{V} \quad (4.49)$$

where V is the volume of the composite, V_{in} indicates the volume of clusters, V_r shows the volume of the CNTs and V_r in stands for the volume of CNTs in the clusters (the agglomerated CNTs). $0 < \mu \leq \eta \leq 1$ in which $\mu \leq \eta = 1$ indicates the complete agglomeration,

$\mu = \eta = 1$ shows the null agglomeration, and $\mu \leq \eta < 1$ implies the partial agglomeration (Figure 4.6)

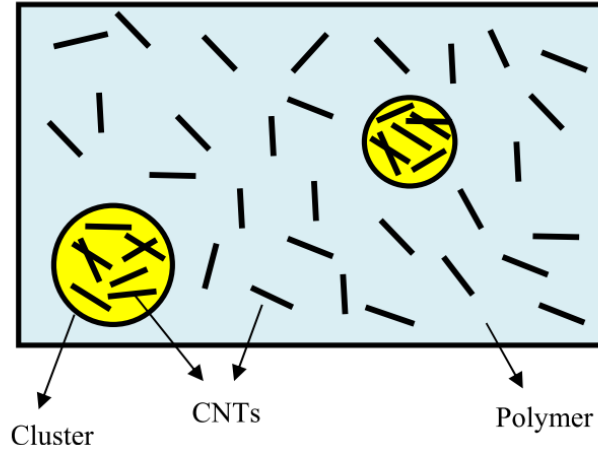


Figure 4.6. Partial agglomeration of CNTs (Source: Yousefi 2020¹⁸⁶)

CNTs are orthotropic materials, but as they are randomly oriented in the polymer, the CNT-reinforced matrix can be considered as an isotropic structure and its elastic modulus (E_m^*) and Poisson's ratio (ν_m^*) can be calculated as ¹⁸⁶.

$$E_m^* = \frac{9 K_m^* G_m^*}{3K_m^* + G_m^*} \quad (4.50)$$

$$\nu_m^* = \frac{3K_m^* - 2G_m^*}{6K_m^* + 2G_m^*} \quad (4.51)$$

in which G_m^* and K_m^* shows the shear and bulk moduli, respectively, and can be calculated based on the Eshelby–Mori–Tanaka scheme as follows ¹⁸⁶:

$$K_m^* = K_{out}^* \left[1 + \frac{\mu \left(\frac{K_{in}^*}{K_{out}^*} - 1 \right)}{1 + (1 - \mu) \left(\frac{K_{in}^*}{K_{out}^*} - 1 \right) \frac{1 + \nu_{out}^*}{3(1 - \nu_{out}^*)}} \right] \quad (4.52)$$

$$G_m^* = G_{out}^* \left[1 + \frac{\mu \left(\frac{G_{in}^*}{G_{out}^*} - 1 \right)}{1 + (1 - \mu) \left(\frac{G_{in}^*}{G_{out}^*} - 1 \right) \frac{8 - 10 \nu_{out}^*}{15(1 - \nu_{out}^*)}} \right] \quad (4.53)$$

where the subscripts “in” and “out” imply the inside and outside of the clusters and in which G_m and K_m specify the shear and bulk moduli of the isotropic matrix, respectively and can be evaluated as¹⁸⁶

$$G_m = \frac{E_m}{2(1 + \nu_m)} \quad (4.54)$$

$$K_m = \frac{E_m}{3(1 - 2\nu_m)} \quad (4.55)$$

where E_m and ν_m are the elastic modulus and Poisson’s ratio of the isotropic matrix, respectively. Also K_{in}^* , G_{in}^* , ν_{out}^* , K_{out}^* , G_{out}^* , α_r , β_r , δ_r and η_r are defined as follows¹⁸⁶:

$$\alpha_r = \frac{3(K_m + G_m) + k_r + l_r}{3(G_m + k_r)} \quad (4.56)$$

$$\beta_r = \frac{1}{5} \left[\frac{4G_m + 2k_r + l_r}{3(G_m + k_r)} + \frac{4G_m}{G_m + p_r} + \frac{4G_m(3K_m + 4G_m)}{G_m(3K_m + G_m) + m_r(3K_m + 7G_m)} \right] \quad (4.57)$$

$$\delta_r = \frac{1}{3} \left[n_r + 2l_r + \frac{(2k_r + l_r)(3K_m + G_m - l_r)}{G_m + k_r} \right] \quad (4.58)$$

$$\eta_r = \frac{1}{5} \left[\frac{2}{3} (n_r - l_r) + \frac{8G_m p_r}{G_m + p_r} + \frac{(2k_r - l_r)(2G_m + l_r)}{3(G_m + k_r)} + \frac{4m_r G_m (3K_m + 4G_m)}{3K_m(m_r + G_m) + G_m(G_m + 7m_r)} \right] \quad (4.59)$$

$$K_{in}^* = K_m + \left[\frac{\eta F_r (\delta_r - 3K_m \alpha_r)}{3[\mu + \eta F_r (\alpha_r - 1)]} \right] \quad (4.60)$$

$$G_{in}^* = G_m + \left[\frac{\eta F_r (\delta_r - 3K_m \alpha_r)}{3[\mu + \eta F_r (\alpha_r - 1)]} \right] \quad (4.61)$$

$$v_{out}^* = \frac{3K_{out}^* - 2G_{out}^*}{6K_{out}^* + 2G_{out}^*} \quad (4.62)$$

$$K_{out}^* = K_m + \left[\frac{(1 - \eta)F_r(\delta_r - 3K_m\alpha_r)}{3[1 - \mu + (1 - \eta)F_r(\alpha_r - 1)]} \right] \quad (4.63)$$

$$G_{out}^* = G_m + \left[\frac{(1 - \eta)F_r(\delta_r - 3G_m\alpha_r)}{3[1 - \mu + (1 - \eta)F_r(\beta_r - 1)]} \right] \quad (4.64)$$

CHAPTER 5

OPTIMIZATION

Optimization can be identified as mathematical process used to form the best design or favourable designs by minimizing or maximizing defined single or multi-objectives that fulfill all the constraints. Optimization is frequently used in engineering problems such as weight, cost, vibration, buckling and failure. In such problems, single and multi-objective optimization approaches are utilized to obtain desired design of structure. In single-objective optimization approach, design and optimization problem comprise of a single-objective function, constraints and bounds. Nevertheless, the design and optimization of the engineering structures need to be maximized and / or minimized often conflicting more than one objectives, simultaneously¹⁸⁵. In this situation, multi-objective approach is used and Pareto optimal solutions are gained. In this approach, it is not possible to obtain the best solution for all objectives, thus only one solution is selected from the set of solutions for practical engineering usage¹⁸⁷.

As design and optimization problems of laminated composites include complicated, highly nonlinear functions, they are unsolvable by the traditional optimization methods. In this situation, the use of stochastic optimization methods such as DE, NM, SA and GA are preferred.

Wolfram Mathematica is one of the most important commercial software used to solve composite design and optimization problems. For solving optimization problems, the software includes stochastic methods such as Differential Evolution (DE), Nelder Mead (NM), Random Search (RS) and Simulated Annealing (SA). All of these methods are being utilized by researchers in the design and optimization of composite structures.

5.1. Single-Objective Optimization

Single-objective optimization approach comprises of objective function, design variables, constraints and bounds of constraints. In this study, the problems that are solved using single-objective optimization approach are expressed as follows

$$\text{Minimize: } f(\theta_1, \theta_2, \dots, \theta_n)$$

$$\text{such that: } h_i(\theta_1, \theta_2, \dots, \theta_n) \geq 0, \quad i = 1, 2, \dots, r$$

$$g_j(\theta_1, \theta_2, \dots, \theta_n) = 0, j = 1, 2, \dots, m$$

$$\theta^L \leq \theta_1, \theta_2, \dots, \theta_n \leq \theta^U$$

where f is objective function, $\theta_1, \theta_2, \dots, \theta_n$ are the design variables and h, g are the constraints of the problem. Here, θ^L and θ^U show lower and upper bounds. In design and optimization of composite structure problems; stiffness, mass, strength, displacements, thickness, vibration frequencies, buckling loads, residual stresses, cost and weight are utilized as objective functions¹⁸⁷. In this thesis, fundamental frequency is taken as objective function of the single-objective optimization problems.

5.2. Multi-objective Optimization

A multi-objective optimization problem can be expressed as follows:

$$\text{Minimize: } f_1(\theta_1, \theta_2, \dots, \theta_n), f_2(\theta_1, \theta_2, \dots, \theta_n), \dots, f_t(\theta_1, \theta_2, \dots, \theta_n)$$

$$\text{such that: } h_i(\theta_1, \theta_2, \dots, \theta_n) \geq 0, i = 1, 2, \dots, r$$

$$g_j(\theta_1, \theta_2, \dots, \theta_n) = 0, j = 1, 2, \dots, m$$

$$\theta^L \leq \theta_1, \theta_2, \dots, \theta_n \leq \theta^U$$

where f_1, f_2, \dots, f_n denote the objective functions to be minimized simultaneously¹⁸⁸. On the contrary to the traditional multi-objective optimization approach, the usage of penalty function formulation may be appropriate because of its advantage of turning constrained optimization problems into the unconstrained ones and thanks to this, it can be applied to the problem by any of the unconstrained methods. In this thesis, penalty approach based on multi-objective optimization is considered to maximize the fundamental frequency and minimize the cost, simultaneously.

5.3. Stochastic Optimization Algorithms

Optimization methods can be categorized as traditional and non-traditional. Traditional methods, such as Lagrange Multipliers and Constrained Variation are analytical and find the optimum solution of only continuous and differentiable functions. Because composite design problems usually have discrete search spaces, the traditional optimization methods cannot be utilized. In these cases, the usage of stochastic optimization methods such as Simulated Annealing (SA), Genetic Algorithms (GA), Differential Evolution (DE) and Nelder-Mead (NM) are appropriate. A detailed discussion of different optimization methods is expressed in¹⁸⁸ for general application of

engineering and in Gurdal et al.¹⁸⁹ for composite design problems. In this thesis, DE, NM, RS and SA methods are used for defined optimizations problems of laminated composites and steps of the algorithms are briefly explained in the following subsections. Related parameters of the algorithms are listed in Table 5.1 used in adjusting the options correctly.

Table 5.1. Three optimization methods options (Source: Rao 1999¹⁸⁸)

Options Name	DE	NM	SA
CrossProbability	0.5	-	-
RandomSeed	0	5/1/2/5	0
ScalingFactor	0.6	-	-
SearchPoints	-	-	1000
Tolerance	0.001	0.001	0.001
ContractRatio	-	0.5	-
ExpandRatio	-	2.0	-
ReflectRatio	-	1.0	-
ShrinkRatio	-	0.5	-
LevelIterations	-	-	50
PerturbationScale	-	-	1.0

5.3.1. Differential Evolution Algorithm

Differential Evolution (DE) is a stochastic optimization method which permits alternative solutions for some of the complex composite design and optimization problems such as increasing frequency and frequency separation and obtaining lightweight design. Differential Evolution algorithm includes the following main stages: initialization, mutation, crossover and selection as shown in Figure 5.1. The optimum results of the algorithm change with the parameters: scaling factor, crossover and population size. Detail description of the DE can be found in¹⁹⁰. DE always considers a population of solutions instead of a single solution at each iteration and is also computationally expensive. It is relatively robust and efficient in finding global optimum of the objective function. However, it is not guaranteed to find the global optima.

The first step of DE optimization process is Initialization. There are several approaches to populate the initial generation. Random generation is widely used approach

for solution. In this step, the algorithm maintains a population of r points, $\{x_1, x_2, \dots, x_k, \dots, x_r\}$, where typically $r \gg m$, with m being the number of variables.

In second step, Mutation, a genetic operator that maintains the genetic variety from one generation of a population to the next generation. In mutation process, the solution can be different from the previous solution and thus a better solution can be gained. In third step, Crossover is used to obtain a richer population. Genetic diversity is encouraged by the interchange of genetic material between chromosomes and then, the gene strings of the related chromosomes are split at the same point in the parents and two parents create a child. Finally, the last step selection is applied and the new individual is added to the new population^{189,191,192}.

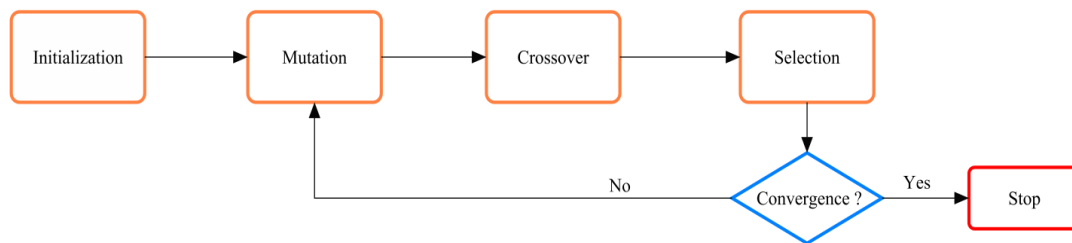


Figure 5.1. Flowchart of the DE algorithm (Source: Vo-Duy 2017⁸⁹)

5.3.2. Nelder-Mead Algorithm

The Nelder–Mead (simplex search) algorithm is a traditional local search method designed by Nelder and Mead (1965) firstly for unconstrained optimization problem⁴⁷. Although Nelder–Mead is not a global optimization algorithm, it is inclined to work fairly well for problems which do not have many local minima in practical usage. The adjustment of the algorithm options is controlled by four basic procedures: reflection, expansion, contraction and shrinkage. One of the characteristic properties of the algorithm is that NM often gives considerable improvements in the first few iterations and rapidly generates quite adequate results. Moreover, the method usually needs only one or two function evaluations per iteration, apart from shrink transformations, which are notably rare in practice. This is very important in applications that each function evaluation is very expensive or time-consuming. Furthermore, the simplex can vary its orientation, size and shape to adapt itself to the local contour of the objective function,

hence NM has high flexibility in exploring difficult domains ¹⁷⁴. The main steps of the algorithm are given in Figure 5.2.

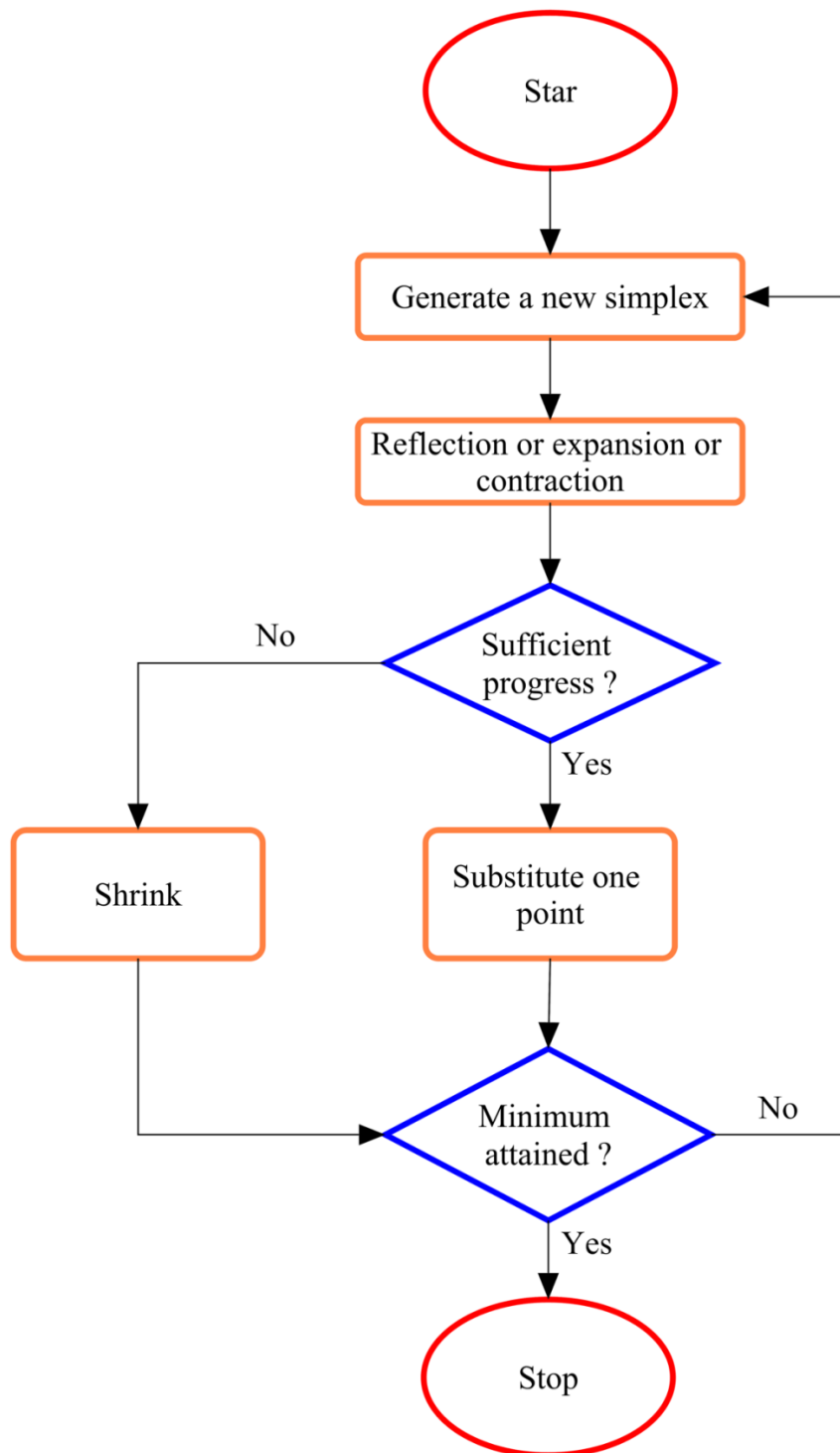


Figure 5.2. Flowchart of the NM algorithm (Source: Reza 2011¹⁹³)

5.3.3. Simulated Annealing Algorithm

One of the most popular random search methods is SA. It is based on the physical process of annealing, that a metal object is warmed up to a high temperature and permit to cool slowly. The melting process lets the atomic structure of the material to pass to a lower energy condition, hence that becoming a tougher material. From the view point of optimization, in SA algorithm, annealing process lets the structure to get away from a local minimum, and to explore and settle on a better global optimum point. The main advantage of SA is that that it enables to solve various optimization problems such as continuous, discrete or mixed-integer. In the working phase of this method, a new point is randomly produced at each iteration and when all stopping criteria are fulfilled the algorithm stops.

The space of the new point from the current point or the extent of the search is based on Boltzmann's probability distribution. The distribution implies the energy of a system in thermal equilibrium at temperature "T". Boltzmann's probability distribution can be expressed in the following form ¹⁸⁸:

$$P(E) = e^{-E/kT} \quad (4.1)$$

where $P(E)$ represents the probability of achieving the energy level E , k is the Boltzmann's constant, and T is temperature. In order to follow the procedure of the algorithm easily, the flowchart of a SA algorithm is presented in Figure 5.3.

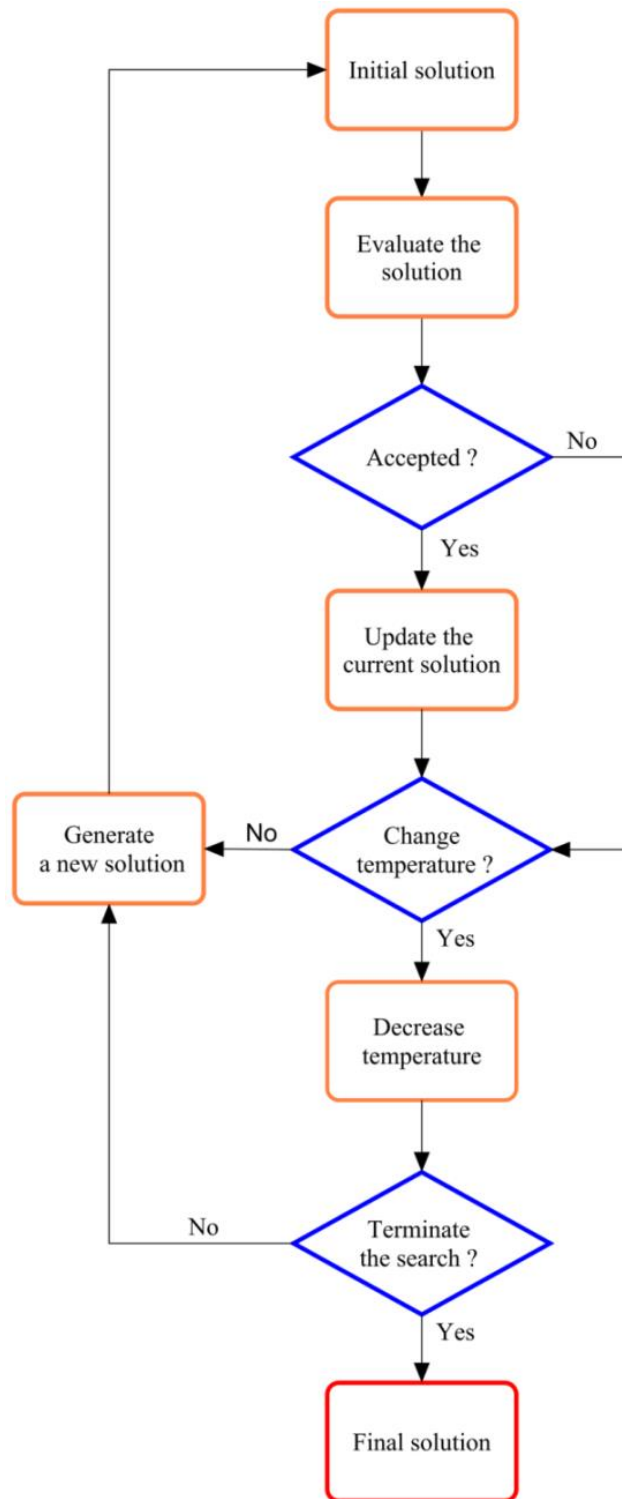


Figure 5.3. Flowchart of the SA algorithm. (Source: Pham 2012¹⁹⁴)

CHAPTER 6

VIBRATION PROBLEMS

6.1. Benchmark Problems

In this study, the non-dimensional natural frequencies of three-phase graphene/fiber-reinforced composite laminates have been maximized by using a number of design variables and then compared with optimum results from the literature for different problems. The objective functions of the problems are fundamental frequencies. There are two main optimization problems which are included in different design variables in this study. In the first problem, distributions of GPLs (Graphene Nano Platelets) are taken as design variables for fiber reinforced plates having uniform layer thicknesses. The total weight of GPLs is defined as a constraint. In the second problem, distributions of the GPLs and volume fraction of the fibers for each layer are used as design variables. The total volume content of fibres as well as the weight content of GPLs and the volume content of fibres in individual layers are utilized as constraints in the optimization problem.

The material properties and dimensions of the graphene nanoplatelets used in the benchmark problems is given in Table 6.1.

Table 6.1. Material Properties of the GPLs, matrix, flax carbon and glass fibers^{37,32}

Material	E_{11} (GPa)	E_{22} (GPa)	G_{12} (GPa)	ν_{12}	Density (kg/m ³)	Cost (\$)
GPL	1010	1010	425.80	0.186	1060	450
Matrix	3	3	1.119	0.34	1200	10
Carbon Fiber	263	19	27.60	0.20	1750	28
Flax Fiber	70	70	29.58	0.183	1400	0.5
Glass Fiber	72.4	72.4	30.66	0.20	2400	2

For the dimensions of the GPLs, $l_{GPL} = 2.5 \mu\text{m}$, $w_{GPL} = 1.5 \mu\text{m}$, $h_{GPL} = 1.5 \text{nm}$ are used.

In order to compare the results in all problems, the non-dimensional form of the fundamental frequency Ω is defined as

$$\Omega = \omega D \sqrt{\frac{\rho_M}{E_M}} \quad (6.1)$$

6.1.1. Problem B1

In problem B1, non-dimensionalized natural frequencies of the fiber-reinforced nanocomposite plates are maximized by using different stochastic algorithms (Differential Evolution Algorithm, Simulated Annealing Algorithm and Nelder Mead Algorithm) under the simply supported boundary conditions. The objective function is defined as non-dimensionalized natural frequency Ω included weight content (W_{GPLi}) of the GPLs for each layer and its sequences as design parameters. The aim of the problem is to compare present optimization results of the Differential Evolution Algorithm solution with results for same problem from the literature. There are two different stacking sequences used in the problem 1, $[0/90/0/90]_{anti-s}$ and $[90/0/90/0]_s$. The laminate is composed of $N=8$ layers and the thickness of each ply is 12.5 mm.

Problem 1 can be defined mathematically as

- Maximize: Non-dimensionalized Natural Frequency $\Omega_{max}(W_{GPL})$
- Constraints: $\frac{1}{8} \sum_{i=1}^8 W_{GPLi} \leq W_{GPLmax}$, $W_{GPLi} \geq 0$

Symmetric & Balanced weight fraction of GPLs sequences;

$[W_{GPL1}/W_{GPL2}/W_{GPL3}/W_{GPL4}]_s$

$t= 12.5$ mm, $N= 8$ ply, $W_{GPLmax}=1.25\%$, $1 < \Omega_{max} / \Omega_0$

In the definition, Ω_0 , W_{GPLi} and W_{GPLmax} shows the non-dimensionalized frequency with uniform graphene weight equal to 1.25% in all layers, weight of graphene platelets for the i^{th} layer and maximum graphene weight for the laminate.

In the results of problem 1, the optimization problems for maximum fundamental frequencies of graphene/fiber reinforced plates are solved by using the Differential Evolution Algorithm. As shown in Table 6.2, there is good agreement between the optimum solution results of the present solution and solution available in the literature³⁷. In Table 6.3, the design efficiency parameters are calculated to determine how the natural frequency is affected by the optimum sequence of the weight content of GPLs.

As a result of the computation for design efficiency factors, It can be seen that optimizing the added amount of the GPLs for each layer is provide a better solution than

adding an equal amount of GPLs to each layer. Therefore, in optimum design problems of the fiber and nano reinforcement composites, using the weight content of the GPLs as design variables might enhance the vibration behaviour of the structures.

Table 6.2. Comparison of optimum results for non-dimensionalized frequencies Ω of graphene/fiber reinforced nanocomposite plates, (for simply supported boundary condition with aspect ratio $a/b=1$)

Stacking Sequence	Fibre Content	Optimal W_{GPL} per layer [Present]	Optimal W_{GPL} per layer ³⁷	Ω_{max} [Present]	Ω_{max}^{37}
[0/90/0/90] anti-s	Glass 30%	[0.0476/0.0024/0/0]s	[0.048/0.0022/0/0]s	0.1749	0.1766
	Glass 60%	[0.0360/0.0140/0/0]s	[0.036/0.014/0/0]s	0.1762	0.1774
[90/0/90/0]s	Glass 30%	[0.0479/0.0021/0/0]s	[0.049/0.0017/0/0]s	0.1750	0.1767
	Glass 60%	[0.0359/0.0141/0/0]s	[0.036/0.014/0.0001/0]s	0.1762	0.1774
[0/90/0/90] anti-s	Carbon 30%	[0.0467/0.0033/0/0]s	[0.047/0.003/0/0]s	0.2019	0.2045
	Carbon 60%	[0.0332/0.0132/0.0036/0]s	[0.033/0.013/0.004/0]s	0.2202	0.2254
[90/0/90/0]s	Carbon 30%	[0.0466/0.0034/0/0]s	[0.047/0.003/0/0]s	0.2013	0.2068
	Carbon 60%	[0.0341/0.0120/0.0039/0]s	[0.034/0.012/0.004/0]s	0.2223	0.2275

Table 6.3. Comparison of design efficiency factors (Ω_{max} / Ω_0) of the optimum design for graphene/fiber reinforced nanocomposite plates, (for simply supported boundary condition with aspect ratio $a/b=1$)

Stacking Sequence	Fibre Contents	Optimal W_{GPL} per layer [Present]	Optimal W_{GPL} per layer ³⁷	Ω_{max} / Ω_0 [Present]	$\Omega_{max} / \Omega_0^{37}$
[0/90/0/90] anti-s	Glass 30%	[0.0476/0.0024/0/0]s	[0.048/0.0022/0/0]s	1.200	1.196
	Glass 60%	[0.0360/0.0140/0/0]s	[0.036/0.014/0/0]s	1.094	1.091
[90/0/90/0]s	Glass 30%	[0.0479/0.0021/0/0]s	[0.049/0.0017/0/0]s	1.200	1.196
	Glass 60%	[0.0359/0.0141/0/0]s	[0.036/0.014/0.0001/0]s	1.094	1.090
[0/90/0/90] anti-s	Carbon 30%	[0.0467/0.0033/0/0]s	[0.047/0.003/0/0]s	1.123	1.108
	Carbon 60%	[0.0332/0.0132/0.0036/0]s	[0.033/0.013/0.004/0]s	1.034	1.033
[90/0/90/0]s	Carbon 30%	[0.0466/0.0034/0/0]s	[0.047/0.003/0/0]s	1.112	1.108
	Carbon 60%	[0.0341/0.0120/0.0039/0]s	[0.034/0.012/0.004/0]s	1.035	1.034

The other significant result observed in problem B1, present optimization problems results demonstrate that the Differential Evolution algorithm and present analytical solution method can be utilized efficiently in order to make the optimum design of GPLs/fiber reinforced nanocomposites problems.

6.1.2. Problem B2

In Problem B2, non-dimensionalized natural frequencies of the fiber reinforced nanocomposite plates are maximized by using Differential Evolution Algorithm for the simply supported boundary conditions. The objective function is defined as non-dimensionalized natural frequency Ω included weight content sequences (W_{GPLi}) of the GPLs as well as fiber volume content of each ply (V_F) as design parameters. The aim of the problem is to compare present optimization results of the Differential Evolution Algorithm solution with results for same problem from the literature. There are two different stacking sequences used in the Problem 1, $[0/90/0/90]_{anti-s}$ and $[90/0/90/0]_s$. The laminate is composed of $N=8$ layers and the thickness of the each ply is 12.5 mm.

Problem 1 can be defined mathematically as

- Maximize: Non-dimensionalized Natural Frequency $\Omega_{max}(W_{GPL}, V_F)$

- Constraints: $\frac{1}{8} \sum_{i=1}^8 W_{GPLi} \leq W_{GPLmax}, W_{GPLi} \geq 0,$

$$\frac{1}{8} \sum_{i=1}^8 V_{Fi} \leq V_{Fmax}, V_{Fi} \geq 0$$

Symmetric weight fraction of GPLs sequences;

$$[W_{GPL1}/W_{GPL2}/W_{GPL3}/W_{GPL4}]_s$$

Symmetric volume of fiber sequences;

$$[V_{F1}/V_{F2}/V_{F3}/V_{F4}]_s, V_{Fmax} = 30\%,$$

$$t = 12.5 \text{ mm}, N = 8 \text{ ply}, W_{GPLmax} = 1.25\%, 1 < \Omega_{max} / \Omega_0$$

In the definition, $\Omega_0, W_{GPLi}, W_{GPLmax}$ and V_{Fmax} shows the non-dimensionalized frequency with uniform graphene weight equal to 1.25% in all layers, weight of graphene platelets for the i_{th} layer, maximum graphene weight for the laminate and maximum fiber volume content of the laminate equal to 30%, respectively.

In Table 6.4, the whole of the results of Problem 2 shows that the present analytical solution and Differential Evolution Algorithm as optimization method provide the same solution for maximizing the fundamental frequencies of graphene/fiber

reinforced plates in case they are compared with the study in the literature. Besides, optimizing fiber volume content in addition to the weight fraction of the GPLs at each layer delivers the increment in the design efficiency factor considering the Problem B1 results. The other outstanding result that the amount of the volume fraction and weight fraction of GPLs give a more increase in natural frequency in the case of arrangement with the high quantity at the top and bottom layers.

Table 6.4. Comparison of optimum results for non-dimensionalized frequencies Ω and design efficiency factors (Ω_{\max}/Ω_0) of GPLs/fiber reinforced nanocomposite plates, (Maximum fundamental frequencies with two design variables subjected to Stacking sequences $[0/90/0/90]_s$ with aspect ratio $a/b=1$)

Fiber	Results	Optimal W_{GPL} per layer	Optimal V_f per layer	Ω_{\max}	Ω_{\max}/Ω_0
Carbon	Present	[0.0416/0.0084/0/0]s	[0.46/0.74/0/0]s	0.2237	1.244
	Ref ³⁷	[0.042/0.008/0/0]s	[0.4/0.6/0.1/0.1]s	0.2209	1.192
Glass	Present	[0.0347/0.0153/0/0]s	[0.6/0.4/0.1/0.1]s	0.1852	1.271
	Ref ³⁷	[0.035/0.015/0/0]s	[0.6/0.4/0.1/.,1]s	0.1864	1.262

6.1.3. Problem B3

In Problem B3, three different stochastic optimization methods (Differential Evolution Algorithm, Simulated Annealing Algorithm, and Nelder Mead Algorithm) have been utilized in order to maximize the non-dimensionalized natural frequencies of the fiber-reinforced nanocomposite plates with the simply supported boundary conditions. The objective function is defined as non-dimensionalized natural frequency Ω included weight content (W_{GPLi}) of the GPLs for each layer and its sequences as design parameters. The objective of the problem is to make comparisons of present optimization results for DE, SA, and NM algorithm solutions with results from the literature for the same problem utilizing SQP. There are two different stacking sequences used in the Problem 1, $[0/90/0/90]_{\text{anti-s}}$ and $[90/0/90/0]_s$. The laminate is composed of $N=8$ layers and the thickness of the each ply is 12.5 mm.

Problem 1 can be defined mathematically as

- Maximize: Non-dimensionalized Natural Frequency $\Omega_{\max}(W_{GPL})$
- Constraints: $\frac{1}{8} \sum_{i=1}^8 W_{GPLi} \leq W_{GPL\max}, W_{GPLi} \geq 0$

Symmetric & Balanced weight fraction of GPLs sequences;

$$[W_{GPL1}/W_{GPL2}/W_{GPL3}/W_{GPL4}]_s$$

$$t= 12.5 \text{ mm, } N= 8 \text{ ply, } W_{GPLmax}=1.25\% , 1 < \Omega_{max} / \Omega_0$$

Algorithms: DE, SA and NM

In the definition, Ω_0 , W_{GPLi} and W_{GPLmax} show the non-dimensionalized frequency with uniform graphene weight equal to 1.25% in all layers, weight of graphene platelets for the i^{th} layer and maximum graphene weight for the laminate.

Table 6.5. Comparison of optimum weight fraction sequence results for non-dimensionalized frequencies Ω of graphene/fiber reinforced nanocomposite plates, (for simply supported boundary condition with aspect ratio a/b=1)

Case	V_f	[Differential Evolution] Optimal W_{GPL} per layer [Present]	[Nelder Mead] Optimal W_{GPL} per layer [Present]	[Simulated Annealing] Optimal W_{GPL} per layer [Present]	SQP Algorithm Optimal W_{GPL} per layer ³⁷
a	Glass 30%	[0.048/0.002/0/0]s	[0.048/0.002/0/0]s	[0.0346/0.0121/0.003/0]s	[0.048/0.0022/0/0]s
	Glass 60%	[0.0359/0.0141/0/0]s	[0.0359/0.0141/0/0]s	[0.0299/0.015/0.0033/0.0011]s	[0.036/0.014/0/0]s
b	Glass 30%	[0.0482/0.0018/0/0]s	[0.0482/0.0018/0/0]s	[0.0368/0.0089/0.0018/0.0012]s	[0.049/0.0017/0/0]s
	Glass 60%	[0.0359/0.0141/0/0]s	[0.0358/0.0142/0/0]s	[0.0262/0.0186/0.0051/0.0001]s	[0.036/0.014/0.0001/0]s
a	Carbon 30%	[0.0467/0.0033/0/0]s	[0.0467/0.0033/0/0]s	[0.0351/0.0137/0/0.0011]s	[0.047/0.003/0/0]s
	Carbon 60%	[0.0332/0.0133/0.0035/0]s	[0.0355/0.0145/0/0]s	[0.0263/0.0105/0.0115/0.0017]s	[0.033/0.013/0.004/0]s
b	Carbon 30%	[0.0466/0.0034/0/0]s	[0.0465/0.0035/0/0]s	[0.0332/0.0156/0.0001/0.0007]s	[0.047/0.003/0/0]s
	Carbon 60%	[0.0341/0.012/0.0039/0]s	[0.0365/0.0135/0/0]s	[0.0272/0.0127/0.0087/0.0005]s	[0.034/0.012/0.004/0]s

a=[0/90/0/90] anti-s, b=[0/90/0/90]s

In the results of Problem B3, the Differential Evolution, Simulated Annealing, and Nelder Mead Algorithms are utilized to solve the optimization problems for maximum fundamental frequencies of graphene/fiber reinforced plates. The optimal solutions of the present and the results that are already available in the literature are in good agreement, as demonstrated in Table 6.5 and Table 6.6. It is clear that three different algorithms, DE, NM, and SA, are capable of achieving precise designs for the multiscale nanocomposite plate optimization problems.

Table 6.6. Comparison of design efficiency factors (Ω_{\max} / Ω_0) of the optimum design for graphene/fiber reinforced nanocomposite plates, (for simply supported boundary condition with aspect ratio a/b=1)

	Algorithms	DE	NM	SA	SQP
Stacking Sequence	Fibre Contents	Ω_{\max} [Present]	Ω_{\max} [Present]	Ω_{\max} [Present]	Ω_{\max}^{37}
a	Glass 30%	0.1750	0.1750	0.1713	0.1766
	Glass 60%	0.1762	0.1762	0.1748	0.1774
b	Glass 30%	0.1753	0.1753	0.1709	0.1767
	Glass 60%	0.1762	0.1760	0.1745	0.1774
a	Carbon 30%	0.2016	0.2016	0.1991	0.2045
	Carbon 60%	0.2223	0.2219	0.2209	0.2254
b	Carbon 30%	0.2013	0.2013	0.1984	0.2068
	Carbon 60%	0.2223	0.2217	0.2211	0.2275

a=[0/90/0/90] anti-s, b=[0/90/0/90]s

Additionally, the optimum results show that the amount of weight fraction of the GPLs changed according to fiber volume fraction and fiber orientation angles. Therefore, combining the weight content of the GPLs and stacking sequences of the fiber orientation angles as design variables may improve the vibration behavior of the structures in optimum design issues of fiber and nano reinforcement composites. Finally, the DE, SA, and NM algorithms provide different configurations for the three-phase multiscale composite problem, thereby approximating the same level of optimal natural frequency.

6.1.4. Problem B4

In Problem B4 the comparison of the present analytical method and Finite element method (Autodesk Inventor NASTRAN) solutions are carried out with benchmark problem results from published literature³⁸. There are two main problems in this part to validate non-dimensional fundamental frequency of the present method and NASTRAN with numerical and ANSYS commercial software from the literature for two-phase e-glass fiber reinforced composite and e-glass fiber/carbon nanotubes (CNTs) reinforced nanocomposite. The description of the problems are given in Table 6.7. The material properties are given in Table 6.8.

In Problem B4.1, fundamental frequency of zero content of CNTs, only glass fiber reinforced plate is calculated for three different stacking sequences. In Problem B4.2, the same fundamental frequencies are calculated for multiphase E-glass fiber/CNTs reinforced nanocomposite plates with constant volume fraction of fiber content and weight content of CNTs in each layer with four different stacking sequences.

Table 6.7. General description of benchmark Problems B4

Reinforcement	Weight Content of Carbon Nanotube for plies	Glass Fiber	Methods
Problem B4.1	Zero	Present	CLPT FEM
Problem B4.2	Constant	Present	CLPT FEM

The non-dimensional form of the fundamental frequency ω_{11} is defined as $\bar{\omega}$ expressed in Equation (6.2):

$$\bar{\omega} = \omega_{11} \sqrt{\rho h / D_0} \quad (6.2)$$

$$D_0 = \frac{E_{11} H_0^3}{12(1 - \nu_{12}^2)}$$

where D_0 , ρ and h are the flexural rigidity, density and thickness of the plate.

Table 6.8. Material properties of the CNTs, matrix, glass fibers³⁸

Material	E_{11} (GPa)	G_{12} (GPa)	ν_{12}	Density(kg/m ³)
Carbon nanotubes	640	$E_{11}/(2(1+\nu))$	0.27	1350
Matrix	3.5	$E_{11}/(2(1+\nu))$	0.35	1200
Glass Fibers	72.4	$E_{11}/(2(1+\nu))$	0.20	2400

For the CNTs, $l_{CNT} = 25\mu\text{m}$, $d_{CNT} = 1.4\text{nm}$, $t_{CNT} = 0.34\text{nm}$ are used.

6.1.4.1. Problem B4.1

In Problem B4.1, the verification of the analytical method of solution in Wolfram Mathematica programming code is presented with analytical and numerical results from published literature.

Four-node shell elements have been used in the commercial software Autodesk NASTRAN based on the plate theory. These results are also compared to the numerical results obtained by using the commercial finite element software NASTRAN. For the presented simulations, the material properties are specified as $E_{11} = 60.7\text{GPa}$, $E_{22} = 24.8\text{GPa}$, $G_{12} = 12.0\text{GPa}$ and $\nu_{12} = 0.23$ for E-glass/epoxy square laminates studied in 87,88.

Table 6.9. Comparison of non-dimensional frequencies Ω obtained by analytical and numerical solution (Autodesk NASTRAN) with different methods from the literature for glass fiber reinforced with SSSS square plate

		Model
Stacking Sequences	Methods	Non-Dimensional Frequency
[0,0,0]	Present Method	14.950
	NASTRAN	14.945
	Anashpaul et al ³⁸	15.115
	ANSYS ³⁸	14.863
	Ref ¹⁹⁵	15.171
	Ref ¹⁹⁶	15.190
[15/-15/15]	Present Method	15.2981
	NASTRAN	15.258
	Anashpaul et al ³⁸	15.491
	ANSYS ³⁸	15.294
	Ref ¹⁹⁵	15.369
	Ref ¹⁹⁶	15.430
[30/-30/30]	Present Method	15.972
	NASTRAN	15.835
	Anashpaul et al ³⁸	16.215
	ANSYS ³⁸	15.902
	Ref ¹⁹⁵	15.583
	Ref ¹⁹⁶	15.900
[45/-45/45]	Present Method	16.298
	NASTRAN	16.039
	Anashpaul et al ³⁸	16.566
	ANSYS ³⁸	16.249
	Ref ¹⁹⁵	16.082
	Ref ¹⁹⁶	16.140

In the analysis results, the non-dimensional frequency values for various stacking sequences demonstrate consistent variance, aligning with angle variations documented in previous studies within the literature. Furthermore, these results in Table 6.9 have been methodically compared to numerical outcomes derived from the widely used commercial finite element analysis software, NASTRAN, to validate the findings and ensure their reliability and accuracy within the context of existing research.

6.1.4.2. Problem B4.2

In Problem B4.2, the non-dimensional natural frequencies of three-phase CNTs-Glass fiber reinforced laminates are calculated using analytical methods and the NASTRAN FEM commercial solver software. These calculated natural frequencies are then compared with recent results found in the literature to verify the accuracy and validity of the methodology employed.

Problem B4.2 can be defined mathematically as

- Calculate: Non-dimensionalized Natural Frequency $\bar{\omega}(\theta_i, W_{CNTi}, V_F)$
 $N= 3 \text{ ply}, a \times b \times h= 1 \times 1 \times 0.001 \text{ m (dimension of the plate)}$

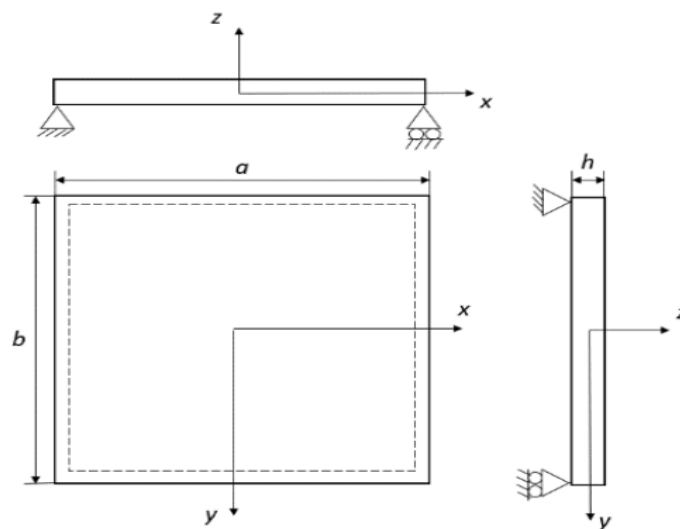


Figure 6.1. Dimensions and boundary conditions of plate (Source: Anashpaul 2023³⁸)

The non-dimensional frequency values across various compositions of CNT content, glass fiber volume fractions, and stacking sequences display consistent variance

and align with changes in angle reported in existing literature see in Table 6.10. This consistency indicates that both the present analytical method and the NASTRAN FEM solver are effectively capable of calculating natural frequencies for configurations with varying weights of carbon nanotubes. This demonstrates the robustness and adaptability of these methods in addressing the complexities of composite material behaviour.

Table 6.10. Comparison of non-dimensional frequencies Ω obtained by analytical and FEM solutions (NASTRAN) with different methods from the literature for CNT/glass fiber reinforced with SSSS square plate

Material Content	Stacking Sequence	Present Study	NASTRAN	Anashpaul et al ³⁸	ANSYS ³⁸
VF= 0,3 Wcnt=0.05	[0/0/0]	16.620	16.450	16.599	16.426
	[-15/15/15]	16.897	16.880	16.901	16.782
	[30/-30/30]	17.378	17.590	17.457	17.359
	[45/-45/45]	17.614	17.900	17.687	17.678
VF= 0,3 Wcnt=0.01	[0/0/0]	13.858	13.980	13.632	13.172
	[-15/15/15]	14.455	14.555	14.210	13.791
	[30/-30/30]	15.581	15.648	15.223	14.727
	[45/-45/45]	16.114	16.250	15.490	15.294
VF= 0,6 Wcnt=0.01	[0/0/0]	13.481	13.650	13.055	13.25
	[-15/15/15]	14.135	14.189	13.700	14.177
	[30/-30/30]	15.361	15.450	14.736	15.423
	[45/-45/45]	15.9382	15.975	15.041	15.996

6.1.5. Problem B5

In Problem B5, the minimum weight design problem of CNT/fiber-reinforced laminates, featuring uniform layer thicknesses and non-uniform distribution of reinforcements, is addressed under a frequency constraint, brief description of problem are given in Table 6.11. Optimal designs for three-phase, CNT/fiber-reinforced composite laminates are developed to maximize fundamental frequency. These designs incorporate various design variables and parameters and utilize advanced optimization techniques such as Differential Evolution (DE), Simulated Annealing (SA), and Nelder Mead (NM) algorithms. The primary objective of this study is to compare the optimization results obtained from the DE, SA, and NM algorithms with those from the Sequential Quadratic Programming (SQP) method documented in the literature, thus evaluating the

effectiveness and efficiency of these contemporary optimization approaches in solving complex engineering problems.

Table 6.11. Description of the optimization problems

Purpose	Material	Objective	Methods	Design Variables
Minimum weight design problem of CNT/Fiber reinforced laminates for frequency constraint	Glass/ CNT /Epoxy	Weight	DE SA NM	$[\theta_1, \theta_2, \theta_3, \theta_4]_s$ $[W_{CNT1}/ W_{CNT2}/ W_{CNT3}/ W_{CNT4}]_s$ $[V_{F1}/ V_{F2}/ V_{F3}/ V_{F4}]_s$

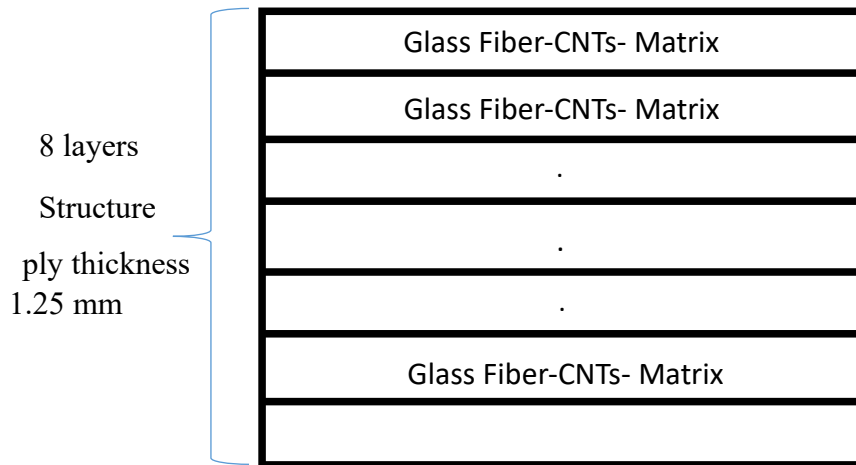


Figure 6.2. Glass fiber/CNTs reinforced nanocomposite plate

Problem B5 can be defined mathematically as

- Minimize: $W_L(\theta_i, W_{CNTi}, V_{Fi})$
- Constraints: $90^\circ \geq \theta_i \geq 0^\circ, \frac{1}{8} \sum_{i=1}^8 W_{CNTi} \leq W_{CNTmax}, W_{GPLi} \geq 0$
 $, W_{CNTmax}=1.25\%, V_{Fk} \leq 0.6, b/a = 1, \Omega_0 \leq \omega_{11}/\omega_{IP}$
 $\theta_i \in \{0^\circ, \pm 15^\circ, \pm 30^\circ, \pm 45^\circ, \pm 60^\circ, \pm 75^\circ, \pm 90^\circ\}$
Symmetric stacking sequences; $[\theta_1, \theta_2, \theta_3, \theta_4]_s$
Symmetric weight fraction of CNT sequences;
 $[W_{CNT1}/W_{CNT2}/W_{CNT3}/W_{CNT4}]_s$
Symmetric volume fraction of Glass Fiber;
 $[V_{F1}/ V_{F2}/ V_{F3}/ V_{F4}]_s$
Algorithms; DE, SA and NM

In the definition, ω_{IP} and ω_{11} shows the frequency of the isotropic plate of the same thickness as the minimum weight laminate made of the matrix material only and the fundamental frequency of CNT-Glass fiber reinforced composite plate, respectively.

For frequency constraints of 1.25, 1.3, and 1.5, the optimal configurations involve zero fiber content in all layers, with the addition of carbon nanotube (CNT) reinforcements alone meeting the frequency requirements for a minimum weight design. As the frequency constraints increase further, CNT reinforcements alone become inadequate, necessitating an increase in fiber contents across all layers, particularly in the surface layers, to satisfy these higher demands.

Table 6.12. Comparison of the optimum stacking sequences result of the weight minimization problem for DE, SA and NM algorithms with SQP³⁸ method for different frequency constraints Ω_0

Ω_0	Fiber Angles			
	DE	SA	NM	SQP ³⁸
1.25	[90/90/90/90] _s	[90/90/90/90] _s	[-45/-45/30/-60] _s	[45/45/30/45] _s
1.30	[90/90/90/90] _s	[90/-75/-75/75] _s	[90/75/90/60] _s	[45/45/30/45] _s
1.50	[90/90/90/90] _s	[45/75/90/90] _s	[-45/90/-45/30] _s	[45/45/30/45] _s
1.75	[45/-75/90/90] _s	[45/90/-30/-75] _s	[45/45/90/-45] _s	[45/45/30/45] _s
2.00	[-45/90/-75/-75] _s	[-45/-45/90/-45] _s	[-45/90/-75/90] _s	[45/60/0/30] _s
2.20	[45/90/0/90] _s	[45/90/90/30] _s	[45/-45/90/90] _s	[45/0/0/30] _s
2.40	[45/-45/90/-75] _s	[-45/30/-75/-75] _s	[45/45/90/0] _s	[45/45/30/45] _s
2.50	[-45/-45/90/90] _s	[45/45/45/45] _s	[45/45/90/90] _s	[45/45/90/45] _s

Table. 6.13. Comparison of the optimum volume fraction design results for each layer in the weight minimization problem using DE, SA, and NM algorithms versus the SQP method for different frequency constraints Ω_0 .

Ω_0	Volume Fraction of Fiber (V_{fk}) per Layer			
	DE	SA	NM	SQP ³⁸
1.25	[0/0/0/0] _s	[0/0/0/0] _s	[0.104/0.02/0/0] _s	[0/0/0/0] _s
1.30	[0/0/0/0] _s	[0/0/0/0] _s	[0.102/0.004/0/0] _s	[0/0/0/0] _s
1.50	[0/0/0/0] _s	[0.101/0/0/0] _s	[0.179/0.004/0.002/0.01] _s	[0/0/0/0] _s
1.75	[0.073/0/0/0] _s	[0.184/0.03/0/0] _s	[0.202/0.031/0/0] _s	[0.063/0/0/0] _s
2.00	[0.0499/0.0001/0/0] _s	[0.452/0/0/0] _s	[0.6/0/0/0.002] _s	[0.26/0/0/0] _s
2.20	[0.47/0/0/0] _s	[0.6/0/0/0] _s	[0.6/0.589/0/0.007] _s	[0.44/0/0/0] _s
2.40	[0.6/0.228/0/0] _s	[0.6/0.6/0/0] _s	[0.6/0.6/0.001/0.052] _s	[0.6/0.08/0/0] _s
2.50	[0.6/0.6/0/0] _s	[0.6/0.6/0/0] _s	[0.597/0.528/0/0.065] _s	[0.6/0.47/0/0] _s

The optimization process not only determines the most efficient stacking sequences but also ensures optimal distribution of fibers and CNTs within the laminate. The impact of escalating frequency constraints on achieving minimum weight is detailed and analyzed with corresponding results displayed in the Table 6.15. This approach helps identify the trade-offs between weight minimization and frequency compliance in composite laminate design.

Table 6.14. Comparison of the DE, SA, and NM algorithms' optimum weight content designs per layer in the weight minimization problem with the SQP approach for various frequency constraints Ω_0

Ω_0	Wcnt per layer			
	DE	SA	NM	SQP ³⁸
1.25	[0.0162/0/0/0]s	[0.0063/0.0183/0.0035/0.0088]s	[0.0004/0/ 0.001/0.0001]s	[0.009/0.011/0.007/0.023]s
1.30	[0.0198/0.0001/0/0]s	[0.0115/0.0077/0.0024/0.0115]s	[0.0003/0.0112/0.0339/0.0042]s	[0.013/0/0.037/0]s
1.50	[0.0359/0/0/0]s	[0.017/0.0084/0.0058/0.0018]s	[0.0023/0.0115/0.0261/0.0092]s	[0.036/0/0/0.014]s
1.75	[0.0499/0.0001/0/0]s	[0.0344/0/0.0105/0.0038]s	[0.0249/0.0097/0.0152/0]s	[0.05/0/0/0]s
2.00	[0.286/0/0/0]s	[0.0145/0.0203/0.0021/0.0067]s	[0.0033/0.0024/0.0037/0.0001]s	[0.05/0/0/0]s
2.20	[0.05/0/0/0]s	[0.0244/0.0102/0.0017/0.0023]s	[0.0011/0.0017/0/0]s	[0.05/0/0/0]s
2.40	[0.05/0/0/0]s	[0.0266/0.0186/0.0008/0.0005]s	[0.0135/0.0358/0.0007/0]s	[0.05/0/0/0]s
2.50	[0.05/0/0/0]s	[0.05/0/0/0]s	[0.0478/0/0/0.0022]s	[0.05/0/0/0]s

Table 6.15. Comparison of the DE, SA, and NM algorithms' minimum weight results for structures in the weight minimization problem with the SQP approach for various frequency constraints

Ω_0	Weight				Reference Weight				Design Efficiency Factor			
	DE	SA	NM	SQP ³⁸	DE	SA	NM	SQP ³⁸	DE	SA	NM	SQP ³⁸
1.25	12.006	12.012	12.370	12.020	15.005	15.060	14.990	15.000	0.801	0.798	0.825	0.801
1.30	12.007	12.011	12.330	12.020	15.600	15.004	15.600	15.600	0.769	0.800	0.790	0.770
1.50	12.012	12.314	12.600	12.020	18.001	18.030	18.250	18.000	0.667	0.683	0.690	0.667
1.75	12.230	12.658	12.710	12.210	1.750	21.220	21.000	21.000	0.583	0.596	0.605	0.581
2.00	12.870	13.370	13.800	12.790	24.000	24.000	24.000	24.000	0.536	0.559	0.605	0.533
2.20	13.420	13.810	15.580	13.330	26.400	26.400	26.180	26.400	0.508	0.521	0.595	0.505
2.40	14.500	15.610	15.770	14.060	28.800	28.800	28.600	28.800	0.500	0.541	0.551	0.488
2.50	15.610	15.670	15.586	15.220	30.000	29.850	29.300	30.000	0.522	0.525	0.532	0.507

As shown in Tables 6.12, 6.13, 6.14 and 6.15 (the results of the Problem B5), the design efficiency decreases as the frequency constraint increases, indicating that the weight of the optimum laminate improves over an isotropic plate at the same frequency constraint.

It shows a good agreement between the optimum solution results of the present algorithms (DE, SA and NM) and available in the literature. Using the weight content of the CNTs and volume fraction of fiber besides stacking sequences as design variables might enhance lightweight structures having better vibration behaviour of the structures. It is clear that three different algorithms, DE, NM, and SA, are capable of achieving different design configurations for the multiscale nanocomposite plate optimization problems.

6.1.6. Problem B6

In this study's chapter, there are a pair of two issues with determining the natural frequency for CNTs-reinforced composite plates and FGM-GNPs, including agglomeration effects. Using the Halpin Tsai Model and FSDT, the functionally graded GNPs composite plate problems for assessing fundamental frequency are solved in the first problem. In the second problem, the Eshelby Mori Tanaka model is implemented to compute Young's modulus of the carbon nanotube-reinforced composite and compare the results to analytical and experimental results from the literature.

6.1.6.1. Problem B6.1

The GPL weight fraction demonstrates layer-wise change to produce a functionally graded structure. Four different GPL distribution patterns which is given Figure 6.3 are taken into consideration in order to investigate the effect of GPL distribution on the dynamic performance of the GPL/polymer plate, of which Pattern 1 is a special case corresponding to an isotropic homogeneous plate in which GPLs are uniformly distributed at the same w.t.% across all layers. Patterns 2-4 all show a graded material composition where the GPL weight fraction varies linearly from layer to layer throughout the plate thickness. In Pattern 2, the GPL weight fraction decreases from the highest in the mid plane to the lowest on the plate's top and bottom surfaces, whereas in

Pattern 3, the weight fraction is maximum on the top and bottom surfaces and the lowest at the plate's mid plane. Additionally, Patterns 2 and 3 are both symmetric; however, Pattern 4 is not, and in Pattern 4, the GPL weight percentage rises linearly from the top surface to the bottom surface.

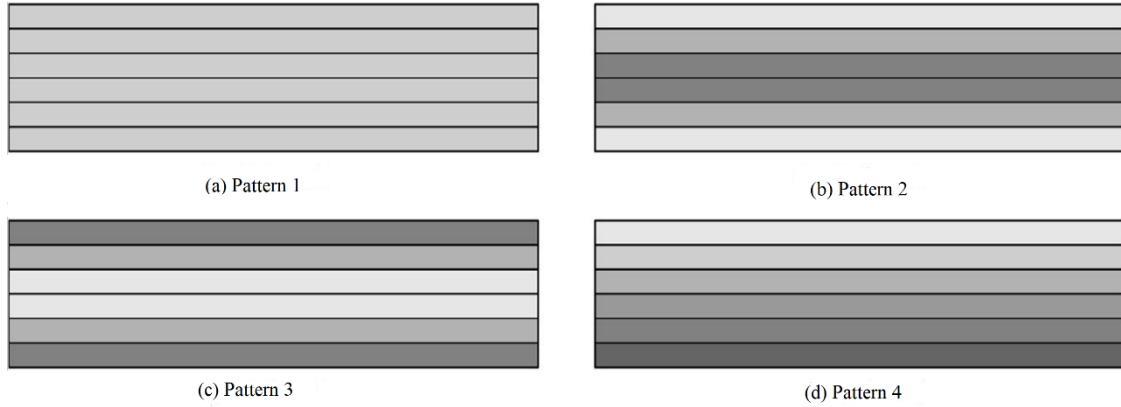


Figure 6.3. Different GPL distribution patterns¹⁹⁷

In the Problem B6.1, material properties of the functionally graded GNPs composite plates are calculated by using modified Halpin-Tsai material model. First order shear deformation plate theory (FSDT) and Navier-solution based technique is utilized to obtain the natural frequencies response of the simply supported plate. The goal is to conduct a non-dimensional natural frequencies analysis of GNPs reinforced plates for various patterns (UD, FG-X, FG-V, FG-O) and compare the results with those that are reported in the literature. The laminate is composed of $N=10$ layers and the total thickness of the laminate is 0.045 m. And the plate ($a \times b \times h = 0.45 \times 0.45 \times 0.045$) is reinforced with graphene nanoplatelets that properties are given; $l_{GPL} = 2.5 \mu\text{m}$, $w_{GPL} = 1.5 \mu\text{m}$, $h_{GPL} = 2.5 \mu\text{m}$, $\rho_{GPL} = 1.06 \text{ g/cm}^3$, $E_{GPL} = 1.01 \text{ TPa}$, $\nu_{GPL} = 0.186$. The epoxy matrix properties are also given as; $E_M = 3.0 \text{ GPa}$, $\rho_M = 1.2 \text{ g/cm}^3$ and $\nu_M = 0.34$.

The comparison results of the FG-GNP plate's natural frequencies for just epoxy and the UD, FG-X, FG-0, and FG-V patterns are shown in Table 6.16. The mode forms' m and n parameters indicate how many half-waves are present in the x and y directions.

It is clear that the present method is capable of offering outcomes that are very comparable as well. Another outcome is that, compared to other grading methods, FG-X epoxy plate attained the highest fundamental frequency. Therefore, using a high amount of GPLs at the top and bottom surfaces as well as a low amount of GPLs at the middle surfaces of the plate, is the most effective way to increase natural frequencies.

Table 6.16. Comparison of the effect of GPL distribution patterns on dimensionless natural frequencies ($\bar{\omega} = \omega t \sqrt{\rho_m/E_m}$) according to different mode shapes

Modes (m,n)	Neat Epoxy		UD		FG-X		FG-V		FG-O	
	Present	Ref. 197	Present	Ref. 197	Present	Ref. 197	Present	Ref. ¹⁹⁷	Present	Ref. 197
1,1	0.0588	0.058	0.122	0.122	0.141	0.141	0.117	0.117	0.097	0.097
2,1	0.141	0.139	0.293	0.290	0.334	0.331	0.281	0.265	0.236	0.234
2,2	0.217	0.213	0.450	0.444	0.509	0.503	0.436	0.41	0.368	0.363
3,1	0.265	0.260	0.553	0.540	0.618	0.612	0.534	0.501	0.453	0.447
3,2	0.334	0.325	0.695	0.677	0.771	0.76	0.675	0.625	0.576	0.564
3,3	0.419	0.426	0.872	0.887	0.96	0.969	0.851	0.824	0.732	0.749

6.1.6.2 Problem B6.2

In Problem B6.2, Young's modulus of the functionally graded CNTs composites is determined by using the Eshelby-Mori Tanaka model, including the agglomeration effect to compare experimental results from the literature. The Hill's moduli of the CNTs considered for this purpose are listed in Table 6.17.

Table 6.17. Hill's moduli of SWCNT

Hill's Elastic Moduli of the SWCNT(GPa) ⁵⁹	
k_r	271
l_r	88
m_r	17
n_r	1089
p_r	442
Density(kg/m ³)	1400

In this instance, the matrix's material's elastic characteristics are $E_m = 0.85$ GPa and $\nu_m = 0.3$. The results of experiments conducted by Odegard et al.⁶⁰, in which the material properties of the present materials were investigated for various values of volume fraction of the reinforcement, served as the basis for this research.

The Eshelby Mori-Tanaka model is capable of estimating experimental results⁶⁰ of Young's modulus with good agreement, in which $\mu = 0.4$ considering a complete agglomerated model where $\eta = 1$, as shown in Figure 6.4. It shows that the employed

agglomeration model based on the EMT method is in good agreement with the prior literature because all CNTs are found in inclusions. It is possible to see that as μ decreases, the increase in the CNT volume fraction does not correspond to the expected increase in mechanical performance due to the severity of the agglomeration effect, using the fully dispersed case as a reference, $\mu = 1$, where Young's modulus has the higher increase in function of the volume fraction.

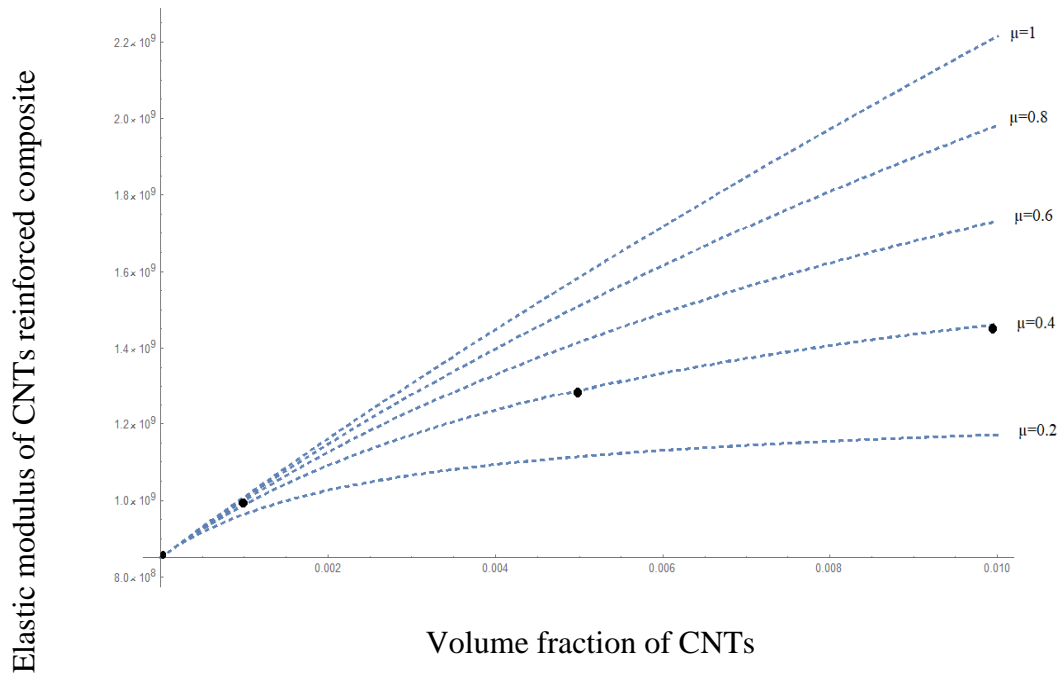


Figure 6.4. Young's modulus of the CNT reinforced matrix for different agglomeration factor and comparison with experimental and analytical results^{60,61}

6.2. Single-Objective Problems

In industrial applications such as automobiles, aircraft and construction, there is a demand for lightweight and cheaper materials having good mechanical properties like high natural frequency and sound reduction ability. To meet these requirements, there is general tendency in investigations on the usage of nanofillers with fiber reinforcement composites and hybridization of the different fiber (one is cheaper than) types in the same matrix materials.

In this chapter of the study, there are four main optimization problems which are solved by the Differential evolution algorithm to see the effect of the hybridization and nano reinforcement on natural frequency, weight and cost. Laminated composite plate under consideration is as shown in Figure 6.5 which has the length a , width b and a total thickness of D in the x , y and z -directions, respectively.

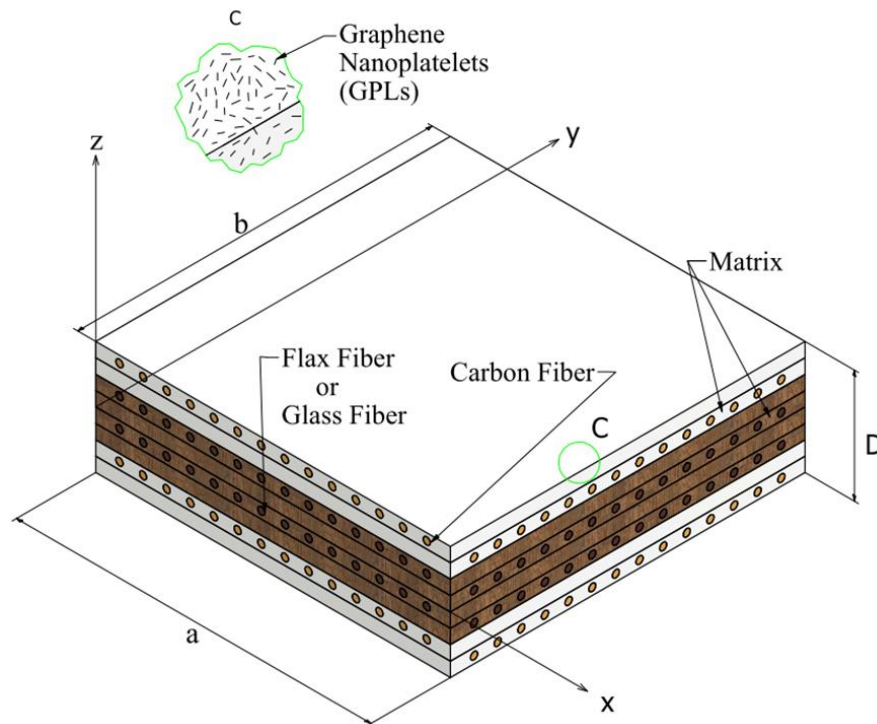


Figure 6.5. Schematic illustration of a unidirectional fiber-reinforced composite laminate

In the first problem, the Carbon, Glass and Flax fiber reinforced composites problems for maximum fundamental frequency are solved to find optimum stacking sequences without nano reinforcement in matrix materials and hybridization of the fibers. In the second problem, the natural frequencies of the composite plates are maximized in order to see the only hybridization of the fibers effect on the fundamental frequencies of the composite plates. As the third problem of this part of the study, the maximum fundamental frequencies of the fiber and graphene nanoplatelets reinforced nanocomposite plates are obtained by using the Differential Evolution algorithm to see the effects of the nano reinforcement on frequencies for fiber-reinforced composite plates. In the last problem, to see the total effects of the hybridization and nano reinforcement

on the natural frequencies of fiber-reinforced composites, the fundamental frequency is maximized as the objective function in each optimization problem.

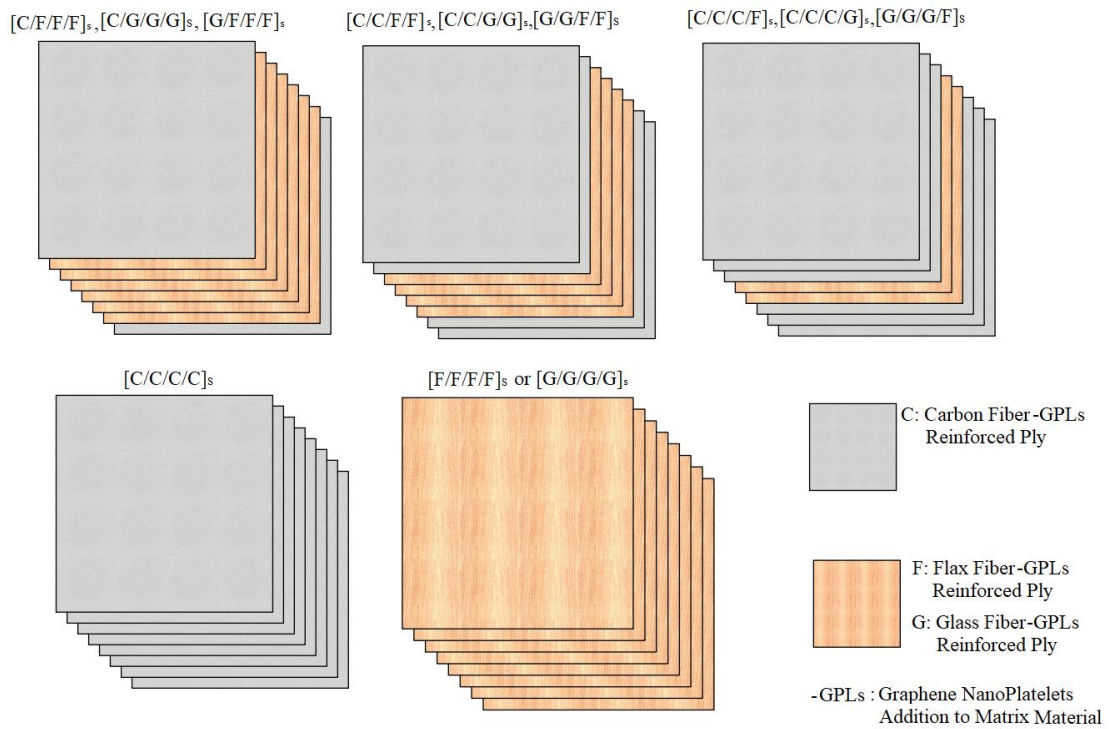


Figure 6.6. Illustration of the symbols for inter ply hybrid fiber/GPLs reinforced nanocomposites layer by layer

Table 6.18. Material properties of the GPLs, matrix, flax carbon and glass fibers^{32,37,198}

Material	E_{11} (GPa)	E_{22} (GPa)	G_{12} (GPa)	ν_{12}	Density (kg/m ³)	Cost (\$)
GPL	1010	1010	425.80	0.186	1060	450
Matrix	3	3	1.119	0.34	1200	10
Carbon Fiber	263	19	27.60	0.20	1750	28
Flax Fiber	70	70	29.58	0.183	1400	0.5
Glass Fiber	72.4	72.4	30.66	0.20	2400	2

For the dimensions of the GPLs, the following values are used: $l_{GPL} = 2.5 \mu\text{m}$, $w_{GPL} = 1.5 \mu\text{m}$, $h_{GPL} = 1.5 \text{nm}$.

The symbols associated with these issues can be illustrated with reference to Figure 6.6. In this subsection, the following demonstration is employed for hybrid and non-hybrid single-objective optimization problems. A comprehensive summary of the

aforementioned issues is also presented in Table 6.18. The material properties and dimensions of the graphene nanoplatelets used in the single-objective problems are given in Table 6.19.

Table 6.19. Description of the optimization problems

Prob. No	Purpose	Material	Objective Function	Design Variables
1	Optimum Stacking Sequences Design of the fiber reinforced composite plates	Carbon/Epoxy Glass/Epoxy Flax/Epoxy	Fundamental Frequency	$[\theta_1, \theta_2, \theta_3, \theta_4]_s$
2	Optimum Stacking Sequences Design of the hybrid Natural Fiber Reinforced Composite Plates	Carbon-Flax/Epoxy Glass- Flax /Epoxy	Fundamental Frequency	$[\theta_1, \theta_2, \theta_3, \theta_4]_s$
3	Optimum Design of the Graphene Nanoplatelets Fiber Reinforced nanocomposite Plates	Carbon/GPLs/Epoxy Glass /GPLs/Epoxy Flax/GPLs/Epoxy	Fundamental Frequency	$[\theta_1, \theta_2, \theta_3, \theta_4]_s$ $[W_{GPL1}/W_{GPL2}$ $/W_{GPL3}/W_{GPL4}]_s$
4	Optimum Design of the Graphene Nanoplatelets hybrid natural Fiber Reinforced nanocomposite Plates	Carbon-Flax/GPLs/Epoxy Carbon-Glass/GPLs/Epoxy Glass-Flax/GPLs/Epoxy	Fundamental Frequency	$[\theta_1, \theta_2, \theta_3, \theta_4]_s$ $[W_{GPL1}/W_{GPL2}$ $/W_{GPL3}/W_{GPL4}]_s$

6.2.1. Problem 1

In design Problem 1, non-dimensionalized natural frequencies of the fiber reinforced composite plates are maximized by using different stochastic algorithms (Differential Evolution Algorithm, Simulated Annealing Algorithm and Nelder Mead Algorithm) under the simply supported boundary conditions. The objective function is defined as non-dimensionalized natural frequency Ω included fiber orientation angle (θ_i) of each layer as design parameters. The aim of the problem is to propose the basic optimum design results of the Carbon/Glass and Flax reinforced composite plates in order to compare the next problem results for seeing the effect of hybridization and nano reinforcement on natural frequency. The laminate is composed of N=8 layers and the thickness of each ply is 12.5 mm.

Problem 1 can be defined mathematically as

- Maximize: Non-dimensionalized Natural Frequency $\Omega_{max}(\theta_i)$
- Constraints: $90^\circ \geq \theta_i \geq 0^\circ$, $t= 12.5$ mm, $N= 8$ ply
Symmetric stacking sequences; $[\theta_1, \theta_2, \theta_3, \theta_4]_s$
 $\theta_i \in \{0^\circ, 15^\circ, 30^\circ, 45^\circ, 60^\circ, 75^\circ, 90^\circ\}$

In the definition, θ_i shows the fiber orientation angles for each layer.

Table 6.20. Optimum stacking sequences results of the carbon, flax and glass fiber reinforced composite plates

Fibre Composition	Natural Frequency (Ω_{max})	Optimum Stacking Sequence	Weight (kg)	Cost (\$)
Carbon	0,166961	[-45/-45/-45/-45]s	136,500	2102,10
Flax	0,113960	[-45/-45/-45/-45]s	126,000	900,00
Glass	0,103555	[-45/-45/-45/-45]s	156,000	1185,00

In a result of the optimization Problem 1, carbon fiber reinforced composite plate case provide the highest natural frequency for the same problem if it is compared with Flax and Glass fiber reinforcement cases. Nevertheless, the cost of the carbon fiber reinforced composite plate is more than others as seen in Table 6.20. The other result shows that Flax came forward as a more advantageous important material when it is compared with glass fiber reinforced case in the view of cost-to-weight ratio, price and biodegradability. Therefore, in Problems 3 and 4, in the outer layer carbon fiber is utilized at the top and bottom layers to achieve the maximum fundamental frequency of either glass or flax fibers with a hybridization effect.

6.2.2. Problem 2

In the optimization Problem 2, non-dimensionalized natural frequencies of the hybrid fiber reinforced composite plates are maximized by using different stochastic algorithms (Differential Evolution Algorithm) under the simply supported boundary conditions. The objective function is defined as non-dimensionalized natural frequency Ω included fiber orientation angle (θ_i) of each layer as design parameters. In the outer layers, carbon fibre is used, while in the inner layer, flax or glass fibre is considered due to the advantage of

the design, as discussed in the study³⁰. It is related that the best option is to choose high volume content of fiber and weight content of GPLs at the top and bottom layers giving better natural frequencies. The laminate is composed of N=8 layers and the thickness of each ply is 12.5 mm. In the definition, θ_i shows the fiber orientation angles for each layer.

Problem 2 can be defined mathematically as

- Maximize: Non-dimensionalized Natural Frequency $\Omega_{max}(\theta_i)$
- Constraints: $90^\circ \geq \theta_i \geq 0^\circ$, $t = 12.5$ mm, $N = 8$ ply,
Symmetric stacking sequences; $[\theta_1, \theta_2, \theta_3, \theta_4]_s$
 $\theta_i \in \{0^\circ, \pm 15^\circ, \pm 30^\circ, \pm 45^\circ, \pm 60^\circ, \pm 75^\circ, \pm 90^\circ\}$

As a result of optimization Problem 2, the natural frequencies of the cases in which Carbon-Flax reinforced indicate better solutions than Carbon-Glass fiber reinforced plates in terms of weight and cost. For the [C/C/C/F]_s case, it obtained higher fundamental frequency than the c-only carbon fiber reinforced case with low cost 14,2% and lightweight 2%.

Table 6.21. Optimum stacking sequences results of the carbon-flax and carbon-glass fiber reinforced composite plates

Fibre Composition	Fiber Sequences for each layer	Optimum Stacking Sequence	Natural Frequency (Ω_{max})	Weight (kg)	Cost (\$)
Carbon-Flax	[C/F/F/F] _s	[-45/45/-45/45] _s	0.153797	128.625	1201.20
Carbon-Flax	[C/C/F/F] _s	[45/45/45/-45] _s	0.166000	131.250	1501.50
Carbon-Flax	[C/C/C/F] _s	[45/45/-45/45] _s	0.168395	133.875	1801.80
Carbon-Glass	[C/G/G/G] _s	[45/-45/-45/45] _s	0.142385	151.125	1414.25
Carbon-Glass	[C/C/G/G] _s	[-45/-45/45/45] _s	0.157526	146.250	1643.85
Carbon-Glass	[C/C/C/G] _s	[-45/-45/45/45] _s	0.163990	141.375	1872.98

In Table 6.21, it is also provided that the low cost 28.6% and lightweight 3.8% design can be achieved by sacrificing just 0.6% natural frequency for [C/C/F/F]_s case. The other important issue is that Flax fiber might be applied more advantageously in the lightweight composite design with Carbon instead of Glass fiber for biodegradability and low carbon emissions in the structures.

6.2.3. Problem 3

In the optimization Problem 3, non-dimensionalized natural frequencies of the hybrid fiber reinforced composite plates are maximized by using different stochastic algorithms (Differential Evolution Algorithm) under the simply supported boundary conditions. The objective function is defined as non-dimensionalized natural frequency Ω included fiber orientation angle (θ_i) of each layer as design parameters. In the outer layers, carbon fiber is used whereas in the inner layer flax or glass fiber is considered due to the being of results coming from the chapter 4 problems. It is related that the best option is to choose high volume content of fiber and weight content of GPLs at the top and bottom layers giving better natural frequencies. The laminate is composed of N=8 layers and the thickness of each ply is 1.25 mm.

Problem 3 can be defined mathematically as

- Maximize: Non-dimensionalized Natural Frequency $\Omega_{max}(\theta_i, W_{GPLi})$
- Constraints: $90^\circ \geq \theta_i \geq 0^\circ$, $t = 1.25$ mm, $N = 8$ ply

Symmetric stacking sequences; $[\theta_1, \theta_2, \theta_3, \theta_4]_s$

Symmetric weight fraction of GPLs sequences;

$[W_{GPL1}/W_{GPL2}/W_{GPL3}/W_{GPL4}]_s$,

$\theta_i \in \{0^\circ, \pm 15^\circ, \pm 30^\circ, \pm 45^\circ, \pm 60^\circ, \pm 75^\circ, \pm 90^\circ\}$

$W_{GPLmax} = 1.25\%$, $\frac{1}{8} \sum_{i=1}^8 W_{GPLi} \leq W_{GPLmax}$, $W_{GPLi} \geq 0$,

In the definition, Ω_0 , W_{GPLi} , W_{GPLmax} and θ_i shows the non-dimensionalized frequency with uniform graphene weight equal to 1.25% in all layers, weight of graphene platelets for the i^{th} layer, maximum graphene weight for the laminate and the fiber orientation angles for each layer, respectively.

As a result of optimization Problem 3, the natural frequencies of the cases in which Carbon/GPLs reinforced with the highest cost show better results than Glass and Flax GPLs reinforced plates, shown in Table 6.22. Flax Graphene nanoplatelets reinforced composite plate is also obtained with 18,2% higher frequency and lower 7.7% weight and 31.3% cost than only carbon fiber reinforced composite plates. The other advantage of using Flax fiber ensures to the designer has the ability of biodegradable and low-cost structures. Although glass fibre/GPLs reinforced designs have 7% higher natural frequency than only carbon fibre reinforced composite plates, they are less advantageous as their weight is 11.7% higher.

Table 6.22. Optimum stacking sequences and weight content of GPLs results of the carbon, flax and glass fiber reinforced composite plates

Fibre Composition	Fiber Sequences for each layer	Optimum Stacking Sequence	Optimal W_{GPL} per layer	Natural Frequency (Ω_{max})	Weight (kg)	Cost (\$)
Carbon with Graphene	[C/C/C/C]s	[45/45/-45/45]s	[0.0465/0.0035/0/0]s	0.224	136.362	2689.44
Flax with Graphene	[F/F/F/F]s	[-45/-45/45/45]s	[0.0467/0.0033/0/0]s	0.197	125.862	1443.87
Glass with Graphene	[G/G/G/G]s	[-45/-45/-45/45]s	[0.05/0/0/0]s	0.178	155.862	1858.52

6.2.4. Problem 4

In the optimization Problem 3, non-dimensionalized natural frequencies of the hybrid fiber reinforced composite plates are maximized by using different stochastic algorithms (Differential Evolution Algorithm) under the simply supported boundary conditions. The objective function is defined as non-dimensionalized natural frequency Ω included fiber orientation angle (θ_i) of each layer as design parameters. In the outer layers, carbon fiber is used whereas in the inner layer flax or glass fiber is considered due to the being of results coming from the chapter 4 problems. It is related that the best option is to choose high volume content of fiber and weight content of GPLs at the top and bottom layers giving better natural frequencies. In the

The laminate is composed of $N=8$ layers and the thickness of the each ply is 1.25 mm.

Problem 4 can be defined mathematically as

- Maximize: Non-dimensionalized Natural Frequency $\Omega_{max}(\theta_i, W_{GPLi})$
- Constraints: $90^\circ \geq \theta_i \geq 0^\circ, \frac{1}{8} \sum_{i=1}^8 W_{GPLi} \leq W_{GPLmax}, W_{GPLi} \geq 0$

Symmetric stacking sequences; $[\theta_1, \theta_2, \theta_3, \theta_4]_s$

Symmetric & Balanced weight fraction of GPLs sequences;

$[W_{GPL1}/W_{GPL2}/W_{GPL3}/W_{GPL4}]_s$

$\theta_i \in \{0^\circ, \pm 15^\circ, \pm 30^\circ, \pm 45^\circ, \pm 60^\circ, \pm 75^\circ, \pm 90^\circ\}$

$W_{GPLmax} = 1.25\% t = 1.25 \text{ mm}, N = 8 \text{ ply}$

In the definition, $\Omega_0, W_{GPLi}, W_{GPLmax}$ and θ_i shows the non-dimensionalized frequency with uniform graphene weight equal to 1.25% in all layers, weight of graphene

platelets for the i^{th} layer, maximum graphene weight for the laminate and the fiber orientation angles for each layer, respectively.

Table 6.23 shows the comparison of the hybridization with nano-reinforcement effects on natural frequency of the simply supported plates. The natural frequency value is achieved of the [C/C/C/F]_s case with 35.7% increment, 2% and decreasing in weight.

The best solution in terms of weight and natural frequency is [C/C/F/F]_s design with %34.2 increase in frequency, a % 0.5 cost and %4 weight reduction as compared with only carbon reinforcement composite plate design. [C/F/F/F]_s design is also another better design from the point of the natural frequency(%35.7 increment) with %15.2 cost and %5.8 weight reduction as compared with only carbon reinforcement composite in Problem 1.

The other significant issue is that the glass hybridization with carbon fiber and GPLs reinforcement has not advantageous in regards to weight and cost. [G/F/F/F]_s hybridization with respect to GPLs nano reinforcement can also be provide important advantageous in terms of the weight and cost, 2% and 6.4%. Additionally, using the flax fiber at one ply in fully carbon reinforcement GPLs laminated composite plate has the highest value of the natural frequency among all cases.

The overall comparison of natural frequencies, costs, and weights for optimum designs of Problems 1–4 is shown in Figure 6.7 to see the total effect on three different parameters under the assumption that the total ply number constant is 8. In comparison to carbon fiber-reinforced designs frequently used in industry, hybridization of conventional carbon fiber-reinforced composite plates with natural fibers, such as flax fibers, clearly improves cost and price by 14 to 42 percent and 1.9 to 5.9 percent, respectively, provided the same natural frequency and constant total ply number. The graph also shows that, in comparison to the simple carbon fiber-reinforced composite design, adding GPLs to the conventional layered flax fiber-reinforced composite and optimizing the weight fraction of GPLs and orientation angle for each layer can result in much lower costs (31%), lightweight structures (7.8%) and superior natural frequency (18.3%). Therefore, to reduce weight, improve frequency, and save costs, multiscale flax fiber-reinforced nanocomposite structures can be utilized instead of that's frequently preferred carbon-reinforced composite structures. Similarly, in applications where weight is not a major concern, a simple glass-reinforced layered composite plate may also be reduced by 11% in price by promoting the frequency by 7% with optimum GPLs embedded each ply.

Table 6.23. Optimum stacking sequences and weight content of GPLs results of the carbon-flax and carbon-glass, glass-flax fiber reinforced composite plates.

Fiber Sequences for each layer	Optimum Stacking Sequence	Optimal WGPL per layer	Natural Frequency	Weight (kg)	Cost (\$)
[C/F/F/F]s-GPLs	[-45/-45/45/45]s	[0.0404/0.0096/0/0]s	0.214	128.487	1781.11
[C/C/F/F]s-GPLs	[-45/-45/45/45]s	[0.0465/0.0035/0/0]s	0.224	131.112	2089.96
[C/C/C/F]s-GPLs	[-45/-45/45/45]s	[0.05/0/0/0]s	0.227	133.737	2390.26
[C/G/G/G]s-GPLs	[-45/-45/45/-45]s	[0.0397/0.0103/0/0]s	0.197	150.987	2019.69
[C/C/G/G]s-GPLs	[45/-45/45/-45]s	[0.0476/0.0024/0/0]s	0.213	146.112	2232.31
[C/C/C/G]s-GPLs	[-45/-45/-45/-45]s	[0.0465/0.0035/0/0]s	0.220	141.237	2461.44
[G/G/G/F]s-GPLs	[-45/45/-45/45]s	[0.05/0/0/0]s	0.183	148.362	2714.17
[G/G/F/F]s-GPLs	[45/45/45/-45]s	[0.05/0/0/0]s	0.188	140.862	2353.07
[G/F/F/F]s-GPLs	[-45/45/45/-45]s	[0.05/0/0/0]s	0.193	133.362	1967.00

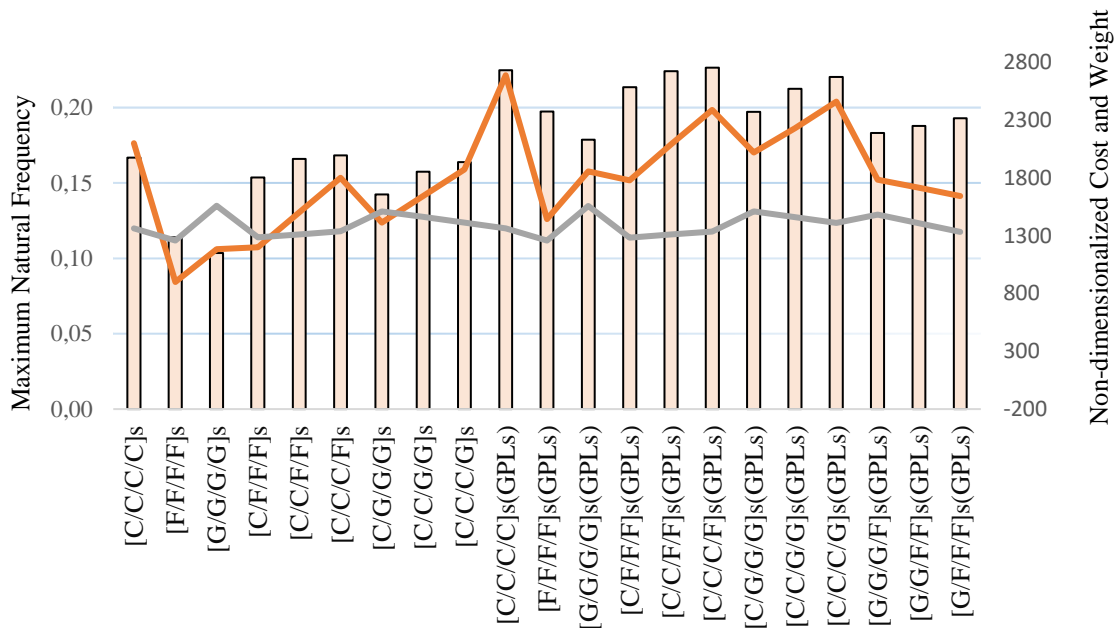


Figure 6.7. Comparison of natural frequencies, costs and weights for optimum designs formulated in Problems 1–4

The graph additionally indicates that, in comparison to traditional carbon-reinforced composite structures, the hybrid application of glass fiber and flax fiber with

GPLs, particularly for the [G/F/F/F]_s case, can achieve a 15.5% frequency increase with a combined cost savings of 21.7% and a 2.2% weight benefit. However, in cases where frequency is at the forefront, the use of flax fiber and carbon fiber reinforced with GPLs hybrid nanocomposite structures is more advantageous in terms of cost and weight, as well as making the design more suitable for environmentally friendly approaches.

6.2.5. Problem 5

In design Problem 5, the Differential Evolution Algorithm is implemented to maximize the non-dimensionalized natural frequencies of the fiber reinforced nanocomposite plates for different aspect ratios (a/b) that range from 0.2 to 2. The objective function is defined as non-dimensionalized natural frequency Ω included weight content sequences (W_{GPLi}) of the GPLs as well as fiber orientation angles of each ply (θ_i) as design parameters. The objective of the problem is to compare and analyze how different aspect ratios affect the best design results delivered by the Differential Evolution Algorithm solution.

Problem 5 can be defined mathematically as

- Maximize: Non-dimensionalized Natural Frequency $\Omega_{max}(W_{GPL}, V_F)$
- Constraints: $90^\circ \geq \theta_i \geq 0^\circ$, $t = 1.25$ mm, $N = 8$ ply

Symmetric weight fraction of GPLs sequences;

$$[W_{GPL1}/W_{GPL2}/W_{GPL3}/W_{GPL4}]_s$$

Symmetric stacking sequences for fibers; $[\theta_1, \theta_2, \theta_3, \theta_4]_s$

$$\theta_i \in \{0^\circ, \pm 15^\circ, \pm 30^\circ, \pm 45^\circ, \pm 60^\circ, \pm 75^\circ, \pm 90^\circ\}$$

$$\frac{1}{8} \sum_{i=1}^8 W_{GPLi} \leq W_{GPLmax}, W_{GPLi} \geq 0, W_{GPLmax} = 1.25\%$$

In the definition, Ω_0 , W_{GPLi} , W_{GPLmax} and θ_i shows the non-dimensionalized frequency with uniform graphene weight equal to 1.25% in all layers, weight of graphene platelets for the i th layer, maximum graphene weight for the laminate and the fiber orientation angles for each layer, respectively

The results achieved of Problem 5 point out that aspect ratios play a significant role in the optimal design of multiscale nanocomposites' maximum fundamental frequency problem. It is apparent from Table 6.24 and 6.25 that variation in aspect ratios resulted in several optimum designs, each of which consists of a different stacking sequence and GPL weight fraction.

Table 6.24. Comparison of optimum design for non-dimensionalized frequencies Ω of carbon, flax and glass fiber reinforced nanocomposite plates for different aspect ratios(a/b),

a/b	Carbon/GPLs-Epoxy			Flax/GPLs-Epoxy			Glass/GPLs-Epoxy		
	Natural Frequency	Cost(\$)	Weight (kg)	Natural Frequency	Cost (\$)	Weight (kg)	Natural Frequency	Cost (\$)	Weight (kg)
0,2	1.960	538.65	27.27	1.767	289.24	25.17	1.597	372.188	31.17
0,4	0.758	1076.79	54.54	0.645	577.65	50.34	0.583	743.525	62.34
0,6	0.414	1614.15	81.82	0.358	866.08	75.52	0.324	1119.72	93.52
0,8	0.282	2151.78	109.09	0.249	1154.48	100.69	0.225	1492.62	124.69
1	0.225	2689.44	136.36	0.198	1443.87	125.86	0.179	1858.52	155.86
1,2	0.193	3227.09	163.64	0.169	1731.72	151.04	0.153	2229.13	187.03
1,4	0.176	3764.52	190.91	0.151	2020.33	176.21	0.137	2600.68	218.21
1,6	0.167	4302.49	218.18	0.140	2308.95	201.38	0.127	2972.21	249.38
1,8	0.162	4840.47	245.45	0.133	2597.57	226.55	0.120	3343.74	280.55
2	0.159	5378.16	272.72	0.128	2886.19	251.72	0.116	3715.26	311.72

Regardless of the aspect ratios, the weight content pattern of the GPLs generally tends to produce outer layers with greater graphene contents and inner layers with lower graphene contents for the optimum maximum fundamental frequency designs.

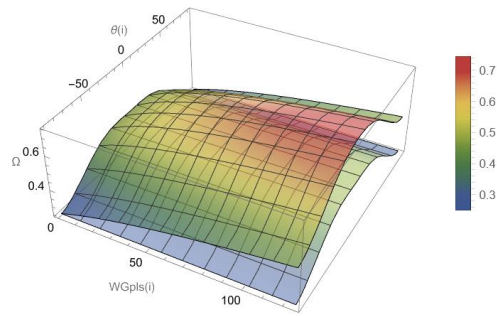
Additionally, a distinct and appropriate design for various aspect ratios also necessitates optimizing fiber orientation angles in addition to the weight percentage of the GPLs at each layer. It is obvious that among the fibers, flax fiber delivers superior design in terms of cost, weight, and environmental friendliness. The other result is that, if weight and cost are not taken into consideration, carbon fiber reinforced with GPLs suggests the highest fundamental frequency. In order to decrease the weight and cost of the designs, hybridizing flax fiber with carbon fiber could offer a successful strategy.

The contour plots in terms of uniform distributed graphene content and fibre orientation angle of [C/C/F/F]_s design are drawn as shown in Figure 6.8 to investigate the sensitivity of the frequency for different aspect ratios (a/b) of 0.4, 1, 1.4 and 2. The $[+\theta/-\theta/+\theta/-\theta]_s$ and $[W_{GPL}/W_{GPL}/W_{GPL}/W_{GPL}]_s$ are taken as the stacking order of the laminates and the weight content of each layer, respectively. The contours with zero graphene content are also plotted in each graph to show the difference between zero content and variable uniformly distributed GPLs on the natural frequency.

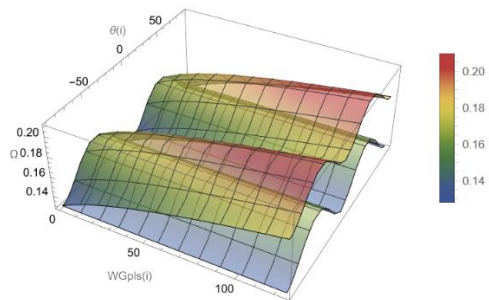
Table 6.25. Comparison of optimum design for non-dimensionalized frequencies Ω of carbon, flax and glass fiber reinforced nanocomposite plates for different aspect ratios(a/b),

a/b	Glass/GPLs-Epoxy			Flax/GPLs-Epoxy			Carbon/GPLs-Epoxy		
	Natural Frequency	Optimal WGPL per layer	Stacking Sequence	Natural Frequency	Optimal WGPL per layer	Stacking Sequence	Natural Frequency	Optimal WGPL per layer	Stacking Sequence
0.2	1.596	[0.0333/0.0129/0.0032 /0.0006]s	[0/0/0/0]s	1.767	[0.0310/0.0148/0.0035 /0.0007]s	[0/0/0/15]s	1.960	[0.0163/0.0128/0.0105 /0.104]s	[0/0/0/0]s
0.4	0.583	[0.0452/0.0048/0/0]s	[0/0/0/0]s	0.645	[0.0452/0.0048/0/0]s	[0/0/0/0]s	0.758	[0.0311/0.0133/0.0031 /0.0025]s	[0/0/0/0]s
0.6	0.324	[0.0484/0.0016/0/0]s	[0/15/-15/0]s	0.358	[0.0484/0.0016/0/0]s	[0/-15/15/0]s	0.414	[0.0423/0.0077/0/0]s	[0/15/-15/-15]s
0.8	0.225	[0.05/0/0]s	[-30/-30/-30/30]s	0.249	[0.0500/0/0]s	[-15/-30/-30 -30]s	0.282	[0.0451/0.0049/0/0]s	[-30/-30/-45/-30]s
1	0.178	[0.05/0/0]s	[-45/-45/-45/45]s	0.198	[0.0467/0.0033/0/0]s	[-45/-45/45/45]s	0.225	[0.0467/0.0033/0/0]s	[45/45/-45/45]s
1.2	0.153	[0.05/0/0]s	[-60/45/-45/45]s	0.169	[0.05/0/0]s	[60/-45/45 /-45]s	0.193	[0.0474/0.0026/0/0]s	[60/45/-45/45]s
1.4	0.137	[0.05/0/0]s	[75/60/-60/-60]s	0.151	[0.05/0/0]s	[90/60/-60 /60]s	0.176	[0.0487/0.0013/0/0]s	[-75/-60/-60/90]s
1.6	0.127	[0.05/0/0]s	[90/75/75/75]s	0.140	[0.05/0/0]s	[90/-75/-75 /75]s	0.167	[0.0482/0.0018/0/0]s	[90/75/60/90]s
1.8	0.120	[0.05/0/0]s	[90/90/90/90]s	0.133	[0.05/0/0]s	[90/90/90 /90]s	0.162	[0.0478/0.0022/0/0]s	[90/90/90/90]s
2	0.116	[0.05/0/0]s	[90/90/90/90]s	0.128	[0.05/0/0]s	[90/90/90 /90]s	0.159	[0.0481/0.0019/0/0]s	[90/90/90/90]s

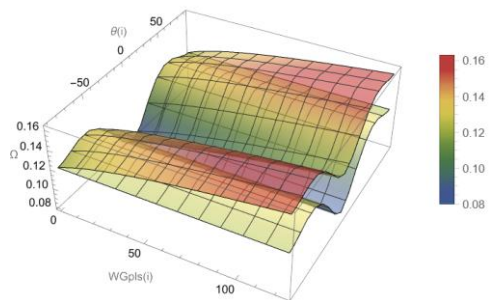
a)



b)



c)



d)

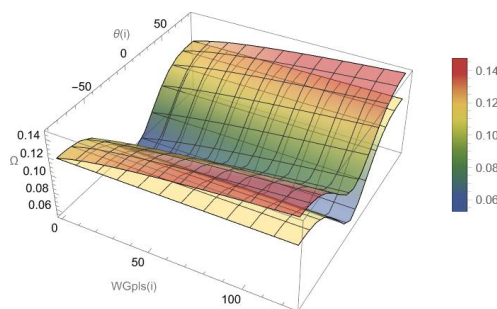


Figure 6.8. Contour plots of the frequency for hybrid [C/C/F/F]_s composite plates with varying graphene weight and fibre orientation angles of each layer a) for aspect ratio 0.4 b) for aspect ratio 1 c) for aspect ratio 1.4 d) for aspect ratio 2

The two horizontal axes show the variation of the angle of the fibre orientation and the weight content of graphene in each layer. For each aspect ratio, not only the increase in the graphene weight content is a critical factor for the natural frequency, but also the fibre orientation angle has an effect on the natural frequency of the laminate. It can be seen from the figure that despite having fewer parameters such as equal graphene distribution and same fibre orientation angle in each layer, the natural frequency is affected differently by combining these two parameters. The behaviour of the surface in each graph is different due to the variable aspect ratios. It is also a statement of the requirements for which optimizing each orientation angle and weight content must be carried out to find the global maximum fundamental frequency for different aspect ratios. The comparison between graphene without and with added graphene surface also shows that the natural frequency is sensitive to changing with increasing weight fraction of GPLs for different aspect ratios.

6.2.6. Problem 6

In the optimization Problem 3, non-dimensionalized natural frequencies of the hybrid carbon/flax fiber reinforced nanocomposite plates are maximized for different flax layer numbers ranging from 0 to 16 by using Differential Evolution Algorithm in conjunction with simply supported boundary conditions. The objective function is defined as non-dimensionalized natural frequency Ω included fiber orientation angle (θ_i) and weight fraction of GPLs of each layer as design variables. Carbon fiber is used in the outside layers, whereas flax fiber is used in the interior layer since it is less expensive and heavier than carbon fiber. This problem aims to see how the quantity of flax fiber affects the natural frequency for a hybrid carbon/flax fiber reinforced nanocomposite plate.

Problem 6 can be defined mathematically as

- Maximize: Non-dimensionalized Natural Frequency $\Omega_{max}(\theta_i, W_{GPLi})$
- Constraints: $90^\circ \geq \theta_i \geq 0^\circ, \frac{1}{16} \sum_{i=1}^{16} W_{GPLi} \leq W_{GPLmax}, W_{GPLi} \geq 0$

Symmetric stacking sequences;

$$[\theta_1, \theta_2, \theta_3, \theta_4, \theta_5, \theta_6, \theta_7, \theta_8]_s$$

Symmetric weight fraction of GPLs sequences;

$$[W_{GPL1}/W_{GPL2}/W_{GPL3}/W_{GPL4}/W_{GPL5}/ \dots / W_{GPL8}]_s$$

$$t = 12.5 \text{ mm}, N = 16, W_{GPLmax} = 1.25\%$$

$$\theta_i \in \{0^\circ, \pm 15^\circ, \pm 30^\circ, \pm 45^\circ, \pm 60^\circ, \pm 75^\circ, \pm 90^\circ\}$$

In the definition, Ω_0 , W_{GPLi} , W_{GPLmax} and θ_i shows the non-dimensionalized frequency with uniform graphene weight equal to 1.25% in all layers, weight of graphene platelets for the i th layer, maximum graphene weight for the laminate and the fiber orientation angles for each layer, respectively.

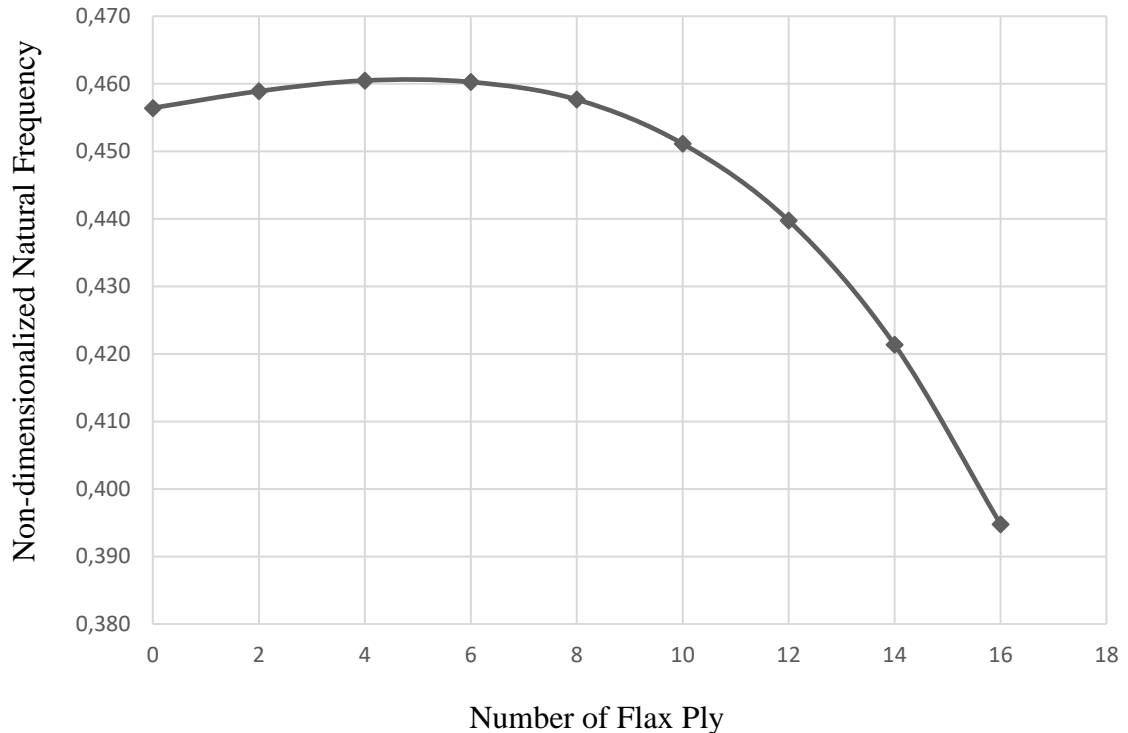


Figure 6.9. Variation of the natural frequencies with increasing in flax ply for constant total ply thickness of the hybrid composite plate

In Table 6.27, it is shown that the comparison effects of hybridization based on various flax fiber and carbon fiber reinforcing ply numbers on the natural frequency in the simply supported nanocomposite plates. The $[C_6/F_2]_s$ case achieves the optimal solution in terms of weight, cost, and natural frequency with a 0.88% increase as well as a decrease in 13% cost and 2% weight. $[C_5/F_3]_s$ design is also another better design from the point of the natural frequency (%0.85 increment) with %19 cost and %2.88 weight reduction as compared with only carbon reinforcement composite in problem. It can be seen in Figure 6.9, the use of the ply number of flax layers, 4 and 6, in hybrid nanocomposite which are composed of a total of 16 layers, gives the highest frequencies. Another significant finding is that, assuming the condition that the total number of layers

remains constant, an increase in the flax ply number in hybrid multiscale nanocomposite structures tends to reduce the natural frequency as it is seen in Figure 6.9.

Table 6.26. Optimum stacking sequences and weight content of GPLs results of the carbon-flax fiber reinforced composite plates according to variation of flax ply number

Total Number of Layer	Nf (Number of Flax Layer)	Natural Frequency Ω_{max}	Optimal WGPL per layer	Optimum Stacking Sequence	Cost (\$)	Weight (kg)
16	0	0.456	[0.0218/0.0119/0.0056/0.073/0.026/0.008/0/0]s	[45/-45/45/-45/45/-45/45/-75]s	3836	218.29
	2	0.459	[0.023/0.0104/0.0081/0.046/0.019/0/0.029/0]s	[45/45/45/-45/-45/-45/90/90]s	3594	216.19
	4	0.460	[0.023/0.0104/0.0081/0.046/0.019/0/0.029/0]s	[45/45/45/-45/-45/-45/90/90]s	3354	214.09
	6	0.460	[0.0199/0.0136/0.0092/0.0033/0.0012/0.0028/0/0]s	[45/-45/-45/-45/45/60/-30/-30]s	3113	211.99
	8	0.458	[0.0238/0.009/0.007/0.027/0.0057/0.0014/0/0.004]s	[45/45/45/45/45/45/30/-60]s	2869	209.89
	10	0.451	[0.0220/0.0093/0.0046/0.0094/0.0029/0.0017/0/0]s	[-45/-45/-45/-45/45/-30/-45/-15]s	2624	207.79
	12	0.439	[0.0194/0.0098/0.0139/0.0065/0.0003/0/0/0]s	[-45/-45/-45/45/-45/-45/45/90]s	2379	205.69
	14	0.421	[0.0143/0.0261/0.0088/0.005/0.003/0/0/0]s	[-45/45/-45/-45/-45/45/-30/45]s	2128	203.59
	16	0.395	[0.0335/0.0144/0.002/0/0/0/0/0]s	[-45/-45/-45/-45/45/45/45/90]s	1877	201.49

6.3. Multi-Objective Optimization Problems

In design Problems 1, 2, and 3 related to laminated composite plates, there are three main objectives as follows: (i) maximizing the fundamental frequency, (ii) minimizing the weight, and (iii) minimizing the cost. To optimize, these objectives are employed using the following combinations of two or three parameters: maximizing frequency while minimizing cost, maximizing frequency while minimizing weight, and maximizing frequency while minimizing both cost and weight. In relation to this, the linear combination of the squares of the values "frequency," "cost," and "weight" is introduced in three different functions like as m_1+m_2 , m_1+m_3 and $m_1+m_2+m_3$, respectively. Here, the functions establish the relationship between "frequency" (m_1), "cost" (m_2), and "weight" (m_3) similarly to a multi-objective approach. The brief description of the problems can be seen in Table 6.27.

Table 6.27. Mathematical definitions of optimization problems for two-phase (fiber/matrix) composites and three phase (fiber/GPLs/matrix) nanocomposite plates

	Two-Phase Composite	Three-Phase Nanocomposite
Minimize	$F_1 = k_1 m_1^2 + k_2 m_2^2 + k_4 (\delta - 0.2)^2 + k_5 (\gamma - 0.2)^2$ (Problem 1) $F_2 = k_1 m_1^2 + k_3 m_3^2 + k_4 (\delta - 0.2)^2 + k_5 (\gamma - 0.2)^2$ (Problem 2) $F_3 = k_1 m_1^2 + k_2 m_2^2 + k_3 m_3^2 + k_4 (\delta - 0.2)^2 + k_5 (\gamma - 0.2)^2$ (Problem 3) $m_1 = \left(\frac{\bar{\omega}_{max} - \bar{\omega}_{mn}}{\bar{\omega}_{max}} \right)$ $m_2 = \left(\frac{Weight}{Weight_{max}} \right)$ $m_3 = \left(\frac{Cost}{Cost_{max}} \right)$	$\bar{\omega}_{mn} \left(\begin{matrix} \theta_1, \theta_2, \dots, \theta_N, \\ V_{F1}, V_{F2}, \dots, V_{FN}, \\ W_{CNT_1}, W_{CNT_2}, \dots, W_{CNT_N} \end{matrix} \right)$ $Weight \left(V_{F1}, V_{F2}, \dots, V_{FN} \right)$ $Cost \left(V_{F1}, V_{F2}, \dots, V_{FN} \right)$ $\bar{\omega}_{mn} \left(\begin{matrix} \theta_1, \theta_2, \dots, \theta_N, \\ V_{F1}, V_{F2}, \dots, V_{FN}, \\ W_{CNT_1}, W_{CNT_2}, \dots, W_{CNT_N} \end{matrix} \right)$ $Weight \left(\begin{matrix} V_{F1}, V_{F2}, \dots, V_{FN} \\ W_{CNT_1}, W_{CNT_2}, \dots, W_{CNT_N} \end{matrix} \right)$ $Cost \left(\begin{matrix} V_{F1}, V_{F2}, \dots, V_{FN} \\ W_{CNT_1}, W_{CNT_2}, \dots, W_{CNT_N} \end{matrix} \right)$
Find	θ_i, V_{Fi} N_{ho} and N_{hi} (for hybrid structure)	$\theta_i, V_{Fk}, W_{CNT_k}$ N_{ho} and N_{hi} (for hybrid structure)
Design Variables	$\{\theta_1, \theta_2, \theta_3, \dots, \theta_N\}$	$\{\theta_1, \theta_2, \theta_3, \dots, \theta_N, W_{CNT_1}, W_{CNT_2}, W_{CNT_3}, \dots, W_{CNT_N}\}$
Constraints	$\theta_i \in \{0^\circ, \pm 15^\circ, \pm 30^\circ, \pm 45^\circ, \pm 60^\circ, \pm 75^\circ, \pm 90^\circ\}$ N_{ho} and N_{hi} (for hybrid structure) $0.10 \leq V_{Fk} \leq 0.60$	$\theta_i \in \{0^\circ, \pm 15^\circ, \pm 30^\circ, \pm 45^\circ, \pm 60^\circ, \pm 75^\circ, \pm 90^\circ\}$ $\frac{1}{N} \sum_{i=1}^N W_{CNT_k} \leq W_{CNT_{max}}$ $W_{CNT_k} \geq 0, W_{CNT_{max}} = 1.25\%$, $0.10 \leq V_{Fk} \leq 0.60$ N_{ho} and N_{hi} (for hybrid structure)

where N_{ho} , N_{hi} , θ_i , V_{Fk} , W_{CNT_k} , are the number of outer and inner layers in hybrid composite structures, fiber orientation angle, volume fraction of fiber and weight content of CNT for each layer, respectively. The total number of layers for hybrid structures can be determined via the equation $N = N_{ho} + N_{hi}$. For non-hybrid structures, N represents directly the total number of plies. For all the design problems, width/ length ratio (aspect ratio) is a/b=1. The lay-up of the hybrid and non-hybrid plies with synthetic and natural fibers are shown in Figure 6.10. The two-phase (fiber and matrix) and three phase (fiber, CNTs and matrix) composite structures can be written by using following style clearly.

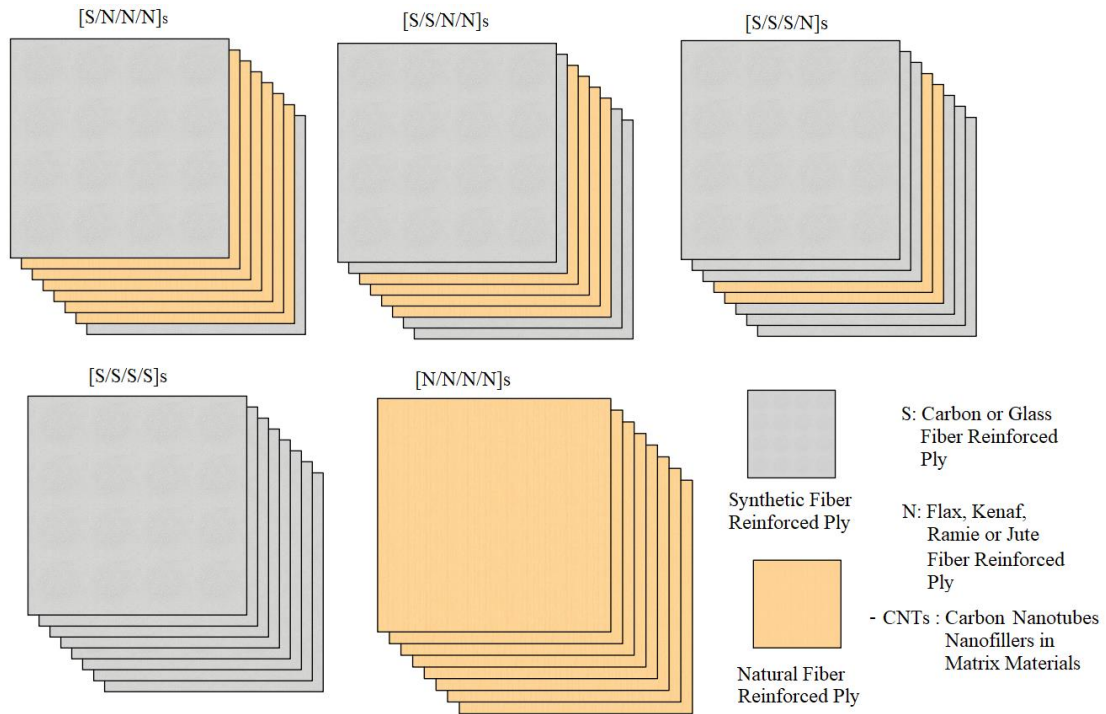


Figure 6.10. Illustration of the symbols for inter ply hybrid and non-hybrid fiber/CNTs reinforced nanocomposites for two-phase and three-phase composites

The material properties of synthetic fibers (carbon, glass), natural fibers (flax, kenaf, ramie, jute), nano-reinforcement (Carbon nanotubes) and matrix used in the present problems are given in Table 6.28.

Table 6.28. Material properties of fibers, CNTs and matrix for Problem 1, 2 and 3^{38,80,86,182,199,200}

	Jute	Kenaf	Ramie	Flax	Carbon	Carbon AS4	Glass	CNTs	Matrix
E ₁ (Gpa)	55,3	52,2	60,9	70	263	225	72,4	450	4,2
E ₂ ,E ₃ (Gpa)	6,7	6,1	7,8	70	19	15	72,4		
G ₁₂ ,G ₁₃ (Gpa)	3,1	2,9	3,7	29,58	27,6	15-7	30,66		1,567
v ₁₂ ,v ₁₃	0,32	0,32	0,32	0,183	0,2	0,2	0,2		0,34
v ₂₃	0,14	0,13	0,17		0,4	0,4	0,2		
Density(kg/m ³)	1340	1300	1550	1400	1750	1800	2400	624,4	1250
Cost (\$/kg)	0,95	0,4	2	0,5	28	28	2	485	10

The parameters $\bar{\omega}_{mn}$, cost, and weight, show optimum natural frequency, optimum cost and weight values. The parameters $\bar{\omega}_{max}$, $cost_{max}$ and $weight_{max}$ denote the maximum

fundamental frequency, maximum cost and the maximum weight for all layers consisting of carbon/epoxy material for 0.60 volume fraction of fiber value and optimum stacking sequences. In this study, the coefficient k_1 is assumed to be equal to four, on the basis that the importance of the fundamental frequency is four times greater than that of weight and cost. The other k_i parameters are equal to 1, which indicates that the importance of cost and weight are equal. The influence of bending-twisting coupling terms δ and γ is assumed as equal to 0.2.

In accordance with the principles of a multi-objective approach for optimization, this part of study addresses the following issues:

- (1) Frequency–weight problems
- (2) Frequency–cost problems
- (3) Frequency–cost–weight problems.

The followings are devoted to detailed descriptions and results of the multi-objective optimization problems (Problems 1–3)

6.3.1. Problem 1

In design problem, multi-objective optimization problems of hybrid and non-hybrid fibers/CNT reinforced composite plates are performed in terms of fundamental frequency and weight with non-uniform distribution of CNT and fiber reinforcements. Additionally, the same multi-objective optimization problems are solved for two-phase fiber reinforced composite plate structures to compare efficiency of optimum design which are defined as penalty function values. The laminate is composed of $N=8$ layers and the length to thickness ratio $a/h = 100$. The natural frequencies of fibre-reinforced nanocomposite plates are optimised through the utilisation of the Modified Differential Evolution Algorithm, while simultaneously minimizing weight for simply supported boundary conditions. The objective function F_I is defined as penalty function which is composed of non-dimensionalized natural frequency $\bar{\omega}_{mn}$ and weight. θ_i , W_{CNT_k} and V_{FK} are the design parameters. The objective of the problem is to make comparisons of multiobjective problem results for maximum natural frequency and minimum weight for Jute, Kenaf, Ramie, Flax, Carbon and Glass fiber reinforcement with and without CNT for hybrid and non-hybrid structures. The first problem is a simple one that looks

at the results of two goals—maximum natural frequency and minimum weight with a couple.

Problem 1 can be defined mathematically as

- Minimize: $F_1 = k_1 m_1^2 + k_2 m_2^2 + k_4 (\delta - 0.2)^2 + k_5 (\gamma - 0.2)^2$

$$m_1 = \left(\frac{\bar{\omega}_{max} - \bar{\omega}_{mn}}{\bar{\omega}_{max}} \right) m_2 = \left(\frac{Weight}{Weight_{max}} \right)$$

- Constraints: $\frac{1}{8} \sum_{i=1}^8 W_{CNTi} \leq W_{CNTmax}, W_{CNTi} \geq 0$

Symmetric stacking sequences; $[\theta_1, \theta_2, \theta_3, \theta_4]_s$

Symmetric weight fraction of GPLs sequences;

$[W_{CNT1}/W_{CNT2}/W_{CNT3}/W_{CNT4}]_s$

Symmetric volume fraction of Fiber; $[V_{F1}/V_{F2}/V_{F3}/V_{F4}]_s$

$a/D = 100, a/b = 1, W_{CNTmax}=1.25\%$,

$0.10 \leq V_{Fk} \leq 0.60$

Algorithms: Differential Evolution

In the definition, W_{CNTi} and W_{CNTmax} show weight of carbon nanotubes for the i^{th} layer and maximum graphene weight for the laminate.

Table 6.29 indicates how different hybrid and non-hybrid designs affect the optimal stacking sequence, from fiber volume fraction, and CNT distribution weight fraction for the highest feasible fundamental frequency and the minimum achievable weight of the composite plates. Results show a tendency toward more efficient design outcomes when large volume fraction and weight content of CNT are placed at the outer layer instead of to the inner layer. In accordance with the benefits of density, CNTs are added to each layer of natural fiber reinforced designs to enhance the fiber volume content and reduce weight. F values also demonstrate the efficiency level of the optimal design in terms of frequency and weight. The minimum F values for [C/C/F/F]_s-CNT, [C/C/C/F]_s-CNT, [C/C/K/K]_s-CNT, [C/C/C/K]_s-CNT, [C/C/R/R]_s-CNT, [C/C/C/R]_s-CNT, [C/C/J/J]_s-CNT, and [C/C/C/J]_s-CNT are less than 0.800. This indicates that the most efficient cases result from the hybridization of flax, jute, kenaf, and ramie fibers with carbon fibers through the addition of CNT into the matrix. Glass fiber reinforced [G/G/G/G]_s-CNT and [G/G/G/G]_s cases are less efficient than both three-phase and two-phase composite designs, totally natural fiber reinforced cases [F/F/F/F]_s-CNT, [J/J/J/J]_s-CNT, [K/K/K/K]_s-CNT, [R/R/R/R]_s-CNT, [F/F/F/F]_s, [J/J/J/J]_s, [K/K/K/K]_s, [R/R/R/R]_s, and their hybridizations each other. When two-phase designs of natural fiber reinforcement and their hybridizations are compared to three-phase natural fiber

reinforced designs with CNT, it can be shown that the natural frequency of the structure may increase by 10% by adding 1% CNT into the matrix. This finding supports the use of natural fibers with CNTs for applications where vibration and lightness control is important. Since cost is not considered an objective in the optimization problem, the fully carbon fiber reinforced [C/C/C/C] s-CNT case is the one of the most efficient design in terms of natural frequency and weight. However, despite the renowned strength and lightweight properties of carbon fiber and CNT, hybrid designs combining carbon fiber with flax, kenaf, ramie, and jute fibers with CNT are more efficient than the fully carbon fiber reinforced case [C/C/C/C] s-CNT.

Table 6.29. Comparison of optimum Stacking sequence, volume fraction of fiber and weight fraction of CNT distribution results for maximum fundamental frequency and minimum weight of composite plates

Design	F-value	Optimum Results		
		Stacking Sequence	Fiber Volume Fraction per layer	Weight Content of CNT per layer
[F/F/F/F]s-CNT	1.139	[45/-45/45/45]s	[0.60/0.60/0.60/0.10]s	[0.0392/0.0108/0/0.0]s
[G/G/G/G]s-CNT	1.655	[45/-45/45/45]s	[0.600/0.100/0.100/0.100]s	[0.05/0.0/0/0]s
[J/J/J/J]s-CNT	1.455	[45/-45/-45/45]s	[0.600/0.600/0.600/0.100]s	[0.05/0.0/0/0]s
[K/K/K/K]-CNT]	1.471	[45/-45/-45/45]s	[0.60/0.60/0.60/0.60]s	[0.05/0.0/0/0]s
[R/R/R/R]-CNT	1.200	[45/-45/45/-45]s	[0.60/0.60/0.60/0.10]s	[0.0472/0.0028/0/0.0]s
[C/C/C/C]s-CNT	0.802	[45/-45/-45/-45]s	[0.495/0.460/0.100/0.100]s	[0.05/0.0/0/0]s
[C/F/F/F]s-CNT	1.000	[90/45/45/45]s	[0.60/0.60/0.10/0.10]s	[0.05/0.0/0/0]s
[C/C/F/F]s-CNT	0.784	[45/-45/-45/-45]s	[0.488/0.483/0.10/0.10]s	[0.50/0.0/0/0]s
[C/C/C/F]s-CNT	0.791	[45/-45/-45/-45]s	[0.492/0.460/0.100/0.100]s	[0.50/0.0/0/0]s
[C/G/G/G]s-CNT	1.228	[90/45/45/45]s	[0.600/0.10/0.10/0.10]s	[0.50/0/0]s
[C/C/G/G]s-CNT	0.851	[45/-45/-45/-45]s	[0.505/0.502/0.10/0.10]s	[0.50/0/0]s
[C/C/C/G]s-CNT	0.824	[45/-45/-45/-45]s	[0.501/0.470/0.10/0.10]s	[0.50/0/0]s
[C/K/K/K]s-CNT	1.079	[90/45/45/45]s	[0.60/0.60/0.60/0.10]s	[0.50/0/0]s
[C/C/K/K]s-CNT	0.780	[45/-45/-45/-45]s	[0.477/0.499/0.10/0.10]s	[0.50/0/0]s
[C/C/C/K]s-CNT	0.789	[45/-45/-45/-45]s	[0.482/0.475/0.10/0.10]s	[0.50/0/0]s
[C/R/R/R]s-CNT	1.078	[90/45/45/45]s	[0.60/0.60/0.10/0.10]s	[0.50/0/0]s
[C/C/R/R]s-CNT	0.796	[45/-45/-45/-45]s	[0.484/0.503/0.100/0.100]s	[0.50/0/0]s
[C/C/C/R]s-CNT	0.798	[45/-45/-45/-45]s	[0.484/0.474/0.100/0.100]s	[0.50/0/0]s
[C/J/J/J]s-CNT	1.016	[90/45/45/45]s	[0.60/0.60/0.60/0.10]s	[0.50/0/0]s
[C/C/J/J]s-CNT	0.783	[45/-45/-45/-45]s	[0.479/0.500/0.10/0.10]s	[0.50/0/0]s
[C/C/C/J]s-CNT	0.791	[45/-45/-45/-45]s	[0.482/0.474/0.100/0.100]s	[0.50/0/0]s

Three Phase Composites

(cont. on next page)

Table 6.29 (cont.)

[F/J/J/J] _s -CNT	1.209	[45/-45/-45/45] _s	[0.60/0.60/0.10/0.10] _s	[0.500/0/0/0] _s
[F/F/J/J] _s -CNT	1.142	[45/-45/-45/45] _s	[0.60/0.60/0.60/0.10] _s	[0.381/0.119/0/0] _s
[F/F/F/J] _s -CNT	1.137	[45/-45/45/45] _s	[0.60/0.60/0.60/0.10] _s	[0.385/0.115/0/0] _s
[F/K/K/K] _s -CNT	1.197	[45/-45/-45/45] _s	[0.60/0.60/0.10/0.10] _s	[0.500/0/0/0] _s
[F/F/K/K] _s -CNT	1.133	[45/-45/45/45] _s	[0.60/0.60/0.60/0.10] _s	[0.377/0.123/0/0] _s
[F/F/F/K] _s -CNT	1.136	[45/-45/45/45] _s	[0.60/0.60/0.60/0.10] _s	[0.385/0.115/0/0] _s
[F/R/R/R] _s -CNT	1.261	[45/-45/45/45] _s	[0.60/0.477/0.10/0.10] _s	[0.500/0/0/0] _s
[F/F/R/R] _s -CNT	1.178	[45/-45/45/45] _s	[0.60/0.60/0.10/0.10] _s	[0.344/0.156/0/0] _s
[F/F/F/R] _s -CNT	1.141	[45/-45/45/45] _s	[0.60/0.60/0.60/0.10] _s	[0.385/0.115/0/0] _s
[F/F/F/F] _s	1.325	[45/-45/45/45] _s	[0.60/0.60/0.60/0.10] _s	-
[G/G/G/G] _s	2.034	[45/-45/-45/-45] _s	[0.521/0.379/0.100/0.100] _s	-
[J/J/J/J] _s	1.564	[45/-45/-45/45] _s	[0.60/0.60/0.60/0.10] _s	-
[K/K/K/K]	1.583	[45/-45/-45/45] _s	[0.60/0.60/0.60/0.10] _s	-
[R/R/R/R]	1.640	[45/-45/45/45] _s	[0.60/0.60/0.10/0.10] _s	-
[C/F/F/F] _s	1.125	[90/45/45/45] _s	[0.60/0.60/0.60/0.10] _s	-
[C/C/F/F] _s	0.888	[45/-45/-45/45] _s	[0.419/0.432/0.60/0.60] _s	-
[C/C/C/F] _s	0.809	[45/-45/-45/-45] _s	[0.510/0.567/0.10/0.10] _s	-
[C/G/G/G] _s	1.410	[90/45/45/45] _s	[0.60/0.10/0.10/0.10] _s	-
[C/C/G/G] _s	0.870	[45/-45/-45/-45] _s	[0.514/0.60/0.10/0.10] _s	-
[C/C/C/G] _s	0.843	[45/-45/-45/-45] _s	[0.515/0.573/0.10/0.10] _s	-
[C/K/K/K] _s	1.143	[90/45/45/45] _s	[0.60/0.60/0.60/0.10] _s	-
[C/C/K/K] _s	0.797	[45/-45/-45/-45] _s	[0.502/0.594/0.10/0.10] _s	-
[C/C/C/K] _s	0.807	[45/-45/-45/-45] _s	[0.504/0.566/0.10/0.10] _s	-
[C/R/R/R] _s	1.223	[90/45/45/45] _s	[0.60/0.60/0.10/0.10] _s	-
[C/C/R/R] _s	0.814	[45/-45/-45/-45] _s	[0.508/0.599/0.10/0.10] _s	-
[C/C/C/R] _s	0.815	[45/-45/-45/-45] _s	[0.509/0.571/0.10/0.10] _s	-
[C/J/J/J] _s	1.153	[90/45/45/45] _s	[0.60/0.60/0.60/0.10] _s	-
[C/C/J/J] _s	0.800	[45/-45/-45/-45] _s	[0.505/0.597/0.10/0.10] _s	-
[C/C/C/J] _s	0.808	[45/-45/-45/-45] _s	[0.505/0.567/0.10/0.10] _s	-
[F/J/J/J] _s	1.400	[45/-45/-45/-45] _s	[0.60/0.60/0.60/0.10] _s	-
[F/F/J/J] _s	1.336	[45/-45/-45/-45] _s	[0.60/0.60/0.528/0.101] _s	-
[F/F/F/J] _s	1.333	[45/-45/45/-45] _s	[0.60/0.60/0.463/0.100] _s	-
[F/K/K/K] _s	1.391	[45/-45/-45/45] _s	[0.60/0.60/0.60/0.10] _s	-
[F/F/K/K] _s	1.327	[45/-45/45/45] _s	[0.60/0.60/0.547/0.10] _s	-
[F/F/F/K] _s	1.332	[45/-45/45/-45] _s	[0.60/0.60/0.453/0.102] _s	-
[F/R/R/R] _s	1.475	[45/-45/45/45] _s	[0.60/0.60/0.10/0.10] _s	-
[F/F/R/R] _s	1.377	[45/-45/45/45] _s	[0.60/0.60/0.10/0.10] _s	-
[F/F/F/R] _s	1.340	[45/-45/45/-45] _s	[0.60/0.60/0.491/0.10] _s	-

Two Phase Composites

Table 6.30 presents the optimum natural frequency and weight results for combinations of hybrid and non-hybrid cases with and without CNT. The cost results are provided as outputs to compare overall results with those of other multi-objective

optimization approaches. Weight and frequency value reductions are expressed as percentages in comparison to the [C/C/C/C] s reference optimum case. The [C/C/K/K]s-CNT and [C/C/F/F]s-CNT cases are the most efficient, with the lowest F values of 0.780 and 0.784, respectively. The results indicate that a 12.2% weight reduction can be achieved by sacrificing the frequency value by about 5.6%, while also using more eco-friendly fibers, and gaining approximately 26% cost reduction advantages. The next most efficient designs after these are [C/C/C/F]s-CNT, [C/C/C/K]s-CNT, [C/C/R/R]s-CNT, [C/C/C/R]s-CNT, [C/C/J/J]s-CNT, and [C/C/C/J]s-CNT. These designs provide optimal solutions to the problem, achieving an 11.5% weight reduction and a 5.5% decrease in natural frequency.

In addition to this, the two-phase hybrid designs [C/C/F/F]s, [C/C/C/F]s, [C/C/K/K]s, [C/C/C/K]s, [C/C/R/R]s, [C/C/C/R]s, [C/C/J/J]s, and [C/C/C/J]s also provide efficient designs with a 10% weight reduction and a 5.7% decrease in frequency. The results also indicate that using natural fiber hybridization without CNT is more efficient when weight reduction is less important. In multi-objective optimization problems where natural frequency and weight are used as objectives, hybrid and non-hybrid natural fiber reinforced design cases with CNTs may provide a 15.5% weight reduction and a 69% cost reduction, albeit with a sacrifice of 31% in natural frequency. For the same design approaches using fully natural fiber reinforced cases in two-phase structures without CNT, it can be observed that less efficient designs with a 12% reduction in frequency values are achievable compared to multiphase designs with CNTs. However, these designs still offer 15% weight reduction and 76% cost savings. The [C/C/C/C] s-CNT design is also among the most efficient designs, leveraging the low density and high strength properties of carbon nanotubes. This is particularly advantageous when biodegradability and cost are not primary concerns for designers.

This graph illustrates the optimal configurations of hybrid and non-hybrid fiber reinforced composites, both with and without the incorporation of carbon nanotubes (CNTs), focusing on achieving maximum natural frequency and minimizing weight. Among all the optimal designs that provide the highest fundamental frequency and lowest weight, the composite plate designs reinforced with carbon and natural fibers ([C/C/N/N]s-CNTs and [C/C/C/N]s, where N represents natural fibers such as Kevlar, Flax, Jute, and Ramie) are the most effective. In general, hybrid synthetic carbon/natural fiber/CNTs reinforced nanocomposites offer a weight reduction of up to 15% and a cost saving of 47%, with a potential decrease of 6% in natural frequency. Although the design

of [C/C/C/F]s-cnt and [C/C/C/F]s indicates same maximum fundamental frequency, [C/C/C/F]s-cnt is more efficient with 0,791 efficiency factor while [C/C/C/F]s case. For fully natural fiber reinforced designs the addition of CNTs may be provide % 12 increment in natural frequency at same weight. Although the designs [C/C/C/F]s-CNT and [C/C/C/F]s achieve the same maximum fundamental frequency, [C/C/C/F]s-CNT demonstrates greater efficiency with an efficiency factor of 0.791 compared to [C/C/C/F]s.

Table 6.30. Comparison of optimum fundamental frequency and minimum weight with the related cost and comparing the results to the reference design

Design	F-value	Objectives		Output	Comparison with [C/C/C/C]s design		
		wmn	Weight (Kg)	Cost (\$)	Cost Reduction (%)	Weight Reduction (%)	Frequency Reduction (%)
[F/F/F/F]s-CNT	1.139	289.548	12.957	98.208	69.1	15.3	31.2
[G/G/G/G]s-CNT	1.655	243.198	14.706	156.892	50.7	3.9	42.2
[J/J/J/J]s-CNT	1.455	239.076	12.672	98.958	68.9	17.2	43.2
[K/K/K/K]s-CNT	1.471	234.553	12.482	94.248	70.4	18.4	44.3
[R/R/R/R]s-CNT	1.200	236.123	13.232	123.478	61.2	13.5	43.9
[C/C/C/C]s-CNT	0.802	397.473	13.596	249.757	21.5	11.1	5.6
[C/F/F/F]s-CNT	1.000	321.989	13.232	181.632	42.9	13.5	23.4
[C/C/F/F]s-CNT	0.784	397.376	13.444	232.814	26.8	12.1	5.6
[C/C/C/F]s-CNT	0.791	397.713	13.505	240.252	24.5	11.7	5.5
[C/G/G/G]s-CNT	1.228	294.878	13.732	203.317	36.1	10.3	30.0
[C/C/G/G]s-CNT	0.851	395.448	13.990	240.561	24.4	8.6	6.1
[C/C/C/G]s-CNT	0.824	396.857	13.781	244.172	23.3	9.9	5.7
[C/K/K/K]s-CNT	1.079	319.062	13.156	166.295	47.7	14.0	27.9
[C/C/K/K]s-CNT	0.780	397.064	13.400	233.461	26.6	12.4	5.7
[C/C/C/K]s-CNT	0.789	397.518	13.487	241.075	24.2	11.8	5.6
[C/R/R/R]s-CNT	1.078	312.858	13.532	187.377	41.1	11.6	28.9
[C/C/R/R]s-CNT	0.796	397.209	13.540	236.148	25.8	11.5	5.7
[C/C/C/R]s-CNT	0.798	396.923	13.550	242.100	23.9	11.4	5.7
[C/J/J/J]s-CNT	1.016	319.151	13.286	169.180	46.8	13.2	27.7
[C/C/J/J]s-CNT	0.783	397.336	13.425	234.125	26.4	12.3	5.6
[C/C/C/J]s-CNT	0.791	397.279	13.495	241.241	24.2	11.8	5.6
[F/J/J/J]s-CNT	1.209	277.221	12.586	112.174	64.8	17.7	34.2
[F/F/J/J]s-CNT	1.142	287.300	12.852	98.684	69.0	16.0	31.8
[F/F/F/J]s-CNT	1.137	289.489	12.942	98.205	69.1	15.4	31.2
[F/K/K/K]s-CNT	1.197	276.544	12.506	110.346	65.3	18.3	34.3
[F/F/K/K]s-CNT	1.133	287.480	12.782	97.111	69.5	16.5	31.7

Three Phase Composites

(cont. on next page)

Table 6.30 (cont.)

[F/F/F/K]s-CNT	1.136	289.590	12.932	97.949	69.2	15.5	31.2
[F/R/R/R]s-CNT	1.261	271.396	12.899	120.241	62.2	15.7	35.5
[F/F/R/R]s-CNT	1.178	280.687	12.782	113.206	64.4	16.5	33.3
[F/F/F/R]s-CNT	1.141	288.969	12.994	99.008	68.9	15.1	31.4
[F/F/F/F]s	1.325	256.767	12.950	70.173	77.9	15.4	39.0
[G/G/G/G]s	2.034	206.979	15.300	116.170	63.5	0.0	50.8
[J/J/J/J]s	1.564	225.782	12.665	71.613	77.5	17.2	46.4
[K/K/K/K]	1.583	221.463	12.475	67.414	78.8	18.5	47.4
[R/R/R/R]	1.640	222.052	13.225	93.470	70.6	13.6	47.3
[C/F/F/F]s	1.125	300.128	13.475	135.543	57.4	11.9	28.7
[C/C/F/F]s	0.888	362.266	13.770	154.999	35.8	11.1	5.5
[C/C/C/F]s	0.809	398.128	13.668	211.986	33.4	10.7	5.4
[C/G/G/G]s	1.410	265.028	13.725	170.640	46.4	10.3	37.1
[C/C/G/G]s	0.870	393.362	14.130	211.642	33.5	7.6	6.6
[C/C/C/G]s	0.843	396.182	13.933	215.785	32.2	8.9	5.9
[C/K/K/K]s	1.143	290.972	13.150	133.618	58.0	14.1	31.5
[C/C/K/K]s	0.797	397.615	13.557	203.916	35.9	11.4	5.6
[C/C/C/K]s	0.807	397.065	13.634	211.077	33.7	10.9	5.7
[C/R/R/R]s	1.223	284.987	13.525	154.700	51.4	11.6	32.8
[C/C/R/R]s	0.814	397.742	13.697	207.077	34.9	10.5	5.5
[C/C/C/R]s	0.815	397.737	13.710	213.079	33.0	10.4	5.5
[C/J/J/J]s	1.153	291.358	13.280	136.503	57.1	13.2	31.4
[C/C/J/J]s	0.800	399.164	13.585	205.000	35.6	11.2	5.4
[C/C/C/J]s	0.808	397.240	13.647	211.523	33.5	10.8	5.7
[F/J/J/J]s	1.400	245.314	12.755	71.132	77.6	16.6	41.7
[F/F/J/J]s	1.336	253.394	12.820	72.588	77.2	16.2	39.8
[F/F/F/J]s	1.333	254.482	12.866	74.085	76.7	15.9	39.6
[F/K/K/K]s	1.391	244.316	12.625	68.248	78.6	17.5	42.0
[F/F/K/K]s	1.327	253.721	12.762	70.622	77.8	16.6	39.7
[F/F/F/K]s	1.332	254.404	12.852	74.050	76.7	16.0	39.6
[F/R/R/R]s	1.475	238.379	13.000	89.330	71.9	15.0	43.4
[F/F/R/R]s	1.377	247.603	12.775	85.190	73.2	16.5	41.2
[F/F/F/R]s	1.340	254.449	12.933	74.101	76.7	15.5	39.6

Two Phase Composites

6.3.2. Problem 2

Problem 2 is similar to Problem 1 with one difference such that cost is utilized as second objective instead of weight together with natural frequency for multi-objective optimization problems of hybrid and non-hybrid fibers/CNT reinforced composite plates with non-uniform distribution of CNT and fiber reinforcements. Additionally, the same multi-objective optimization problems are solved for two-phase fiber reinforced composite plate structures to compare efficiency of optimum design which are defined as penalty function values. The effect of minimization approach for weight with maximization of natural frequency are investigated for optimum results. Number of plies and length to thickness ratio are same for Problem 2. The objective function F_2 is also defined as penalty function which is composed of non-dimensionalized natural frequency $\bar{\omega}_{mn}$ and cost. θ_i , W_{CNTk} and V_{Fk} are the design parameters for multiphase composite plates. For two-phase fiber reinforced composites problems, θ_i and V_{Fk} are also employed as design variables. The objective of the problem is to make comparisons of multiobjective problem results for maximum natural frequency and minimum cost for Jute, Kenaf, Ramie, Flax, Carbon and Glass fiber reinforcement with and without CNT for hybrid and non-hybrid structures.

Problem 2 can be defined mathematically as

- Minimize: $F_2 = k_1 m_1^2 + k_3 m_3^2 + k_4 (\delta - 0.2)^2 + k_5 (\gamma - 0.2)^2$

$$m_1 = \left(\frac{\bar{\omega}_{max} - \bar{\omega}_{mn}}{\bar{\omega}_{max}} \right) \quad m_3 = \left(\frac{Cost}{Cost_{max}} \right)$$

- Constraints: $\frac{1}{8} \sum_{i=1}^8 W_{CNTi} \leq W_{CNTmax}, W_{CNTi} \geq 0$

Symmetric stacking sequences; $[\theta_1, \theta_2, \theta_3, \theta_4]_s$

Symmetric weight fraction of CNTs sequences;

$[W_{CNT1}/W_{CNT2}/W_{CNT3}/W_{CNT4}]_s$

Symmetric volume fraction of fiber; $[V_{F1}/V_{F2}/V_{F3}/V_{F4}]_s$

$a/D = 100, a/b = 1, W_{CNTmax}=1.25\%$,

$0.10 \leq V_{Fk} \leq 0.60$

Algorithms: Differential Evolution

Table 6.31 illustrates the impact of various hybrid and non-hybrid designs on the optimal stacking sequence, fiber volume fraction, and CNT distribution weight fraction, aiming to achieve the highest possible fundamental frequency and the lowest achievable

cost of the composite plates. The findings suggest that designs tend to be more efficient when a larger volume fraction and weight content of CNTs are placed in the outer layer rather than the inner layer similar to multi-objective Problem 1.

Table 6.31. Comparison of optimum Stacking sequence, volume fraction of fiber and weight fraction of CNT distribution results for maximum fundamental frequency and minimum cost of composite plates,

Design	F-value	Optimum Results		
		Stacking Sequence	Fiber Volume Fraction per layer	Weight Content of CNT per layer
[F/F/F/F] _s -CNT	0.501	[45/-45/45/45] _s	[0.60/0.60/0.60/0.60] _s	[0.0397/0.0103/0/0.0] _s
[G/G/G/G] _s -CNT	0.895	[45/-45/45/45] _s	[0.600/0.600/0.600/0.100] _s	[0.0473/0.0077/0/0] _s
[J/J/J/J] _s -CNT	0.844	[45/-45/-45/45] _s	[0.60/0.60/0.60/0.60] _s	[0.05/0.0/0/0] _s
[K/K/K/K]-CNT	0.866	[45/-45/-45/45] _s	[0.60/0.60/0.60/0.60] _s	[0.05/0.0/0/0] _s
[R/R/R/R]-CNT	0.885	[45/-45/45/-45] _s	[0.60/0.60/0.60/0.10] _s	[0.0484/0.0016/0/0.0] _s
[C/C/C/C] _s -CNT	0.597	[45/-45/-45/-45] _s	[0.594/0.600/0.270/0.100] _s	[0.0004/0.0/0.0/0.0] _s
[C/F/F/F] _s -CNT	0.559	[90/45/45/45] _s	[0.60/0.60/0.60/0.60] _s	[0.0392/0.00/0/0.0] _s
[C/C/F/F] _s -CNT	0.306	[45/-45/-45/-45] _s	[0.463/0.486/0.60/0.60] _s	[0.0/0.0/0/0.0] _s
[C/C/C/F] _s -CNT	0.389	[45/-45/-45/-45] _s	[0.453/0.491/0.100/0.600] _s	[0.0/0.0/0/0.0] _s
[C/G/G/G] _s -CNT	0.738	[90/45/45/45] _s	[0.60/0.60/0.10/0.10] _s	[0.0356/0/0/0] _s
[C/C/G/G] _s -CNT	0.443	[45/-45/-45/-45] _s	[0.449/0.520/0.10/0.10] _s	[0/0/0/0] _s
[C/C/C/G] _s -CNT	0.454	[45/-45/-45/-45] _s	[0.443/0.485/0.10/0.10] _s	[0/0/0/0] _s
[C/K/K/K] _s -CNT	0.551	[90/45/45/45] _s	[0.60/0.60/0.60/0.60] _s	[0.0181/0/0/0] _s
[C/C/K/K] _s -CNT	0.301	[45/-45/-45/-45] _s	[0.458/0.499/0.60/0.60] _s	[0/0/0/0] _s
[C/C/C/K] _s -CNT	0.384	[45/-45/-45/-45] _s	[0.448/0.491/0.10/0.60] _s	[0/0/0/0] _s
[C/R/R/R] _s -CNT	0.594	[90/45/45/45] _s	[0.60/0.60/0.60/0.60] _s	[0.0173/0/0/0] _s
[C/C/R/R] _s -CNT	0.351	[45/-45/-45/-45] _s	[0.471/0.507/0.600/0.600] _s	[0/0/0/0] _s
[C/C/C/R] _s -CNT	0.412	[45/-45/-45/-45] _s	[0.455/0.498/0.100/0.600] _s	[0/0/0/0] _s
[C/J/J/J] _s -CNT	0.522	[90/45/45/45] _s	[0.60/0.60/0.60/0.60] _s	[0.0175/0/0/0] _s
[C/C/J/J] _s -CNT	0.312	[45/-45/-45/-45] _s	[0.459/0.497/0.60/0.60] _s	[0/0/0/0] _s
[C/C/C/J] _s -CNT	0.390	[45/-45/-45/-45] _s	[0.446/0.488/0.100/0.600] _s	[0/0/0/0] _s
[F/J/J/J] _s -CNT	0.599	[45/-45/-45/45] _s	[0.60/0.60/0.60/0.60] _s	[0.0500/0/0/0] _s
[F/F/J/J] _s -CNT	0.514	[45/-45/45/45] _s	[0.60/0.60/0.60/0.60] _s	[0.0372/0.0128/0/0] _s
[F/F/F/J] _s -CNT	0.498	[45/-45/45/45] _s	[0.60/0.60/0.60/0.60] _s	[0.0394/0.0106/0/0] _s
[F/K/K/K] _s -CNT	0.585	[45/-45/-45/45] _s	[0.60/0.60/0.60/0.60] _s	[0.0500/0/0/0] _s
[F/F/K/K] _s -CNT	0.503	[45/-45/45/-45] _s	[0.60/0.60/0.60/0.60] _s	[0.0369/0.0131/0/0] _s
[F/F/F/K] _s -CNT	0.485	[45/-45/45/45] _s	[0.60/0.60/0.60/0.60] _s	[0.0393/0.0107/0/0] _s
[F/R/R/R] _s -CNT	0.673	[45/-45/-45/45] _s	[0.60/0.60/0.60/0.10] _s	[0.0500/0/0/0] _s
[F/F/R/R] _s -CNT	0.552	[45/-45/45/45] _s	[0.60/0.60/0.60/0.10] _s	[0.0391/0.0109/0/0] _s
[F/F/F/R] _s -CNT	0.515	[45/-45/45/45] _s	[0.60/0.60/0.60/0.10] _s	[0.0388/0.0112/0/0] _s

Three Phase Composites

(cont. on next page)

Table 6.31 (cont.)

	[F/F/F/F]s	0.648	[45/-45/45/45]s	[0.60/0.60/0.60/0.60]s	-
	[G/G/G/G]s	1.166	[45/-45/-45/-45]s	[0.521/0.379/0.100/0.100]s	-
	[J/J/J/J]s	0.914	[45/-45/-45/45]s	[0.60/0.60/0.60/0.60]s	-
	[K/K/K/K]	0.943	[45/-45/-45/45]s	[0.60/0.60/0.60/0.60]s	-
	[R/R/R/R]	0.934	[45/-45/-45/45]s	[0.60/0.60/0.60/0.10]s	-
	[C/F/F/F]s	0.505	[90/45/45/45]s	[0.60/0.60/0.60/0.60]s	-
	[C/C/F/F]s	0.306	[45/-45/-45/-45]s	[0.463/0.486/0.60/0.60]s	-
	[C/C/C/F]s	0.389	[45/-45/-45/-45]s	[0.453/0.491/0.10/0.60]s	-
	[C/G/G/G]s	0.773	[90/45/45/45]s	[0.60/0.60/0.10/0.10]s	-
	[C/C/G/G]s	0.443	[45/-45/-45/-45]s	[0.449/0.520/0.10/0.10]s	-
	[C/C/C/G]s	0.454	[45/-45/-45/-45]s	[0.443/0.485/0.10/0.10]s	-
	[C/K/K/K]s	0.563	[90/45/45/45]s	[0.60/0.60/0.60/0.60]s	-
	[C/C/K/K]s	0.301	[45/-45/-45/-45]s	[0.458/0.499/0.60/0.60]s	-
	[C/C/C/K]s	0.383	[45/-45/-45/-45]s	[0.448/0.491/0.10/0.60]s	-
	[C/R/R/R]s	0.635	[90/45/45/45]s	[0.60/0.60/0.60/0.60]s	-
	[C/C/R/R]s	0.351	[45/-45/-45/-45]s	[0.472/0.507/0.60/0.60]s	-
	[C/C/C/R]s	0.412	[45/-45/-45/-45]s	[0.455/0.498/0.10/0.60]s	-
	[C/J/J/J]s	0.571	[90/45/45/45]s	[0.60/0.60/0.60/0.60]s	-
	[C/C/J/J]s	0.312	[45/-45/-45/-45]s	[0.406/0.431/0.60/0.60]s	-
	[C/C/C/J]s	0.390	[45/-45/-45/-45]s	[0.446/0.488/0.10/0.60]s	-
	[F/J/J/J]s	0.742	[45/-45/-45/-45]s	[0.60/0.60/0.60/0.60]s	-
	[F/F/J/J]s	0.665	[45/-45/45/-45]s	[0.60/0.60/0.60/0.60]s	-
	[F/F/F/J]s	0.646	[45/-45/45/-45]s	[0.60/0.60/0.598/0.600]s	-
	[F/K/K/K]s	0.745	[45/-45/45/45]s	[0.596/0.60/0.594/0.60]s	-
	[F/F/K/K]s	0.658	[45/-45/45/45]s	[0.60/0.60/0.60/0.60]s	-
	[F/F/F/K]s	0.668	[45/-45/45/-45]s	[0.596/0.60/0.594/0.60]s	-
	[F/R/R/R]s	0.796	[45/-45/-45/45]s	[0.60/0.60/0.60/0.10]s	-
	[F/F/R/R]s	0.709	[45/-45/45/-45]s	[0.60/0.60/0.60/0.489]s	-
	[F/F/F/R]s	0.668	[45/-45/45/-45]s	[0.60/0.60/0.60/0.448]s	-

Two Phase Composites

This approach leverages the benefits of density and strength properties, integrating CNTs into each layer of natural fiber reinforced designs to increase fiber volume content and lower costs. In hybrid carbon and natural fiber reinforced designs, algorithms often favour two-phase designs without CNTs due to their lower cost compared to incorporating CNTs. The F values also indicate the efficiency level of the optimal design concerning both frequency and cost. The minimum F values for [C/C/F/F]s-CNT, [C/C/C/F]s-CNT, [C/C/K/K]s-CNT, [C/C/C/K]s-CNT, [C/C/R/R]s-CNT, [C/C/C/R]s-CNT, [C/C/J/J]s-CNT, [C/C/C/J]s-CNT are identical to those of the two-phase design cases [C/C/N/N]s and [C/C/C/N]s, all below 0.400. In these designs, where cost is prioritized over weight in a multi-objective approach, there is no distinction

between optimal hybrid carbon-natural fiber reinforced composite [C/C/N/N] s and [C/C/C/N] s designs. The glass fiber reinforced [G/G/G/G]s-CNT and [G/G/G/G]s cases are less efficient compared to optimal designs among two-phase and three-phase composite structures. Among the non-hybrid fiber/CNT reinforced optimal designs, the most efficient case is [F/F/F/F]s-CNT, which achieves a design efficiency factor of 0.500. The efficiency of [F/F/F/F]s-CNT arises from the synergistic combination of the relatively economical flax fiber and the strategic incorporation of a small, yet impactful, amount of 1% CNT, despite its higher cost. In completely natural fiber reinforced cases such as [F/F/F/F]s, [J/J/J/J]s, [K/K/K/K]s, [R/R/R/R]s, and their hybridizations, the strategic addition and optimization of CNT at each ply result in a 10% increase in frequency, a 70% reduction in cost, and a 15% weight savings. This finding supports the use of hybridizing natural fibers with carbon fibers in applications where vibration control and cost efficiency are critical, especially in scenarios where carbon nanotubes (CNTs) are not utilized. Given that the price of carbon fiber is lower than that of CNTs, incorporating CNTs may not be feasible for achieving maximum natural frequency and minimizing costs in multi-objective optimization problems. In contrast to the previous problem, where weight was not considered in the objective function of the optimization problem, the fully carbon fiber reinforced [C/C/C/C]s-CNT case is not an efficient design in terms of natural frequency and cost. However, for achieving a cost-effective and high natural frequency design, combining flax, kenaf, ramie, and jute fibers with CNTs proves more advantageous compared to [G/G/G/G]s designs.

Table 6.32 provides the optimum outcomes for natural frequency and cost across different hybrid and non-hybrid scenarios, including configurations with and without CNT. It also includes weight values to facilitate comparisons with other approaches in multi-objective optimization. Reductions in cost and frequency are expressed as a percentage compared to the [C/C/C/C] s reference optimal case. The two-phase cases of [C/C/K/K]s, [C/C/J/J]s, and [C/C/F/F]s are the most efficient, achieving the lowest F values of 0.301, 0.312, and 0.306, respectively. The results suggest that by accepting a 9.9% reduction in frequency, a cost reduction of 48.8% is achievable, while at the same time using greener fibres and achieving a weight reduction of approximately 9%. The [C/C/C/F]s, [C/C/C/K]s, and [C/C/C/J]s designs also exhibit F values of 0.389, 0.384, and 0.390, respectively. These designs offer a 41% cost reduction and 11% weight savings, achieved by sacrificing 11% of the natural frequency, making them the second feasible designs. C/F/F/F]s-CNT, [C/R/R/R]s-CNT, [C/J/J/J]s-CNT, and [C/R/R/R]s-

CNT are the next most efficient designs. With a 53% reduction in cost and a 23% reduction in natural frequency, these designs offer optimal solutions. Additionally, three-phase hybrid designs fully reinforced with natural fibers—such as [F/J/J/J]s-CNT, [F/F/J/J]s-CNT, [F/F/F/J]s-CNT, [F/K/K/K]s-CNT, [F/F/K/K]s-CNT, [F/F/F/K]s-CNT, [F/R/R/R]s-CNT, [F/F/R/R]s-CNT, and [F/F/F/R]s-CNT—offer efficient solutions. These designs achieve a 72% cost reduction, albeit with a 31% decrease in frequency.

Table 6.32. Comparison of optimum fundamental frequency and minimum cost with the related weight and comparing the results to the reference design

Design	F-value	Objectives		Output	Comparison with [C/C/C/C]s design		
		Fundamental Frequency	Cost	Weight	Cost Reduction (%)	Weight Reduction (%)	Frequency Reduction (%)
[F/F/F/F]s-CNT	0.501	288.180	84.790	13.207	73.4	13.7	31.6
[G/G/G/G]s-CNT	0.895	251.381	146.017	17.706	54.1	-15.7	40.3
[J/J/J/J]s-CNT	0.844	238.568	86.024	12.847	73.0	16.0	43.3
[K/K/K/K]-CNT	0.866	234.622	80.258	12.606	74.8	17.6	44.3
[R/R/R/R]-CNT	0.885	240.639	113.406	13.669	64.4	10.7	42.8
[C/C/C/C]s-CNT	0.597	421.000	245.918	14.151	22.7	7.5	0.0
[C/F/F/F]s-CNT	0.559	320.408	147.708	13.730	53.6	10.3	23.9
[C/C/F/F]s-CNT	0.306	378.031	163.826	13.904	48.5	9.1	10.2
[C/C/C/F]s-CNT	0.389	375.262	186.214	13.735	41.5	10.2	10.9
[C/G/G/G]s-CNT	0.738	295.061	188.457	15.223	40.8	0.5	29.8
[C/C/G/G]s-CNT	0.443	371.135	198.052	13.932	37.8	8.9	11.9
[C/C/C/G]s-CNT	0.454	371.418	200.933	13.714	36.9	10.4	11.8
[C/K/K/K]s-CNT	0.551	302.671	131.402	13.277	58.7	13.2	29.9
[C/C/K/K]s-CNT	0.301	379.476	162.903	13.616	48.8	11.0	9.9
[C/C/C/K]s-CNT	0.384	375.822	184.930	13.579	41.9	11.3	10.7
[C/R/R/R]s-CNT	0.594	294.124	145.802	14.402	54.2	5.9	30.0
[C/C/R/R]s-CNT	0.351	374.201	174.863	14.390	45.1	5.9	11.1
[C/C/C/R]s-CNT	0.412	373.187	191.180	13.973	39.9	8.7	11.4
[C/J/J/J]s-CNT	0.522	302.070	134.952	13.457	57.6	12.0	28.3
[C/C/J/J]s-CNT	0.312	378.239	165.436	13.735	48.0	10.2	10.2
[C/C/C/J]s-CNT	0.390	374.270	185.788	13.632	41.6	10.9	11.1
[F/J/J/J]s-CNT	0.599	281.124	86.307	12.937	72.9	15.4	33.2
[F/F/J/J]s-CNT	0.514	286.076	85.746	13.026	73.1	14.9	32.0
[F/F/F/J]s-CNT	0.498	288.665	85.276	13.117	73.2	14.3	31.4
[F/K/K/K]s-CNT	0.585	281.368	82.366	12.757	74.1	16.6	33.2
[F/F/K/K]s-CNT	0.503	287.030	83.120	12.906	73.9	15.6	31.8
[F/F/F/K]s-CNT	0.485	289.523	83.962	13.057	73.6	14.7	31.2

Three Phase Composites

(cont. on next page)

Table 6.32 (cont.)

[F/R/R/R]s-CNT	0.673	278.459	107.363	13.444	66.3	12.1	33.9
[F/F/R/R]s-CNT	0.552	284.696	103.150	13.219	67.6	13.6	32.4
[F/F/F/R]s-CNT	0.515	289.282	99.008	12.994	68.9	15.1	31.3
[F/F/F/F]s	0.648	255.760	56.760	13.200	82.2	13.7	39.3
[G/G/G/G]s	1.166	206.979	116.158	15.300	63.5	0.0	50.8
[J/J/J/J]s	0.914	225.431	58.678	12.840	81.6	16.1	46.5
[K/K/K/K]	0.943	221.518	53.424	12.600	83.2	17.6	47.4
[R/R/R/R]	0.934	227.307	83.395	13.662	73.8	10.7	46.0
[C/F/F/F]s	0.505	298.565	135.725	13.725	57.4	10.3	29.1
[C/C/F/F]s	0.306	378.031	163.826	13.905	48.5	9.1	10.2
[C/C/C/F]s	0.389	375.262	186.214	13.735	41.5	10.2	10.9
[C/G/G/G]s	0.773	275.311	165.240	15.225	48.1	0.5	34.6
[C/C/G/G]s	0.443	371.135	198.052	13.932	37.8	8.9	11.9
[C/C/C/G]s	0.454	371.418	200.933	13.714	36.9	10.4	11.8
[C/K/K/K]s	0.563	287.775	119.628	13.275	62.4	13.2	31.7
[C/C/K/K]s	0.301	379.476	162.903	13.616	48.8	11.0	9.9
[C/C/C/K]s	0.383	375.822	184.930	13.578	41.9	11.3	10.7
[C/R/R/R]s	0.635	281.741	134.550	14.400	57.7	5.9	33.1
[C/C/R/R]s	0.351	374.416	174.863	14.396	45.1	5.9	11.1
[C/C/C/R]s	0.412	373.187	191.180	13.972	39.9	8.7	11.4
[C/J/J/J]s	0.571	287.840	123.569	13.455	61.2	12.1	31.6
[C/C/J/J]s	0.312	378.239	165.436	13.570	48.0	11.3	10.2
[C/C/C/J]s	0.390	374.270	185.788	13.632	41.6	10.9	11.1
[F/J/J/J]s	0.742	244.738	58.190	12.930	81.7	15.5	41.9
[F/F/J/J]s	0.665	253.560	57.719	13.050	81.9	14.7	39.8
[F/F/F/J]s	0.646	256.110	57.298	13.109	82.0	14.3	39.2
[F/K/K/K]s	0.745	243.571	56.217	13.045	82.3	14.7	42.2
[F/F/K/K]s	0.658	254.084	55.092	12.900	82.7	15.7	39.7
[F/F/F/K]s	0.668	256.078	56.217	13.045	82.3	14.7	39.2
[F/R/R/R]s	0.796	242.859	79.255	13.437	75.1	12.2	42.4
[F/F/R/R]s	0.709	249.399	67.578	13.553	78.8	11.4	40.8
[F/F/F/R]s	0.668	254.177	64.333	13.292	79.8	13.1	39.6

Two Phase Composites

In multi-objective optimization problems where natural frequency and cost serve as objectives, hybrid and non-hybrid natural fiber reinforced designs with CNTs may also achieve a 15.5% weight reduction. It can be seen that less efficient designs with a 10% reduction in frequency values are disadvantageous compared to multiphase designs with CNTs for the same design approaches using fully natural fibre-reinforced cases in two-phase structures without CNTs. Nevertheless, these designs still achieve an 82% reduction in cost and a 17% decrease in weight.

This graph presents the optimal design in terms of maximum natural frequency and minimum cost for both hybrid and non-hybrid fiber reinforced composites, including configurations with and without carbon nanotubes (CNTs). The most effective designs in terms of both cost and natural frequency are [C/C/N/N]s and [C/C/C/N]s (where N represents natural fibres such as Kevlar, flax, jute and ramie). Of all the cases, [C/C/K/K]s emerges as the most efficient design both in terms of cost and in terms of natural frequency. In general, two-phase composite designs using carbon and natural fibers can achieve up to a 48% cost reduction and a 10% weight reduction, while potentially experiencing an 11% decrease in natural frequency. This is because the optimization aims to strike a balance between minimizing costs and maximizing fundamental frequency objectives. For the hybrid natural fiber reinforced [F/F/F/K]s-CNT design, it is possible to achieve a 48% weight reduction and a 15% cost saving, albeit with a sacrifice of 31% in natural frequency compared to traditional carbon fiber reinforced composite structures.

6.3.3. Problem 3

Problem 3 examines the effect of three different objectives; natural frequency, weight and cost in multi-objective optimization approach for hybrid and non-hybrid fibers/CNT reinforced nanocomposite plates with non-uniform distribution of CNT and fiber reinforcements. The alternative hybrid and non-hybrid natural fiber reinforced composite designs with and without carbon nanotubes are proposed in terms of optimum fundamental frequency, cost and weight to traditional carbon and glass fiber reinforced composite structures. The effect of minimization approach for weight and cost while maximizing of natural frequency are investigated for optimum results. The efficiency factor F (penalty function values) values and increment and decreasing in frequency, weight and cost values are compared with Problem 1 and Problem 2 results in order to investigate the effect of different multi-objective optimization approach for three and two phase fiber reinforced composite structures. Number of plies and length to thickness ratio are same with Problem 1 and 2. The objective function F_3 is also defined as penalty function which is composed of non-dimensionalized natural frequency $\bar{\omega}_{mn}$, weight and cost. θ_i , W_{CNT_k} and V_{Fk} are the design parameters for multiphase composite plates. For two-phase fiber reinforced composites problems, θ_i and V_{Fk} are also employed as design variables. The objective of the problem is to make comparisons of multiobjective problem

results for maximum natural frequency and minimum cost and weight for Jute, Kenaf, Ramie, Flax, Carbon and Glass fiber reinforcement with and without CNT for hybrid and non-hybrid structures.

Problem 3 can be defined mathematically as

- Minimize:

$$F_3 = k_1 m_1^2 + k_2 m_2^2 + k_3 m_3^2 + k_4 (\delta - 0.2)^2 + k_5 (\gamma - 0.2)^2$$

$$m_1 = \left(\frac{\bar{\omega}_{max} - \bar{\omega}_{mn}}{\bar{\omega}_{max}} \right) m_2 = \left(\frac{Weight}{Weight_{max}} \right) m_2 = \left(\frac{Cost}{Cost_{max}} \right)$$

- Constraints: $\frac{1}{8} \sum_{i=1}^8 W_{CNTi} \leq W_{CNTmax}, W_{CNTi} \geq 0$

Symmetric stacking sequences; $[\theta_1, \theta_2, \theta_3, \theta_4]_s$

Symmetric weight fraction of CNTs sequences;

$[W_{CNT1}/W_{CNT2}/W_{CNT3}/W_{CNT4}]_s$

Symmetric volume fraction of Fiber; $[V_{F1}/V_{F2}/V_{F3}/V_{F4}]_s$

$a/D = 100, a/b = 1, W_{CNTmax}=1.25\%$,

$0.10 \leq V_{Fk} \leq 0.60$

Algorithms: Differential Evolution

Table 6.33 shows the influence of different hybrid and non-hybrid designs with CNT on the optimal stacking sequence, fibre volume fraction and CNT weight fraction distribution. The aim is to achieve the maximum possible fundamental frequency and the minimum possible cost and weight of the two phase and three phase composite plates. The results suggest that, similar to the multi-objective Problems 1 and 2, designs tend to be more efficient when a high weight content of CNTs is placed in the outer layer rather than the inner layer. To achieve optimum designs for three different objectives—maximum frequency, minimum cost, and minimum weight—variable fiber volume content and CNT weight content are proposed according to different fiber types and their hybridizations. The [C/C/F/F]_s CNT, [C/C/K/K]_s CNT, [C/C/J/J]_s CNT, [C/C/C/J]_s CNT, [C/C/C/K]_s and [C/C/K/K]_s designs have the minimum F values below the 1,200 value and thus provide the optimum solutions in terms of natural frequency, cost and weight. However, the frequency, cost and weight values of the designs differ from each other due to the variable material properties, which are advantageous for natural fibres and CNTs. For instance, although the F values of [C/C/F/F]_s-CNT, [C/C/C/K]_s-CNT, [C/C/K/K]_s-CNT, [C/C/K/K]_s, [C/C/F/F]_s, and [C/C/C/K]_s are identical, the frequency values, costs, and weights of these designs vary significantly. This variation allows

designers to select the optimal design based on the specific priorities of their application areas.

Table 6.33. Comparison of optimum Stacking sequence, volume fraction of fiber and weight fraction of CNT distribution results for maximum fundamental frequency and minimum weight of composite plates

Design	F-value	Optimum Results		
		Stacking Sequence	Fiber Volume Fraction per layer	Weight Content of CNT per layer
[F/F/F/F]s-CNT	1.235	[45/-45/45/45]s	[0.60/0.60/0.60/0.10]s	[0.039/0.0110/0/0.0]s
[G/G/G/G]s-CNT	1.893	[45/-45/45/45]s	[0.600/0.100/0.100/0.100]s	[0.05/0.0/0/0]s
[J/J/J/J]s-CNT	1.549	[45/-45/45/45]s	[0.600/0.100/0.100/0.100]s	[0.05/0.0/0/0]s
[K/K/K/K]-CNT]	1.546	[45/-45/-45/45]s	[0.60/0.60/0.60/0.60]s	[0.05/0.0/0/0]s
[R/R/R/R]-CNT	1.200	[45/-45/45/-45]s	[0.60/0.60/0.60/0.10]s	[0.0472/0.0028/0/0.0]s
[C/C/C/C]s-CNT	1.412	[45/-45/-45/-45]s	[0.578/0.600/0.100/0.100]s	[0.0190/0.0/0.0027/0.0]s
[C/F/F/F]s-CNT	1.272	[90/45/45/45]s	[0.60/0.60/0.60/0.60]s	[0.0388/0.00/0/0.0]s
[C/C/F/F]s-CNT	1.134	[45/-45/-45/-45]s	[0.424/0.425/0.60/0.60]s	[0.0060/0.0/0/0.0]s
[C/C/C/F]s-CNT	1.212	[45/-45/-45/-45]s	[0.411/0.422/0.100/0.600]s	[0.0080/0.0/0.0027/0.0]s
[C/G/G/G]s-CNT	1.635	[90/45/45/45]s	[0.60/0.10/0.10/0.10]s	[0.0457/0/0/0]s
[C/C/G/G]s-CNT	1.279	[45/-45/-45/-45]s	[0.406/0.450/0.10/0.10]s	[0.0080/0/0/0]s
[C/C/C/G]s-CNT	1.261	[45/-45/-45/-45]s	[0.404/0.424/0.10/0.10]s	[0.0060/0/0/0]s
[C/K/K/K]s-CNT	1.265	[90/45/45/45]s	[0.60/0.60/0.60/0.60]s	[0.0178/0/0/0]s
[C/C/K/K]s-CNT	1.100	[45/-45/-45/-45]s	[0.415/0.431/0.60/0.60]s	[0.0072/0/0.0028/0]s
[C/C/C/K]s-CNT	1.404	[45/-45/-45/-45]s	[0.439/0.386/0.60/0.60]s	[0.01/0/0/0]s
[C/R/R/R]s-CNT	1.434	[90/45/45/45]s	[0.60/0.60/0.10/0.10]s	[0.0136/0/0/0]s
[C/C/R/R]s-CNT	1.206	[45/-45/-45/-45]s	[0.40/0.444/0.101/0.100]s	[0.0100/0/0/0]s
[C/C/C/R]s-CNT	1.222	[45/-45/-45/-45]s	[0.398/0.421/0.100/0.100]s	[0.0060/0/0/0]s
[C/J/J/J]s-CNT	1.296	[90/45/45/45]s	[0.60/0.60/0.60/0.60]s	[0.0172/0/0/0]s
[C/C/J/J]s-CNT	1.118	[45/-45/-45/-45]s	[0.417/0.433/0.60/0.60]s	[0.0058/0/0.0002/0]s
[C/C/C/J]s-CNT	1.187	[45/-45/-45/-45]s	[0.404/0.424/0.100/0.600]s	[0.0059/0/0.0001]s
[F/J/J/J]s-CNT	1.315	[45/-45/-45/45]s	[0.60/0.60/0.60/0.60]s	[0.0500/0/0/0]s
[F/F/J/J]s-CNT	1.232	[45/-45/45/45]s	[0.60/0.60/0.60/0.306]s	[0.0382/0.0118/0/0]s
[F/F/F/J]s-CNT	1.226	[45/-45/45/45]s	[0.60/0.60/0.60/0.10]s	[0.0384/0.0116/0/0]s
[F/K/K/K]s-CNT	1.282	[45/-45/-45/45]s	[0.60/0.60/0.60/0.60]s	[0.0500/0/0/0]s

Three Phase Composites

(cont. on next page)

Table 6.33 (cont.)

[F/F/K/K]s-CNT	1.211	[45/-45/45/45]s	[0.60/0.60/0.60/0.60]s	[0.0382/0.0118/0/0]s
[F/F/F/K]s-CNT	1.214	[45/-45/45/45]s	[0.60/0.60/0.60/0.60]s	[0.0390/0.0110/0/0]s
[F/R/R/R]s-CNT	1.386	[45/-45/45/45]s	[0.60/0.60/0.60/0.10]s	[0.0500/0/0/0]s
[F/F/R/R]s-CNT	1.300	[45/-45/45/45]s	[0.60/0.60/0.60/0.10]s	[0.0388/0.0112/0/0]s
[F/F/F/R]s-CNT	1.238	[45/-45/45/45]s	[0.60/0.60/0.60/0.10]s	[0.0385/0.0115/0/0]s
[F/F/F/F]s	1.373	[45/-45/45/45]s	[0.60/0.60/0.60/0.10]s	-
[G/G/G/G]s	2.166	[45/-45/-45/-45]s	[0.521/0.379/0.100/0.100]s	-
[J/J/J/J]s	1.615	[45/-45/-45/45]s	[0.60/0.60/0.60/0.10]s	-
[K/K/K/K]	1.621	[45/-45/-45/45]s	[0.60/0.60/0.60/0.60]s	-
[R/R/R/R]	1.734	[45/-45/-45/45]s	[0.60/0.60/0.60/0.60]s	-
[C/F/F/F]s	1.306	[90/45/45/45]s	[0.60/0.60/0.60/0.10]s	-
[C/C/F/F]s	1.125	[45/-45/-45/45]s	[0.419/0.432/0.60/0.60]s	-
[C/C/C/F]s	1.187	[45/-45/-45/-45]s	[0.410/0.438/0.10/0.60]s	-
[C/G/G/G]s	1.697	[90/45/45/45]s	[0.60/0.10/0.10/0.10]s	-
[C/C/G/G]s	1.265	[45/-45/-45/-45]s	[0.406/0.467/0.10/0.10]s	-
[C/C/C/G]s	1.250	[45/-45/-45/-45]s	[0.404/0.437/0.10/0.10]s	-
[C/K/K/K]s	1.300	[90/45/45/45]s	[0.60/0.60/0.60/0.60]s	-
[C/C/K/K]s	1.085	[45/-45/-45/-45]s	[0.415/0.445/0.60/0.60]s	-
[C/C/C/K]s	1.164	[45/-45/-45/-45]s	[0.404/0.436/0.10/0.60]s	-
[C/R/R/R]s	1.473	[90/45/45/45]s	[0.60/0.60/0.10/0.10]s	-
[C/C/R/R]s	1.187	[45/-45/-45/-45]s	[0.40/0.464/0.10/0.10]s	-
[C/C/C/R]s	1.210	[45/-45/-45/-45]s	[0.40/0.435/0.10/0.10]s	-
[C/J/J/J]s	1.345	[90/45/45/45]s	[0.60/0.60/0.60/0.60]s	-
[C/C/J/J]s	1.110	[45/-45/-45/-45]s	[0.406/0.431/0.60/0.60]s	-
[C/C/C/J]s	1.177	[45/-45/-45/-45]s	[0.406/0.438/0.10/0.60]s	-
[F/J/J/J]s	1.450	[45/-45/-45/-45]s	[0.60/0.60/0.60/0.10]s	-
[F/F/J/J]s	1.386	[45/-45/-45/-45]s	[0.60/0.60/0.60/0.396]s	-
[F/F/F/J]s	1.380	[45/-45/45/-45]s	[0.60/0.60/0.598/0.598]s	-
[F/K/K/K]s	1.434	[45/-45/-45/45]s	[0.60/0.60/0.60/0.60]s	-
[F/F/K/K]s	1.369	[45/-45/45/45]s	[0.60/0.60/0.60/0.60]s	-
[F/F/F/K]s	1.371	[45/-45/45/-45]s	[0.60/0.60/0.574/0.60]s	-
[F/R/R/R]s	1.553	[45/-45/45/-45]s	[0.60/0.60/0.257/0.10]s	-
[F/F/R/R]s	1.448	[45/-45/45/45]s	[0.60/0.60/0.385/0.10]s	-
[F/F/F/R]s	1.395	[45/-45/45/-45]s	[0.60/0.60/0.491/0.10]s	-

Two Phase Composites

Integrating CNTs into each layer of natural fiber reinforced designs can enhance the optimal design in terms of cost, weight, and frequency. The results indicate that algorithms tend to use a very low level of CNT addition to improve efficiency. This approach also enables more efficient designs compared to two-phase optimal results for multi-objective optimization problems focused on achieving maximum frequency and

minimizing cost and weight. In these designs, where cost and weight are equally prioritized in a multi-objective approach, there is a distinction between the optimal hybrid carbon-natural fiber reinforced composite three-phase [C/C/N/N]_s-CNT and two-phase [C/C/C/N]_s designs. When considering the CNT addition difference in the multi-objective approach, the designs achieve a 5% higher natural frequency compared to the two-phase designs by incorporating just 2% CNT into the outer layer of the structures. The glass fiber reinforced [G/G/G/G]_s-CNT and [G/G/G/G]_s cases are also less efficient compared to optimal designs among two-phase and three-phase composite structures.

Among the fully hybrid and non-hybrid natural fiber/CNT reinforced optimal designs, [F/F/K/K]_s-CNT, [F/F/F/K]_s-CNT, [F/F/J/J]_s-CNT, and [F/F/F/J]_s-CNT represent the second most efficient cases, offering approximately 70% cost savings and a 15% weight reduction, albeit with a 30% frequency reduction. Optimal distribution of 5% CNTs in natural fiber reinforced composite designs provides a 13% increase in frequency at the expense of a 9% cost increase. It is possible to achieve a design with 1.369 F values by reducing the cost by 82% and the weight by 15% for the optimal two-phase fully natural fibre reinforced composite designs [F/F/K/K]_s. In fully natural fibre reinforced cases such as [F/F/F/F]_s CNT, [J/J/J/J]_s CNT, [K/K/K/K]_s CNT, [R/R/R/R]_s CNT, the strategic addition and optimization of CNT at each ply results in up to 13.2% increase in frequency with 1.235 F value compared to two-phase cases; [F/F/F/F]_s, [J/J/J/J]_s, [K/K/K/K]_s, [R/R/R/R]_s.

The results supports that the use of CNTs in mutiphase hybrid and non-hybrid fully natural fiber reinforced composites are more beneficial in multiobjective optimum solution for applications where minimum weight, cost and maximum natural frequency are requested. For carbon/natural fiber and CNT reinforced nanocomposite cases, algorithm tend to give optimum results by decreasing volume content of fiber in inner layer by adding CNT into outer layers.

Table 6.34 outlines the optimal results for natural frequency, cost, and weight across various hybrid and non-hybrid configurations, including those with and without CNT. Reductions in weight, cost, and frequency are quantified as percentages relative to the baseline [C/C/C/C]_s reference case. Among the configurations evaluated, the [C/C/K/K]_s-CNT, [C/C/F/F]_s-CNT, [C/C/J/J]_s-CNT, [C/C/K/K]_s, and [C/C/F/F]_s cases emerged as the most efficient, recording the lowest F values of 1.100, 1.134, 1.118, 1.085, and 1.125 respectively. The findings suggest that a cost reduction of up to 50% and a weight reduction of 12.8% are achievable by allowing a frequency reduction of about

13%, while also incorporating more eco-friendly fibers. In terms of natural frequency, the fully carbon fiber reinforced [C/C/C/C] s-CNT case has the highest natural frequency which is capable of giving reference optimal design behaviour with more advantageous that by decreasing 23% cost and 10% weight. It also shows that by using CNT fillers in the outer layers of carbon fiber reinforced structures, the price and weight may be decreased of traditional carbon fiber reinforced composite structures for the same natural frequency value.

Table 6.34. Comparison of optimum fundamental frequency, minimum cost and weight and comparing the results to the reference design

Design	F-value	Objectives		Output	Comparison with [C/C/C/C]s design		
		wmn	Weight	cost	Cost Reduction (%)	Weight Reduction (%)	Frequency Reduction (%)
[F/F/F/F]s-CNT	1.235	289.503	12.956	98.200	69.1	15.3	31.2
[G/G/G/G]s-CNT	1.893	243.198	14.706	156.892	50.7	3.9	42.2
[J/J/J/J]s-CNT	1.549	210.356	12.322	124.825	60.8	19.5	50.0
[K/K/K/K]-CNT]	1.546	234.478	12.606	80.258	74.8	17.6	44.3
[R/R/R/R]-CNT	1.200	240.642	13.669	113.396	64.4	10.7	42.8
[C/C/C/C]s-CNT	1.412	420.007	13.898	243.971	23.3	9.2	0.2
[C/F/F/F]s-CNT	1.272	320.220	13.730	147.446	53.7	10.3	23.9
[C/C/F/F]s-CNT	1.134	365.014	13.768	160.073	49.7	10.0	13.3
[C/C/C/F]s-CNT	1.212	361.115	13.584	186.597	42.4	11.2	14.2
[C/G/G/G]s-CNT	1.635	292.925	13.731	200.488	37.0	10.3	30.4
[C/C/G/G]s-CNT	1.279	356.621	13.778	194.982	38.7	9.9	15.3
[C/C/C/G]s-CNT	1.261	357.920	13.577	197.363	38.0	11.3	15.0
[C/K/K/K]s-CNT	1.265	302.488	13.277	131.206	58.8	13.2	29.9
[C/C/K/K]s-CNT	1.100	365.091	13.465	160.763	49.5	12.0	13.3
[C/C/C/K]s-CNT	1.404	379.770	14.111	225.850	29.0	7.8	9.8
[C/R/R/R]s-CNT	1.434	294.487	13.527	163.541	48.6	11.6	31.3
[C/C/R/R]s-CNT	1.206	360.543	13.337	191.780	39.7	12.8	14.4
[C/C/C/R]s-CNT	1.222	358.916	13.352	194.658	38.8	12.7	14.8
[C/J/J/J]s-CNT	1.296	301.887	13.457	134.756	57.7	12.0	29.9
[C/C/J/J]s-CNT	1.118	363.958	13.590	161.106	49.4	11.2	13.6
[C/C/C/J]s-CNT	1.187	359.725	13.487	181.725	42.9	11.8	14.6
[F/J/J/J]s-CNT	1.315	281.124	12.937	86.307	72.9	15.4	33.2
[F/F/J/J]s-CNT	1.232	286.900	12.924	93.547	70.6	15.5	31.9
[F/F/F/J]s-CNT	1.226	289.466	12.942	98.205	69.1	15.4	31.3
[F/K/K/K]s-CNT	1.282	281.094	12.757	82.366	74.1	16.6	33.2

Three Phase Composites

(cont. on next page)

Table 6.34 (cont.)

	[F/F/K/K]s-CNT	1.211	287.063	12.906	83.123	73.9	15.6	31.8
	[F/F/F/K]s-CNT	1.214	289.168	13.057	83.960	73.6	14.7	31.3
	[F/R/R/R]s-CNT	1.386	278.196	13.444	107.363	66.3	12.1	33.9
	[F/F/R/R]s-CNT	1.300	284.351	13.219	103.149	67.6	13.6	32.5
	[F/F/F/R]s-CNT	1.238	288.924	12.994	99.008	68.9	15.1	31.4
Two Phase Composites	[F/F/F/F]s	1.373	256.767	12.950	70.127	78.0	15.4	39.0
	[G/G/G/G]s	2.166	206.979	15.300	116.158	63.5	0.0	50.8
	[J/J/J/J]s	1.615	225.782	12.665	71.613	77.5	17.2	46.4
	[K/K/K/K]	1.621	221.518	12.600	53.424	83.2	17.6	47.4
	[R/R/R/R]	1.734	223.180	13.319	91.608	71.2	12.9	47.0
	[C/F/F/F]s	1.306	300.128	13.475	135.543	57.4	11.9	28.7
	[C/C/F/F]s	1.125	362.266	13.770	154.999	51.3	10.0	14.0
	[C/C/C/F]s	1.187	359.500	13.604	177.573	44.2	11.1	14.6
	[C/G/G/G]s	1.697	265.028	13.725	170.640	46.4	10.3	37.1
	[C/C/G/G]s	1.265	355.367	13.800	189.343	40.5	9.8	15.6
	[C/C/C/G]s	1.250	356.966	13.590	193.126	39.3	11.2	15.2
	[C/K/K/K]s	1.300	290.435	13.275	119.628	62.4	13.2	31.7
	[C/C/K/K]s	1.085	363.678	13.483	154.141	51.6	11.9	13.6
	[C/C/C/K]s	1.164	359.436	13.443	176.033	44.7	12.1	14.6
	[C/R/R/R]s	1.473	282.780	13.525	154.700	51.4	11.6	32.8
	[C/C/R/R]s	1.187	358.825	13.363	184.635	42.0	12.7	14.8
	[C/C/C/R]s	1.210	358.547	13.373	190.642	40.1	12.6	14.8
	[C/J/J/J]s	1.345	287.840	13.455	123.569	61.2	12.1	31.6
	[C/C/J/J]s	1.110	358.786	13.570	154.723	51.4	11.3	14.8
	[C/C/C/J]s	1.177	359.400	13.508	177.701	44.2	11.7	14.6
	[F/J/J/J]s	1.450	245.315	12.755	71.133	77.6	16.6	41.7
	[F/F/J/J]s	1.386	253.826	12.948	63.187	80.1	15.4	39.7
	[F/F/F/J]s	1.380	256.113	13.108	57.353	82.0	14.3	39.2
	[F/K/K/K]s	1.434	244.151	12.750	54.258	83.0	16.7	42.0
	[F/F/K/K]s	1.369	254.084	12.900	55.092	82.7	15.7	39.7
	[F/F/F/K]s	1.371	256.189	13.037	56.682	82.2	14.8	39.2
	[F/R/R/R]s	1.553	239.785	13.137	86.544	72.8	14.1	43.1
	[F/F/R/R]s	1.448	249.934	13.024	79.876	74.9	14.9	40.6
[F/F/F/R]s	1.395	254.449	12.933	74.101	76.7	15.5	39.6	

For fully natural fiber reinforced cases, 82% weight saving is enhanced by decreasing 39% natural frequency with 15% cost reduction. [C/C/N/N]s-CNT, [C/C/C/N]s-CNT and [C/C/N/N]s cases are the other most efficient optimal designs in terms of cost and weight by achieving an 45-80% weight reduction and 11-12% cost reduction with decrease in frequency between the range of 13-14.6%. In addition to this, among the two-phase designs [C/C/J/J]s, [C/C/K/K]s, [C/C/C/K]s, [C/C/R/R]s,

[C/C/C/R]s, [C/C/J/J]s, and [C/C/C/J]s also provide more efficient designs with a 12% weight and 51% cost savings with a about the 14.8% decrease in frequency. Generally, the efficiency of multi-objective optimal designs for multiphase composite structures for maximum natural frequency, minimum weight and cost, it can be seen that to use optimal non-uniform volume content of fiber and weight content of cnt distributions enable to be use more cost and weight effective engineering structures in terms of natural frequency. The multi-objective optimization approaches also illustrate that by using CNT in hybrid and nonhybrid natural fiber reinforced structures, the cost and weight may be decreased up to 80% and 16%, respectively.

This graph shows the optimal configuration for hybrid and non-hybrid fiber reinforced composites with and without carbon nanotubes (CNTs), taking into account the maximum natural frequency as well as the minimum possible cost and weight. Considering cost, weight, and natural frequency, the [C/C/F/F]s-CNT, [C/C/K/K]s-CNT and [C/C/J/J]s-CNT designs are the most effective out of all the scenarios. By using these design, 49% weight and 13% cost savings can be achieved by sacrificing 9% in natural frequency in spite of CNT utilization as nanofillers. Of all the cases, [C/C/C/K]s emerges as the most efficient design both in terms of decreasing cost and weight with maximum natural frequency. For Hybrid natural fiber reinforced [F/F/F/K]s-CNT design, 14% weight and 73% cost saving can be provided with sacrificing 31% natural frequency compared to traditional carbon fiber reinforced composite structures. Hybrid natural fiber reinforced composites come forward with more cost effective designs up to 83% decreasing cost. In this graph, it is obviously seen that [C/C/K/K]s-CNT and [C/C/C/K]s-CNT are the most optimal design in terms of cost, weight and natural frequency.

6.3.3.1 Finite Element Analysis of the Optimum Cases

In this study, the Finite Element Method (FEM) is applied to conduct a free vibration analysis of optimized hybrid nanocomposite designs reinforced with Carbon/Kenaf and Carbon/Flax/CNTs. The FEM simulations are performed using Autodesk Inventor NASTRAN Commercial Software under an Educational License. To perform the vibration analysis of the hybrid fiber-reinforced nanocomposite plates, an appropriate mesh is generated. Given that the composite plate has a side-to-thickness ratio greater than 10, linear quadrilateral 4-node shell elements are chosen as an effective meshing option for the model. The plates are composed of eight unidirectional layers, with the square plate dimensions being 1 m × 1 m and a total laminate thickness of 10 mm.

Fully simply supported boundary (SSSS) conditions are applied to multiscale nanocomposite plates. The boundary conditions (BCs) for displacement constraints on the simply supported plate are defined as follows:

$$\begin{aligned} v = w = 0 \text{ at } x = 0 \text{ and } x = a, & \quad u = w = 0 \text{ at } y = 0 \text{ and } y = b \\ M_x = 0 \text{ at } x = 0 \text{ and } x = a, & \quad M_y = 0 \text{ at } y = 0 \text{ and } y = b \end{aligned}$$

The model has undergone convergence testing with respect to mesh density, leading to the selection of a mesh consisting of 20 elements per side, each with a dimension of 50 mm. This configuration results in a total of 1,281 nodes and 400 elements being employed to achieve the final solution.

The optimum non-uniform weight content of CNTs, fiber orientation angles, and fiber volume fraction for each layer of the hybrid Carbon/Flax/CNTs and Carbon/Kenaf/CNT nanocomposite plates are provided in the accompanying Table 6.35. These values are derived from the results of a multi-objective optimization problem aimed at maximizing natural frequency while minimizing both cost and weight.

Using the optimum volume fraction and CNT weight content for each layer, non-uniform material properties are calculated as shown in Table 6.36. The analysis considers two different symmetric designs, [C/C/K/K]_s and [C/C/F/F]_s, where each layer exhibits distinct properties, mirrored symmetrically across the laminate (Figure 6.14).

Table 6.35. Optimum design results of the Problem 3.

Design	F-value	Design Variables		
		Stacking Sequence	Fiber Volume Fraction	Weight Content of CNTs
[C/C/K/K]s-CNTs	1.100	[45/-45/-45/-45]s	[0.415/0.431/0.60/0.60]s	[0.0072/0/0.0028/0]s
[C/C/F/F]s-CNTs	1.134	[45/-45/-45/-45]s	[0.424/0.425/0.60/0.60]s	[0.0060/0.0/0/0.0]s

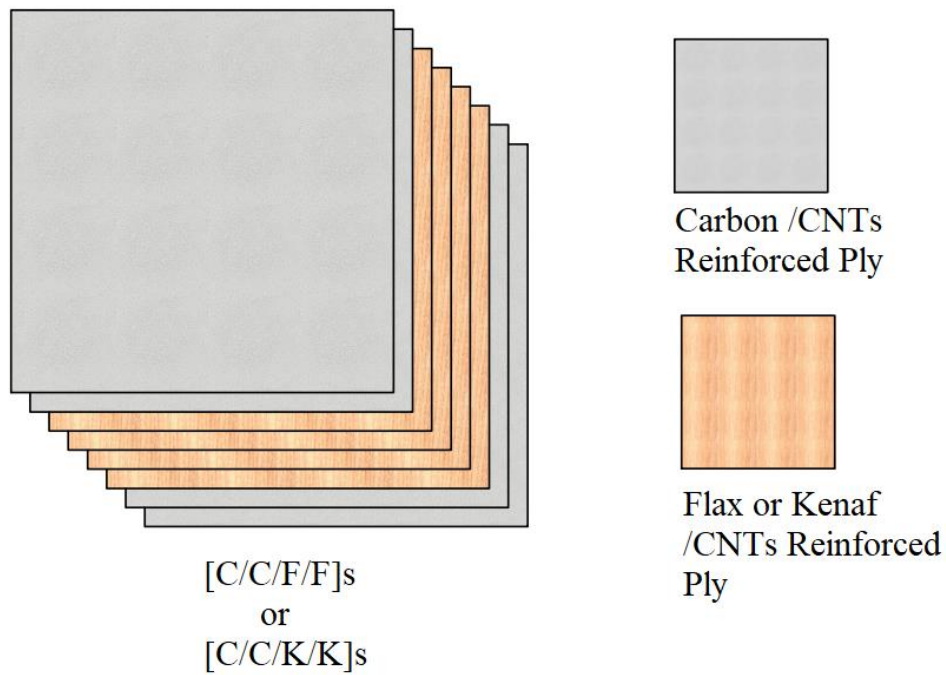


Figure 6.14. Representation of the designs

Table 6.36. Optimum material properties for layer by layer

[C/C/K/K]s-CNTs	Carbon/CNTs[1]	Carbon/CNTs[2]	Kenaf/CNTs[3]	Kenaf/CNTs[4]
E1 (Mpa)	112081.00	115345.00	32956.20	32720.00
E2 (Mpa)	7638.20	5799.41	5130.47	4753.81
G12 (Mpa)	3033.42	2199.66	2123.65	1939.98
V12	0.29	0.29	0.33	0.33
qq	1428.81	1437.05	1260.15	1260.00
[C/C/F/F]s-CNTs	Carbon/CNTs[1]	Carbon/CNTs[2]	Flax/CNTs[3]	Flax/CNTs[4]
E1 (Mpa)	114257.00	113788.00	43400.00	43400.00
E2 (Mpa)	7402.16	5755.16	9090.26	9090.26
G12 (Mpa)	2927.07	2927.07	3040.85	3040.85
V12	0.29	0.29	0.25	0.25
qq	1433.66	1433.75	1320.00	1320.00

In the Table 6.37, a strong agreement can be observed between the FEM results and analytical results for the optimum designs' angular frequencies (ω). Angular frequency (ω) can be converted to frequency (f) in Hertz by using equality $\omega = 2\pi f$. The optimum inter-ply hybrid fiber/CNT-reinforced nanocomposite designs were derived using the Halpin-Tsai model and Classical Lamination Plate Theory (CLPT), with the FEM results demonstrating an error margin of only 1.6%. By using the present approach, FEM analysis of fiber-reinforced nanocomposite plates can effectively account for the non-uniform material properties of each ply when assessing vibration behavior. By integrating multiscale modelling with micromechanical equations, Finite Element Methods are accurately applied to three-phase fiber/CNT-reinforced nanocomposite structures using Autodesk NASTRAN.

Table 6.37. Comparison of the FEM results with analytical method for optimum cases

Design	F-value	FEM (NASTRAN)	Analytical	Error (%)	Cost	Weight
[C/C/K/K]s-CNTs	1.100	359.341	365.091	1.6	160.763	13.465
[C/C/F/F]s-CNTs	1.134	359.379	365.014	1.6	160.073	13.768

The natural frequencies and mode shapes of composite plates can be numerically calculated, with a focus on several fundamental bending mode shapes of rectangular plates. The structure of the first three fundamental modes is primarily determined by the plate's geometric and stiffness characteristics. The first ten fundamental bending mode shapes of the square plate are illustrated in the accompanying Figure 6.15.

Using the stochastic optimization algorithm Differential Evolution (DE) in conjunction with multiscale modelling, the vibration behaviour of hybrid fiber/CNT-reinforced nanocomposite plates is optimized, aiming to maximize performance while minimizing cost and weight.

The proposed FEM analysis procedure integrates multiscale modelling with the inclusion of CNTs within the matrix. Dispersion of CNT particles in the matrix is a significant challenge, with a practical limit to CNT addition (maximum 10 wt%) due to agglomeration formation. Consequently, the present approach serves as an effective design tool for low volume fractions. It is able to identify the optimum vibrational performance, taking into account the non-uniform distribution of nanoparticles in the matrix.

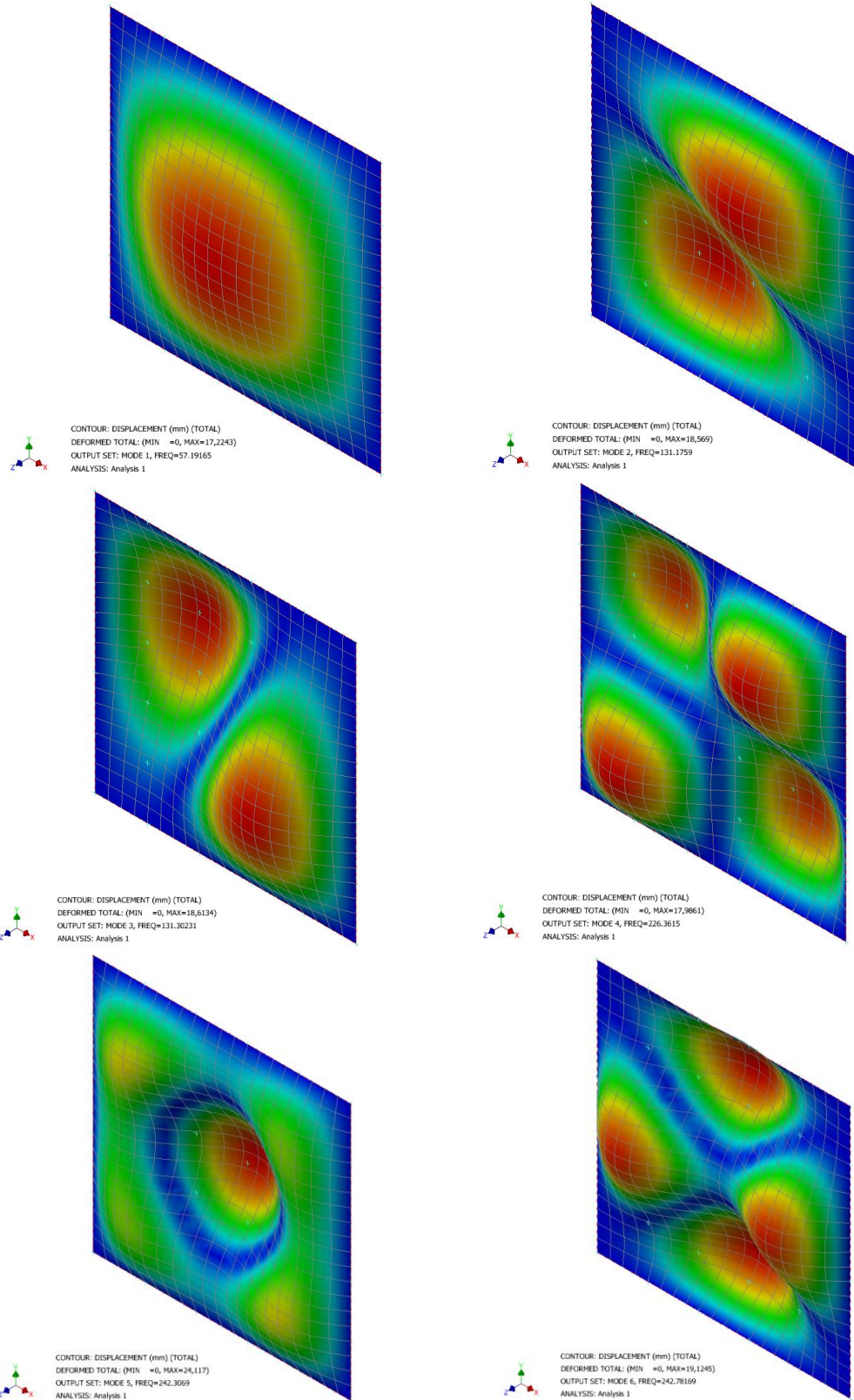
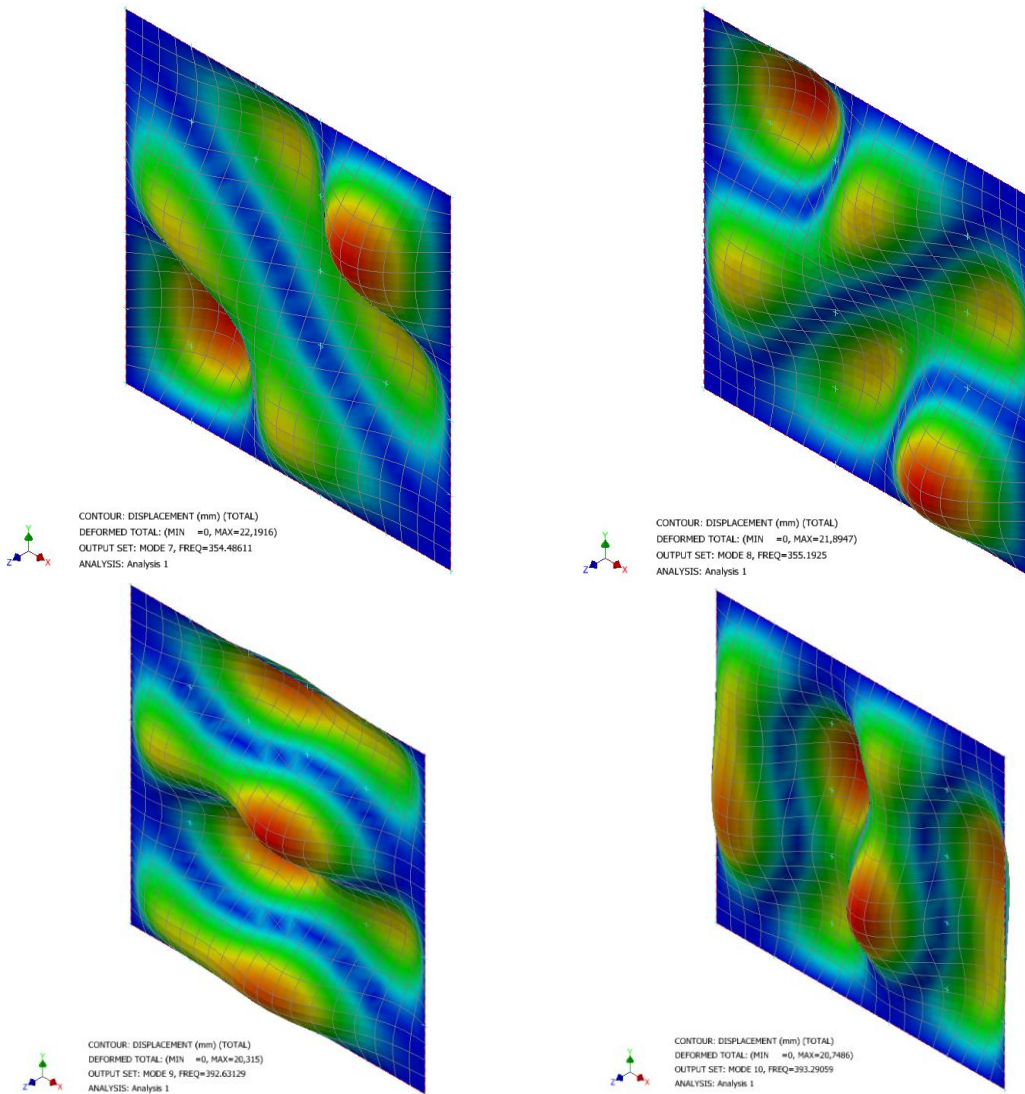


Figure 6.15. Mode shapes of vibration of [C/C/K/K]s-CNT multiscale nanocomposite plate with SSSS boundary condition

(cont. on next page)

Figure 6.15 (cont.)



CHAPTER 7

BUCKLING PROBLEMS

In this section of the thesis, the critical buckling load factors of three-phase, graphene or carbon nanotubes (CNTs)/fiber-reinforced nanocomposite laminates have been maximized. This was achieved through the use of various design variables and load cases. Both single-objective and multi-objective optimization problems were addressed to identify solutions that provide the maximum critical buckling loads while minimizing weights. This section is organized into three main parts: i) benchmark problems, which set the baseline for comparisons, ii) single-objective optimization problems focusing solely on optimizing one parameter, and iii) multi-objective optimization problems that balance conflicting objectives to derive an optimal solution.

7.1. Benchmark Problem

In the benchmark problems section, the design and optimization of fiber-reinforced composite plates are undertaken to assess various optimization approaches for maximizing critical buckling loads and to evaluate multiphase material models. This portion of the study comprises four verification problems:

Problem B1: Stacking sequence design and optimization challenges are addressed for different load cases (LC) as reported in the literature. The solutions are compared with the maximum critical buckling loads from recent studies to gauge their effectiveness.

Problem B2: The critical buckling load analysis for composite plates under biaxial and uniaxial loadings is performed using the First-order Shear Deformation Theory (FSDT) and Navier's solution. The outcomes are benchmarked against results obtained from both analytical methods and Finite Element Method (FEM) to ensure consistency and accuracy.

Problem B3: Material properties of MWCNT-reinforced nanocomposite laminae are calculated using the modified Halpin-Tsai Model. This problem aims to validate the calculation approach by comparing it with documented results from the literature, ensuring the model's relevance and reliability.

Problem B4: This involves examining how the agglomeration and waviness of MWCNTs affect the mechanical properties and critical buckling loads of nanocomposite plates. The findings from these analyses are juxtaposed with experimental results from existing studies to verify theoretical predictions and understand material behaviour under practical conditions.

Each of these problems serves to validate the theoretical approaches used, ensuring that the optimization strategies are grounded in practical, verifiable outcomes.

7.1.1. Problem B1

The design and optimization of the stacking sequence for a 64-layer symmetrically balanced graphite/epoxy composite are focused on maximizing the critical buckling load, which serves to validate the current optimization methods against documented results in the literature ²⁰¹. In this subsection, the primary objective is to enhance the buckling load factor of a laminated composite plate comprised of graphite/epoxy layers. This effort involves considering various load cases, which are detailed in the specified Table 7.1, ensuring a comprehensive approach to evaluating the structural capabilities of the composite under different stress scenarios. The schematic view of the problem can be seen in Figure 7.1.

Table 7.1. Different load cases, lengths, and widths considered for 64-layer laminated composite plate.

Load cases	a(m)	b(m)	N_x (N/m)	N_y (N/m)
LC1	0.508	0.254	1	1
LC2	0.508	0.508	1	1
LC3	0.508	1.016	1	1
LC4	0.508	0.254	1	0.5
LC5	0.508	0.508	1	0.5
LC6	0.508	1.016	1	0.5
LC7	0.508	0.254	1	2
LC8	0.508	0.508	1	2
LC9	0.508	1.016	1	2

Problem B1 can be defined mathematically as

- Maximize: Buckling Load Factor $\lambda_{(m,n)} (\theta_i)$
- Design Variables: θ_i

- Constraints: $\theta_k \in \{0, 45, 90\}$, N=64 ply
Symmetric & balanced stacking sequences; $[\theta_1, \theta_2, \theta_3, \theta_4]_s$

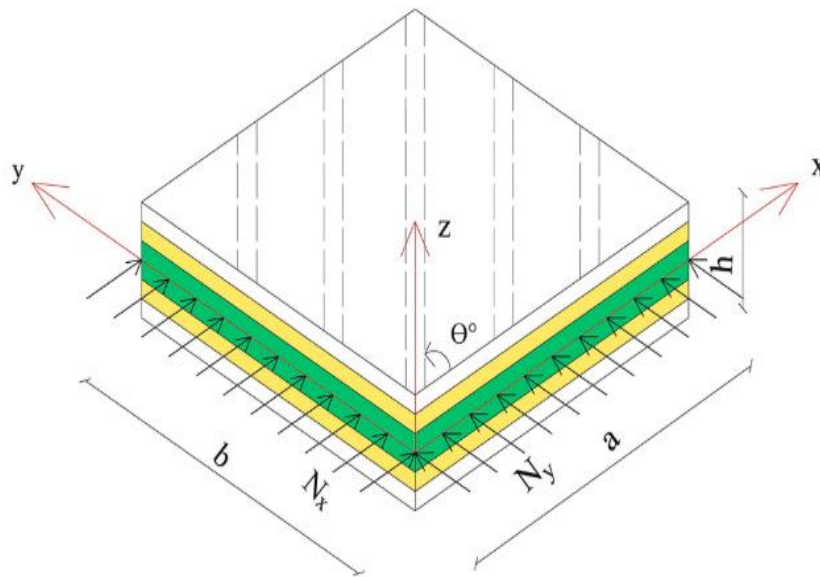


Figure 7.1. Laminated composite plate with 64 layers Structure (Source: Jalili 2021²⁰¹)

Table 7.2. Optimum stacking sequences and buckling load factors obtained for 64-layer laminated composite plate with graphite/epoxy layers under different load cases

Load Cases	Stacking Sequence		Critical Buckling Load	
	Present Study (DE)	Jalili et al.(PSO) ²⁰¹	Present Study	Jalili et al ²⁰¹
LC1	$[90_4/\pm 45/90_4/\pm 45_2/90_4/\pm 45/90_6/\pm 45/90_2]_s$	$[\pm 45/90_8/\pm 45/90_{18}/\pm 45]_s$	685822	695781,3
LC2	$[\pm 45_{16}]_s$	$[\pm 45_{16}]_s$	242823	242823
LC3	$[0_2/\pm 45/0_{10}/\pm 45_2/0_6/\pm 45/0_4/\pm 45]_s$	$[0_{10}/\pm 45_2/0_2/\pm 45_3/0_2/\pm 45_4]_s$	173956	173945,3
LC4	$[\pm 45/90_4/\pm 45/90_4/\pm 45_6/90_4/\pm 45/90_2]_s$	$[\pm 45/90_6/\pm 45_5/90_8/\pm 45_2/90_2]_s$	1057950	1057648
LC5	$[\pm 45_{16}]_s$	$[\pm 45_{16}]_s$	323792	323764
LC6	$[0_{16}/\pm 45/0_6/\pm 45/0_2/\pm 45/0_2]_s$	$[0_{16}/\pm 45/0_6/\pm 45/0_2/\pm 45/0_2]_s$	206492,9	206492,9
LC7	$[90_{16}/\pm 45/90_6/\pm 45/90_2/\pm 45/90_2]_s$	$[90_{16}/\pm 45/90_6/\pm 45/90_2/\pm 45/90_2]_s$	412985	412985
LC8	$[\pm 45_{16}]_s$	$[\pm 45_{16}]_s$	161896	161882
LC9	$[0_2/\pm 45/0_2/\pm 45/0_2/\pm 45_4/0_6/\pm 45/0_2/\pm 45_2]_s$	$[\pm 45/0_4/(\pm 45/0_2)_2/\pm 45_4/0_6/\pm 45/0_2]_s$	132245	132243,5

The design variables are limited to fiber orientations. To validate the analytical model, the optimal orientations and buckling load factors obtained through the Differential Evolution algorithm are compared with those reported by Jalili et al.²⁰¹. The comparison in Table 7.2 reveals a strong agreement between the maximum buckling load factors (λ_{\max}) obtained in this study and those reported by Jalili et al.²⁰¹ using PSO algorithm. However, the stacking sequences optimized by DE and PSO differ for some load cases, indicating the existence of multiple optimal stacking sequences with the same buckling load factors.

7.1.2. Problem B2

To validate analytical solution in determining the critical buckling load by FSDT, it was compared against both analytical and numerical results from the existing literature. The results were specifically contrasted with findings from studies by various researchers including Anish et al.²⁰², Nguyen-Van et al.²⁰³, Liu et al.²⁰⁴, Reddy and Phan²⁰⁵, Khdeir and Librescu²⁰⁶, Singh et al.²⁰⁷, Sayyad and Ghugal²⁰⁸, Noor²⁰⁹ and Vescovini and Dozio²¹⁰. These comparisons were made across different theoretical frameworks and methodologies.

The analysis focused on a simply supported (SSSS) cross-ply laminated square plate configured in stacking sequences $[0^\circ/90^\circ/90^\circ/0^\circ]$ and $[0^\circ/90^\circ/0^\circ]$, subjected to uniaxial compression. In this example, the analysis of a square plate was performed by using an a/h ratio equal to 10; an a/b ratio equal to 1, $G_{12} = G_{13} = 0.6E_2$, $G_{23} = 0.5E_2$, $\nu_{12} = 0.25$; and an E_1/E_2 elastic modulus ratio equal to 3/10/20/30 and 40, respectively. The method can deal with any material. The mechanical properties specified in this example were selected purely for benchmarking purposes to facilitate comparison with results cited in references^{202–210}. The outcomes from the current FE model, as detailed in Table 7.3, show excellent consistency with the analytical findings documented in the aforementioned studies.

Furthermore, effect of thickness ratio an analysis for a simply supported cross-ply laminated square plate stacked as $[0^\circ/90^\circ/0^\circ]$ under the effect of biaxial compression was conducted.

In this comparison example, the buckling analysis of a rectangular plate was performed with a thickness ratio, a/h , equal to 10/20/50; an a/b ratio equal to 1, $G_{12} = G_{13} = 0.6E_2$,

$G_{23} = 0.5E_2$, $\nu_{12} = 0.25$; and an E_1/E_2 elastic modulus ratio equal to 10 and 25. The results from the present FE model, presented in Table 7.4, are in very good agreement compared with the results provided by studies from the literature.

Table 7.3. Comparison of nondimensional buckling loads, $N = N_{cr}\alpha^2/E_2h^3$, for simply supported cross-ply laminated rectangular plates under uniaxial compressions ($G_{12} = G_{13} = 0.6E_2$, $G_{23} = 0.5E_2$, $\nu_{12} = 0.25$, $\alpha/b = 1$, $\alpha/h = 10$).

(N_x, N_y)	Lamination	Studies	3	10	20	30	40
(1, 0)	[0°/90°/90°/0°]	Present	5.399	9.965	15.352	19.756	23.453
		182	4.997	9.580	14.950	19.303	22.919
		202	5.319	9.808	15.103	19.419	23.056
		203	5.321	9.809	15.064	19.339	22.912
		204	5.412	10.01	15.309	19.778	23.412
		204	5.401	9.985	15.374	19.537	23.154
		205	5.114	9.774	15.298	19.957	23.340
		206	5.442	10.26	15.418	19.813	23.489
(1, 0)	[0°/90°/0°]	Present	5.396	9.871	14.985	19.026	22.315
		182	4.994	9.486	14.567	18.548	21.764
		202	5.314	9.698	14.692	18.634	21.841
		207	5.379	9.827	14.970	19.099	22.513
		207	5.410	9.895	15.032	19.122	22.488
		208	-	9.923	15.002	19.001	22.329
		209	5.304	9.762	15.019	19.304	22.881

Table 7.4. Comparison of nondimensional buckling loads, $N = N_{cr}\alpha^2/E_2h^3$, for simply supported cross-ply laminated rectangular plates under biaxial compressions ($G_{12} = G_{13} = 0.6E_2$, $G_{23} = 0.5E_2$, $\nu_{12} = 0.25$, $\alpha/b = 1$, $\alpha/h = 10$, [0°/90°/0°])

(N_x, N_y)	E_1/E_2	Studies	10	20	50
(1, 1)	10	Present	4.9355	5.5175	5.7079
		182	4.7421	5.4192	5.6901
		202	4.8441	5.489	5.7084
		210	4.9095	5.5082	5.7063
		(1, 1)	25	Present	8.305
182	7.864	9.8656	10.7262		
202	7.9066	10.0852	10.704		
210	8.682	10.8768	11.732		

7.1.3. Material Model Verification

The material properties of the MWCNT-reinforced nanocomposite lamina were determined using the modified Halpin-Tsai equations including agglomeration and waviness effects. The volume fractions of the fiber and the matrix in the composite were set at 60% and 40%, respectively. Utilizing the methodology outlined in the previous section, the engineering constants derived from this analysis and comparison with result available in the literature are presented in Table 7.5.

Using the modified H–T equation, a parametric study was carried out to determine Young’s modulus of CNT/polymer nanocomposites for agglomeration factors. The variation of Young’s modulus with the CNT agglomeration factor is presented in Figure 7.2. The CNT/polymer nanocomposite mechanical property is shown to be significantly sensitive to the CNT agglomeration. It is observed that the elastic modulus of the CNT/polymer nanocomposite increases when the CNT agglomeration factor increases. The presence of CNT agglomeration in the matrix results in a negative effect on its reinforcement role.

Table 7.5. Comparison of the modified Halpin Tsai Model results for variable V_{cnt} ,
Mechanical properties of MWCNT-reinforced nanocomposite matrix.

Volume Fraction of MCNT	Present	Ref ¹⁸²	Present	Ref ¹⁸²	Present	Ref ¹⁸²
	E ₁	E ₁	E ₂	E ₂	G ₁₂	G ₁₂
0	136.680	136.680	9.026	9.026	4.537	4.537
0.25	136.751	136.751	9.194	9.194	4.676	4.676
0.5	136.818	136.818	9.345	9.345	4.803	4.803
1	136.938	136.938	9.606	9.606	5.025	5.025
1.5	137.042	137.042	9.823	9.823	5.213	5.213
2	137.133	137.133	10.003	10.003	5.372	5.372
3	137.279	137.279	10.281	10.281	5.619	5.619
4	137.385	137.385	10.473	10.473	5.792	5.792
6	137.505	137.505	10.682	10.682	5.982	5.982
8	137.535	137.535	10.734	10.734	6.029	6.029
10	137.506	137.506	10.655	10.685	5.985	5.985

(cont. on next page)

Table 7.5 (cont.)

Volume Fraction of MCNT	Present	Ref ¹⁸²	Present	Ref ¹⁸²	Present	Ref ¹⁸²	Present	Ref ¹⁸²
	G23	G23	v12	v12	v23	v23	ρ	ρ
0	3.492	3.492	0.257	0.260	0.374	0.370	1.580	1.580
0.25	3.577	3.577	0.257	0.260	0.374	0.370	1.581	1.581
0.5	3.654	3.654	0.257	0.260	0.374	0.370	1.582	1.582
1	3.786	3.786	0.257	0.260	0.374	0.370	1.584	1.584
1.5	3.896	3.896	0.257	0.260	0.374	0.370	1.586	1.586
2	3.989	3.989	0.257	0.260	0.375	0.370	1.588	1.588
3	4.131	4.131	0.257	0.260	0.374	0.370	1.592	1.592
4	4.229	4.229	0.257	0.260	0.374	0.370	1.596	1.596
6	4.336	4.336	0.257	0.260	0.374	0.370	1.604	1.604
8	4.363	4.363	0.256	0.260	0.374	0.370	1.612	1.612
10	4.338	4.338	0.257	0.260	0.374	0.370	1.620	1.620

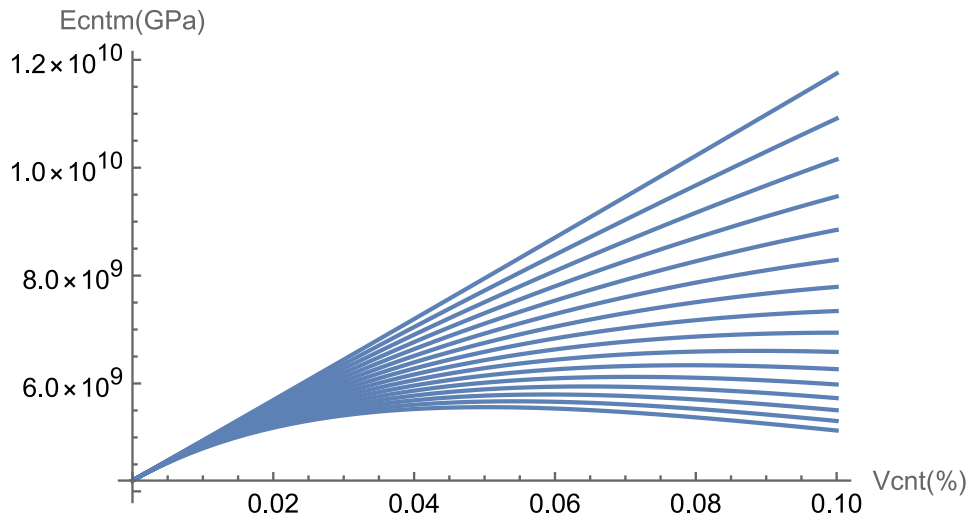


Figure 7.2. Young's modulus of CNT-reinforced matrix as a function of V_{cnt} (vol%) for various f_A agglomeration factors

It is observed that the elastic modulus of the CNT/polymer nanocomposite increases when the CNT agglomeration factor decreases. The presence of CNT agglomeration in the matrix results in a negative effect on its reinforcement role.

Using the modified H–T equation, a parametric study was carried out to determine Young's modulus of CNT/polymer nanocomposites for various waviness efficiency factors. The variation of Young's modulus with the CNT waviness efficiency factor is

presented in Figure 7.3. The CNT/polymer nanocomposite mechanical property is shown to be significantly sensitive to the CNT waviness. It is observed that the elastic modulus of the CNT/polymer nanocomposite increases when the CNT waviness correction factor increases. The presence of CNT waviness in the matrix results in a negative effect on its reinforcement role.

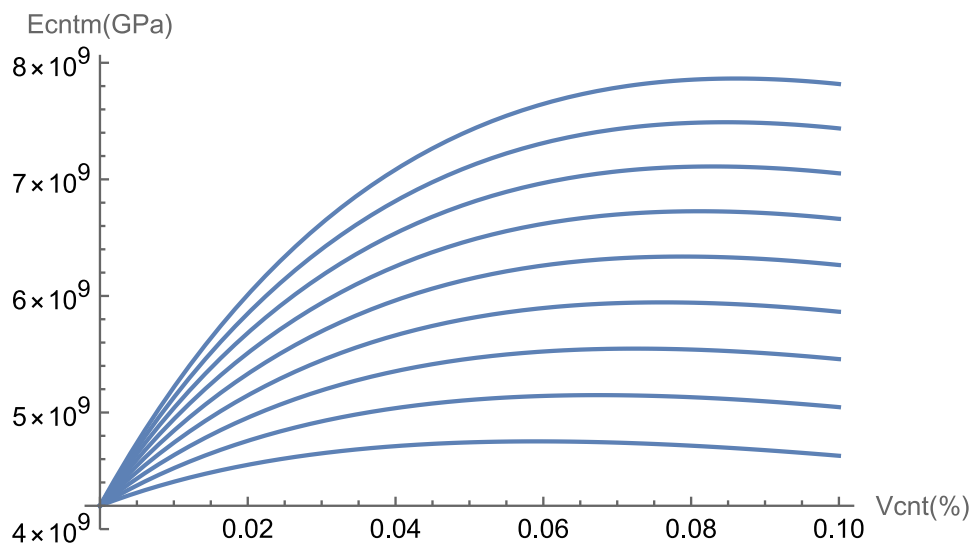


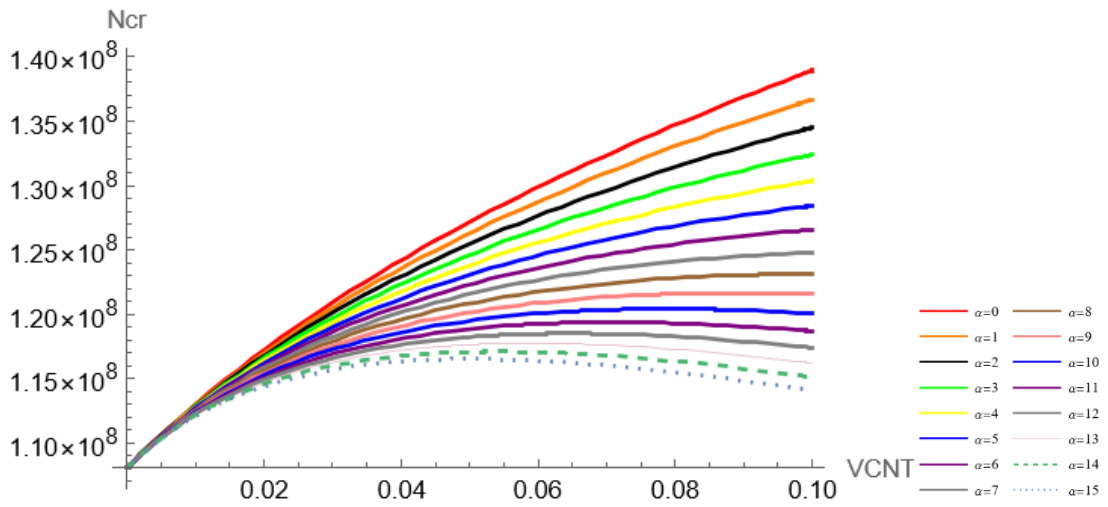
Figure 7.3. Young's modulus of CNT-reinforced matrix as a function of V_{cnt} (vol%) for various f_w waviness factors

It is observed that the elastic modulus of the CNT/polymer nanocomposite increases when the CNT waviness correction factor increases. The presence of CNT waviness in the matrix results in a negative effect on its reinforcement role.

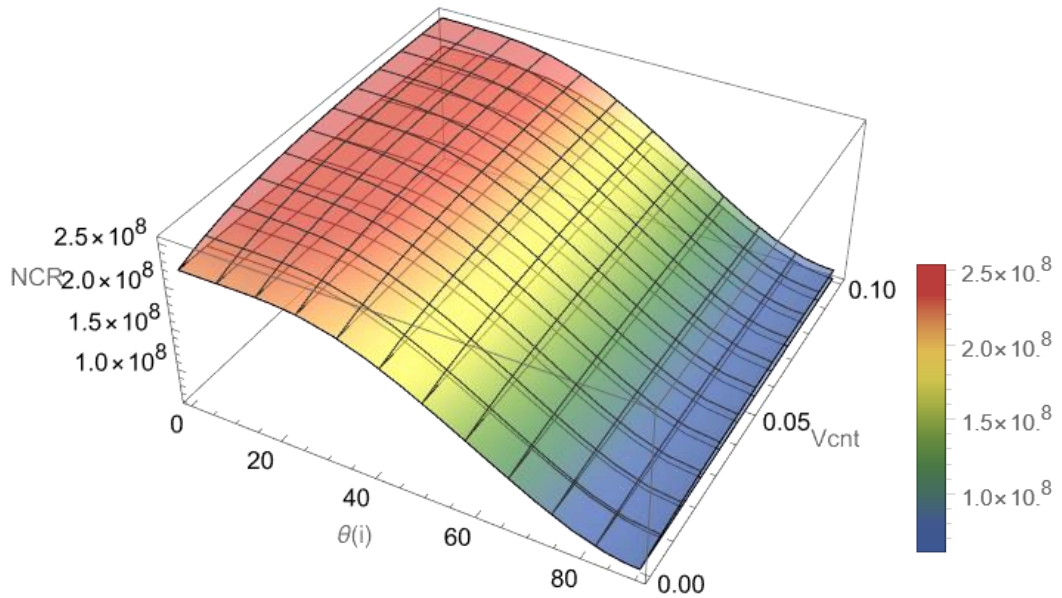
The Figure 7.4 (a) shows the the influence of volume fraction increment on N_{cr} . Using the modified H–T model, parametric study of fiber reinforced nanocomposite plate was carried out to determine agglomeration effects on critical buckling load. This graph shows how increasing the agglomeration coefficient beyond a certain point causes the critical buckling load to decrease. At 0.08 volume percent of CNTs, the critical buckling load increment begins to decrease for a low agglomeration factor.

For the design with the same fibre orientation angle of each ply, the effect of varying the angle between 0° and 90° on the critical buckling load is shown in Figure 7.4(b). It is also seen that even if angle optimization is made, the addition of CNT to the matrix material increases the critical buckling load in spite of uniform addition. It can be

concluded that the optimization process of fiber volume fraction and V_{cnt} for each ply is crucial to increase efficiency of design.



(a)



(b)

Figure 7.4. (a) Agglomeration effects on Critical Buckling Load for [90/90/90/90]_s plates with 0.60 volume fraction of fiber and $a/b=0.5$. (b) comparison of how variations in fiber orientation angle and volume fraction affect N_{cr}

7.2. Single-objective Optimization Problem

In this part of the study, the critical buckling load behaviours of 16-layer carbon/epoxy, glass/epoxy, and flax/epoxy composites were compared, and the effect of CNTs weight content optimization on the critical buckling load of multiphase laminated nanocomposites was examined. Fiber angle orientation and CNTs weight ratio in each layer were considered design parameters and aimed to obtain designs that would maximize the critical buckling load. In this process, a modified version of Differential Evolution, one of the stochastic optimization methods, was used. The results showed that The addition of CNTs significantly improved the critical buckling load of carbon/epoxy, glass/epoxy, and flax/epoxy laminated composites.

7.2.1. Problem 1

Considered laminated composite has 16 layered symmetric-balanced stacking sequences, and each edge is simply supported. The non-dimensional buckling load was computed for the number of half waves $m=1$, $n=1$, and the compression ratio was $N_x/N_y=1$ (Figure 7.5). The thickness of each composite plate is $h=0.508\text{mm}$, while the length and width values are taken as Problem B1 for nine different load cases LC1 to LC9. The material properties of materials in optimization problem are given in Table 7.6.

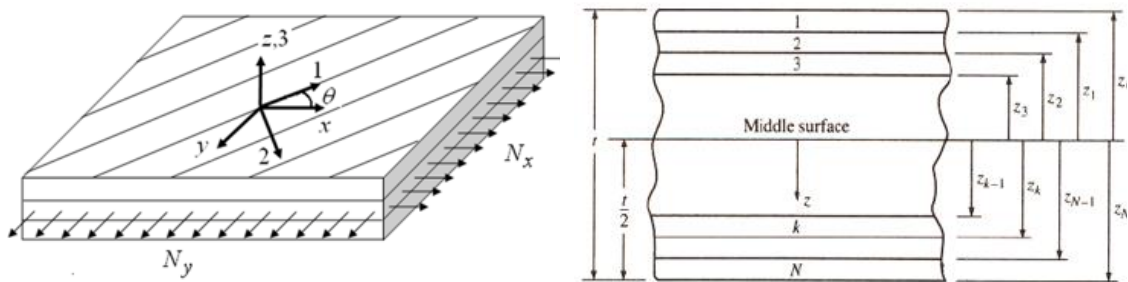


Figure 7.5. Layered symmetric-balanced laminated composite (Source: Reddy 2003¹⁷⁶)

Problem can be defined mathematically as

- Maximize: Buckling Load Factor $\lambda_{(m, n)}(\theta_i, W_{cnti})$
- Design Variables: θ_i, W_{cnti}

- Constraints: Symmetric & balanced stacking sequences; $[\theta_1, \theta_2, \theta_3, \theta_4]_s$
Symmetric weight fraction of CNT sequences;
 $[W_{CNT1}/W_{CNT2}/W_{CNT3}/W_{CNT4}]_s$
 $\theta_i \in \left\{ 0^\circ, \pm 15^\circ, \pm 30^\circ, \pm 45^\circ, \right. \\ \left. \pm 60^\circ, \pm 75^\circ, \pm 90^\circ \right\} \frac{1}{N} \sum_{i=1}^N W_{CNT_k} \leq W_{CNTmax},$
 $W_{CNTk} \geq 0, W_{CNTmax}=1.25\% , 0.10 \leq V_{Fk} \leq 0.60, b/a =1$

Table 7.6. Material Properties of the CNT, matrix, flax carbon and glass fibers ^{32,38}

Material	E ₁₁ (GPa)	E ₂₂ (GPa)	G ₁₂ (GPa)	v ₁₂	Density (kg/m ³)
Matrix	3	3	1.119	0.34	1200
CarbonNanotube	640	640	251.96	0.27	1350
Carbon Fiber	263	19	27.60	0.20	1750
Flax Fiber	70	70	29.58	0.183	1400
Glass Fiber	72.4	72.4	30.66	0.20	2400

Table 7.7 shows the optimum designs of carbon/epoxy-CNTs, glass/epoxy-CNTs, and flax/epoxy-CNTs laminated composites regarding critical buckling load. Each layer's fiber orientation and CNTs weight ratio were considered design parameters. When the results are examined, it can be seen that the obtained stacking sequences for the maximum critical buckling load are distinct. However, the optimum CNTs ratio in each layer is the same, and adding 0.05 CNTs only to the first layer is sufficient for optimum design.

The critical buckling load value of [C/C/C/C]_s is achieved with CNTs cases with 6.6% and 8% increment at the same weight compared to carbon fibre only cases for two different load cases. The addition of 1% CNTs to the matrix material increased the critical buckling load by 19.50% and 23.52% for glass and flax fiber reinforced composite laminates for the same weight. It can be shown that the anti-buckling performance of the natural fiber reinforced design may be improved by adding a very little quantity of CNTs without increasing weight.

Adding CNTs to composites improved critical buckling load of 10%, 20%, and 24% compared to the carbon/epoxy, glass/epoxy, and flax/epoxy laminated composites without CNTs. This improvement was achieved without any increase in the weight of the composites. In this respect, it is seen that the addition of CNTs has a remarkably positive effect on the critical buckling behavior of the layered composite. Another significant result is that flax, as a natural material, can be an alternative to glass material in critical

buckling load problems. Although the critical buckling load of the flax/epoxy-CNTs layered composite is 2% lower than glass/epoxy-CNTs, it is also 28% lighter, making flax stand out as an alternative material to glass.

Table 7.7. Comparison of critical buckling load capacity, stacking sequences and weight for 16 layered symmetric-balanced CNTs added laminated composites

	Fiber Sequences for each layer	Critical Buckling Load	Cost(\$)	Weight (kg)	Optimal WGPL per layer	Optimum Stacking Sequence
LC1	[C/C/C/C]s	439807	20.915	1.358	[0/0/0/0]s	[±75/±60/±90/±60]s
	[F/F/F/F]s	149751	8.923	1.248	[0/0/0/0]s	[90 ₂ /±75/90 ₂ /±60]s
	[G/G/G/G]s	153666	12.211	1.606	[0/0/0/0]s	[90 ₂ /±75 ₂ /90 ₂]s
	[C/C/C/C]s-GPLs	468819	23.601	1.359	[0.05/0 ₇]s	[-75/75/60 ₂ /90 ₄]s
	[F/F/F/F]s-GPLs	178853	11.383	1.249	[0.05/0 ₇]s	[90 ₈]s
	[G/G/G/G]s-GPLs	183119	15.369	1.608	[0.05/0 ₇]s	[90 ₈]s
LC2	[C/C/C/C]s	150926	41.831	2.716	[0/0/0/0]s	[±45 ₄]s
	[F/F/F/F]s	51954	17.847	2.496	[0/0/0/0]s	[45/45/-45/-45]s
	[G/G/G/G]s	53211	24.422	3.123	[0/0/0/0]s	[45/45/-45/-45]s
	[C/C/C/C]s-GPLs	162862	47.200	2.719	[0.05/0 ₇]s	[±45/45/45]s
	[F/F/F/F]s-GPLs	64175	22.767	2.499	[0.05/0 ₇]s	[-45/45/-45/-45]s
	[G/G/G/G]s-GPLs	65449	30.739	3.216	[0.05/0 ₇]s	[45/-45/45/-45/-45/45/-45/45]s
LC3	[C/C/C/C]s	109952	83.663	5.432	[08]s	[15/-15/30/-30/0/0/30/-30]s
	[F/F/F/F]s	37437	35.693	4.992	[08]s	[0/0/15/-15/0/0/30/-30]s
	[G/G/G/G]s	38416	48.844	6.423	[08]s	[0/0/15/-15/15/-15/0/0]s
	[C/C/C/C]s-GPLs	117205	94.404	5.438	[0.05/0 ₇]s	[-15/15/-30/30/0/0/0/0]s
	[F/F/F/F]s-GPLs	44713	45.534	4.997	[0.05/0 ₇]s	[08]s
	[G/G/G/G]s-GPLs	45783	61.479	6.432	[0.05/0 ₇]s	[08]s
LC4	[C/C/C/C]s	686543	20.915	1.358	[08]s	[60/60/90/90/75/75]s
	[F/F/F/F]s	235511	8.923	1.248	[08]s	[60/-60/75/-75/90/90/90/90]s
	[G/G/G/G]s	241364	12.211	1.606	[08]s	[60/-60/75/-75/90/90/60/-60]s
	[C/C/C/C]s-GPLs	736437	23.601	1.359	[0.05/0 ₇]s	[-60/60/60/-60/90/90/90/90]s
	[F/F/F/F]s-GPLs	286651	11.383	1.249	[0.05/0 ₇]s	[-60/60/90/90/90/90/90/90]s
	[G/G/G/G]s-GPLs	293069	15.369	1.608	[0.05/0 ₇]s	[-60/60/90/90/90/90/90/90]s
LC5	[C/C/C/C]s	201234	41.833	2.716	-	[±45 ₄]s
	[F/F/F/F]s	69273	17.847	2.496	-	[±45 ₄]s
	[G/G/G/G]s	70948	24.420	3.213	-	[±45 ₄]s
	[C/C/C/C]s-GPLs	217149	47.200	2.719	[0.05/0 ₇]s	[45/-45/-45/45/45/-45/45/-45]s
	[F/F/F/F]s-GPLs	85567	22.767	2.498	[0.05/0 ₇]s	[-45/45/45/-45/-45/45/-45/45]s
	[G/G/G/G]s-GPLs	87265	30.739	3.216	[0.05/0 ₇]s	[45/-45/45/-45/-45/45/-45/45]s

(cont. on next page)

Table 7.7 (cont.)

LC6	[C/C/C/C]s	127395	83.660	5.432	-	[15/-15/0/0/0/0/30/-30]s
	[F/F/F/F]s	41947	35.690	4.992	-	[908]s
	[G/G/G/G]s	43092	48.844	6.426	-	[908]s
	[C/C/C/C]s-GPLs	136507	94.400	5.438	[0.05/0 ₇]s	[0/0/15/-15/0/0/0/0]s
	[F/F/F/F]s-GPLs	49681	45.534	4.997	[0.05/0 ₇]s	[908]s
	[G/G/G/G]s-GPLs	50870	61.479	6.432	[0.05/0 ₇]s	[908]s
LC7	[C/C/C/C]s	254789	20.915	1.358	-	[75/-75/90/90/90/90/60/-60]s
	[F/F/F/F]s	83894	8.923	1.248	-	[908]s
	[G/G/G/G]s	86158	12.211	1.606	-	[908]s
	[C/C/C/C]s-GPLs	273015	23.600	1.359	[0.05/0 ₇]s	[0/0/-75/75/0/0/0/0]s
	[F/F/F/F]s-GPLs	99363	11.383	1.249	[0.05/0 ₇]s	[908]s
	[G/G/G/G]s-GPLs	101733	15.369	1.608	[0.05/0 ₇]s	[908]s
LC8	[C/C/C/C]s	100617	41.831	2.716	[0/0/0/0]s	[±45 ₄]s
	[F/F/F/F]s	34636	17.847	2.496	[0/0/0/0]s	[±45 ₄]s
	[G/G/G/G]s	35474	24.422	3.213	[0/0/0/0]s	[±45 ₄]s
	[C/C/C/C]s-GPLs	108574	47.200	2.719	[0.05/0 ₇]s	[±45 ₄]s
	[F/F/F/F]s-GPLs	42784	22.767	2.499	[0.05/0 ₇]s	[±45 ₂ /-45/45/-45/45]s
	[G/G/G/G]s-GPLs	43633	30.739	3.216	[0.05/0 ₇]s	[±45 ₂ /-45/45/-45/45]s
LC9	[C/C/C/C]s	85818	83.663	5.432	-	[30/-30/30/-30/0/0/15/-15]s
	[F/F/F/F]s	29439	35.695	4.992	-	[30/-30/15/-15/0/0/0/0]s
	[G/G/G/G]s	30170	48.844	6.427	-	[30/-30/15/-15/0/0/30/-30]s
	[C/C/C/C]s-GPLs	92055	94.405	5.438	[0.05/0 ₇]s	[-30/30/30/-30/0/0/0/0]s
	[F/F/F/F]s-GPLs	36010	45.534	4.997	[0.05/0 ₇]s	[-15/15/30/-30/0/0/0/0]s
	[G/G/G/G]s-GPLs	36636	61.479	6.432	[0.05/0 ₇]s	[-30/30/0/0/0/0/0/0]s

In results of the problem, the critical buckling load behaviors of 16-layer carbon/epoxy, glass/epoxy, and flax/epoxy composites were compared, and the effect of CNTs addition on the critical buckling load of multiphase laminated composites was examined. Fiber angle orientation and CNTs weight ratio in each layer were considered design parameters and aimed to obtain designs that would maximize the critical buckling load. In this process, a modified version of Differential Evolution, one of the stochastic optimization methods, was used. The results showed that the highest critical buckling load was obtained using carbon/epoxy and carbon/epoxy- CNTs laminated composites. The main focus here was to determine whether nano-reinforced natural materials can be used as an alternative to synthetic materials to optimize the critical buckling load behavior.

The following inferences can be made about the study:

- For both natural and synthetic composite plates, the addition of CNTs provided a remarkable increase in the critical buckling load.

- Considering only the critical buckling load as an objective, using multiphase carbon/epoxy and carbon/epoxy-CNTs nanocomposites allows the highest critical buckling load.
- When weight is considered as a parameter in addition to the critical buckling load, it is more advantageous to use flax/epoxy composite instead of glass/epoxy composite and flax/epoxy-CNTs instead of glass/epoxy-CNTs.
- The addition of CNTs improved the critical buckling load of carbon/epoxy, glass/epoxy, and flax/epoxy laminated composites by 10%, 20%, and 24%, respectively.

In line with all these results, it has been observed that natural composites with CNTs addition do not have as high a critical buckling load as carbon fiber-reinforced laminated composites. Still, they can be an excellent alternative to glass fiber-reinforced laminated composites. As a further study, examining the critical buckling behavior of hybrid composites with CNTs on this subject may be useful.

7.3. Multi-objective Optimization Problem

In this section, the multi-objective optimization of hybrid and non-hybrid fiber/CNTs reinforced composite plates focuses on achieving maximum critical buckling loads and minimum weights, utilizing a non-uniform distribution of CNTs and fiber reinforcements. The primary objectives in the design process are: (i) maximizing critical buckling loads, and (ii) minimizing weight. Optimization involves these objectives by strategically balancing the two parameters: enhancing critical buckling loads while simultaneously reducing weights. A penalty function is used which is a linear combination of the squares of the "critical buckling loads" and "weight", denoted as m_1 and m_2 respectively. This function describes the relationship between "buckling" (m_1) and "weight" (m_2). It reflects the principles of multi-objective optimization and brief summary of problem are given in Table 7.8. This approach makes it possible to evaluate the trade-offs between these main goals in the design.

In the defined framework, N_{ho} and N_{hi} , represent the number of outer and inner layers, respectively, in hybrid composite structures. θ_i denotes the fiber orientation angle, V_{F_k} indicates the volume fraction of fiber, and V_{CNT_k} refers to the volume fraction of CNT

for each layer. The total number of layers in hybrid structures is calculated using the equation $N = N_{ho} + N_{hi}$. For non-hybrid structures, N directly represents the total number of plies. Across all design scenarios, the width-to-length ratio (aspect ratio) is maintained at $a/b=0.5$.

Table 7.8. Mathematical definitions of optimization problems for two-phase (fiber /matrix) composites and three phase (fiber/GPLs/matrix) nanocomposite plates

	Three-Phase Nanocomposite
Minimize	$F_1 = k_1 m_1^2 + k_2 m_2^2$ $m_1 = \left(\frac{\lambda_{max} - \lambda_{mn}}{\lambda_{max}} \right)$ $m_2 = \left(\frac{Weight}{Weight_{max}} \right)$ <hr/> $\lambda_{mn} \left(\begin{array}{c} \theta_1, \theta_2, \dots, \theta_N, \\ V_{F1}, V_{F2}, \dots, V_{FN}, \\ V_{CNT_1}, V_{CNT_2}, \dots, V_{CNT_N} \end{array} \right)$ $Weight \left(\begin{array}{c} V_{F1}, V_{F2}, \dots, V_{FN} \\ V_{CNT_1}, V_{CNT_2}, \dots, V_{CNT_N} \end{array} \right)$
Find	$\theta_i, V_{Fk}, V_{CNTk}$ $N_{ho} \text{ and } N_{hi} \text{ (for hybrid structure)}$
Design Variables	$\left\{ \begin{array}{c} \theta_1, \theta_2, \theta_3, \dots, \theta_N, \\ V_{CNT_1}, V_{CNT_2}, V_{CNT_3}, \dots, V_{CNT_N} \end{array} \right\}$
Constraints	$\theta_i \in \left\{ 0^\circ, \pm 15^\circ, \pm 30^\circ, \pm 45^\circ, \right. \\ \left. \pm 60^\circ, \pm 75^\circ, \pm 90^\circ \right\}$ $\frac{1}{N} \sum_{i=1}^N V_{CNTk} \leq V_{CNTmax},$ $V_{CNTk} \geq 0,$ $V_{CNTmax} = 5\% ,$ $0.10 \leq V_{Fk} \leq 0.60$ $N_{ho} \text{ and } N_{hi} \text{ (for hybrid structure)}$

The material properties of synthetic (glass, carbon) and natural (flax, kenaf, ramie, jute) fibers, CNTs and matrix material used in the present study are given in Table 7.9.

Table 7.9. Material properties of fiber and matrix for buckling Problem 1^{38,80,86,182,199,200}

	Jute	Kenaf	Ramie	Flax	Carbon AS4	Glass	CNTs	Matrix
E_1 (Gpa)	55.3	52.2	60.9	70	225	72.4	450	4.2
E_2, E_3 (Gpa)	6.7	6.1	7.8	70	15	72.4		
G_{12}, G_{13} (Gpa)	3.1	2.9	3.7	29.58	15-7	30.66		1.567
ν_{12}, ν_{13}	0.32	0.32	0.32	0.183	0.2	0.2		0.34
ν_{23}	0.14	0.13	0.17		0.4	0.2		
Density(kg/m ³)	1340	1300	1550	1400	1800	2400	624.4	1250
Cost (\$/kg)	0.95	0.4	2	0.5	28	2	485	10

7.3.1. Problem 1

In this study, the determination of the mechanical properties of CNT-reinforced nanocomposites is conducted using a combination of theoretical models. Specifically, the modified Halpin–Tsai (H–T) equations and the rule of mixtures are utilized, which incorporate the effects of CNT agglomeration within the matrix materials. This approach allows for a comprehensive understanding of the composite behavior under various loading conditions. First-order shear deformation theory (FSDT) is implemented in the solution of the problem

In this analysis, the parameters λ_{mn} and weight, represent the maximum critical buckling load and minimum weight values, respectively. The parameters λ_{max} and $weight_{max}$ denote the highest critical buckling loads and the lowest weight across all layers, which consist of carbon/epoxy material at a 0.60 volume fraction of fiber and with optimized stacking sequences. For the purposes of this study, the coefficients k_1 and k_2 are set to one, reflecting the assumption that the importance of critical buckling load and weight are considered equally.

The laminate structure is configured with 8 layers and features a length to thickness ratio (a/h) of 15 and aspect ratio (a/b) of 0.5. Optimization of the critical buckling loads in fiber-reinforced nanocomposite plates is achieved through the application of the Modified Differential Evolution Algorithm. This optimization effort aims to minimize the weight of the plates while adhering to simply supported boundary

conditions. The objective function F_l is formulated as a penalty function that incorporates non-dimensionalized critical buckling load λ_{mn} and weight as its components.

The design parameters include the fiber orientation angle (θ_i), volume fraction of CNT (V_{CNT_k}), and volume fraction of fiber (V_{Fk}).

The multi-objective optimization problem for multiphase hybrid/non-hybrid fiber/CNT reinforced nanocomposites targets two primary objectives: achieving the maximum critical buckling load and minimizing weight. This optimization employs a coupled approach to simultaneously address these goals.

Problem 1 can be defined mathematically as

- Minimize: $F_1 = k_1 m_1^2 + k_2 m_2^2$

$$m_1 = \left(\frac{\lambda_{max} - \lambda_{mn}}{\lambda_{max}} \right) m_2 = \left(\frac{Weight}{Weight_{max}} \right)$$
- Constraints: $\frac{1}{8} \sum_{i=1}^8 V_{CNTi} \leq V_{CNTmax}, V_{CNTi} \geq 0,$
 $N_x = N_y = 1$ (biaxial compression)
 Symmetric stacking sequences; $[\theta_1, \theta_2, \theta_3, \theta_4]_s$
 Symmetric weight fraction of GPLs sequences;
 $[V_{CNT1}/V_{CNT2}/V_{CNT3}/V_{CNT4}]_s$
 Symmetric volume fraction of Fiber; $[V_{F1}/V_{F2}/V_{F3}/V_{F4}]_s$
 $a/h = 15, a/b = 0.5, N = 8$ ply,
 $V_{CNTmax} = 5\%, 0.10 \leq V_{Fk} \leq 0.60$
 Algorithm; Differential Evolution Algorithm

Table 7.10 demonstrates how various hybrid and non-hybrid designs influence the optimal stacking sequence, fiber volume fraction, and distribution of CNT volume fraction, aimed at achieving the highest possible critical buckling load and the lowest achievable weight of the composite plates. This Table provides a detailed comparison of how design variations impact the mechanical performance objectives. Optimal designs for various synthetic/natural fiber/CNT-reinforced multiphase composite structures display variations in fiber orientation angles, fiber volume fractions, and CNT weight content. This variability underscores the necessity for a unique optimization approach for each design case, focusing on non-uniform distribution of fibers and CNTs to maximize critical buckling load and minimize weight. F values effectively reflect the efficiency level of the optimal design, particularly in terms of critical buckling load and weight.

Table 7.10. Comparison of optimum Stacking sequence, volume fraction of fiber and weight fraction of CNT distribution results for maximum critical buckling load and minimum weight of composite plates

Design	F-value	Design Variables		
		Stacking Sequence	Fiber Volume Fraction	Volume Content of CNT
[F/F/F/F]s-CNT	0.836	[0/0/0/0]s	[0.600/0.100/0.600/0.100]s	[0.049/0.043/0.037/0.071]s
[G/G/G/G]s-CNT	1.213	[0/0/0/0]s	[0.600/0.100/0.100/0.100]s	[0.048/0.055/0.050/0.047]s
[J/J/J/J]s-CNT	1.042	[0/15/0/0]s	[0.600/0.600/0.600/0.100]s	[0.044/0.038/0.033/0.085]s
[K/K/K/K]-CNT	1.045	[0/-15/0/0]s	[0.600/0.600/0.600/0.100]s	[0.044/0.038/0.033/0.085]s
[R/R/R/R]-CNT	1.097	[0/0/0/0]s	[0.600/0.600/0.100/0.100]s	[0.038/0.032/0.065/0.065]s
[C/C/C/C]s-CNT	0.826	[-15/15/15/0]s	[0.600/0.515/0.100/0.100]s	[0.037/0.038/0.063/0.062]s
[C/F/F/F]s-CNT	0.753	[15/15/30/15]s	[0.600/0.600/0.600/0.100]s	[0.030/0.036/0.034/0.100]s
[C/C/F/F]s-CNT	0.772	[15/-15/-30/-30]s	[0.600/0.100/0.600/0.600]s	[0.032/0.100/0.035/0.033]s
[C/C/C/F]s-CNT	0.793	[-15/-15/15/30]s	[0.600/0.117/0.100/0.600]s	[0.037/0.061/0.063/0.039]s
[C/G/G/G]s-CNT	0.897	[-15/-30/30/-30]s	[0.600/0.100/0.100/0.100]s	[0.042/0.054/0.052/0.052]s
[C/C/G/G]s-CNT	0.861	[-15/-30/30/-30]s	[0.600/0.100/0.100/0.100]s	[0.042/0.054/0.052/0.052]s
[C/C/C/G]s-CNT	0.843	[15/15/15/-30]s	[0.600/0.500/0.100/0.100]s	[0.037/0.039/0.062/0.062]s
[C/K/K/K]s-CNT	0.808	[-15/-15/15/0]s	[0.600/0.600/0.600/0.100]s	[0.053/0.032/0.030/0.085]s
[C/C/K/K]s-CNT	0.805	[15/-15/-15/0]s	[0.600/0.600/0.100/0.100]s	[0.036/0.034/0.065/0.065]s
[C/C/C/K]s-CNT	0.814	[-15/15/-15/0]s	[0.600/0.600/0.100/0.100]s	[0.036/0.036/0.064/0.064]s
[C/R/R/R]s-CNT	0.843	[-15/15/-15/0]s	[0.600/0.100/0.100/0.100]s	[0.044/0.053/0.052/0.051]s
[C/C/R/R]s-CNT	0.817	[-15/-15/-15/0]s	[0.600/0.600/0.100/0.100]s	[0.035/0.034/0.066/0.065]s
[C/C/C/R]s-CNT	0.821	[-15/15/15/0]s	[0.600/0.548/0.100/0.100]s	[0.036/0.037/0.064/0.063]s
[C/J/J/J]s-CNT	0.816	[-15/-15/-15/0]s	[0.600/0.600/0.600/0.100]s	[0.052/0.032/0.030/0.086]s
[C/C/J/J]s-CNT	0.806	[15/15/15/0]s	[0.600/0.600/0.100/0.100]s	[0.036/0.034/0.065/0.065]s
[C/C/C/J]s-CNT	0.815	[15/-15/-15/0]s	[0.600/0.557/0.100/0.100]s	[0.036/0.036/0.064/0.064]s

The designs [C/F/F/F]s-CNT, [C/C/F/F]s-CNT, and [C/C/C/F]s-CNT exhibit the lowest F values, below 0.800, indicating that they are the most efficient cases among the considered designs. This suggests that the most efficient outcomes are achieved through the hybridization of flax and carbon fibers with the integration of CNTs into the matrix. The glass fiber reinforced [G/G/G/G]s-CNT case, with an F value of 1.213, is less efficient compared to other three-phase composite designs. It also underperforms relative to totally natural fiber reinforced cases like [F/F/F/F]s-CNT, [J/J/J/J]s-CNT, [K/K/K/K]s-CNT, [R/R/R/R]s-CNT, and their various hybridizations. This finding indicates that the use of CNTs in conjunction with natural fibers is advantageous for applications where controlling buckling load and weight is critical. Given that weight is a key objective in the optimization problem, the fully carbon fiber reinforced [C/C/C/C]s-CNT case

emerges as one of the most efficient designs in terms of critical buckling load and weight. However, despite the well-known strength and lightweight properties of carbon fiber and CNTs, hybrid designs that combine carbon fiber with natural fibers such as flax, kenaf, ramie, and jute, along with CNTs, prove to be more efficient than the solely carbon fiber reinforced [C/C/C/C]s-CNTs configuration.

Table 7.11 presents the optimal critical buckling load and weight results for various hybrid and non-hybrid configurations that include CNTs. Reductions in weight and critical buckling load are quantified as percentages, providing a comparative analysis against the [C/C/C/C]s reference optimum case. The [C/F/F/F]s-CNT, [C/C/F/F]s-CNT, [C/C/C/F]s-CNT, and [C/C/K/K]s-CNT designs are the most efficient, achieving the lowest F values of 0.75, 0.77, 0.79, and 0.80, respectively.

Table 7.11. Comparison of optimum critical buckling loads and minimum weights and comparing the results to the reference design

Design	Objective Function				
	F-value	λ_{mn}	Weight	Weight Reduction	Buckling Load Reduction
[F/F/F/F]s-CNT	0.84	106.21	65.16	17.52	39.50
[G/G/G/G]s-CNT	1.21	74.67	74.22	6.05	57.47
[J/J/J/J]s-CNT	1.04	65.51	63.68	19.39	62.68
[K/K/K/K]s-CNT	1.04	62.60	62.73	20.60	64.34
[R/R/R/R]s-CNT	1.10	66.46	66.62	15.68	62.14
[C/C/C/C]s-CNT	0.83	144.13	70.40	10.88	17.90
[C/F/F/F]s-CNT	0.75	157.23	68.05	13.87	10.43
[C/C/F/F]s-CNT	0.77	150.66	68.55	13.23	14.18
[C/C/C/F]s-CNT	0.79	136.49	68.14	13.75	22.25
[C/G/G/G]s-CNT	0.90	115.09	69.69	11.78	34.44
[C/C/G/G]s-CNT	0.86	117.34	68.94	12.73	33.16
[C/C/C/G]s-CNT	0.84	143.10	71.04	10.08	18.48
[C/K/K/K]s-CNT	0.81	120.21	66.48	15.85	31.53
[C/C/K/K]s-CNT	0.80	147.69	69.74	11.72	15.87
[C/C/C/K]s-CNT	0.81	146.50	70.08	11.29	16.55
[C/R/R/R]s-CNT	0.84	111.21	66.51	15.81	36.65
[C/C/R/R]s-CNT	0.82	148.23	70.36	10.93	15.56
[C/C/C/R]s-CNT	0.82	145.88	70.32	10.99	16.90
[C/J/J/J]s-CNT	0.82	121.77	67.13	15.03	30.63
[C/C/J/J]s-CNT	0.81	147.87	69.84	11.59	15.77
[C/C/C/J]s-CNT	0.82	146.40	70.12	11.25	16.60

The results indicate that a 14% reduction in weight is possible with a 10% decrease in critical buckling load, while also benefiting from the use of more eco-friendly fibers. The next most efficient designs after these are [C/C/R/R]_s-CNT, [C/C/C/R]_s-CNT, [C/C/J/J]_s-CNT, [C/C/C/J]_s-CNT and [C/C/C/K]_s-CNT. These designs provide optimal solutions to the problem, achieving up to 11.72% weight reduction and a 15% decrease in critical buckling load.

For the highly efficient [C/F/F/F]_s design, it is evident that using flax fiber in the inner layers, combined with non-uniformly distributed CNT nanofillers, is the most effective strategy for achieving maximum critical buckling loads and minimum weights. Additionally, leveraging the beneficial properties of CNTs enables a more biodegradable design with potential weight savings of up to 14%. In contrast to the [C/F/F/F]_s design, the [C/C/N/N]_s-CNT configurations, which utilize Kenaf, Ramie, and Jute fibers, prove to be more efficient for hybrid optimal designs in terms of weight and buckling loads. These designs also facilitate the creation of optimal structures that achieve a weight saving of 11.50% while accepting a decrease in critical buckling load of about 15%. The [C/C/C/C]_s-CNT design is also among the most efficient designs, leveraging the low density and high strength properties of carbon nanotubes. It gives up to 11% weight saving with 18% decrease in critical buckling load.

This graph displays the optimal configurations of multiphase hybrid and non-hybrid fiber/CNT reinforced nanocomposites, aimed at maximizing critical buckling load and minimizing weight. In Figure 7.6, it can be seen that integrating carbon nanotubes (CNTs) into the matrix material enhances the hybridization of natural and carbon fibers, leading to improved outcomes in terms of F-value design parameters within the multi-objective optimization problem. The carbon/natural fiber reinforced composite plate designs are more efficient than the optimal designs that only employ natural fiber reinforcement for the highest critical buckling load. The [C/F/F/F]_s design, which exhibits the lowest F-value of 0.376, is identified as the most suitable in terms of weight and buckling loads. Compared to the [C/C/C/C]_s reference design, it is evident that a 14% weight reduction can be achieved by sacrificing 11% of the critical buckling load in the [C/F/F/F]_s case. The [C/C/K/K]_s case also facilitates a more eco-friendly design compared to the [C/C/C/C]_s design, achieving up to a 12% weight reduction and a 15% decrease in critical buckling load.

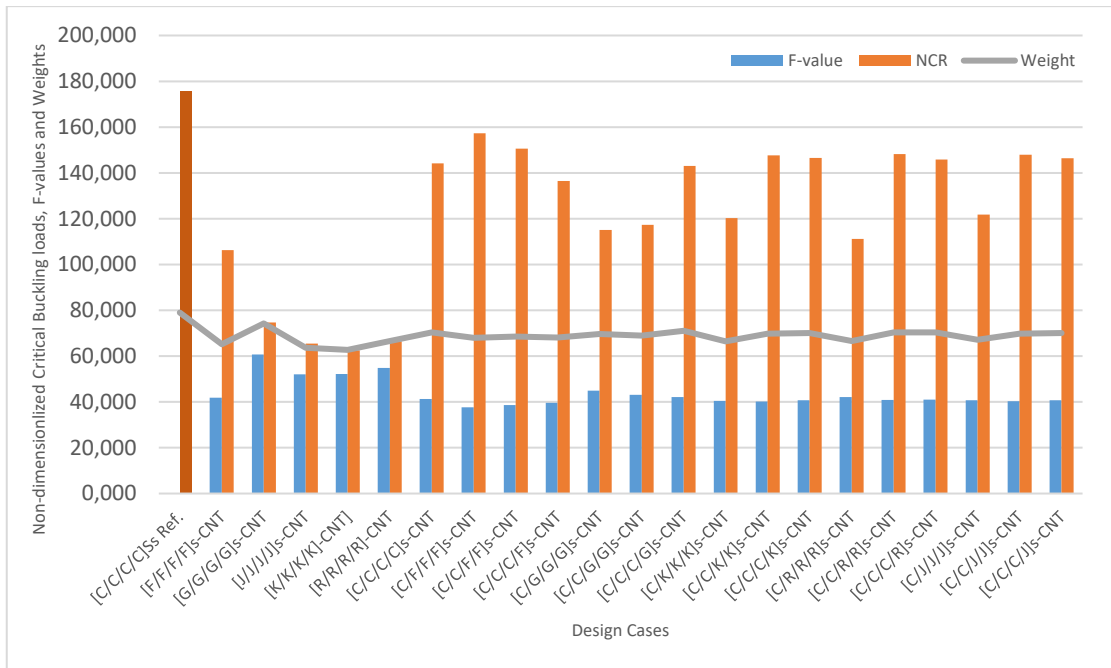


Figure 7.6. Comparison of the optimum design results for maximum critical buckling load and minimum weight

In conclusion, despite the potential for agglomeration, the inclusion of CNTs in material models enhances the efficiency and eco-friendliness of synthetic natural fiber reinforced composites. This approach effectively compensates for the lower strength properties of natural fibers, leading to more robust and sustainable design outcomes thanks to stochastic optimization approaches.

CHAPTER 8

NANOCOMPOSITE DRIVESHAFT PROBLEM

Driveshafts are crucial components in vehicle transmission systems, responsible for transmitting motion from the differential to the wheels. During operation, driveshafts are subjected to various types of stress, including torsional, bending, and normal forces. These forces are integral to the functioning of the driveshaft but also present challenges in terms of durability and performance, necessitating careful design and material selection to ensure reliability and efficiency in power transmission. The picture of driveshaft can be seen in Figure 8.1.

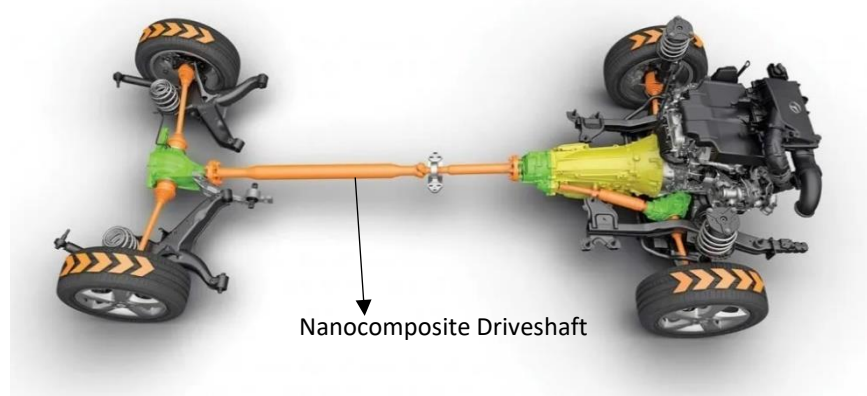


Figure 8.1. General visual representation of the placement and role of the driveshaft in the vehicle's transmission system (Source: Markel 2024²¹¹)

In the current chapter of the thesis, the analysis and optimization of non-hybrid and hybrid fiber/CNTs reinforced nanocomposite driveshafts are thoroughly investigated. Initially, a benchmark problem involving Carbon/Epoxy, Carbon/CNTs/Epoxy, and Basalt/bio-epoxy composites is addressed to determine fundamental frequency, torsional critical buckling load, and the factor of safety. These parameters are evaluated according to Tsai-Wu and Puck failure theories using analytical methods, specifically classical lamination theory, and the Finite Element Method (FEM) utilizing NASTRAN software. The results of problem are compared with available results from the literature. Subsequently, the original optimization problem for multiphase hybrid carbon/flax fiber

/CNTs reinforced nanocomposite driveshafts is addressed using a modified differential evolution algorithm, aimed at refining the design and enhancing the mechanical properties requirements of the driveshafts. This two-fold approach allows for a comprehensive assessment and optimization of driveshaft designs under varied material compositions and structural conditions.

8.1. Benchmark Problem

In this comprehensive study, the structural behaviour of a laminated composite driveshaft reinforced with multi-walled carbon nanotubes (MWCNTs) was meticulously analysed through modal and linear buckling analysis, coupled with detailed failure analysis employing both Tsai-Wu and Puck failure theories. The investigation was conducted using both an analytical approach and the finite element method (FEM), providing a robust comparison with existing literature on similar studies. Two distinct methodologies were implemented for the analyses: the Classical Laminate Theory (CLT) served as the analytical method, while FEM calculations were executed using the Autodesk NASTRAN software. These methods were utilized to precisely calculate critical torsional buckling loads, determine fundamental frequencies, and evaluate failure indices. Stress analysis was carried out for various composite driveshaft configurations including Carbon/Epoxy, Carbon/CNTs/Epoxy, and Basalt/bio-epoxy, aiming to understand the enhancement in mechanical performance and failure resistance offered by the integration of MWCNTs into traditional and bio-based epoxy composites.

The foundational example of a composite driveshaft used in this study is drawn from Kaw's authoritative text, "Mechanics of Composite Materials." In this reference, Kaw introduces a composite driveshaft to illustrate the analysis, design, and failure of composite laminates using classical laminate theory. The specific example provided describes a single-piece driveshaft typically found in civil vehicles, measuring 1480 mm in length and 100 mm in outside diameter, and it is shown in Figure 8.2.

Key design constraints include a maximum torque capacity of 550 N m, a minimum bending natural frequency above 80 Hz (corresponding to 4800 rpm), and a minimum factor of safety (FoS) of 3. Detailed design specifications for this driveshaft are outlined in Table 8.1.

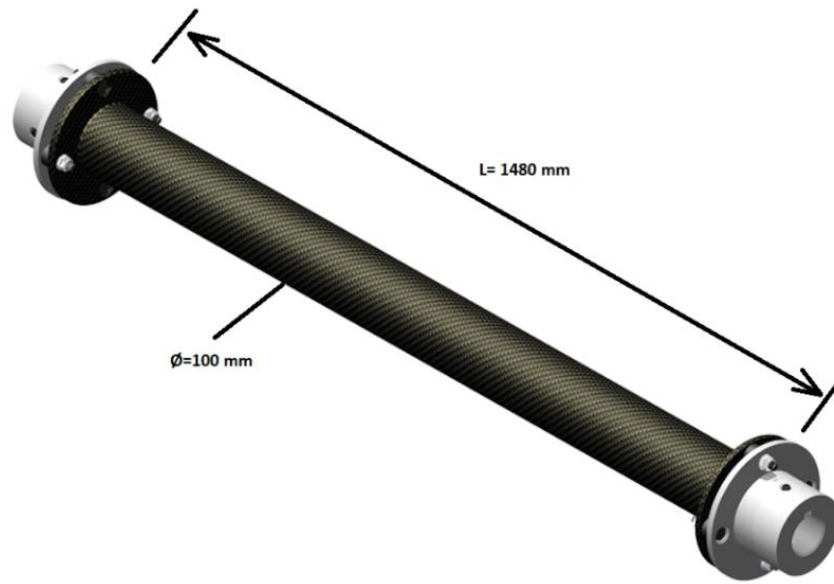


Figure 8.2. General dimension of the composite driveshaft (Source: Baltimoreaircoil 2024²¹²)

In this study, three critical evaluation criteria were considered to assess the performance and safety of the composite driveshaft. These criteria include: (i) the factor of safety, calculated based on the stress limit to ensure durability and reliability under operational conditions; (ii) the critical torsional buckling load, which determines the shaft's ability to withstand torsional loads without failure; and (iii) the natural frequency, important for avoiding resonance and ensuring stability at operational speeds. These parameters are essential for the comprehensive evaluation of the driveshaft's design and functionality. For benchmark and original optimization problems, these parameters are utilized to achieve designs with minimum weight for different fiber materials and their combinations.

Table 8.1. Design specification of the driveshaft

Torque (Nm)	550
Minimum natural frequency (Hz)	80
FoS	3
Length (mm)	1480
Outside radius (mm)	50

8.1.1. Finite Element Analysis of Composite Driveshafts

The performance evaluation of the driveshaft utilized both Finite Element Analysis (FEA) and Classical Laminate Theory (CLT). Autodesk Inventor NASTRAN is used for the FEA modelling, while the CLT analysis was conducted using Wolfram Mathematica. Additionally, Autodesk Inventor NASTRAN in-CAD was employed to develop the driveshaft model, defining the composite layup and executing the simulation. Given that the ratio of the radius to thickness of the hollow tube is greater than 10, shell theory was deemed appropriate and consequently, shell elements were utilized for the FEA modelling. This approach provides a comprehensive framework for assessing the structural integrity and response of the driveshaft under operational loads. Then, 2D geometric model of the composite tube is created. The second step involves meshing of 2D surface and the creating laminate under idealizations command by defining mechanical properties of composite plies given in Table 8.2 as orthotropic shell element material. The 2D finite element model of the composite tube (Figure 8.3) was created. In total, 4526 SHELL 3 elements having 13640 nodes were used.

Table 8.2. Mechanical Properties of the Carbon/Epoxy, Carbon/CNT/Epoxy and Basalt /bio-epoxy composite materials²¹³

	B/E	C/E	C/CNT/E
E_1 (GPa)	54.9	139	140
$E_2=E_3$ (GPa)	8.9	6.4	8.3
$\nu_{12} = \nu_{13}$	0.26	0.31	0.32
ν_{23}	0.35	0.45	0.47
$G_{12}=G_{13}$ (GPa)	4.9	3.7	4.4
G_{23} (GPa)	2.2	2.4	2.8
S_1 (MPa)	1310	2172	2389
S_1^c (MPa)	776	1448	1593
S_2 (MPa)	50	44	49
S_2^c (MPa)	135	199	219
S_{12} (MPa)	51	86	95
ρ (kg/m ³)	2072	1490	1490

Then, the boundary and loading conditions were applied to the 3D finite element model by creating two cylindrical coordinate systems (r, Θ, z) at the ends of the composite tube.

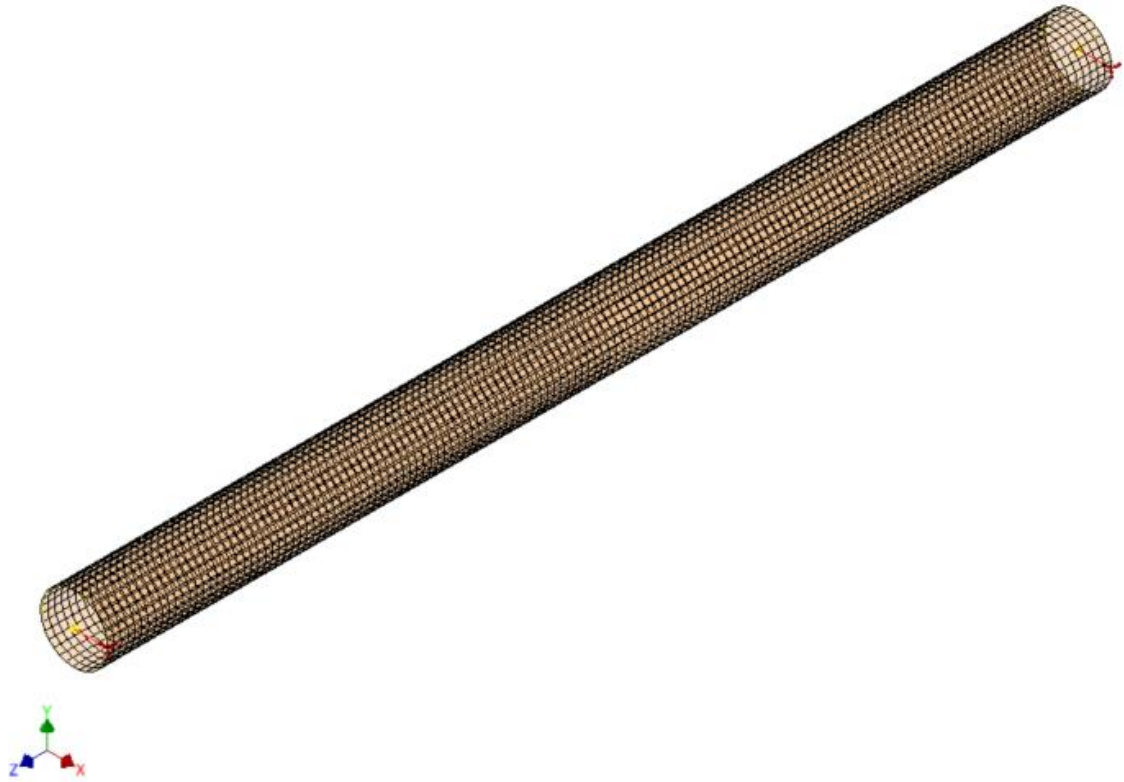


Figure 8.3. Mesh used in FEA model

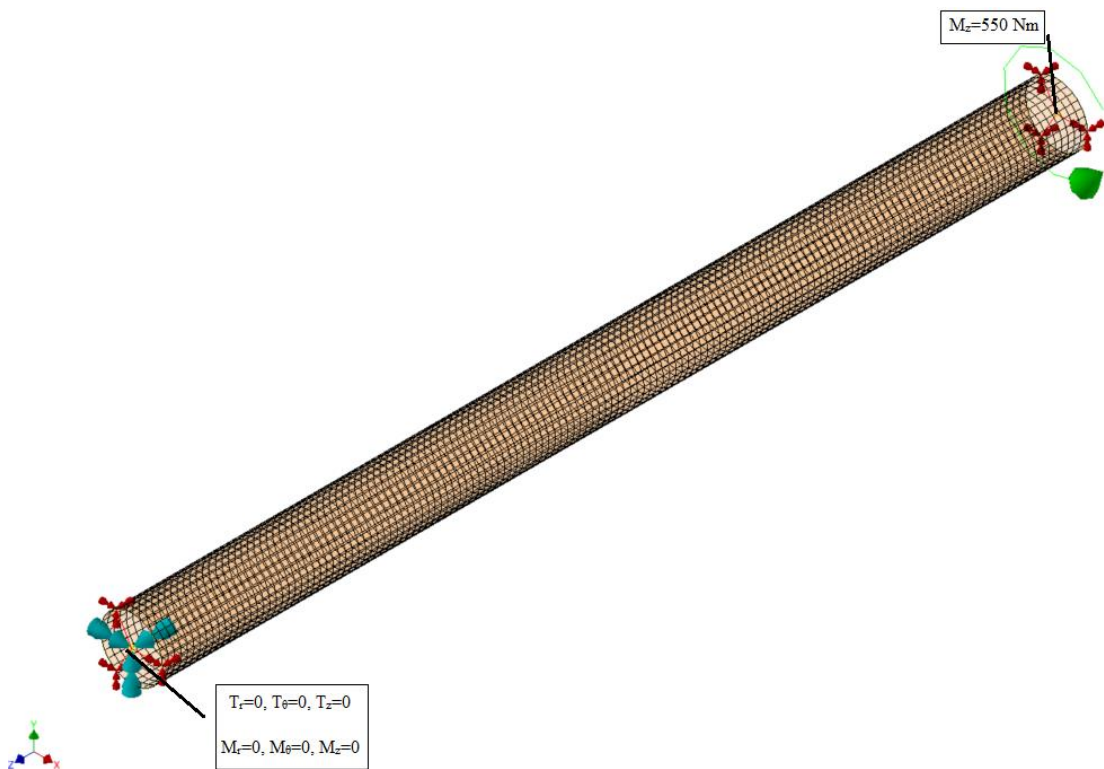


Figure 8.4. Boundary conditions and loadings of static and buckling analysis in Autodesk Inventor NASTRAN Software

Figure 8.4 shows the boundary and loading conditions used for the torsional buckling of the composite tube. One end is fixed in both translation and rotation in r , Θ , and z axes, whereas the translation is fixed in the r -axis for static stress analysis and buckling analysis. The other end of the driveshaft, which connects to the engine, was subjected to a torque of 550 N m around the axis of the shaft to simulate the driving force typically transmitted during operation.

In Figure 8.5. The boundary conditions of normal modes analysis in commercial software are given as; both ends are fixed for radial and circumferential translation.

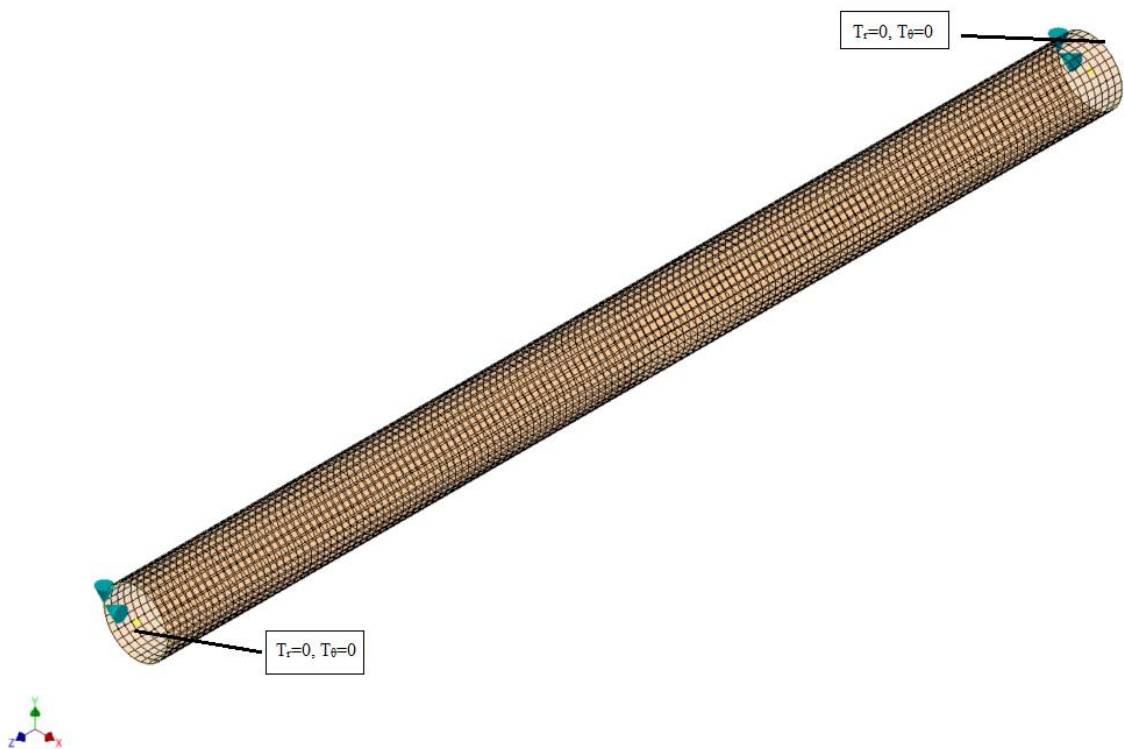


Figure 8.5. Boundary conditions and loadings of normal modes analysis in Autodesk Inventor NASTRAN Software

Mesh properties and set up are given in Table 8.3 for running analysis of the composite driveshafts. Stress components equalise when element size is above 10 mm, as shown in ref²¹³. Therefore, an element size of 10 mm was chosen for the composite model.

The results for fundamental frequency, critical buckling torque, and safety factor calculations, derived from both finite element analysis and analytical methods for various fiber orientation angles and material combinations, align well with each other and corroborate existing findings in the literature as seen in Table 8.4.

Table 8.3. Mesh Set up in Autodesk NASTRAN

Mesh Type	Quad Shell Element
Element Size (mm)	10
Max Element Growth Rate	1.5
Refinement Ratio	0.6
Max and Min Triangle Angle	20 - 30

The factor of safety is calculated using the Tsai-Wu failure theory in analytical approaches, while the Puck failure theory is applied in Finite Element Software to determine the FoS. Additionally, four-node shell elements, based on plate theory, are employed in the commercial software NASTRAN to enhance the accuracy and reliability of the simulations.

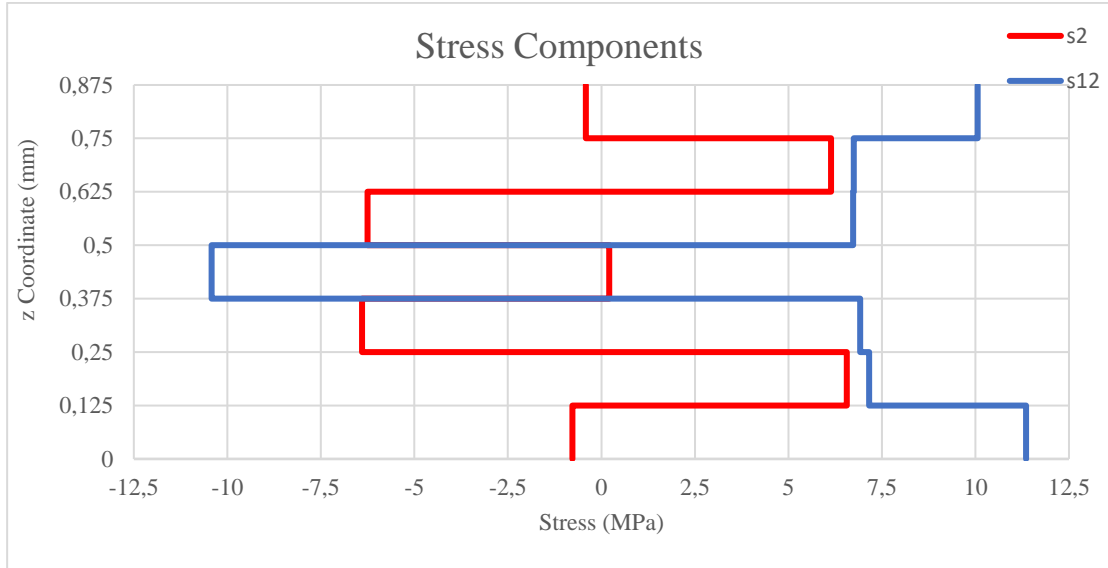
Table 8.4. A summary of comparison for composite driveshaft design parameters calculations; critical torsional buckling load, fundamental frequency and factor of safety (Tsai-Wu for CLT and Puck for FEA)

		Carbon/Epoxy		C/CNTs/Epoxy		B/Bepoxy	
		Present	Searle et al. ²¹³	Present	Searle et al. ²¹³	Present	Searle et al. ²¹³
T _c (Nm)	CLT	575.67	580.00	591.00	572.00	595.84	598.00
	FEA	591.70	612.00	660.00	762.00	674.00	823.00
	Difference (FEA/CLT)%	0.03	0.05	0.10	0.25	0.12	0.27
f _n (Hz)	CLT	106.75	107.00	109.77	109.00	80.65	80.00
	FEA	125.00	123.00	134.58	135.00	82.50	99.00
	Difference (FEA/CLT)%	0.15	0.13	0.18	0.19	0.02	0.19
FoS	CLT	5.32	5.17	5.30	5.34	4.82	5.47
	FEA	6.68	6.67	6.37	6.58	4.60	4.76
	Difference (FEA/CLT)%	0.20	0.22	0.17	0.19	-0.05	-0.15

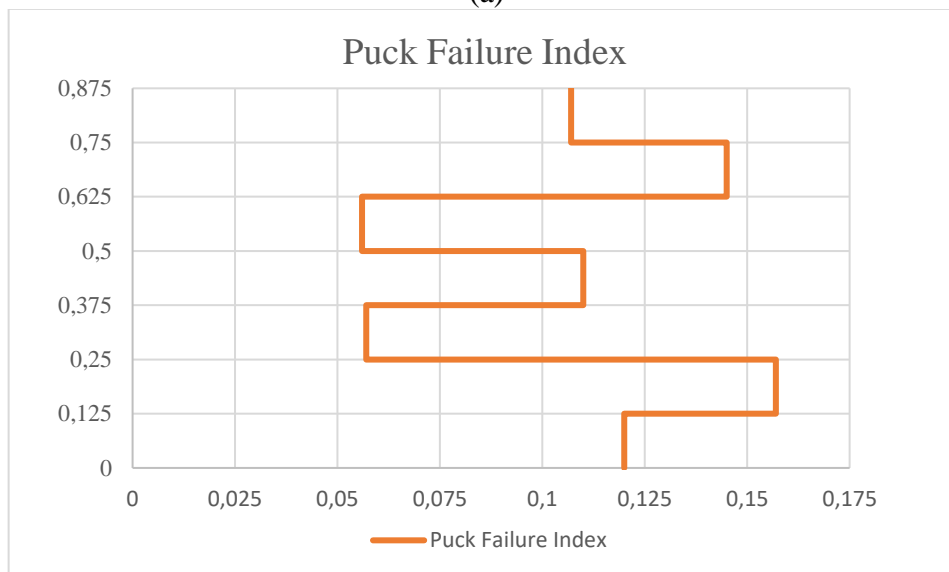
Results of the failure index are also in good agreement with results of FEM by ref Searle et al. agreement with each other. The results were verified with data available in the open literature, where possible.

In Figure 8.6, s₁₂ (shear) and s₂ (normal) stress components and biggest puck failure criterion indexes of matrix or fiber fault are given to compare results from the literature. The failure indexes indicate the potential failure of composite by matrix

dominated tensile failure, matrix dominated shear according to three failure modes. The stress component s_1 was not presented in the figures because it was far lower than the unidirectional strength.



(a)



(b)

Figure 8.6. Finite element analysis results for (a) stress components and (b) Puck failure indexes

Figure 8.6 shows the comparison of stress components and failure index values of C/CNT/E composite driveshaft by FEM with (Autodesk NASTRAN) and available results (ANSYS) by ref. ²¹³ In the Carbon/Epoxy (C/E) and Carbon/CNT/Epoxy

(C/CNT/E) shafts, the Interlaminar Failure (IRF) values in the 65° plies were found to be higher than in either the unidirectional or transverse plies. The stress components and failure indexes obtained from the present NASTRAN finite element analysis and those obtained from the literature⁸¹ using ANSYS are in good agreement.

8.2. Nanocomposite Driveshaft Optimization Problem

In this problem, weight minimization of hybrid and nonhybrid fiber/CNT reinforced nanocomposite driveshaft problems are obtained by using Modified Differential Evolution Algorithm by considering fundamental frequency(f_n), critical buckling load (T_{cr}) and Tsai-Wu failure index ($FoS_{(Tsai-Wu)i}$) as design constraints. The determination of the mechanical properties of CNTs-reinforced nanocomposites is conducted using a combination of theoretical models. Specifically, the modified Halpin–Tsai (H–T) equations and the rule of mixtures are utilized, which incorporate the effects of CNTs agglomeration within the matrix materials. Flax, Carbon and Glass fibers, CNTs and matrix material properties are also given in Table 8.5.

Table 8.5. Material Properties for driveshaft optimization problems

	Flax ²¹⁴	Carbon ^{213,215}	Glass ²¹⁵	Matrix ²¹³	CNTs ²¹³
E_1 (GPa)	50	230	85	3.45	450
E_2, E_3 (GPa)	12	15.41	85		
G_{12}, G_{13} (GPa)	3.4	10.04	35.42	1.26	
ν_{12}, ν_{13}	0.178	0.29	0.2	0.36	
ν_{23}	0.178	0.46	0.2		
Density(kg/m ³)	1400	18	2400	1250	624.4
S_1^T (MPa)	750	3350	1550	68	150000
S_1^C (MPa)	150	2500	1550	250	
S_2^T (MPa)	150	0	1550	0	
S_2^C (MPa)	150	0	1550	0	
S_{12} (MPa)	20	95	35	70	

Stacking sequences of fibers, volume fraction of carbon fiber and volume content of the CNT at each layer are selected as design variables. Additionally, carbon fiber

reinforced driveshaft without CNT inclusion is also optimized with constant volume fraction $V_f = 0.60$ to use basic design to see efficiency of design parameter increments.

Problem can be defined mathematically as

- Minimize: $Weight(V_{Fk}, W_{NTck}, \theta_k)$
- Constraints: $T_{cr}(V_{Fk}, W_{NTck}, \theta_k) \geq 550 Nm,$
 $f_n(V_{Fk}, W_{NTck}, \theta_k) \geq 80 Hz,$
 $FoS_{(Tsai-Wu_i)} \geq 3$
 $\frac{1}{n} \sum_{i=1}^n V_{CNTi} \leq V_{CNTmax}, V_{CNTtotal} \leq 0.20\% \text{ or } 0.30\%,$
 $V_{Fk} \leq 0.6, V_{CNTmax}=10\%,$
 $\theta_k \in \{0, 15, 30, 45, 60, 75, 90\}$
 Symmetric stacking sequences; $[\theta_1, \theta_2, \theta_3, \theta_4]_s$
 Symmetric weight fraction of CNT sequences;
 $[W_{CNT1}/W_{CNT2}/W_{CNT3}/W_{CNT4}]_s$
 Symmetric volume fraction of Fiber; $[V_{F1}/V_{F2}/V_{F3}/V_{F4}]_s$
 Algorithm: Differential Evolution

Table 8.6. Optimum stacking sequences, volume fraction of fiber and carbon nanotubes sequences for composite driveshaft

Designs	Stacking Sequence	Volume Fraction of Fiber	Volume Fraction of CNT
[C/C/C/C]s	[0/90/75/90]s	[0.60/0.60/0.60/0.60]s	-
[C/C/C/C]s	[75/90/90/0]s	[0.31/0.60/0.40/0.60]s	-
[G/G/G/G/G]s	[-30/-75/90/90/15]s	[0.49/0.53/0.46/0.47/0.51]s	-
[C/C/C/C]s-CNT	[90/90/90/0]s	[0.60/0.54/0.10/0.60]s	[0.088/0.100/0.100/0.012]s
[F/F/F/F/F]s-CNT	[90/90/0/0/90/90]s	[0.53/0.40/0.57/0.54/0.29/0.50]s	[0.043/0.067/0.043/0.090/0.035/0.017]s
[G/G/G/G/G]s-CNT	[90/90/90/90/0]s	[0.57/0.46/0.52/0.45/0.60]s	[0.088/0.10/0.036/0.024/0.042]s
[C/C/C/E]s-cnt	[0/90/90/90]s	[0.36/0.60/0.57/0.27]s	[0.10/0.10/0.056/0.088]s
[F/C/C/C]s-cnt	[90/90/90/0]s	[0.57/0.56/0.55/0.60]s	[0.068/0.088/0.10/0.088]s

In this problem, stacking sequences optimization of carbon fiber reinforced composite driveshaft problem are solved by using modified differential algorithm with constant fiber volume fraction 60% for each layer. The calculated weight of driveshaft is given as 0.774 kg. First of all, this result is utilized to compare weight minimization optimization approach results includes volume fraction of fiber and fiber orientation angle

as design variables for same carbon fiber reinforced composite driveshaft. The optimum stacking sequences, volume fraction of fibers and volume fraction of CNTs are given in Table 8.6. It is resulted that utilizing the volume fraction of carbon fibers as the sole design variable, the optimization of a composite driveshaft is achieved, resulting in a 8.8% reduction in weight. In Table 8.7, it can be seen that the driveshaft weight may be reduced by 11.49% compared to traditional optimum fiber reinforced driveshaft with constant volume fraction of fiber, for [C/C/C/C]s-CNT case. In comparison to an optimally designed fiber-reinforced driveshaft without carbon nanotubes (CNTs), incorporating a typical 5% addition of CNTs to the matrix material led to a further weight reduction of approximately 2%.

Table 8.7. Minimum weight, natural frequencies, critical torsional buckling loads and safety factor results of optimum multiphase fiber reinforced nanocomposite driveshafts

Designs	Weight	fn	Tcr	FoS	Weight Reduction
[C/C/C/C]s	0.774	123.062	694.777	3.195	
[C/C/C/C]s	0.706	96.438	551.171	4.489	8.786
[G/G/G/G/G]s	1.028	83.884	556.047	3.014	-32.752
[C/C/C/C]s-CNTs	0.685	99.523	550.117	3.065	11.499
[F/F/F/F/F]s-CNTs	0.879	84.072	579.790	7.376	-13.566
[G/G/G/G/G]s-CNTs	0.929	80.643	551.337	6.261	-20.052
[C/C/C/E]s-CNTs	0.687	106.661	555.809	8.350	11.240
[F/C/C/C]s-CNTs	0.683	101.138	550.049	4.680	11.757

The [G/G/G/G/G]s case is the least efficient in terms of weight, with 1.028 kg, but it has been demonstrated that incorporating a maximum of 10% volume fraction of CNT into each ply can reduce the weight of the driveshaft by 9.65% in the [G/G/G/G/G]s-CNT case. Moreover, using a fully flax fiber/CNT reinforced nanocomposite driveshaft ([F/F/F/F/F]s-CNT) results in approximately 15% less weight compared to the glass fiber/CNTs reinforced design, showcasing significant weight savings and more ecofriendly design. For the [F/C/C/C]s-CNT design, incorporating flax fiber in the outer layers enhances the driveshaft by achieving a 12% weight saving compared to traditional carbon fiber reinforced composite driveshafts. This substitution effectively reduces the overall weight while maintaining the structural integrity necessary for performance.

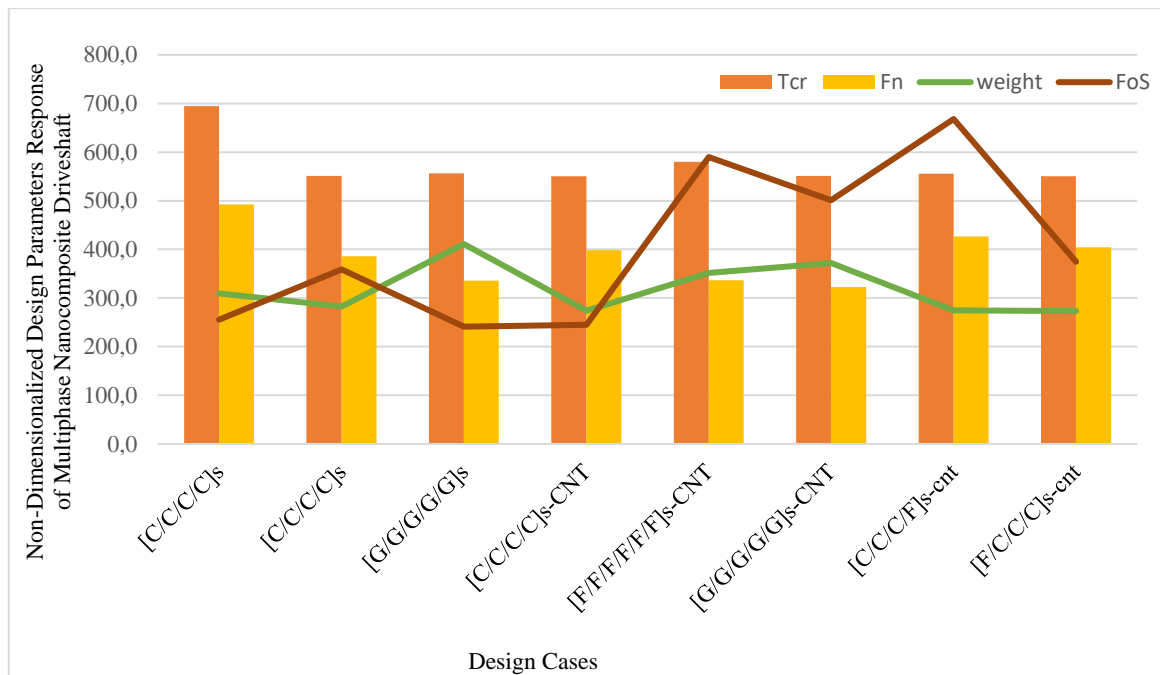


Figure 8.7. Comparison of the optimum design results minimum weight design results for multiphase hybrid and non-hybrid fiber/CNTs reinforced nanocomposite driveshafts

The Figure 8.7 shows the optimal configurations of multiphase hybrid and non-hybrid fiber/CNTs reinforced nanocomposites driveshafts, aimed at minimizing weight providing critical buckling loads, fundamental frequency and safety factor for failure index design constraints limits. In this figure, it can be seen that integrating carbon nanotubes (CNTs) into the matrix material with the hybridization of natural and carbon fibers provides the optimum solution in terms of minimum weight. As can be seen from the Figure 8.7, just optimizing the fiber volume fraction non-uniformly can reduce the weight by 8.8 %, while optimizing by adding cnt provides a 11.5% percent weight advantage. Additionally, the fully flax fiber reinforced nanocomposite driveshaft ([F/F/F/F/F]s-CNT) presents an eco-friendly alternative to the glass fiber/CNTs reinforced driveshaft ([G/G/G/G/G]s-CNT), offering a lighter and more biodegradable solution.

In this section of the thesis, the Finite Element Method (FEM) is employed to conduct a comprehensive analysis of optimized hybrid flax/carbon/CNT-reinforced nanocomposite driveshaft designs. The analyses include free vibration analysis, torsional buckling analysis, and stress-strain analysis, all performed using the Autodesk

NASTRAN Solver. To perform the eigenvalue buckling, vibration, and stress-strain analyses of the optimum multiscale nanocomposite driveshaft design, an appropriate mesh is generated using linear quadrilateral 4-node shell elements, which serve as an effective meshing option for the structure. The composite driveshaft is composed of seven hybrid flax and carbon layers, with dimensions as previously outlined in Table 8.1. The boundary conditions (BCs) for displacement constraints, provided at the beginning of the section, are consistently applied across all analyses. These same BCs are used for the normal modes, eigenvalue buckling, and static analysis of the hybrid nanocomposite driveshaft. The model was subjected to a convergence test in terms of mesh density, which led to the selection of a mesh consisting of 13640 nodes and 4526 elements, which were used to obtain the final solution.

The optimum non-uniform CNT weight content, fibre orientation angle and fibre volume fraction for each layer of the hybrid flax/carbon/CNT nanocomposite driveshaft are obtained by [F/C/C/C]s-cnt design and the properties of each layer for this design are given in Table 8.8. These values are derived from the results of an optimization problem designed to minimize weight while adhering to the specified constraints.

Table 8.8. Material properties of each ply for optimum inter-ply hybrid flax/carbon/CNTs nanocomposite driveshafts with modified Halpin-Tsai model

	Flax	Carbon ¹	Carbon ²	Carbon ³
E ₁ (MPa)	30422.20	130751.00	128472.00	139774.00
E ₂ (MPa)	7927.53	8943.66	8784.88	9385.65
G ₁₂ (MPa)	2457.62	3836.21	3740.14	4113.80
G ₂₃ (MPa)	2457.62	2999.65	2945.15	3142.84
V ₁₂	0.32	0.32	0.32	0.32
V ₂₃	0.26	0.41	0.41	0.42
ρ (kg/m ³)	1297.17	1849.71	1834.10	1899.74
S ₁ ^T (MPa)	627.78	2086.56	2056.62	2201.42
S ₂ ^T (MPa)	285.78	210.56	1666.63	1761.75
S ₁ ^C (MPa)	363.97	1687.92	214.12	191.42
S ₂ ^C (MPa)	363.97	287.92	291.63	261.75
T ₁₂ (MPa)	212.68	264.73	267.33	249.30

Table 8.9 shows a strong agreement between the FEM results and analytical results for the optimum designs, particularly in terms of the fundamental frequency, critical torsional buckling load, and factor of safety values for the nanocomposite driveshaft. For the normal mode analysis results of the hybrid fiber/CNT-reinforced

nanocomposite driveshaft, a 14% difference is observed compared to the results calculated using the analytical method. Similarly, there is a 10% difference for the critical torsional buckling load values. The factor of safety can be determined using both analytical methods and FEA, with a 4% difference between the two approaches.

Table 8.9. A comparison of the natural frequencies, critical torsional buckling load, and factor of safety results obtained from finite element analysis (FEA) and analytical methods for the optimum hybrid nanocomposite driveshaft

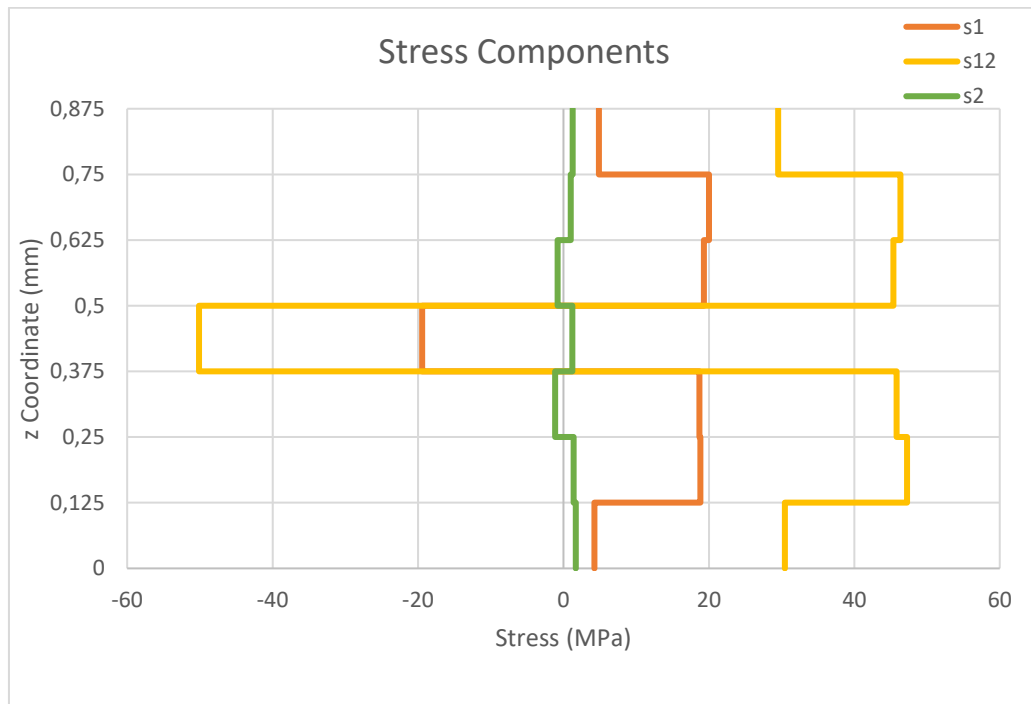
[F/C/C/C]s-cnt	fn (Hz)	Tcr (Nm)	FoS
Analytical	101.138	550.049	4.680
FEA (NASTRAN)	115.619	500.750	4.878
Difference (%)	14	10	4.2

The optimum interlayer hybrid fibre/CNT reinforced nanocomposite driveshaft was derived using the Halpin-Tsai model and Classical Lamination Plate Theory (CLPT), with the FEM results showing a maximum error margin of only 14%. The present approach allows the non-uniform material properties in each layer to be accurately considered in the FEM analysis of fibre-reinforced nanocomposite driveshafts. Using Autodesk NASTRAN, FEM is effectively applied to multi-scale hybrid fibre/CNT-reinforced nanocomposites by combining multi-scale modelling with micromechanical equations.

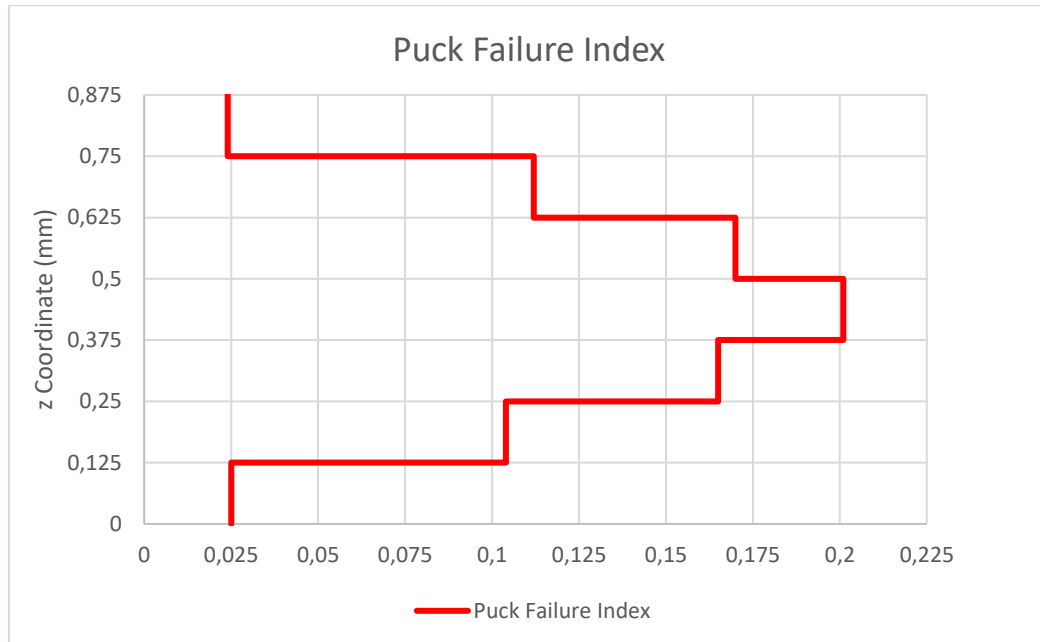
The factor of safety is calculated based on stress-strain analysis results using the Puck Failure Theory, applied layer by layer in Autodesk NASTRAN Software. The normal stresses and shear stress distributions are illustrated in Figure 8.9a. Additionally, the Puck failure values for the nanocomposite driveshaft are also depicted in Figure 8.9b.

Figures 8.8a and 8.8b display the composite layups, stress components (s_1 , s_2 , and s_{12}), and Puck failure index results for the [F/C/C/C]s nanocomposite driveshaft design. It is evident that the s_2 stress components are significantly lower than the unidirectional strength due to the presence of 90° layers. The maximum shear stress (s_{12}) and normal stress (s_1) occur in the middle layer of the nanocomposite driveshaft, where the highest Puck failure index is also observed. The three failure states of the Puck criterion are also shown, indicating the potential failure of the composite by matrix dominated tensile failure, matrix dominated shear failure and matrix dominated

compression failure. Additionally, the shear stress (s_{12}) and Puck failure index for matrix tension are illustrated in Figures 8.9 (a) and 8.9 (b).

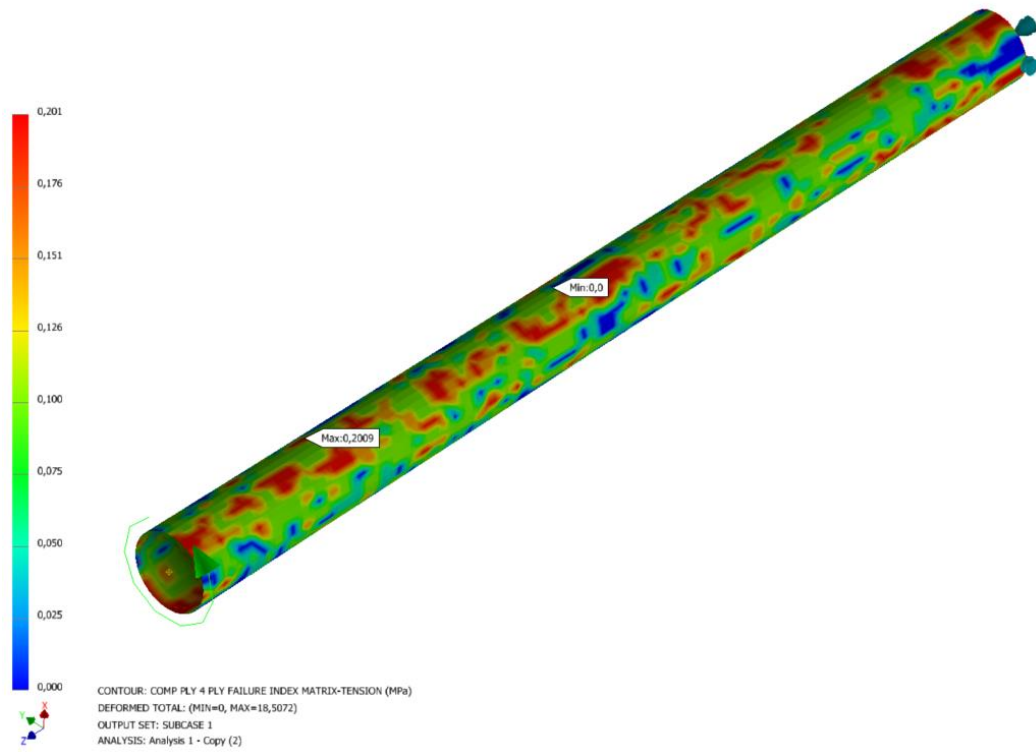


(a)

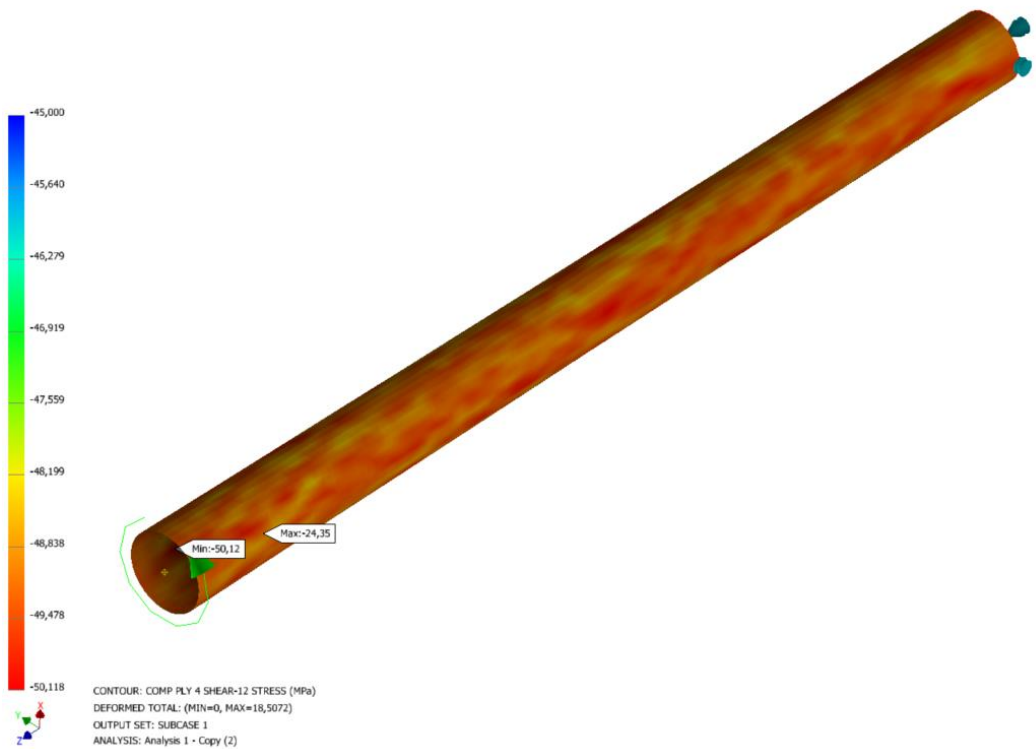


(b)

Figure 8.8. Finite element analysis results for a) stress components and b) puck failure indexes for multiphase hybrid flax/carbon/CNTs reinforced nanocomposite driveshafts



(a)



(b)

Figure 8.9. Finite element analysis results for 4th carbon/CNTs ply of hybrid nanocomposite driveshaft a) shear stress component (s12) and b) puck failure index

An eigenvalue buckling analysis was conducted to determine the deformation and critical buckling load, with the model fully fixed at one end and subjected to torsional loading at the other end. The analytical method yielded a corresponding buckling torque value of 550 N·m, while the FEA result was 500.75 N·m. The mode shape from the eigenvalue buckling analysis is illustrated in Figure 8.10.

A set of the first ten mode shapes of the natural frequency for a simply supported nanocomposite driveshaft is presented in Figure 8.11, with the first mode excluded due to its value being zero. FEM analysis was conducted using Autodesk NASTRAN Software to detect deformation and natural frequencies. The corresponding frequency values were as follows: (a) 115.61 Hz, (b) 115.63 Hz, (c) 156.10 Hz, (d) 156.54 Hz, (e) 224.13 Hz, (f) 224.36 Hz, (g) 289.54 Hz, and (h) 289.64 Hz.

In conclusion, although there is a risk of agglomeration, incorporating CNT into material models significantly boosts the efficiency and environmental sustainability of synthetic natural fiber reinforced composites. This strategy effectively mitigates the inherent lower strength properties of natural fibers, resulting in more robust and sustainable designs. The utilization of stochastic optimization approaches for hybrid nanocomposite driveshaft design further enhances these outcomes, enabling the development of high-performance, eco-friendly composite structures. The FEA analysis approach, combined with the modified Halpin-Tsai method, can be effectively utilized for designing nanocomposite driveshafts with non-uniform material properties layer by layer.

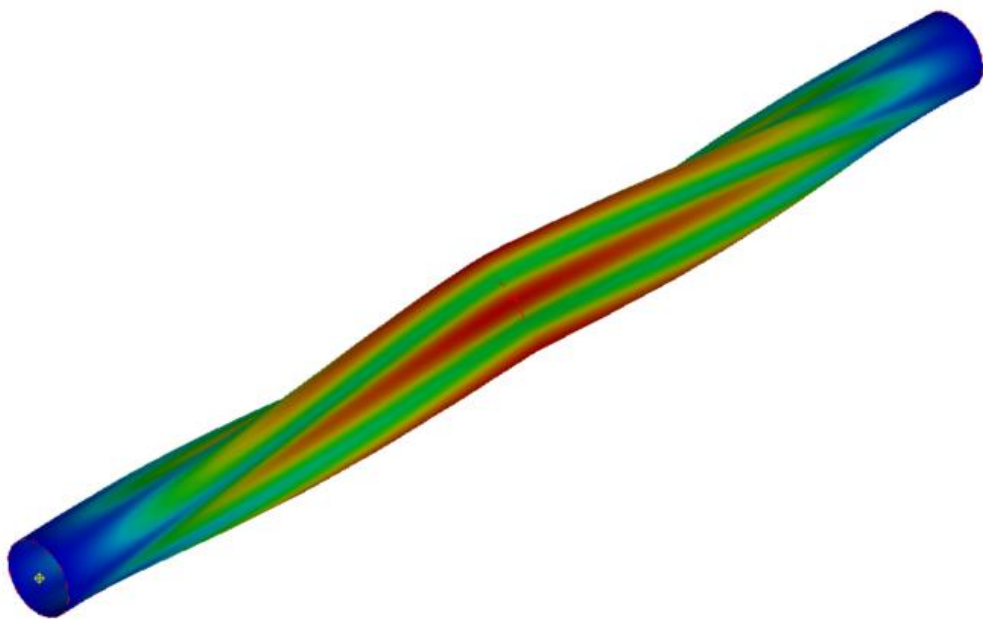


Figure 8.10 First buckling mode shape of a hybrid nanocomposite driveshaft

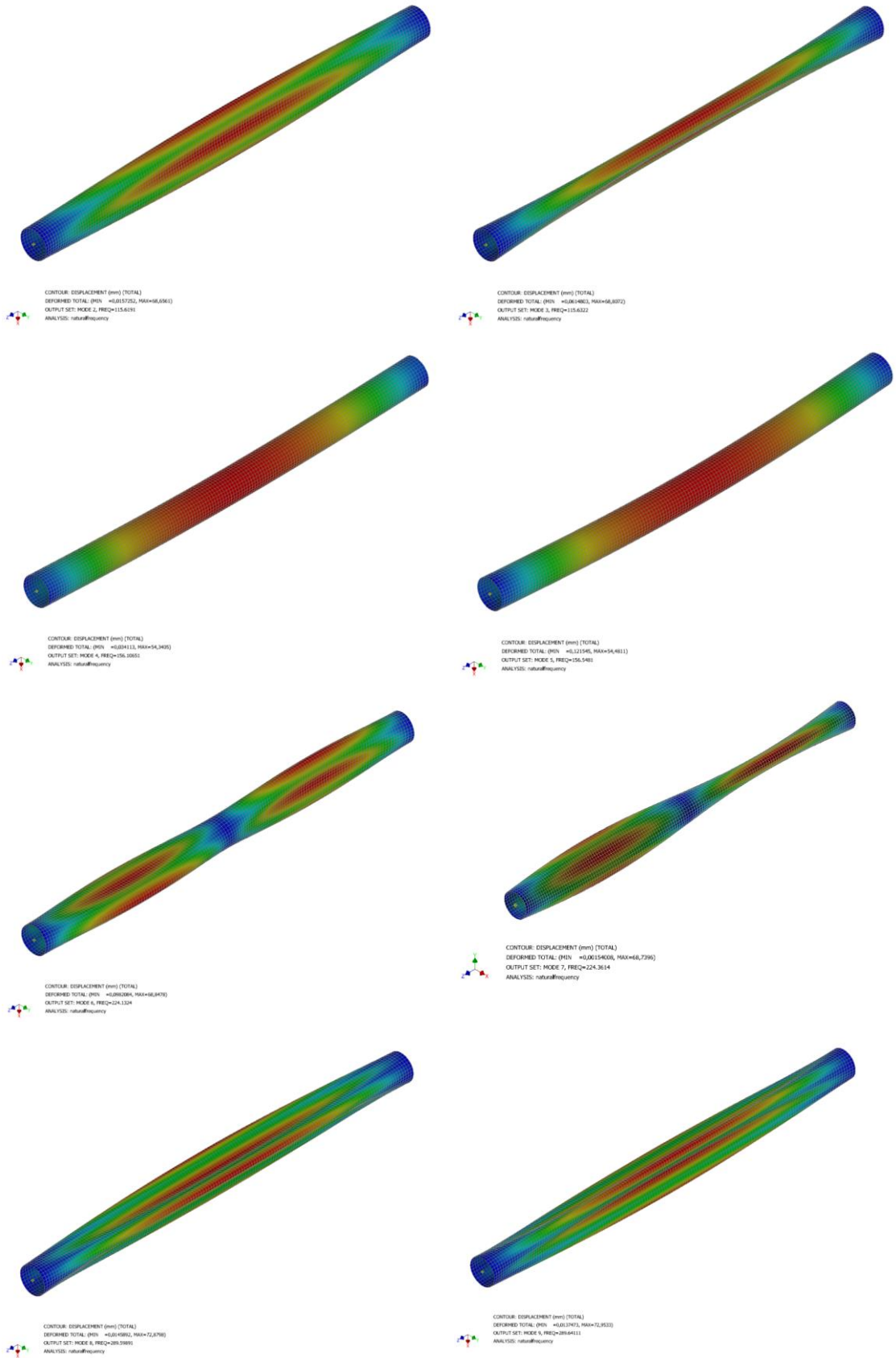


Figure 8.11. The first eight mode shapes of natural frequency of a simply supported composite driveshaft

CHAPTER 9

CONCLUSION

This thesis presents a study on designing a hybrid fiber-reinforced multiscale nanocomposite using stochastic optimization methods. The composite comprises multiscale components: a macroscale matrix, microscale fiber, and nanoscale CNTs or GPLs. The development of these multiscale nanocomposite structures aims to meet conditions of higher natural frequency, increased buckling load, reduced failure index, lower weight, and cost-effectiveness. These composites are intended for applications in automotive, aerospace, and aviation industries, offering environmentally friendly properties. Multiscale hybrid fiber-reinforced nanocomposites can satisfy the requirements of applications with appropriate stacking sequences, volume fraction of each ply and weight content of nanofillers (CNTs and GPLs). By using a comprehensive set of design variables in the optimal design of nanocomposite structures, more environmentally friendly hybrid natural fibre reinforced nanocomposite structures can be proposed for applications where vibration, buckling and failure behaviour are critical factors. These designs also offer minimum cost and weight compared to traditional fully synthetic fibre reinforced composite structures.

The other concluding points of this thesis can be written as follows;

- Optimum design of multiscale hybrid and non-hybrid natural/synthetic fibers-reinforced nanocomposite laminates has been proposed by using CLPT, FSDT, Navier solution, and stochastic optimization methods.
- Halpin-Tsai and Modified Halpin-Tsai models were utilized to determine the elastic properties of each ply which is composed of fiber, nanofillers and matrix materials by considering agglomeration and waviness effects.
- The weight fraction of the graphene nanoplatelets (GPLs), the stacking sequences, and the volume fraction of fibers have been optimized by using Differential Evolution (DE), Simulated Annealing (SA), and Nelder Mead (NM) algorithms for multiscale hybrid and non-hybrid nanocomposite plates.
- The comparison of the different multi-objective approaches (natural frequency-cost, natural frequency-weight, and natural frequency-cost-

weight) have been carried out for inter-ply hybrid/non-hybrid two-phase (fiber+matrix) and inter-ply hybrid/non-hybrid three-phase (fiber+nanofillers+matrix) composite structures.

- Using inter-ply hybrid fibers with GPLs nano-reinforcement in composite structures, it is feasible to design high-frequency, low-cost, and low-weight multilayer composites with high stiffness-to-weight ratios. In this respect, as a substitute for carbon fiber composites and carbon/glass composites, the use of flax fiber with GPLs reinforcement in hybrid structures has a significant potential with 18.2% higher frequency, 7.7% lower weight and 31.3% lower cost.
- Regarding the effect of the aspect ratio on the optimal design of multiscale nanocomposites. it can be concluded that the weight content of GPLs is evenly distributed across both the outer and inner layers for aspect ratios between 0.2 and 0.6. However, for aspect ratios between 0.6 and 2 the weight content is more concentrated on the outer layers as compared to the inner layers.
- For multi-objective designs of composite structures, while carbon fibers and CNTs or GPLs are commonly used, combining natural fibers (Flax, Kevlar, Jute, and Ramie) with CNTs and GPLs in interply hybrid designs can achieve superior results with 30% weight savings and 13% cost savings.
- Considering only the critical buckling load as an objective, the use of multiphase carbon/epoxy and carbon/epoxy-CNTs nanocomposites allows the highest critical buckling load.
- Multi-objective optimization of multiscale hybrid and non-hybrid fiber/CNTs reinforced nanocomposites was achieved for maximum critical buckling loads and minimum weights. Using Kenaf and Flax natural fibers with carbon fiber and adding CNTs can reduce weight by up to 14% with a 10% decrease in critical buckling load, while also benefiting from more eco-friendly fibers.
- As expected, placing fiber and CNTs reinforcements in or near the outer layers is more effective for minimizing weight due to their higher contribution to laminate stiffness. Numerical results indicated that

increasing the amount of CNTs reduces the amount of fiber to satisfy the frequency or buckling constraints in weight minimization problems.

- For driveshaft design with minimum weight, using variable volume fraction of carbon fibers in addition to stacking sequences can achieve a 8.8% weight reduction compared to traditional constant volume fraction designs. Moreover, incorporating flax fiber in the outer layers of the nanocomposite driveshaft enhances it by achieving a 12% weight saving compared to traditional carbon fiber-reinforced composite driveshafts
- In conclusion, despite the risk of agglomeration, incorporating small amount of CNTs into material models significantly alters the efficiency and mechanical response of natural fiber-reinforced composites.
- The approaches used in the thesis study increase the inherent low strength of natural fibres. The result is more robust and sustainable designs. Using stochastic optimization approaches for nanocomposite design further developing these outcomes, enabling the development of high-performance, eco-friendly composite structures.

For future research on multiscale inter-ply hybrid fiber-reinforced nanocomposites, the followings can be suggested:

- Conduct experimental investigations of hybrid natural fiber/CNTs reinforced composite driveshafts and compare the results with optimization outcomes.
- Extend the study by incorporating objective functions for hygrothermal effects using a multi-objective optimization approach tailored for aerospace applications.
- Enhance material models for nano-reinforcement by incorporating more accurate agglomeration models that are better supported by experimental data.
- Investigate the performance of hybrid natural fiber-reinforced composites in cryogenic environments, particularly for liquid hydrogen storage, using nanofillers such as CNTs and GPLs.

REFERENCES

1. Talapatra, A.; Datta, D. Graphene-Reinforced Thermoplastic Polyurethane Nanocomposites: A Simulation and Experimental Study. *J. Thermoplast. Compos. Mater.* **2021**, *34* (2), 143–161. <https://doi.org/10.1177/0892705719839459>.
2. Bernard, C.; Goodwin, D. G.; Gu, X.; Celina, M.; Nyden, M.; Jacobs, D.; Sung, L.; Nguyen, T. Graphene Oxide/Waterborne Polyurethane Nanocoatings: Effects of Graphene Oxide Content on Performance Properties. *J. Coatings Technol. Res.* **2020**, *17* (1), 255–269. <https://doi.org/10.1007/s11998-019-00267-6>.
3. Mittal, G.; Dhand, V.; Rhee, K. Y.; Park, S. J.; Lee, W. R. A Review on Carbon Nanotubes and Graphene as Fillers in Reinforced Polymer Nanocomposites. *J. Ind. Eng. Chem.* **2015**, *21*, 11–25. <https://doi.org/10.1016/j.jiec.2014.03.022>.
4. Mittal, V.; Chaudhry, A. U. Polymer - Graphene Nanocomposites: Effect of Polymer Matrix and Filler Amount on Properties. *Macromol. Mater. Eng.* **2015**, *300* (5), 510–521. <https://doi.org/10.1002/mame.201400392>.
5. Kim, M.; Park, Y. Bin; Okoli, O. I.; Zhang, C. Processing, Characterization, and Modeling of Carbon Nanotube-Reinforced Multiscale Composites. *Compos. Sci. Technol.* **2009**, *69* (3–4), 335–342. <https://doi.org/10.1016/J.COMPSCITECH.2008.10.019>.
6. Zaman, I.; Kuan, H. C.; Dai, J.; Kawashima, N.; Michelmore, A.; Sovi, A.; Dong, S.; Luong, L.; Ma, J. From Carbon Nanotubes and Silicate Layers to Graphene Platelets for Polymer Nanocomposites. *Nanoscale* **2012**, *4* (15), 4578–4586. <https://doi.org/10.1039/C2NR30837A>.
7. Mittal, G.; Dhand, V.; Rhee, K. Y.; Park, S. J.; Lee, W. R. A Review on Carbon Nanotubes and Graphene as Fillers in Reinforced Polymer Nanocomposites. *J. Ind. Eng. Chem.* **2015**, *21*, 11–25. <https://doi.org/10.1016/J.JIEC.2014.03.022>.
8. Rafiee, M. A.; Rafiee, J.; Wang, Z.; Song, H.; Yu, Z. Z.; Koratkar, N. Enhanced Mechanical Properties of Nanocomposites at Low Graphene Content. *ACS Nano* **2009**, *3* (12), 3884–3890.

https://doi.org/10.1021/NN9010472/SUPPL_FILE/NN9010472_SI_001.PDF.

9. Kumar, A.; Sharma, K.; Dixit, A. R. Effects of Various Functional Groups in Graphene on the Tensile and Flexural Properties of Epoxy Nanocomposites: A Comparative Study. *https://doi.org/10.1080/1536383X.2022.2077332* **2022**, *30* (11), 1123–1133. <https://doi.org/10.1080/1536383X.2022.2077332>.
10. Saiah, B.; Bachene, M.; Guemana, M.; Chiker, Y.; Attaf, B. On the Free Vibration Behavior of Nanocomposite Laminated Plates Contained Piece-Wise Functionally Graded Graphene-Reinforced Composite Plies. *Eng. Struct.* **2022**, *253*. <https://doi.org/10.1016/j.engstruct.2021.113784>.
11. Rahman, M. Z. Mechanical and Damping Performances of Flax Fibre Composites – A Review. *Composites Part C: Open Access*. Elsevier B.V. March 1, 2021. <https://doi.org/10.1016/j.jcomc.2020.100081>.
12. Bledzki, A. K.; Faruk, O.; Sperber, V. E. Cars from Bio-Fibres. *Macromol. Mater. Eng.* **2006**, *291* (5), 449–457. <https://doi.org/10.1002/mame.200600113>.
13. Moudood, A.; Rahman, A.; Öchsner, A.; Islam, M.; Francucci, G. Flax Fiber and Its Composites: An Overview of Water and Moisture Absorption Impact on Their Performance. *https://doi.org/10.1177/0731684418818893* **2018**, *38* (7), 323–339. <https://doi.org/10.1177/0731684418818893>.
14. Javanshour, F.; Ramakrishnan, K. R.; Layek, R. K.; Laurikainen, P.; Prapavesis, A.; Kanerva, M.; Kallio, P.; Van Vuure, A. W.; Sarlin, E. Effect of Graphene Oxide Surface Treatment on the Interfacial Adhesion and the Tensile Performance of Flax Epoxy Composites. *Compos. Part A Appl. Sci. Manuf.* **2021**, *142*, 106270. <https://doi.org/10.1016/J.COMPOSITESA.2020.106270>.
15. De Prez, J.; Van Vuure, A. W.; Ivens, J.; Aerts, G.; Van de Voorde, I. Effect of Enzymatic Treatment of Flax on Fineness of Fibers and Mechanical Performance of Composites. *Compos. Part A Appl. Sci. Manuf.* **2019**, *123*, 190–199. <https://doi.org/10.1016/J.COMPOSITESA.2019.05.007>.
16. Prabhakaran, S.; Krishnaraj, V.; Senthil Kumar, M.; Zitoune, R. Sound and Vibration Damping Properties of Flax Fiber Reinforced Composites. In *Procedia Engineering*; Elsevier Ltd, 2014; Vol. 97, pp 573–581. <https://doi.org/10.1016/j.proeng.2014.12.285>.

17. Andersons, J.; Spārniņš, E.; Joffe, R. Stiffness and Strength of Flax Fiber/Polymer Matrix Composites. *Polym. Compos.* **2006**, *27* (2), 221–229. <https://doi.org/https://doi.org/10.1002/pc.20184>.
18. Zhang, D.; Milanovic, N. R.; Zhang, Y.; Su, F.; Miao, M. Effects of Humidity Conditions at Fabrication on the Interfacial Shear Strength of Flax/Unsaturated Polyester Composites. *Compos. Part B Eng.* **2014**, *60*, 186–192. <https://doi.org/10.1016/J.COMPOSITESB.2013.12.031>.
19. Ng, L. F.; Yahya, M. Y.; Muthukumar, C. Mechanical Characterization and Water Absorption Behaviors of Pineapple Leaf/Glass Fiber-Reinforced Polypropylene Hybrid Composites. *Polym. Compos.* **2022**, *43* (1), 203–214. <https://doi.org/10.1002/PC.26367>.
20. Al-Hajaj, Z.; Zdero, R.; Bougherara, H. Mechanical, Morphological, and Water Absorption Properties of a New Hybrid Composite Material Made from 4 Harness Satin Woven Carbon Fibres and Flax Fibres in an Epoxy Matrix. *Compos. Part A Appl. Sci. Manuf.* **2018**, *115*, 46–56. <https://doi.org/10.1016/J.COMPOSITESA.2018.09.015>.
21. Liu, Z.; Wang, H.; Yang, L.; Du, J. Research on Mechanical Properties and Durability of Flax/Glass Fiber Bio-Hybrid FRP Composites Laminates. *Compos. Struct.* **2022**, *290*. <https://doi.org/10.1016/J.COMPSTRUCT.2022.115566>.
22. LI, S. A.; DUFFY, K. J. MINIMUM COST DESIGN OF VIBRATING LAMINATES BY HYBRIDIZATION. <http://dx.doi.org/10.1080/03052159208941231> **2007**, *19* (4), 255–267. <https://doi.org/10.1080/03052159208941231>.
23. Ma, X.; Tian, K.; Li, H.; Zhou, Y.; Hao, P.; Wang, B. Concurrent Multi-Scale Optimization of Hybrid Composite Plates and Shells for Vibration. *Compos. Struct.* **2020**, *233* (May 2019), 111635. <https://doi.org/10.1016/j.compstruct.2019.111635>.
24. Abachizadeh, M.; Tahani, M. An Ant Colony Optimization Approach to Multi-Objective Optimal Design of Symmetric Hybrid Laminates for Maximum Fundamental Frequency and Minimum Cost. *Struct. Multidiscip. Optim.* **2009**, *37* (4), 367–376. <https://doi.org/10.1007/s00158-008-0235-6>.

25. An, H.; Chen, S.; Huang, H. Multi-Objective Optimal Design of Hybrid Composite Laminates for Minimum Cost and Maximum Fundamental Frequency and Frequency Gaps. *Compos. Struct.* **2019**, *209*, 268–276. <https://doi.org/10.1016/J.COMPSTRUCT.2018.10.075>.
26. Prabhakaran, S.; Krishnaraj, V.; Senthil Kumar, M.; Zitoune, R. Sound and Vibration Damping Properties of Flax Fiber Reinforced Composites. *Procedia Eng.* **2014**, *97*, 573–581. <https://doi.org/10.1016/J.PROENG.2014.12.285>.
27. Zhong, Y.; Kureemun, U.; Tran, L. Q. N.; Lee, H. P. Natural Plant Fiber Composites-Constituent Properties and Challenges in Numerical Modeling and Simulations. *Int. J. Appl. Mech.* **2017**, *9* (4). <https://doi.org/10.1142/S1758825117500454>.
28. Shah, D. U.; Schubel, P. J.; Clifford, M. J. Composites : Part B Can Flax Replace E-Glass in Structural Composites ? A Small Wind Turbine Blade Case Study. *Compos. PART B* **2013**, *52*, 172–181. <https://doi.org/10.1016/j.compositesb.2013.04.027>.
29. Ben Ameer, M.; El Mahi, A.; Rebiere, J. L.; Abdennadher, M.; Haddar, M. Damping Analysis of Unidirectional Carbon/Flax Fiber Hybrid Composites. *Int. J. Appl. Mech.* **2018**, *10* (5). <https://doi.org/10.1142/S1758825118500503>.
30. Savran, M.; Aydin, L. Stochastic Optimization of Graphite-Flax/Epoxy Hybrid Laminated Composite for Maximum Fundamental Frequency and Minimum Cost. *Eng. Struct.* **2018**, *174*, 675–687. <https://doi.org/10.1016/j.engstruct.2018.07.043>.
31. Hosseinzadeh, Y.; Jalili, S.; Khani, R. Investigating the Effects of Flax Fibers Application on Multi-Objective Optimization of Laminated Composite Plates for Simultaneous Cost Minimization and Frequency Gap Maximization. *J. Build. Eng.* **2020**, *32* (April), 101477. <https://doi.org/10.1016/j.jobbe.2020.101477>.
32. Megahed, M.; Abo-bakr, R. M.; Mohamed, S. A. Optimization of Hybrid Natural Laminated Composite Beams for a Minimum Weight and Cost Design. *Compos. Struct.* **2020**, *239*. <https://doi.org/10.1016/j.compstruct.2020.111984>.
33. Thai, C. H.; Ferreira, A. J. M.; Tran, T. D.; Phung-Van, P. Free Vibration, Buckling and Bending Analyses of Multilayer Functionally Graded Graphene

- Nanoplatelets Reinforced Composite Plates Using the NURBS Formulation. *Compos. Struct.* **2019**, 220 (April), 749–759. <https://doi.org/10.1016/j.compstruct.2019.03.100>.
34. Kamarian, S.; Shakeri, M.; Yas, M. H. Natural Frequency Analysis and Optimal Design of CNT/Fiber/Polymer Hybrid Composites Plates Using Mori-Tanaka Approach, GDQ Technique, and Firefly Algorithm. *Polym. Compos.* **2018**, 39 (5), 1433–1446. <https://doi.org/10.1002/pc.24083>.
 35. Xiang, R.; Pan, Z. Z.; Ouyang, H.; Zhang, L. W. A Study of the Vibration and Lay-up Optimization of Rotating Cross-Ply Laminated Nanocomposite Blades. *Compos. Struct.* **2020**, 235. <https://doi.org/10.1016/j.compstruct.2019.111775>.
 36. Yousefi, A. H.; Memarzadeh, P.; Afshari, H.; Hosseini, S. J. Optimization of CNT/Polymer/Fiber Laminated Truncated Conical Panels for Maximum Fundamental Frequency and Minimum Cost. *Mech. Based Des. Struct. Mach.* **2021**. <https://doi.org/10.1080/15397734.2021.1945932>.
 37. Jeawon, Y.; Drosopoulos, G. A.; Foutsitzi, G.; Stavroulakis, G. E.; Adali, S. Optimization and Analysis of Frequencies of Multi-Scale Graphene/Fibre Reinforced Nanocomposite Laminates with Non-Uniform Distributions of Reinforcements. *Eng. Struct.* **2021**, 228. <https://doi.org/10.1016/j.engstruct.2020.111525>.
 38. Anashpaul, S.; Drosopoulos, G. A.; Adali, S. Minimum Weight Design of CNT/Fiber Reinforced Laminates Subject to a Frequency Constraint by Optimal Distribution of Reinforcements across the Thickness. *Compos. Struct.* **2023**, 319 (May), 117112. <https://doi.org/10.1016/j.compstruct.2023.117112>.
 39. Drosopoulos, G. A.; Gogos, C.; Foutsitzi, G. Multi-Objective Optimization for Maximum Fundamental Frequency and Minimum Cost of Hybrid Graphene/Fibre-Reinforced Nanocomposite Laminates. *Structures* **2023**, 54, 1593–1607. <https://doi.org/10.1016/j.istruc.2023.05.118>.
 40. Jeawon, Y.; Drosopoulos, G. A.; Foutsitzi, G.; Stavroulakis, G. E.; Adali, S. Optimization of Graphene/Fibre Reinforced Cantilever Skew Laminates for Maximum Fundamental Frequency via Non-Uniform Distribution of Reinforcements. *Thin-Walled Struct.* **2023**, 189 (February), 110903.

- <https://doi.org/10.1016/j.tws.2023.110903>.
41. Radebe, I. S.; Drosopoulos, G. A.; Adali, S. Effect of Non-Uniform Fibre Distribution along Thickness and Non-Uniform Ply Thicknesses on Frequencies of Symmetric Angle-Ply Laminates. *Fibers Polym.* **2022**, *23* (8), 2250–2260. <https://doi.org/10.1007/s12221-022-4440-5>.
 42. Kuriakose, V. M.; Rohith Sai, P.; Sanjaay Kumar, M.; Sreehari, V. M. Influence of CNT Fillers in the Vibration Characteristics of Natural Fiber Reinforced Composite Plates. *Compos. Struct.* **2022**, 282. <https://doi.org/10.1016/j.compstruct.2021.115012>.
 43. Singh, P.; Bala, Y. G. Thermal and Vibrational Analysis of Flax Fiber Composite and Effect of the Addition of Expandable Graphite. *Proc. Inst. Mech. Eng. Part L J. Mater. Des. Appl.* **2022**, *236* (10), 2116–2126. <https://doi.org/10.1177/14644207221101961>.
 44. Shanmugam, S.; Meenakshisundaram, O. Experimental Investigation of Graphene Filled Flax/E-Glass/Epoxy Hybrid Nanocomposites on Physical, Mechanical, and Thermal Properties. *Fullerenes Nanotub. Carbon Nanostructures* **2022**. <https://doi.org/10.1080/1536383X.2022.2110080>.
 45. Muc, A. Optimal Fibre Orientation for Simply-Supported, Angle-Ply Plates under Biaxial Compression. *Compos. Struct.* **1988**, *9* (2), 161–172. [https://doi.org/10.1016/0263-8223\(88\)90005-0](https://doi.org/10.1016/0263-8223(88)90005-0).
 46. Zor, M.; Şen, F.; Toygar, M. E. An Investigation of Square Delamination Effects on the Buckling Behavior of Laminated Composite Plates with a Square Hole by Using Three-Dimensional FEM Analysis. <http://dx.doi.org/10.1177/0731684405048836> **2005**, *24* (11), 1119–1130. <https://doi.org/10.1177/0731684405048836>.
 47. Nemeth, M. P. Importance of Anisotropy on Buckling of Compression-Loaded Symmetric composite Plates. <https://doi.org/10.2514/3.9531> **1986**, *24* (11), 1831–1835. <https://doi.org/10.2514/3.9531>.
 48. Kaw, A. K. Mechanics of Composite Materials. **2006**, 466.
 49. Thostenson, E. T.; Ren, Z.; Chou, T.-W. Advances in the Science and

Technology of Carbon Nanotubes and Their Composites: A Review.

50. Wuite, J.; Adali, S. Deflection and Stress Behaviour of Nanocomposite Reinforced Beams Using a Multiscale Analysis.
<https://doi.org/10.1016/j.compstruct.2005.09.011>.
51. Liew, K. M.; Lei, Z. X.; Zhang, L. W. Mechanical Analysis of Functionally Graded Carbon Nanotube Reinforced Composites: A Review. **2014**.
<https://doi.org/10.1016/j.compstruct.2014.09.041>.
52. Fidelus, J. D.; Wiesel, E.; Gojny, F. H.; Schulte, K.; Wagner, H. D. Thermo-Mechanical Properties of Randomly Oriented Carbon/Epoxy Nanocomposites.
<https://doi.org/10.1016/j.compositesa.2005.02.006>.
53. Kang, I.; Yeo Heung, Y.; Kim, J. H.; Lee, J. W.; Gollapudi, R.; Subramaniam, S.; Narasimhadevara, S.; Hurd, D.; Kirikera, R.; Shanov, V.; Schulz, M. J.; Shi, D.; Boerio, J.; Mall, S.; Ruggles-Wren, M. Introduction to Carbon Nanotube and Nanofiber Smart Materials. **2006**.
<https://doi.org/10.1016/j.compositesb.2006.02.011>.
54. Tarfaoui, M.; Moumen, A. El; Boehle, M.; Shah, O.; Lafdi, K. Self-Heating and Deicing Epoxy/Glass Fiber Based Carbon Nanotubes Buckypaper Composite.
<https://doi.org/10.1007/s10853-018-2917-9>.
55. Malekzadeh, P.; Zarei, A. R. Free Vibration of Quadrilateral Laminated Plates with Carbon Nanotube Reinforced Composite Layers.
<https://doi.org/10.1016/j.tws.2014.04.016>.
56. Sankar, A.; Natarajan, S.; Ganapathi, M. Dynamic Instability Analysis of Sandwich Plates with CNT Reinforced Facesheets. **2016**.
<https://doi.org/10.1016/j.compstruct.2016.03.026>.
57. Shahrabaki, E. A.; Alibeigloo, A. Three-Dimensional Free Vibration of Carbon Nanotube-Reinforced Composite Plates with Various Boundary Conditions Using Ritz Method. <https://doi.org/10.1016/j.compstruct.2014.01.013>.
58. Ansari, R.; Torabi, J.; Shojaei, M. F. Buckling and Vibration Analysis of Embedded Functionally Graded Carbon Nanotube-Reinforced Composite Annular Sector Plates under Thermal Loading. **2016**.

<https://doi.org/10.1016/j.compositesb.2016.10.050>.

59. Apuzzo, A.; Barretta, R.; Luciano, R.; Marotti De Sciarra, F.; Penna, R. Free Vibrations of Bernoulli-Euler Nano-Beams by the Stress-Driven Nonlocal Integral Model. **2017**. <https://doi.org/10.1016/j.compositesb.2017.03.057>.
60. Madenci, E.; Özkılıç, Y. O.; Aksoylu, C.; Asyraf, M. R. M.; Syamsir, A.; Supian, A. B. M.; Mamaev, N. Buckling Analysis of CNT-Reinforced Polymer Composite Beam Using Experimental and Analytical Methods. *Mater.* **2023**, *Vol. 16*, Page 614 **2023**, *16* (2), 614. <https://doi.org/10.3390/MA16020614>.
61. Madenci, E.; Madenci, E. Advances in Nano Research. *Adv. Nano Res.* **2021**, *11* (2), 157. <https://doi.org/10.12989/ANR.2021.11.2.157>.
62. Qian, D.; Wagner, G. J.; Liu, W. K.; Yu, M. F.; Ruoff, R. S. Mechanics of Carbon Nanotubes. *Appl. Mech. Rev.* **2002**, *55* (6), 495–533. <https://doi.org/10.1115/1.1490129>.
63. Zhu, J.; Peng, H.; Rodriguez-Macias, F.; Margrave, J. L.; Khabashesku, V. N.; Imam, A. M.; Lozano, K.; Barrera, E. V. Reinforcing Epoxy Polymer Composites Through Covalent Integration of Functionalized Nanotubes. *Adv. Funct. Mater.* **2004**, *14* (7), 643–648. <https://doi.org/10.1002/ADFM.200305162>.
64. Tarfaoui, M.; Lafdi, K.; Moumen, A. El. Mechanical Properties of Carbon Nanotubes Based Polymer Composites. **2016**. <https://doi.org/10.1016/j.compositesb.2016.08.016>.
65. Godec, M.; Mandrino, D.; Jenko, M. Investigation of the Fracture of a Car's Drive Shaft. *Eng. Fail. Anal.* **2009**, *16* (4), 1252–1261. <https://doi.org/10.1016/j.engfailanal.2008.08.022>.
66. . P. P. S. Design and Analysis of Drive Shaft for Heavy Duty Truck. *Int. J. Res. Eng. Technol.* **2016**, *05* (01), 52–57. <https://doi.org/10.15623/ijret.2016.0501009>.
67. Nehe, S. R.; Ghogare, A.; Vatsa, S.; Tekade, L.; Thakare, S.; Yadav, P.; Shool, P.; Wankhade, P.; Dhakane, V.; Charjan, S. Design, Analysis, Simulation and Validation of Automobile Suspension System Using Drive-Shaft as a Suspension Link. *SAE Int. J. Passeng. Cars - Mech. Syst.* **2018**, *11*, 129+.
68. Cho, D. H.; Lee, D. G.; Choi, J. H. Manufacture of One-Piece Automotive Drive

- Shafts with Aluminum and Composite Materials. *Compos. Struct.* **1997**, 38 (1), 309–319. [https://doi.org/https://doi.org/10.1016/S0263-8223\(97\)00065-2](https://doi.org/https://doi.org/10.1016/S0263-8223(97)00065-2).
69. Gong, L.; Gao, X.; Yang, H.; Liu, Y.; Yao, X. Design on the Driveshaft of 3D 4-Directional Carbon Fiber Braided Composites. *Compos. Struct.* **2018**, 203, 466–473. <https://doi.org/https://doi.org/10.1016/j.compstruct.2018.06.103>.
70. Nadeem, S. K. S.; Giridhara, G.; Rangavittal, H. K. A Review on the Design and Analysis of Composite Drive Shaft. *Mater. Today Proc.* **2018**, 5 (1, Part 3), 2738–2741. <https://doi.org/https://doi.org/10.1016/j.matpr.2018.01.058>.
71. Shinde, R. M.; Sawant, S. M. Investigation on Glass-Epoxy Composite Drive Shaft for Light Motor Vehicle. *Int. J. Des. Eng.* **2019**, 9 (1), 22–35. <https://doi.org/10.1504/IJDE.2019.104124>.
72. Bilalis, E. P.; Keramidis, M. S.; Tsouvalis, N. G. Structural Design Optimization of Composite Materials Drive Shafts. *Mar. Struct.* **2022**, 84, 103194. <https://doi.org/https://doi.org/10.1016/j.marstruc.2022.103194>.
73. Samir Mohamed Mohamed Soliman, E. Optimization of Ply-Laminated Stacking Sequence for Composite Drive Shaft. *J. Fail. Anal. Prev.* **2022**, 23. <https://doi.org/10.1007/s11668-022-01562-y>.
74. Debski, H.; Rozylo, P.; Teter, A. Buckling and Limit States of Thin-Walled Composite Columns under Eccentric Load. *Thin-Walled Struct.* **2020**, 149, 106627. <https://doi.org/https://doi.org/10.1016/j.tws.2020.106627>.
75. Solazzi, L.; Bertoli, D.; Ghidini, L. Static and Dynamic Study of the Industrial Vehicle Transmission Adopting Composite Materials. *Compos. Struct.* **2023**, 316, 117042. <https://doi.org/https://doi.org/10.1016/j.compstruct.2023.117042>.
76. Isaac, C. W.; Ezekwem, C. A Review of the Crashworthiness Performance of Energy Absorbing Composite Structure within the Context of Materials, Manufacturing and Maintenance for Sustainability. *Compos. Struct.* **2021**, 257, 113081. <https://doi.org/https://doi.org/10.1016/j.compstruct.2020.113081>.
77. Zhao, J.; Wu, L.; Zhan, C.; Shao, Q.; Guo, Z.; Zhang, L. Overview of Polymer Nanocomposites: Computer Simulation Understanding of Physical Properties. *Polymer (Guildf)*. **2017**, 133, 272–287.

- <https://doi.org/https://doi.org/10.1016/j.polymer.2017.10.035>.
78. Taşyürek, M.; Tarakçıoğlu, N. Enhanced Fatigue Behavior under Internal Pressure of CNT Reinforced Filament Wound Cracked Pipes. *Compos. Part B Eng.* **2017**, *124*, 23–30.
<https://doi.org/https://doi.org/10.1016/j.compositesb.2017.05.050>.
 79. Solak, Z. A.; Kartav, O.; Tanoglu, M. Enhancement of Filament Wound Glass Fiber/Epoxy-Based Cylindrical Composites by Toughening with Single-Walled Carbon Nanotubes. *Polym. Polym. Compos.* **2022**, *30*, 09673911221086718.
<https://doi.org/10.1177/09673911221086718>.
 80. Georgantzinou, S. K.; Antoniou, P. A.; Markolefas, S. I. A Multi-Scale Method for Designing Hybrid Fiber-Reinforced Composite Drive Shafts with Carbon Nanotube Inclusions. *J. Compos. Sci.* **2021**, *5* (6).
<https://doi.org/10.3390/jcs5060157>.
 81. Searle, J.; Meng, M.; Summerscales, J. FEA Modelling and Environmental Assessment of a Thin-Walled Composite Drive Shaft. *Thin-Walled Struct.* **2022**, *180* (April), 109799. <https://doi.org/10.1016/j.tws.2022.109799>.
 82. Garg, A.; Chalak, H. D.; Belarbi, M.-O.; Zenkour, A. M.; Sahoo, R. Estimation of Carbon Nanotubes and Their Applications as Reinforcing Composite Materials—An Engineering Review. *Compos. Struct.* **2021**, *272*, 114234.
<https://doi.org/https://doi.org/10.1016/j.compstruct.2021.114234>.
 83. Kumar, A.; Sharma, K.; Dixit, A. R. Carbon Nanotube- and Graphene-Reinforced Multiphase Polymeric Composites: Review on Their Properties and Applications. *J. Mater. Sci.* **2020**, *55* (7), 2682–2724.
<https://doi.org/10.1007/s10853-019-04196-y>.
 84. Bilisik, K.; Akter, M. Graphene Nanoplatelets/Epoxy Nanocomposites: A Review on Functionalization, Characterization Techniques, Properties, and Applications. *J. Reinf. Plast. Compos.* **2022**, *41* (3–4), 99–129.
<https://doi.org/10.1177/07316844211049277>.
 85. Davim, J. P. *Mechanical and Industrial Engineering Historical Aspects and Future Directions: Historical Aspects and Future Directions*; 2022.
<https://doi.org/10.1007/978-3-030-90487-6>.

86. De Joardar, S.; Neog, A.; Parvez, S.; Kirtania, S.; Kashyap, S.; Banerjee, S. Micromechanics Based Finite Element Analysis of Effective Elastic Properties of Natural Fiber Reinforced Composites. *J. Nat. Fibers* **2022**, *19* (17), 15790–15807. <https://doi.org/10.1080/15440478.2022.2134265>.
87. Sharma, H.; Kumar, A.; Rana, S.; Sahoo, N. G.; Jamil, M.; Kumar, R.; Sharma, S.; Li, C.; Kumar, A.; Eldin, S. M.; Abbas, M. Critical Review on Advancements on the Fiber-Reinforced Composites: Role of Fiber/Matrix Modification on the Performance of the Fibrous Composites. *J. Mater. Res. Technol.* **2023**, *26*, 2975–3002. <https://doi.org/https://doi.org/10.1016/j.jmrt.2023.08.036>.
88. Nikbakt, S.; Kamarian, S.; Shakeri, M. A Review on Optimization of Composite Structures Part I: Laminated Composites. *Compos. Struct.* **2018**, *195*, 158–185. <https://doi.org/https://doi.org/10.1016/j.compstruct.2018.03.063>.
89. Vo-Duy, T.; Ho-Huu, V.; Do-Thi, T. D.; Dang-Trung, H.; Nguyen-Thoi, T. A Global Numerical Approach for Lightweight Design Optimization of Laminated Composite Plates Subjected to Frequency Constraints. *Compos. Struct.* **2017**, *159*, 646–655. <https://doi.org/10.1016/J.COMPSTRUCT.2016.09.059>.
90. Jones, R. M. *Mechanics Of Composite Materials*; CRC Press, 1999. <https://doi.org/https://doi.org/10.1201/9781498711067>.
91. Sahmaran, M.; Li, V. C.; Andrade, C. Corrosion Resistance Performance of Steel-Reinforced Engineered Cementitious Composite Beams. *ACI Mater. J.* **2008**, *105* (3), 243 – 250.
92. Naslain, R. R.; Pomeroy, M. R. B. T.-R. M. in M. S. and M. E. *Ceramic Matrix Composites: Matrices and Processing*; Elsevier, 2016. <https://doi.org/https://doi.org/10.1016/B978-0-12-803581-8.02317-1>.
93. Rajak, D. K.; Pagar, D. D.; Kumar, R.; Pruncu, C. I. Recent Progress of Reinforcement Materials: A Comprehensive Overview of Composite Materials. *J. Mater. Res. Technol.* **2019**, *8* (6), 6354–6374. <https://doi.org/10.1016/j.jmrt.2019.09.068>.
94. Ray, B. C. Temperature Effect during Humid Ageing on Interfaces of Glass and Carbon Fibers Reinforced Epoxy Composites. *J. Colloid Interface Sci.* **2006**, *298* (1), 111–117. <https://doi.org/https://doi.org/10.1016/j.jcis.2005.12.023>.

95. Xu, Y.; Chung, D. D. L.; Mroz, C. Thermally Conducting Aluminum Nitride Polymer-Matrix Composites. *Compos. Part A Appl. Sci. Manuf.* **2001**, *32* (12), 1749–1757. [https://doi.org/https://doi.org/10.1016/S1359-835X\(01\)00023-9](https://doi.org/https://doi.org/10.1016/S1359-835X(01)00023-9).
96. Mukherjee, M.; Das, C. K.; Kharitonov, A. P. Fluorinated and Oxyfluorinated Short Kevlar Fiber-Reinforced Ethylene Propylene Polymer. *Polym. Compos.* **2006**, *27* (2), 205–212. <https://doi.org/https://doi.org/10.1002/pc.20195>.
97. Dang, Z.-M.; Yuan, J.-K.; Zha, J.-W.; Zhou, T.; Li, S.-T.; Hu, G.-H. Fundamentals, Processes and Applications of High-Permittivity Polymer–Matrix Composites. *Prog. Mater. Sci.* **2012**, *57* (4), 660–723. <https://doi.org/https://doi.org/10.1016/j.pmatsci.2011.08.001>.
98. Kaw, A. K. *Mechanics of Composite Materials*, 2nd ed.; CRC Press, 2005. <https://doi.org/https://doi.org/10.1201/9781420058291>.
99. Wisnom, M. R.; Gigliotti, M.; Ersoy, N.; Campbell, M.; Potter, K. D. Mechanisms Generating Residual Stresses and Distortion during Manufacture of Polymer–Matrix Composite Structures. *Compos. Part A Appl. Sci. Manuf.* **2006**, *37* (4), 522–529. <https://doi.org/https://doi.org/10.1016/j.compositesa.2005.05.019>.
100. Zhang, C. 14 - Understanding the Wear and Tribological Properties of Ceramic Matrix Composites. In *Advances in Ceramic Matrix Composites*; Low, I. M., Ed.; Woodhead Publishing, 2014; pp 312–339. <https://doi.org/https://doi.org/10.1533/9780857098825.2.312>.
101. Richerson, D.W., & Lee, W. E. *Modern Ceramic Engineering: Properties, Processing, and Use in Design*, Fourth Edi.; 2018. <https://doi.org/https://doi.org/10.1201/9780429488245>.
102. Hunt, W. H. 6.05 - Metal Matrix Composites. In *Comprehensive Composite Materials*; Kelly, A., Zweben, C., Eds.; Pergamon: Oxford, 2000; pp 57–66. <https://doi.org/https://doi.org/10.1016/B0-08-042993-9/00134-0>.
103. Li, J.; Laghari, R. A. A Review on Machining and Optimization of Particle-Reinforced Metal Matrix Composites. *Int. J. Adv. Manuf. Technol.* **2019**, *100* (9), 2929–2943. <https://doi.org/10.1007/s00170-018-2837-5>.

104. De Araújo, M. 1 - Natural and Man-Made Fibres: Physical and Mechanical Properties. In *Fibrous and Composite Materials for Civil Engineering Applications*; Figueiro, R., Ed.; Woodhead Publishing Series in Textiles; Woodhead Publishing, 2011; pp 3–28.
<https://doi.org/https://doi.org/10.1533/9780857095583.1.3>.
105. Singh, T. J.; Samanta, S. Characterization of Kevlar Fiber and Its Composites: A Review. *Mater. Today Proc.* **2015**, 2 (4), 1381–1387.
<https://doi.org/https://doi.org/10.1016/j.matpr.2015.07.057>.
106. Davis, D. C.; Wilkerson, J. W.; Zhu, J.; Ayewah, D. O. O. Improvements in Mechanical Properties of a Carbon Fiber Epoxy Composite Using Nanotube Science and Technology. *Compos. Struct.* **2010**, 92 (11), 2653–2662.
<https://doi.org/https://doi.org/10.1016/j.compstruct.2010.03.019>.
107. Husić, S.; Javni, I.; Petrović, Z. S. Thermal and Mechanical Properties of Glass Reinforced Soy-Based Polyurethane Composites. *Compos. Sci. Technol.* **2005**, 65 (1), 19–25. <https://doi.org/https://doi.org/10.1016/j.compscitech.2004.05.020>.
108. Osorio, L.; Trujillo, E.; Vuure, A. W. Van; Verpoest, I. Morphological Aspects and Mechanical Properties of Single Bamboo Fibers and Flexural Characterization of Bamboo/ Epoxy Composites. *J. Reinf. Plast. Compos.* **2011**, 30 (5), 396–408. <https://doi.org/10.1177/0731684410397683>.
109. Kamarudin, S. H.; Mohd Basri, M. S.; Rayung, M.; Abu, F.; Ahmad, S.; Norizan, M. N.; Osman, S.; Sarifuddin, N.; Desa, M. S. Z. M.; Abdullah, U. H.; Mohamed Amin Tawakkal, I. S.; Abdullah, L. C. A Review on Natural Fiber Reinforced Polymer Composites (NFRPC) for Sustainable Industrial Applications. *Polymers (Basel)*. **2022**, 14 (17). <https://doi.org/10.3390/polym14173698>.
110. Manu, T.; Nazmi, A. R.; Shahri, B.; Emerson, N.; Huber, T. Biocomposites: A Review of Materials and Perception. *Mater. Today Commun.* **2022**, 31, 103308.
<https://doi.org/https://doi.org/10.1016/j.mtcomm.2022.103308>.
111. Muhammed Shameem, M.; Sasikanth, S. M.; Annamalai, R.; Ganapathi Raman, R. A Brief Review on Polymer Nanocomposites and Its Applications. *Mater. Today Proc.* **2021**, 45, 2536–2539.
<https://doi.org/https://doi.org/10.1016/j.matpr.2020.11.254>.

112. Reduwan Billah, S. M. Composites and Nanocomposites BT - Functional Polymers; Jafar Mazumder, M. A., Sheardown, H., Al-Ahmed, A., Eds.; Springer International Publishing: Cham, 2019; pp 1–67. https://doi.org/10.1007/978-3-319-92067-2_15-1.
113. Darwish, M. A.; Abd-Elaziem, W.; Elsheikh, A.; Zayed, A. A. Advancements in Nanomaterials for Nanosensors: A Comprehensive Review. *Nanoscale Adv.* **2024**, *6* (16), 4015–4046. <https://doi.org/10.1039/D4NA00214H>.
114. Naganuma, T.; Kagawa, Y. Effect of Particle Size on the Optically Transparent Nano Meter-Order Glass Particle-Dispersed Epoxy Matrix Composites. *Compos. Sci. Technol.* **2002**, *62* (9), 1187–1189. [https://doi.org/https://doi.org/10.1016/S0266-3538\(02\)00059-3](https://doi.org/https://doi.org/10.1016/S0266-3538(02)00059-3).
115. Yan, Q.-L.; Gozin, M.; Zhao, F.-Q.; Cohen, A.; Pang, S.-P. Highly Energetic Compositions Based on Functionalized Carbon Nanomaterials. *Nanoscale* **2016**, *8* (9), 4799–4851. <https://doi.org/10.1039/C5NR07855E>.
116. Domun, N.; Hadavinia, H.; Zhang, T.; Sainsbury, T.; Liaghat, G. H.; Vahid, S. Improving the Fracture Toughness and the Strength of Epoxy Using Nanomaterials – a Review of the Current Status. *Nanoscale* **2015**, *7* (23), 10294–10329. <https://doi.org/10.1039/C5NR01354B>.
117. Qian, D.; Dickey, E. C.; Andrews, R.; Rantell, T. Load Transfer and Deformation Mechanisms in Carbon Nanotube-Polystyrene Composites. *Appl. Phys. Lett.* **2000**, *76* (20), 2868–2870. <https://doi.org/10.1063/1.126500>.
118. Yee, K.; Ghayesh, M. H. A Review on the Mechanics of Graphene Nanoplatelets Reinforced Structures. *Int. J. Eng. Sci.* **2023**, *186*, 103831. <https://doi.org/https://doi.org/10.1016/j.ijengsci.2023.103831>.
119. Hu, K.; Kulkarni, D. D.; Choi, I.; Tsukruk, V. V. Graphene-Polymer Nanocomposites for Structural and Functional Applications. *Prog. Polym. Sci.* **2014**, *39* (11), 1934–1972. <https://doi.org/https://doi.org/10.1016/j.progpolymsci.2014.03.001>.
120. Gojny, F. H.; Wichmann, M. H. G.; Köpke, U.; Fiedler, B.; Schulte, K. Carbon Nanotube-Reinforced Epoxy-Composites: Enhanced Stiffness and Fracture Toughness at Low Nanotube Content. *Compos. Sci. Technol.* **2004**, *64* (15),

- 2363–2371. <https://doi.org/https://doi.org/10.1016/j.compscitech.2004.04.002>.
121. AJAYAN, P. M.; Schadler, L.; Giannaris, C.; Rubio, A. Single-Walled Carbon Nanotube-Polymer COMPOSITES: Strength and Weakness. *Adv. Mater.* **2000**, *12*, 750–+. [https://doi.org/10.1002/\(SICI\)1521-4095\(200005\)12:103.O.CO;2-6](https://doi.org/10.1002/(SICI)1521-4095(200005)12:103.O.CO;2-6).
122. Xie, X.-L.; Mai, Y.-W.; Zhou, X.-P. Dispersion and Alignment of Carbon Nanotubes in Polymer Matrix: A Review. *Mater. Sci. Eng. R Reports* **2005**, *49* (4), 89–112. <https://doi.org/https://doi.org/10.1016/j.mser.2005.04.002>.
123. Hernández-Pérez, A.; Avilés, F.; May-Pat, A.; Valadez-González, A.; Herrera-Franco, P. J.; Bartolo-Pérez, P. Effective Properties of Multiwalled Carbon Nanotube/Epoxy Composites Using Two Different Tubes. *Compos. Sci. Technol.* **2008**, *68* (6), 1422–1431. <https://doi.org/https://doi.org/10.1016/j.compscitech.2007.11.001>.
124. Kwon, S. C.; Adachi, T. Strength and Fracture Toughness of Nano and Micron-Silica Particles Bidispersed Epoxy Composites: Evaluated by Fragility Parameter. *J. Mater. Sci.* **2007**, *42* (14), 5516–5523. <https://doi.org/10.1007/s10853-006-1025-4>.
125. Ayatollahi, M. R.; Shadlou, S.; Shokrieh, M. M. Fracture Toughness of Epoxy/Multi-Walled Carbon Nanotube Nano-Composites under Bending and Shear Loading Conditions. *Mater. Des.* **2011**, *32* (4), 2115–2124. <https://doi.org/https://doi.org/10.1016/j.matdes.2010.11.034>.
126. Hsieh, T. H.; Kinloch, A. J.; Taylor, A. C.; Kinloch, I. A. The Effect of Carbon Nanotubes on the Fracture Toughness and Fatigue Performance of a Thermosetting Epoxy Polymer. *J. Mater. Sci.* **2011**, *46* (23), 7525–7535. <https://doi.org/10.1007/s10853-011-5724-0>.
127. Tang, L.; Zhang, H.; Han, J.; Wu, X.; Zhang, Z. Fracture Mechanisms of Epoxy Filled with Ozone Functionalized Multi-Wall Carbon Nanotubes. *Compos. Sci. Technol.* **2011**, *72* (1), 7–13. <https://doi.org/https://doi.org/10.1016/j.compscitech.2011.07.016>.
128. Naebe, M.; Wang, J.; Amini, A.; Khayyam, H.; Hameed, N.; Li, L. H.; Chen, Y.; Fox, B. Mechanical Property and Structure of Covalent Functionalised Graphene/Epoxy Nanocomposites. *Sci. Rep.* **2014**, *4* (1), 4375.

<https://doi.org/10.1038/srep04375>.

129. T.K., B. S.; Nair, A. B.; Abraham, B. T.; Beegum, P. M. S.; Thachil, E. T. Microwave Exfoliated Reduced Graphene Oxide Epoxy Nanocomposites for High Performance Applications. *Polymer (Guildf)*. **2014**, *55* (16), 3614–3627. <https://doi.org/https://doi.org/10.1016/j.polymer.2014.05.032>.
130. Atif, R.; Shyha, I.; Inam, F. The Degradation of Mechanical Properties Due to Stress Concentration Caused by Retained Acetone in Epoxy Nanocomposites. *RSC Adv*. **2016**, *6* (41), 34188–34197. <https://doi.org/10.1039/C6RA00739B>.
131. Kumar, A.; Anant, R.; Kumar, K.; Chauhan, S. S.; Kumar, S.; Kumar, R. Anticorrosive and Electromagnetic Shielding Response of a Graphene/TiO₂–Epoxy Nanocomposite with Enhanced Mechanical Properties. *RSC Adv*. **2016**, *6* (114), 113405–113414. <https://doi.org/10.1039/C6RA15273B>.
132. Baruah, P.; Karak, N. Bio-Based Tough Hyperbranched Epoxy/Graphene Oxide Nanocomposite with Enhanced Biodegradability Attribute. *Polym. Degrad. Stab*. **2016**, *129*, 26–33. <https://doi.org/https://doi.org/10.1016/j.polymdegradstab.2016.03.021>.
133. Chatterjee, S.; Wang, J. W.; Kuo, W. S.; Tai, N. H.; Salzmann, C.; Li, W. L.; Hollertz, R.; Nüesch, F. A.; Chu, B. T. T. Mechanical Reinforcement and Thermal Conductivity in Expanded Graphene Nanoplatelets Reinforced Epoxy Composites. *Chem. Phys. Lett*. **2012**, *531*, 6–10. <https://doi.org/https://doi.org/10.1016/j.cplett.2012.02.006>.
134. Qi, B.; Lu, S. R.; Xiao, X. E.; Pan, L. L.; Tan, F. Z.; Yu, J. H. Enhanced Thermal and Mechanical Properties of Epoxy Composites by Mixing Thermotropic Liquid Crystalline Epoxy Grafted Graphene Oxide. *Express Polym. Lett*. **2014**, *8* (7), 467–479. <https://doi.org/10.3144/expresspolymlett.2014.51>.
135. Ahmadi-Moghadam, B.; Sharafimasooleh, M.; Shadlou, S.; Taheri, F. Effect of Functionalization of Graphene Nanoplatelets on the Mechanical Response of Graphene/Epoxy Composites. *Mater. Des*. **2015**, *66*, 142–149. <https://doi.org/https://doi.org/10.1016/j.matdes.2014.10.047>.
136. Wan, Y.-J.; Gong, L.-X.; Tang, L.-C.; Wu, L.-B.; Jiang, J.-X. Mechanical Properties of Epoxy Composites Filled with Silane-Functionalized Graphene

- Oxide. *Compos. Part A Appl. Sci. Manuf.* **2014**, *64*, 79–89.
<https://doi.org/https://doi.org/10.1016/j.compositesa.2014.04.023>.
137. Bortz, D. R.; Heras, E. G.; Martin-Gullon, I. Impressive Fatigue Life and Fracture Toughness Improvements in Graphene Oxide/Epoxy Composites. *Macromolecules* **2012**, *45* (1), 238–245. <https://doi.org/10.1021/ma201563k>.
138. Denver, H.; Heiman, T.; Martin, E.; Gupta, A.; Borca-Tasciuc, D.-A. Fabrication of Polydimethylsiloxane Composites with Nickel Nanoparticle and Nanowire Fillers and Study of Their Mechanical and Magnetic Properties. *J. Appl. Phys.* **2009**, *106* (6), 64909. <https://doi.org/10.1063/1.3224966>.
139. Balguri, P. K.; Samuel, D. G. H.; Aditya, D. B.; Bhaskar, S. V.; Thumu, U. Enhanced Flexural Strength of Tellurium Nanowires/Epoxy Composites with the Reinforcement Effect of Nanowires. *IOP Conf. Ser. Mater. Sci. Eng.* **2018**, *310* (1), 12157. <https://doi.org/10.1088/1757-899X/310/1/012157>.
140. Mahmoud Zaghoul, M. Y.; Yousry Zaghoul, M. M.; Yousry Zaghoul, M. M. Developments in Polyester Composite Materials – An in-Depth Review on Natural Fibres and Nano Fillers. *Compos. Struct.* **2021**, *278*, 114698. <https://doi.org/https://doi.org/10.1016/j.compstruct.2021.114698>.
141. Gholampour, A.; Ozbakkaloglu, T. A Review of Natural Fiber Composites: Properties, Modification and Processing Techniques, Characterization, Applications. *J. Mater. Sci.* **2020**, *55* (3), 829–892. <https://doi.org/10.1007/s10853-019-03990-y>.
142. Rahman, R.; Zhafer Firdaus Syed Putra, S. 5 - Tensile Properties of Natural and Synthetic Fiber-Reinforced Polymer Composites. In *Woodhead Publishing Series in Composites Science and Engineering*; Jawaid, M., Thariq, M., Saba Fibre-Reinforced Composites and Hybrid Composites, N. B. T.-M. and P. T. of B., Eds.; Woodhead Publishing, 2019; pp 81–102. <https://doi.org/https://doi.org/10.1016/B978-0-08-102292-4.00005-9>.
143. Muzyczek, M. 4 - The Use of Flax and Hemp for Textile Applications. In *The Textile Institute Book Series*; Kozłowski, R. M., Mackiewicz-Talarczyk, M. B. T.-H. of N. F. (Second E., Eds.; Woodhead Publishing, 2020; pp 147–167. <https://doi.org/https://doi.org/10.1016/B978-0-12-818782-1.00004-3>.

144. Zhang, Y.; Li, Y.; Ma, H.; Yu, T. Tensile and Interfacial Properties of Unidirectional Flax/Glass Fiber Reinforced Hybrid Composites. *Compos. Sci. Technol.* **2013**, *88*, 172–177.
<https://doi.org/https://doi.org/10.1016/j.compscitech.2013.08.037>.
145. Yan, L.; Chouw, N.; Jayaraman, K. Flax Fibre and Its Composites – A Review. *Compos. Part B Eng.* **2014**, *56*, 296–317.
<https://doi.org/https://doi.org/10.1016/j.compositesb.2013.08.014>.
146. Kamaraj, M.; Dodson, E. A.; Datta, S. Effect of Graphene on the Properties of Flax Fabric Reinforced Epoxy Composites. *Adv. Compos. Mater.* **2020**, *29* (5), 443–458. <https://doi.org/10.1080/09243046.2019.1709679>.
147. Shen, M.; Wang, L.; Long, J.-J. Biodegumming of Ramie Fiber with Pectinases Enhanced by Oxygen Plasma. *J. Clean. Prod.* **2015**, *101*, 395–403.
<https://doi.org/https://doi.org/10.1016/j.jclepro.2015.03.081>.
148. Li, W.; Du, W.; Li, W.; Chen, D.; Liu, Y.; Ouyang, Y. Hygrothermal Aging Behavior and Mechanical Properties of Modified Ramie Fiber Reinforced Polyethylene Terephthalate Glycol Composites. *Cellulose* **2023**, *30* (5), 3061–3072. <https://doi.org/10.1007/s10570-023-05064-4>.
149. Hasan, K. M. F.; Horváth, P. G.; Alpár, T. Potential Natural Fiber Polymeric Nanobiocomposites: A Review. *Polymers (Basel)*. **2020**, *12* (5).
<https://doi.org/10.3390/polym12051072>.
150. Nik Baihaqi, N. M. Z.; Khalina, A.; Mohd Nurazzi, N.; Aisyah, H. A.; Sapuan, S. M.; Ilyas, R. A. Effect of Fiber Content and Their Hybridization on Bending and Torsional Strength of Hybrid Epoxy Composites Reinforced with Carbon and Sugar Palm Fibers. *Polimery* **2021**, *66* (1 SE-Articles), 36–43.
<https://doi.org/10.14314/polimery.2021.1.5>.
151. Zhao, X.; Li, W.; Ouyang, Y.; Xu, W.; Liu, Y. Hygrothermal Aging Behavior and Mechanical Degradation of Ramie/Carbon Fiber Reinforced Thermoplastic Polymer Hybrid Composites. *Ind. Crops Prod.* **2023**, *193*, 116212.
<https://doi.org/https://doi.org/10.1016/j.indcrop.2022.116212>.
152. Saroj, S.; Nayak, S.; Kumar Jesthi, D. Effect of Hybridization of Carbon/Glass/Flax/Kenaf Fibre Composite on Flexural and Impact Properties.

- Mater. Today Proc.* **2022**, *49*, 502–506.
<https://doi.org/https://doi.org/10.1016/j.matpr.2021.03.094>.
153. Etri, H. E. L.; Polat, M. Z.; Özyılmaz, E. B. Classification, Applications, and Impact Behavior of Composite Materials: A Review. *Mech. Adv. Mater. Struct.* 1–44. <https://doi.org/10.1080/15376494.2024.2326665>.
154. Adekomaya, O.; Majozi, T. Sustainable Reclamation of Synthetic Materials as Automotive Parts Replacement: Effects of Environmental Response on Natural Fiber Vulnerabilities. *Environ. Sci. Pollut. Res.* **2024**, *31* (12), 18396–18411. <https://doi.org/10.1007/s11356-024-32436-5>.
155. Moudood, A.; Rahman, A.; Öchsner, A.; Islam, M.; Francucci, G. Flax Fiber and Its Composites: An Overview of Water and Moisture Absorption Impact on Their Performance. *J. Reinf. Plast. Compos.* **2019**, *38* (7), 323–339. <https://doi.org/10.1177/0731684418818893>.
156. Mann, G. S.; Singh, L. P.; Kumar, P.; Singh, S. Green Composites: A Review of Processing Technologies and Recent Applications. *J. Thermoplast. Compos. Mater.* **2020**, *33* (8), 1145–1171. <https://doi.org/10.1177/0892705718816354>.
157. Wu, Y.; Cai, L.; Mei, C.; Lam, S. S.; Sonne, C.; Shi, S. Q.; Xia, C. Development and Evaluation of Zinc Oxide-Blended Kenaf Fiber Biocomposite for Automotive Applications. *Mater. Today Commun.* **2020**, *24*, 101008. <https://doi.org/https://doi.org/10.1016/j.mtcomm.2020.101008>.
158. Bachmann, J.; Yi, X.; Gong, H.; Martinez, X.; Bugada, G.; Oller, S.; Tserpes, K.; Ramon, E.; Paris, C.; Moreira, P.; Fang, Z.; Li, Y.; Liu, Y.; Liu, X.; Xian, G.; Tong, J.; Wei, J.; Zhang, X.; Zhu, J.; Ma, S.; Yu, T. Outlook on Ecologically Improved Composites for Aviation Interior and Secondary Structures. *CEAS Aeronaut. J.* **2018**, *9* (3), 533–543. <https://doi.org/10.1007/s13272-018-0298-z>.
159. *Natural fibre reinforced satellite panel*. <https://www.bcomp.com/news/natural-fibre-reinforced-satellite-panel/> (accessed 2024-07-14).
160. *Natural fibres threaded into satellites for safer missions*. The European Space Agency. https://www.esa.int/Enabling_Support/Space_Engineering_Technology/Natural_fibres_threaded_into_satellites_for_safer_missions (accessed 2024-07-14).

161. K.A. Henschel. Biocomposites in Aviation Structures on the Example of Flax and Its Hybrids, Technische Universität München, 2020.
<https://doi.org/https://mediatum.ub.tum.de/doc/1488689/1488689.pdf>.
162. Gomez-Campos, A.; Vialle, C.; Rouilly, A.; Hamelin, L.; Rogeon, A.; Hardy, D.; Sablayrolles, C. Natural Fibre Polymer Composites - A Game Changer for the Aviation Sector? *J. Clean. Prod.* **2021**, *286*, 124986.
<https://doi.org/https://doi.org/10.1016/j.jclepro.2020.124986>.
163. Elseify, L. A.; Midani, M.; El-Badawy, A.; Jawaid, M. Natural Fiber Composite Qualification in the Automotive Industry BT - Manufacturing Automotive Components from Sustainable Natural Fiber Composites; Elseify, L. A., Midani, M., El-Badawy, A., Jawaid, M., Eds.; Springer International Publishing: Cham, 2021; pp 53–65. https://doi.org/10.1007/978-3-030-83025-0_4.
164. Kausar, A. 4 - Aerospace Applications of Polymer/Carbonaceous Nanofiller Nanocomposites: Mechanical, Thermal, Nonflammability, and Physical Aspects. In *Polymeric Nanocomposites with Carbonaceous Nanofillers for Aerospace Applications*; Kausar, A., Ed.; Woodhead Publishing Series in Composites Science and Engineering; Woodhead Publishing, 2023; pp 85–111.
<https://doi.org/https://doi.org/10.1016/B978-0-323-99657-0.00012-0>.
165. Al Faruque, M. A.; Syduzzaman, M.; Sarkar, J.; Bilisik, K.; Naebe, M. A Review on the Production Methods and Applications of Graphene-Based Materials. *Nanomaterials* **2021**, *11* (9). <https://doi.org/10.3390/nano11092414>.
166. Jennifer Lynch. High Performance, Lightweight Graphene Enhanced Polymer Matrix Composites for Defense Applications. In *Journal of the Science and Technology Organization*; 2020; pp 18–28. <https://doi.org/10.14339/STO-J-02-01>.
167. P. Ferreira, D.; Abreu, I.; Fangueiro, R. *Versatile Graphene-Based Fibrous Systems for Military Applications*; 2019. <https://doi.org/10.14339/STO-MP-AVT-304>.
168. Tomasi, J.; Pisani, W.; Chinkanjanarot, S.; Krieg, A.; Jaszczak, D.; Pineda, E.; Bednarczyk, B.; Miller, S.; King, J.; Miskioglu, I.; Odegard, G. Modeling-Driven Damage Tolerant Design of Graphene Nanoplatelet/Carbon Fiber/Epoxy Hybrid

- Composite Panels for Full-Scale Aerospace Structures; 2019.
<https://doi.org/10.2514/6.2019-1273>.
169. Scalia, T.; Bonventre, L.; Terranova, M. L. From Protosolar Space to Space Exploration: The Role of Graphene in Space Technology and Economy. *Nanomaterials* **2023**, *13* (4). <https://doi.org/10.3390/nano13040680>.
170. Defence Turkey. *F-35 Lightning*.
<https://www.defenceturkey.com/en/content/turaf-f-35a-makes-its-maiden-flight-3030>.
171. National Aeronautics and Space Administration. *Space Launch System Core Stage*. https://www.nasa.gov/wp-content/uploads/2020/02/sls_core_stage_fact_sheet_04262021_508.pdf?emrc=9a5714.
172. Al, M. M. et. *Nanotechnology Roadmap Technology Area*; 2012.
173. Reddy, J. N. Mechanics of Laminated Composite Plates and Shells : Theory and Analysis, Second Edition. *Mech. Laminated Compos. Plates Shells* **2003**.
<https://doi.org/10.1201/B12409>.
174. Aydin, L. Artem, H. S. Oterkus, E. Gundogdu, O. Akbulut, H. Mechanics of Fiber Composites. In *Fiber Technology for Fiber Reinforced Composite*; Woodhead Publishing Press, 2017; pp 5–48.
175. Badie, M. A.; Mahdi, A.; Abutalib, A. R.; Abdullah, E. J.; Yonus, R. AUTOMOTIVE COMPOSITE DRIVESHAFTS : INVESTIGATION OF THE DESIGN. **2006**, *3* (2), 227–237.
176. Reddy, J. N. Mechanics of Laminated Composite Plates and Shells : Theory and Analysis, Second Edition. *Mech. Laminated Compos. Plates Shells* **2003**.
<https://doi.org/10.1201/B12409>.
177. Gholami, R.; Ansari, R.; Gholami, Y. Numerical Study on the Nonlinear Resonant Dynamics of Carbon Nanotube/Fiber/Polymer Multiscale Laminated Composite Rectangular Plates with Various Boundary Conditions. *Aerosp. Sci. Technol.* **2018**, *78*, 118–129. <https://doi.org/10.1016/j.ast.2018.03.043>.
178. Rafiee, M.; Nitzsche, F.; Labrosse, M. R. Modeling and Mechanical Analysis of

- Multiscale Fiber-Reinforced Graphene Composites: Nonlinear Bending, Thermal Post-Buckling and Large Amplitude Vibration. *Int. J. Non. Linear. Mech.* **2018**, *103* (February), 104–112. <https://doi.org/10.1016/j.ijnonlinmec.2018.05.004>.
179. Godara, S. S.; Sharma, N. Multifunctional Applications of Carbon Nanotube Based Polymer Composites BT - Handbook of Carbon Nanotubes; Abraham, J., Thomas, S., Kalarikkal, N., Eds.; Springer International Publishing: Cham, 2020; pp 1–15. https://doi.org/10.1007/978-3-319-70614-6_48-1.
180. Shen, H.-S. A Comparison of Buckling and Postbuckling Behavior of FGM Plates with Piezoelectric Fiber Reinforced Composite Actuators. *Compos. Struct.* **2009**, *91* (3), 375–384. <https://doi.org/https://doi.org/10.1016/j.compstruct.2009.06.005>.
181. Hassanzadeh-Aghdam, M. K.; Jamali, J. A New Form of a Halpin–Tsai Micromechanical Model for Characterizing the Mechanical Properties of Carbon Nanotube-Reinforced Polymer Nanocomposites. *Bull. Mater. Sci.* **2019**, *42* (3), 117. <https://doi.org/10.1007/s12034-019-1784-6>.
182. Georgantzinou, S. K.; Antoniou, P. A.; Giannopoulos, G. I.; Fatsis, A.; Markolefas, S. I. Design of Laminated Composite Plates with Carbon Nanotube Inclusions against Buckling: Waviness and Agglomeration Effects. *Nanomaterials* **2021**, *11* (9). <https://doi.org/10.3390/nano11092261>.
183. Taş, H.; Soykok, I. F. Effects of Carbon Nanotube Inclusion into the Carbon Fiber Reinforced Laminated Composites on Flexural Stiffness: A Numerical and Theoretical Study. *Compos. Part B Eng.* **2019**, *159*, 44–52. <https://doi.org/https://doi.org/10.1016/j.compositesb.2018.09.055>.
184. García-Macías, E.; Rodríguez-Tembleque, L.; Sáez, A. Bending and Free Vibration Analysis of Functionally Graded Graphene vs. Carbon Nanotube Reinforced Composite Plates. *Compos. Struct.* **2018**, *186*, 123–138. <https://doi.org/https://doi.org/10.1016/j.compstruct.2017.11.076>.
185. Eshelby John Douglas. The Determination of the Elastic Field of an Ellipsoidal Inclusion, and Related Problems. *Proc. R. Soc. Lond. A* **1957**, *241*, 376–396. <https://doi.org/https://doi.org/10.1098/rspa.1957.0133>.
186. Yousefi, A. H.; Memarzadeh, P.; Afshari, H.; Hosseini, S. J. Agglomeration

- Effects on Free Vibration Characteristics of Three-Phase CNT/Polymer/Fiber Laminated Truncated Conical Shells. *Thin-Walled Struct.* **2020**, *157*.
<https://doi.org/10.1016/j.tws.2020.107077>.
187. Pelletier, J. L.; Vel, S. S. Multi-Objective Optimization of Fiber Reinforced Composite Laminates for Strength, Stiffness and Minimal Mass. *Comput. Struct.* **2006**, *84* (29–30), 2065–2080. <https://doi.org/10.1016/j.compstruc.2006.06.001>.
188. Rao, S. S. Introduction to Optimization. In *Engineering Optimization Theory and Practice*; 2019; pp 1–56.
<https://doi.org/https://doi.org/10.1002/9781119454816.ch1>.
189. Gürdal, Z.; Haftka, R. T.; Hajela, P. *Design and Optimization of Laminated Composite Materials*; 1999.
190. Storn, R.; Price, K. Differential Evolution – A Simple and Efficient Heuristic for Global Optimization over Continuous Spaces. *J. Glob. Optim.* **1997**, *11* (4), 341–359. <https://doi.org/10.1023/A:1008202821328>.
191. Roque, C. M. C.; Martins, P. A. L. S. Differential Evolution Optimization for the Analysis of Composite Plates with Radial Basis Collocation Meshless Method. *Compos. Struct.* **2015**, *124*, 317–326.
<https://doi.org/https://doi.org/10.1016/j.compstruct.2015.01.019>.
192. S.N. Sivanandam, S. N. D. *Introduction to Genetic Algorithms*; Springer Berlin, Heidelberg, 2007. <https://doi.org/https://doi.org/10.1007/978-3-540-73190-0>.
193. Reza, B. Parameter Estimation of Nonlinear Muskingum Models Using Nelder-Mead Simplex Algorithm. *J. Hydrol. Eng.* **2011**, *16* (11), 946–954.
[https://doi.org/10.1061/\(ASCE\)HE.1943-5584.0000379](https://doi.org/10.1061/(ASCE)HE.1943-5584.0000379).
194. D. T. Pham, D. K. *Intelligent Optimisation Techniques*; Publisher Springer London, 2012. <https://doi.org/https://doi.org/10.1007/978-1-4471-0721-7>.
195. Wang, X.; Wang, Y.; Xu, S. DSC Analysis of a Simply Supported Anisotropic Rectangular Plate. *Compos. Struct.* **2012**, *94* (8), 2576–2584.
<https://doi.org/https://doi.org/10.1016/j.compstruct.2012.03.005>.
196. Leissa, A. W.; Narita, Y. Vibration Studies for Simply Supported Symmetrically Laminated Rectangular Plates. *Compos. Struct.* **1989**, *12* (2), 113–132.

- [https://doi.org/https://doi.org/10.1016/0263-8223\(89\)90085-8](https://doi.org/https://doi.org/10.1016/0263-8223(89)90085-8).
197. Song, M.; Kitipornchai, S.; Yang, J. Free and Forced Vibrations of Functionally Graded Polymer Composite Plates Reinforced with Graphene Nanoplatelets. *Compos. Struct.* **2017**, *159*, 579–588.
<https://doi.org/https://doi.org/10.1016/j.compstruct.2016.09.070>.
 198. <https://www.cheaptubes.com/product/graphene-nanoplatelets/>.
 199. Ali, A.; Shaker, K.; Nawab, Y.; Ashraf, M.; Basit, A.; Shahid, S.; Umair, M. Impact of Hydrophobic Treatment of Jute on Moisture Regain and Mechanical Properties of Composite Material. *J. Reinf. Plast. Compos.* **2015**, *34* (24), 2059–2068. <https://doi.org/10.1177/0731684415610007>.
 200. Peças, P.; Carvalho, H.; Salman, H.; Leite, M. Natural Fibre Composites and Their Applications: A Review. *J. Compos. Sci.* **2018**, *2* (4), 1–20.
<https://doi.org/10.3390/jcs2040066>.
 201. Jalili, S.; Khani, R.; Hosseinzadeh, Y. On the Performance of Flax Fibres in Multi-Objective Design of Laminated Composite Plates for Buckling and Cost. *Structures* **2021**, *33* (June), 3094–3106.
<https://doi.org/10.1016/j.istruc.2021.06.026>.
 202. Anish; Chaubey, A.; Kumar, A.; Kwiatkowski, B.; Barnat-Hunek, D.; Widomski, M. K. Bi-Axial Buckling of Laminated Composite Plates Including Cutout and Additional Mass. *Materials (Basel)*. **2019**, *12* (11).
<https://doi.org/10.3390/ma12111750>.
 203. Nguyen-Van, H.; Mai-Duy, N.; Karunasena, W.; Tran-Cong, T. Buckling and Vibration Analysis of Laminated Composite Plate/Shell Structures via a Smoothed Quadrilateral Flat Shell Element with in-Plane Rotations. *Comput. Struct.* **2011**, *89* (7), 612–625.
<https://doi.org/https://doi.org/10.1016/j.compstruc.2011.01.005>.
 204. Liu, L.; Chua, L. P.; Ghista, D. N. Mesh-Free Radial Basis Function Method for Static, Free Vibration and Buckling Analysis of Shear Deformable Composite Laminates. *Compos. Struct.* **2007**, *78* (1), 58–69.
<https://doi.org/https://doi.org/10.1016/j.compstruct.2005.08.010>.

205. Reddy, J. N.; Phan, N. D. Stability and Vibration of Isotropic, Orthotropic and Laminated Plates According to a Higher-Order Shear Deformation Theory. *J. Sound Vib.* **1985**, *98* (2), 157–170. [https://doi.org/https://doi.org/10.1016/0022-460X\(85\)90383-9](https://doi.org/https://doi.org/10.1016/0022-460X(85)90383-9).
206. Khdeir, A. A.; Librescu, L. Analysis of Symmetric Cross-Ply Laminated Elastic Plates Using a Higher-Order Theory: Part II—Buckling and Free Vibration. *Compos. Struct.* **1988**, *9* (4), 259–277. [https://doi.org/https://doi.org/10.1016/0263-8223\(88\)90048-7](https://doi.org/https://doi.org/10.1016/0263-8223(88)90048-7).
207. Singh, S.; Singh, J.; Shukla, K. K. Buckling of Laminated Composite Plates Subjected to Mechanical and Thermal Loads Using Meshless Collocations. *J. Mech. Sci. Technol.* **2013**, *27* (2), 327–336. <https://doi.org/10.1007/s12206-012-1249-y>.
208. Sayyad, A. S.; Ghugal, Y. M. On the Buckling of Isotropic, Transversely Isotropic and Laminated Composite Rectangular Plates. *Int. J. Struct. Stab. Dyn.* **2014**, *14* (07), 1450020. <https://doi.org/10.1142/S0219455414500205>.
209. Noor, A. K. Stability of Multilayered Composite Plates. *Fibre Sci. Technol.* **1975**, *8* (2), 81–89. [https://doi.org/https://doi.org/10.1016/0015-0568\(75\)90005-6](https://doi.org/https://doi.org/10.1016/0015-0568(75)90005-6).
210. Vescovini, R.; Dozio, L. Exact Refined Buckling Solutions for Laminated Plates under Uniaxial and Biaxial Loads. *Compos. Struct.* **2015**, *127*, 356–368. <https://doi.org/https://doi.org/10.1016/j.compstruct.2015.03.003>.
211. Andrew Markel. *How Well Do You Know Your Driveshaft?* <https://www.brakeandfrontend.com/how-well-do-you-know-your-driveshaft/> (accessed 2024-07-15).
212. *Composite Drive Shaft*. <https://baltimoreaircoil.com/parts/drive-system/composite-drive-shafts>.
213. Searle, J.; Meng, M.; Summerscales, J. FEA Modelling and Environmental Assessment of a Thin-Walled Composite Drive Shaft. *Thin-Walled Struct.* **2022**, *180* (July), 109799. <https://doi.org/10.1016/j.tws.2022.109799>.
214. Chegiani, F.; El Mansori, M.; T. S. Bukkapatnam, S.; Reddy, J. N.

Micromechanical Modeling of the Machining Behavior of Natural Fiber-Reinforced Polymer Composites. *Int. J. Adv. Manuf. Technol.* **2019**, *105* (1–4), 1549–1561. <https://doi.org/10.1007/s00170-019-04271-3>.

215. Soden, P. D.; Hinton, M. J.; Kaddour, A. S. Lamina Properties, Lay-up Configurations and Loading Conditions for a Range of Fibre-Reinforced Composite Laminates. *Compos. Sci. Technol.* **1998**, *58* (7), 1011–1022. [https://doi.org/https://doi.org/10.1016/S0266-3538\(98\)00078-5](https://doi.org/https://doi.org/10.1016/S0266-3538(98)00078-5).

VITA

Ozan AYAKDAŞ

26.04.1991, Aydın/ TURKEY

EDUCATION

- **Ph.D.** in English, 2024, Mechanical Engineering, İzmir Institute of Technology.
- **M.Sc.** in English, 2018, Mechanical Engineering, İzmir Katip Çelebi University.
- **B.Sc.** in Turkish, 2014, Mechanical Engineering, Dokuz Eylül University.

PUBLICATIONS

SCI-Expanded Publications

1. Ayakdas, O.; Artem, S.; Savran, M.; Aydın, L.; Adalı, S.; Vibration Analysis and Optimal Design of Multiscale Hybrid Flax Fiber/Graphene Nanoplatelets Reinforced Laminates Using Modified Differential Evolution Algorithm, Composite Structures, 2024. (Under Review)
2. Kangal, S.; Harun Sayl, A.; Ayakdaş, O.; Kartav, O.; Aydın, L.; Seçil Artem, H.; Aktaş, E.; Yüçetürk, K.; Tanoğlu, M.; Kandemir, S.; Beylergil, B. A Comprehensive Study on Burst Pressure Performance of Aluminum Liner for Hydrogen Storage Vessels. J. Press. Vessel Technol. Trans. ASME 2021, 143 (4), 1–11. <https://doi.org/10.1115/1.4049644>.
3. Ayakdas, O.; Aydın, L.; Savran, M.; Kuçukdoğan, N.; Öztürk, S. Optimum Design of the Type III Pressure Vessel for Different Carbon/Epoxy Materials by using Stochastic Optimization Methods. Research on Engineering Structures and Materials, 2018 DOI: <http://dx.doi.org/10.17515/resm2019.65is0909>

Book Chapters

1. Savran, M.; Ayakdas, O.; Aydın, L.; Dizlek, M.; “Design and Optimization of Glass Reinforced Composite Driveshafts for Automotive Industry”, Designing Engineering Structures Using Stochastic Optimization Methods, CRC Press, 2020.
2. Sayi, H.; Ayakdas, O.; Aydın, L.; Artem, S.; “Development of Optimum Hydrogen Storage Vessels”, Designing Engineering Structures Using Stochastic Optimization Methods, CRC Press, 2020.
3. Savran, M.; Ayakdas, O.; Aydın, L.; “Free Vibration Analysis of Laminated Composite Plates”, The Most Recent Studies in Science and Art, Book Chapter, 2018

Selected International Conference Proceedings

1. Ayakdas, O.; Artem, S.; Savran, M.; Aydın, L.; “Optimum Designs and Analysis of Natural Frequency for Multiscale Graphene/Carbon Jute Fiber Reinforced Nanocomposite Laminates”, V. International Black Sea Modern Scientific Research Congress, November, 2023. (Oral Presentation)
2. Ayakdas, O.; Artem, S.; Savran, M.; Aydın, L.; “The Optimum Design Of Multiphase Natural/Synthetic Cnt-fiber Reinforced Nanocomposite Plate Under Different Loading Cases For Maximum Critical Buckling Load Capacity” 6th International Latin American Scientific Research Congress February 1-3, 2024 / Havana, Cuba.(Full paper submission)